Title

Steady-State and Excited State Kinetics And Photochromism of Spiropyrans in Solution and in Nanocrystalline Suspensions and the Solution and Solid State Transient Kinetics of a 1,1'-Biphenyl-2-Phenyl Diazomethane

Author

Breslin, Vanessa

Publication Date

2018

Peer reviewed|Thesis/dissertation

UNIVERSITY OF CALIFORNIA

Los Angeles

Steady-State and Excited State Kinetics and Photochromism of Spiropyrans in Solution and in Nanocrystalline Suspensions and the Solution and Solid State Transient Kinetics of a 1,1'-Biphenyl-2-Phenyl Diazomethane

A dissertation submitted in partial satisfaction of the

requirements for the degree Doctor of Philosophy

in Chemistry

by

Vanessa Marie Breslin

2018

ABSTRACT OF THE DISSERTATION

Steady-State and Excited State Kinetics and Photochromism of Spiropyrans in Solution and in Nanocrystalline Suspensions and the Solution and Solid State Transient Kinetics of a 1,1'-Biphenyl-2-Phenyl Diazomethane

by

Vanessa Marie Breslin

Doctor of Philosophy in Chemistry

University of California, Los Angeles, 2018

Professor Miguel A. Garcia-Garibay, Chair

The field of organic solid state photochemistry has great potential for new and exciting discoveries as a result of its youth in being able to determine the identities of the intermediates produced upon irradiation of a photochemically active molecule. Studying solid state photochemical reaction mechanisms has proven quite challenging due to the inherent optical properties of crystalline solids, such as birefringence, dichroism, and scattering, that must be overcome in order to observe the true photochemistry of the system under investigation. The rigid environment within a solid, in particular crystalline solids, is advantageous because it essentially programs a certain amount of chemical information into the system that will dictate if and how the photochemical reaction proceeds. The work described in this dissertation demonstrates the utility of using nanocrystalline suspensions as a simple and robust method to

significantly reduce the difficulties associated with studying reactions in crystals. Specifically the solid state kinetics and photochemical mechanism of diarylcarbenes and the spiropyran-merocyanine photochromic system have been investigated using nanocrystalline suspensions in order to expand our knowledge of photochemical reactivity in the solid state.

Chapter One introduces the field of organic solid state photochemistry and uses historical examples to demonstrate several of its fundamental principles, such as the topochemical postulate. The advantages to using solid state photochemistry is also discussed along with the challenges associated with studying photochemical reactions in solids. Specifically, the use of nanocrystalline suspensions is examined as a method capable of addressing the optical problems that are connected with studying solid state photochemical reactions spectroscopically. Additionally, the photochemistry of photochromic molecules and carbenes is highlighted in order to briefly illustrate the utility of solid state photochemistry.

In Chapter Two, the solid state photochromism of spiropyrans is investigated under steady-state irradiation conditions. A homologous set of nitro-substituted spiropyrans with different *N*-alkyl substituents was selected in order to study the effects of crystal packing on the thermal decay kinetics. It was found that the merocyanine has a biexponential lifetime 10–100 times longer in nanocrystalline suspensions than the single exponential lifetime found in solution, which indicated that the crystal lattice might impede multiple merocyanine structures from interconverting rapidly enough to produce a single kinetic signature.

In Chapter Three, nanosecond transient absorption spectroscopy was used to study the photochemical ring-opening reaction for a 6-nitroindolinospiropyran (**SP1**) in solution and in nanocrystalline (NC) suspension. The kinetics in argon-purged and air-saturated acetonitrile were measured and evidence of a triplet excited state species was found along with evidence for

two ground state species. Laser flash photolysis studies performed in NC suspensions initially showed a very broad, featureless absorption spectrum that decayed uniformly for ca. 70 ns before revealing a more defined spectrum that is consistent with a mixture of the ground state *Z*- and *E*-merocyanine structures. DFT calculations suggested that the broad, featureless transient absorption spectrum results from the contribution of the transition structure and other high-energy species during the *Z*- to *E*-merocyanine isomerization.

In Chapter Four, the nanosecond laser flash photolysis of a 1,1'-biphenyl-2-phenyldiazomethane was investigated both in solution and in the solid state. Our results showed the presence of a single transient species both in *n*-hexane and in nanocrystalline (NC) suspension that we hypothesize to be the triplet excited state of the 9-phenylfluorenyl product. UV-vis analysis of our solutions and NC suspensions pre and post laser flash photolysis strongly support the formation of the cyclized 9-phenylfluorenyl product, which also indicates that the photochemical mechanism could be the same in both media. The only difference we observed between the solution and solid state data was the decay lifetime for the transient species in NC suspension was much longer (47 μs) than the solution lifetime (1.3 μs).

The dissertation of Vanessa Marie Breslin is approved.

Harold G. Monbouquette

Heather D. Maynard

Miguel A. Garcia-Garibay, Committee Chair

University of California, Los Angeles

2018

To my family and friends for their unwavering support

TABLE OF CONTENTS

Abstract of the Dissertation.....ii

List of Schemes.....x

List of Figures.....xi

List of Tables.....xiv

List of Abbreviations.....xv

Acknowledgments.....xix

Vita.....xxii

Publications and Presentations.....xxiii

CHAPTER 1. Introduction: Organic Solid State Photochemistry and Nanocrystalline Suspensions.....1

1.1. Introduction.....2

1.2. Organic Solid State Photochemistry: Origins and the Topochemical Postulate.....3

1.3. Observing Reactive Intermediates in Crystals.....6

1.4. Aqueous Nanocrystalline Suspensions.....8

1.5. Photochromism in the Solid State.....11

1.6. Conclusions.....15

1.7. References.....16

CHAPTER 2. Transmission Spectroscopy and Kinetics in Crystalline Solids Using Aqueous Nanocrystalline Suspensions: The Spiropyran-Merocyanine Photochromic System.....21

2.1. Abstract.....22

2.2. Introduction.....23

2.3. Results and Discussion....26
2.4. Conclusions....35
2.5. Experimental....36
2.6. Appendix....47
2.7. References....65

CHAPTER 3. Nanosecond Laser Flash Photolysis of a 6-Nitroinolinospiropyran in Solution and in Nanocrystalline Suspension Under Single Excitation Conditions....68
3.1. Abstract....69
3.2. Introduction....69
3.3. General Methods....74
3.4. Results and Discussion....75
3.4.1. Sample Characterization and Flash Photolysis Setup....75
3.4.2. Solution Photochemical Studies....76
3.4.3. Mechanistic Analysis....80
3.4.4. Solid State Photochemical Studies....85
3.5. Conclusions....90
3.6. Experimental....91
3.7. Appendix....94
3.8. References....129

CHAPTER 4. Nanosecond Transient Absorption Spectroscopic Investigation of a 1,1'-Biphenyl-2-Phenyl Diazomethane in Solution and in the Solid State....134
4.1. Introduction....135

4.2. Results and Discussion.....137

4.3. Conclusions.....154

4.4. Experimental.....155

4.5. Appendix.....165

4.6. References.....184

List of Schemes

Scheme 1.2.1.....3

Scheme 1.2.2.....5

Scheme 1.3.1.....7

Scheme 1.5.1.....11

Scheme 1.5.2.....13

Scheme 1.5.3.....15

Scheme 2.2.1.....23

Scheme 2.2.2.....25

Scheme 2.3.1.....30

Scheme 3.2.1.....70

Scheme 3.4.3.1.....82

Scheme 4.1.1.....137

Scheme 4.2.1.....138

Scheme 4.2.2.....148

Scheme 4.2.3.....151

List of Figures

Figure 1.4.1. Differences between how bulk solids/large crystals and nanocrystals interact with incident laser beam.....9

Figure 1.4.2. Powder X-ray diffraction (PXRD) patterns of bulk crystals (bottom blue line) and nanocrystals (top red line) of **SP1**.....10

Figure 1.5.1. Representative examples of common photochromic molecules.....12

Figure 1.5.2. Representative structures for some of the first spiropyran and spirooxazine molecules reported to be photochromic in the solid state.....14

Figure 2.1.1. The spiropyran–*Z*-merocyanine–*E*-merocyanine photochromic reaction in the solid state under stead-state irradiation conditions along with corresponding UV-vis and fluorescence spectra.....22

Figure 2.3.1. Comparison of PXRD from nanocrystals (top, red) and bulk powders (middle, blue) with the one calculated from data available from the Cambridge Crystallographic Data Centre (bottom, green) for (a) **SP1** and (b) **SP5**. High quality nanocrystals were obtained in the case of **SP1–SP4** (Appendix 2.6.4), but only semicrystalline samples could be obtained in the case of **SP5**.....27

Figure 2.3.2. UV-vis absorption spectra showing the MC thermal decay for MC1 in (a) MeCN and (b) in NC suspension. Insets: pictures of the cuvettes before and after irradiation at 365 nm (see Appendix 2.6.3 for **SP1–SP5** absorption spectra and decay plots).....28

Figure 2.3.3. Thermal decay kinetic plots with trendline (red line) for **MC1** at 557 nm (a) in MeCN and (b) in NC suspension.....29

Figure 2.3.4. Fluorescence intensity at 614 nm vs. time with excitation at 530 nm for **SP1** (a) in MeCN with UV irradiation (365 nm) for 540 s and in the dark for 3000 s and (b) in NC

suspension upon UV irradiation (365 nm) for 780 s and in the dark after UV irradiation followed with white light irradiation. Note: in panel b, the *x*-axis scale changes between 0.8 and 5.3 x 10^3 s. 35

Figure 3.4.1.1. UV-vis absorption spectra of **SP1** in acetonitrile (blue) and in nanocrystalline (NC) suspension (red).....76

Figure 3.4.2.1. (a) Transient absorption spectrum for **SP1** at various time points in argon degassed acetonitrile along with the corresponding transient kinetic plots showing (b) a decay at 440 nm with the earliest portion of the decay shown in the inset, (c) a growth at 550 nm, and (d) a growth followed by a decay at 590 nm. Fit lines are shown in black.....78

Figure 3.4.2.2. (a) Transient absorption spectrum for **SP1** at various time points in air saturated acetonitrile along with the corresponding transient kinetic plots showing (b) a decay at 440 nm, (c) a growth at 550 nm, and (d) a decay at 590 nm. Fit lines are shown in black.....80

Figure 3.4.3.1. Calculated 0-0 transitions for the ***Z*-** and ***E*-MC** from $\mathbf{S_0} \rightarrow \mathbf{S_1}$ with transition energies provided in nm and eV following a procedure reported by Adamo and Jacquemin[55] using (TD)-CAM-B3LYP-(D3BJ)/6-311++G(d,p) IEFPCM-(CH_3CN).....84

Figure 3.4.4.1. Transient absorption spectrum for **SP1** at various time points in NC suspension. Red box: expansion of spectrum at longer times. Laser output (λ=355 nm, 36–40 mJ/pulse, 5–8 ns, 10 Hz).....87

Figure 3.4.4.2. Calculated energies for each geometry along the scanned coordinate based on the dihedral angle highlighted in green. Energies are relative to the optimized ***E*-MC** isomer (0 kcal mol^{-1}, θ_{dih} = 178°). The red plot points correspond to the structures shown, which are the optimized stationary points for the ***Z*-MC**, ***E*-MC**, and transition state structures. Calculations were done at the CAM-B3LYP-(D3BJ)/6-31+G(d,p) IEFPCM-(CH_3CN) level of theory.....89

Figure 3.4.4.3. Calculated UV-vis absorbance spectra (normalized) for selected merocyanine geometries from Figure 3.4.4.2. Spectra were predicted using the (TD)-CAM-B3LYP/6-311++G(d,p) method. The solid black line corresponds to the structure closest to the transition state between ***Z*-** and ***E*-MC**. The yellow, orange, and red solid lines correspond to ***Z*-**like **MC**s, and the green and blue dashed lines correspond to ***E*-**like **MC**s.....90

Figure 4.2.1. Variable temperature (VT) ^{1}H NMR spectra of Weinreb amide **11** in C_6D_6 collected at 298 K, 323 K, and 343 K.....139

Figure 4.2.2. Variable temperature (VT) ^{13}C NMR spectra of Weinreb amide **11** in C_6D_6 collected at 298 K and 343 K.....139

Figure 4.2.3. PXRD of the bulk powder for diaryldiazomethane **1** along with a microscope image of the dark pink powder.....140

Figure 4.2.4. UV-vis spectra for diaryldiazomethane **1** in NC suspension recorded every 5 min for 30 min.....141

Figure 4.2.5. ^{1}H NMR analysis for the photolysis of **1** in C_6D_6 before irradiation (0 min) and 2 min, 8 min, and 13 min post irradiation ($\lambda_{ex} > 290$ nm).....141

Figure 4.2.6. Time-dependent transient absorption spectrum for **1** at various time points in *n*-hexane solution collected between 0 and 1.4 μs.....143

Figure 4.2.7. UV-vis spectra for **1** pre (red line) and post (blue line) pulsed laser irradiation in *n*-hexane solution.....144

Figure 4.2.8. Transient decay at 370 nm for **1** measured in argon degassed *n*-hexane at 298 K. Fit line is shown in black.....144

Figure 4.2.9. Transient decay at 370 nm for **1** measured in air saturated *n*-hexane at 298 K. Fit line is shown in black.....145

Figure 4.2.10. Time-dependent transient absorption spectrum for **4** at various time points in *n*-hexane solution collected between 0 and 900 ns.....146

Figure 4.2.11. Transient decay at 370 nm for **4** measured in air saturated *n*-hexane at 298 K. Fit line is shown in black.....146

Figure 4.2.12. Transient decay at 370 nm for **4** measured in argon degassed *n*-hexane at 298 K. Fit line is shown in black.....147

Figure 4.2.13. Excitation (blue line) and emission spectra (red line) for **4** in methylcyclohexane at 77 K. Excitation spectrum was collected using an emission wavelength of 318 nm, and emission spectrum using an excitation wavelength of 266 nm.....150

Figure 4.2.14. Time-dependent transient absorption spectrum for **1** at various time points in NC suspension collected between 0 and 400 ns.....153

Figure 4.2.15. UV-vis spectra for **1** pre (red line) and post (blue line) pulsed laser irradiation in NC suspension. Picture: NC suspension of **1** with a green laser pointer shining through it to illustrate that suspended particles scatter light.....154

Figure 4.2.16. Transient decay at 370 nm for **1** in NC suspension at 298 K. Fit line is shown in black.....154

List of Tables

Table 2.2.1. Compound Information for **SP1–SP5**.....25

Table 2.3.1. Thermal Decay Lifetimes for **SP1–SP5**.....30

List of Abbreviations

ATR	attenuated total reflectance (infrared spectroscopy)
b	broad (NMR)
^{13}C NMR	carbon-13 nuclear magnetic resonance spectroscopy
ca.	approximately
calcd.	calculated
CCDC	Cambridge Crystallographic Data Centre
C_6D_6	deuterated benzene
$CDCl_3$	deuterated chloroform
CD_3CN	deuterated acetonitrile
$CHCl_3$	chloroform
cm	centimeter
cryst	crystal
CSD	crystal structure database
CTAB	cetyltrimethylammonium bromide (surfactant)
d	doublet (NMR)
DART	direct analysis in real time (mass spectrometry)
DCM	dichloromethane
dd	doublet of doublets (NMR)
DFT	density functional theory
DI	deionized
DLS	dynamic light scattering
DMF	dimethylformamide

dt	doublet of triplets (NMR)
eq.	equivalent
ESI	electrospray ionization
Et	ethyl
et al.	et alia (and others)
EtOH	ethanol
g	gram
h	hour
^{1}H NMR	proton nuclear magnetic resonance spectroscopy
HRMS	high resolution mass spectrometry
[1,5]-H shift	hydrogen atom rearrangement
Hz	hertz
i.e.	id est (namely)
IR	infrared (spectroscopy)
ISC	intersystem crossing
J	coupling constant (NMR)
K	Kelvin
kcal	kilocalories
λ_{ex}	excitation wavelength
λ_{max}	wavelength of maximum absorption
LFP	laser flash photolysis
m	multiplet (NMR)
M	molar

MC	merocyanine
MeCN	acetonitrile
MHz	megahertz
min	minute
mJ	millijoule
mL	milliliter
μL	microliter
μm	micrometer
mM	millimolar
mmol	millimole
mol	mole
m.p.	melting point
μs	microsecond
m/z	mass to charge ratio
NC	nanocrystalline or nanocrystals
nm	nanometer
Nd:YAG	neodymium-doped yttrium aluminum garnet (solid state laser)
ns	nanosecond
Ph	phenyl
pH	measure of acidity
PMMA	poly(methyl methacrylate)
ppm	parts per million
ps	picosecond

PSS	photostationary state
PXRD	powder X-ray diffraction
R	general alkyl group substituent
rt	room temperature
s	singlet (NMR)
s	second
S_0	singlet ground state
S_1	first excited singlet state
soln	solution
SP	spiropyran
t	triplet (NMR)
τ	lifetime
td	triplet of doublets (NMR)
θ_{dih}	dihedral angle
TOF	time of flight (mass spectrometry)
UV-vis	ultraviolet-visible spectroscopy
vs.	versus
VT	variable temperature
X	halogen substituent

Acknowledgments

My time at UCLA as a chemistry graduate student has been a rewarding experience that has been instrumental in making me the scientist I am today, and I am grateful to have been given the opportunity to conduct research at such a prestigious university. Furthermore, the individuals who I have had the fortune of getting to know throughout my scientific career are the ones truly responsible for my academic and research success, and I would like to thank each one in turn.

Firstly, I would like to thank my advisor Professor Miguel Garcia-Garibay for accepting me into his group and for introducing me to the exciting field of photochemistry. His enthusiasm for chemistry inspired me to learn as much as possible about my own research because you can never know too much. He also gave me the freedom to explore my ideas as well as the mentorship, guidance, and support I needed to become a successful, confident, and well-rounded scientist.

Next, I would like to thank my undergraduate research advisor Professor Adam Kiefer for being an incredible teacher and mentor. He taught me organic chemistry before I even took the class and also impressed upon me the value of learning from wrong answers and trying out ideas even if they might not work, which required great patience on his part. Without him, I would not have applied to graduate school and would not be where I am today.

I have been incredibly lucky to have forged many new relationships with some exceptionally talented people throughout my graduate career, many of whom I am grateful to call friends. Thank you to all of my current and former labmates for your support and friendship, especially Dr. Ira Staehle, Dr. Patrick Commins, Dr. Salvador Perez-Estrada, Dr. Xing Jiang, Dr. Geeta Vadehra, Dr. Tim Chung, Dr. Saori Shiraki, Jin Park, Morgan Howe, and Jordan Dotson. I

had the pleasure of mentoring Nicole Barbour, a phenomenal undergraduate student, for three years and would like to thank her for her hard work and dedication to the spiropyran project she helped me to complete. I would also like to thank Dr. Courtney Roberts and Dr. Samantha Paluck for being there whenever I needed advice or just wanted to talk, I truly cherish your friendship.

And last but certainly not least, I would like to thank my wonderful boyfriend Dave and my amazing family for their unconditional support and encouragement. They always believed that I could solve whatever problem I was facing in my research, and they helped keep me grounded when I needed it most. I couldn't have done this without them.

Associated Publications and Author Contributions

Chapter 2 is adapted with permission from the following publication: Breslin, V. M.; Garcia-Garibay, M. A. "Transmission Spectroscopy and Kinetics in Crystalline Solids Using Aqueous Nanocrystalline Suspensions: The Spiropyran-Merocyanine Photochromic System." *Cryst. Growth Des.* **2017**, *17*, 637–642. Copyright 2017 American Chemical Society (**DOI**: 10.1021/acs.cgd.6b01476). All authors were involved in the project development. I synthesized and characterized all compounds and performed all of the photochemical studies. Prof. Garcia-Garibay and I analyzed all of the data and contributed to writing and editing the manuscript and supporting information. This work was supported by National Science Foundation grant CHE1566041.

Chapter 3 is a manuscript that has been submitted for publication as: Breslin, V. M.; Barbour, N. A.; Dang, D.-K.; Lopez, S. A.; Garcia-Garibay, M. A. "Nanosecond Laser Flash Photolysis of a 6-Nitroindolinospiropyran in Solution and in Nanocrystalline Suspension Under Single Excitation Conditions" *Photochem. Photobiol. Sci.* **2018**. Prof. Garcia-Garibay and I were involved in the project development. I synthesized and characterized all compounds. N. A. Barbour and I performed all of the photochemical studies. Prof. Garcia-Garibay, N. A. Barbour, and I analyzed all of the photochemical data. Prof. Lopez and D.-K. Dang performed all of the computational studies and analyzed the associated data. All authors contributed to writing and editing the manuscript and supporting information. This work was supported by National Science Foundation grants CHE1566041 and TG-CHE170074.

VITA

B.S. Chemistry, Mercer University Minor in Biology with Honors, *magna cum laude*	May 2012
Graduate Researcher, University of California, Los Angeles Advisor: Miguel A. Garcia-Garibay, Ph.D	July 2013–2018
Graduate Teaching Fellow, University of California, Los Angeles	September 2012–2017
High School Nanoscience Program–Leader	January 2013–2018
NSF Research Experience for Undergraduates, University of Kansas Advisor: Paul R. Hanson, Ph.D	2011
Mercer on Mission, Mercer University Advisors: Adam M. Kiefer, Ph.D and Kevin Drace, Ph.D	2010
Undergraduate Researcher, Mercer University Advisor: Adam M. Kiefer, Ph.D	June 2009–2012
Mercer Undergraduate Biomedical Scholar Advisor: Adam M. Kiefer, Ph.D	2009

Publications and Presentations

Publications

1. Breslin, V. M.; Garcia-Garibay, M. A. "Nanosecond Transient Absorption Spectroscopic Investigation of a 1,1'-Biphenyl-2-Phenyl Diazomethane in Solution and in the Solid State." *Manuscript in preparation.*

2. Breslin, V. M.; Barbour, N. A.; Dang, D.-K.; Lopez, S. A.; Garcia-Garibay, M. A. "Nanosecond Laser Flash Photolysis of a 6-Nitroindolinospiropyran in Solution and in Nanocrystalline Suspension Under Single Excitation Conditions." *Submitted.*

3. Park, J. H.; Hughs, M.; Chung, T. S.; Ayitou, A. J.-L.; Breslin, V. M.; Garcia-Garibay, M. A. "Generation and Reactivity Studies of Diarylmethyl Radical Pairs in Crystalline Tetraarylacetones via Laser Flash Photolysis Using Nanocrystalline Suspensions." *J. Am. Chem. Soc.* **2017**, *139*, 13312–13317.

4. Chung, T. S.; Ayitou, A. J.-L.; Park, J. H.; Breslin, V. M.; Garcia-Garibay, M. A. "Photochemistry and Transmission Pump-Probe Spectroscopy of 2-Azidobiphenyls in Aqueous Nanocrystalline Suspensions: Simplified Kinetics in Crystalline Solids." *J. Phys. Chem. Lett.* **2017**, *8*, 1845–1850.

5. Breslin, V. M.; Garcia-Garibay, M. A. "Transmission Spectroscopy and Kinetics in Crystalline Solids Using Aqueous Nanocrystalline Suspensions: The Spiropyran-Merocyanine Photochromic System." *Cryst. Growth Des.* **2017**, *17*, 637–642.

Presentations

Photochemistry Gordon Research Conference, Bates College, ME, Summer 2017
"Analysis of a Photochromic Spiropyran in Solution and the Solid State Using Nanosecond Laser Flash Photolysis" (poster) Vanessa M. Breslin and Miguel A. Garcia-Garibay

International Symposium on Photochromism, Shanghai, China, Fall 2016
"Photochromism of Spiropyrans in Solution and in Nanocrystalline Suspension" (oral) Vanessa M. Breslin and Miguel A. Garcia-Garibay

Inter-American Photochemical Society Meeting, Santiago, Chile, Spring 2016
"Thermal Decay Kinetics of Photochromic Spiropyrans in Solution and in Nanocrystalline Suspensions" (poster) Vanessa M. Breslin and Miguel A. Garcia-Garibay

Photocatalysis, Photoconversion, and Photoelectrochemistry: Fundamentals, Techniques, and Applications for the 21st Century, Santiago, Chile, Spring 2016 (NSF sponsored workshop)
"Photocatalysis Involving Photocages" (oral) Vanessa M. Breslin and Ana L. Moore

American Chemical Society National Conference, Boston, MA, Fall 2015
"Solution and Solid State Photochromism of Spiropyrans" (oral) Vanessa M. Breslin and Miguel A. Garcia-Garibay

CHAPTER 1

Introduction:

Organic Solid State Photochemistry and Nanocrystalline Suspensions

1.1 Introduction

Organic solid state photochemistry is a field dedicated to studying the chemical transformations of organic compounds induced by light in the solid state. This requires an understanding of the specific spatial orientation of not only individual atoms within a molecule, but also individual molecules within the solid's framework. Prior to the development of single crystal X-ray diffraction, little was known about the structures of crystals, which hindered the progress in understanding how molecular structure influences solid state photochemical reactivity. Although the development of X-ray diffraction had a profound impact on the field of organic solid state photochemistry as will be discussed shortly, other challenges, such as homogeneous excitation of crystals and their spectroscopic analysis, remained. In Sections 1.3 and 1.4 of this introductory chapter, the optical challenges associated with studying solid state photochemical reactions spectroscopically will be examined as well as how nanocrystalline suspensions can be used to overcome them.

A design principle central to organic solid state photochemistry is that molecules are locked in place within the crystalline lattice, which restricts their conformational degrees of freedom and hence the number of available reaction pathways. This means that we can use the rigidity of the crystal lattice to control chemical reactivity. Although our group has previously focused on designing stereospecific photochemical reactions that rely on the crystalline environment only allowing very minimal molecular motion from reactant to product,[1–9] I wanted to investigate whether the crystalline lattice could tolerate a greater degree of molecular motion in the form of a reversible photochemical reaction. The work described in this dissertation expands our understanding of organic solid state photochemical reactions through studying the kinetics and crystal lattice tolerance to molecular motion of both the spiropyran-merocyanine

photochromic system and a 1,1'-biphenyl-2-phenyl carbene. The purpose of this introductory chapter is to provide an overview of the history of organic solid state photochemistry by discussing the discovery of the first reaction in this field, the advancements that led to the foundational concepts that define the field today, and the complications involved with observing reactive intermediates and measuring kinetics in the solid state along with the use of nanocrystalline suspensions in overcoming them. The subject of photochromism will also be discussed in order to give context to Chapters 2 and 3.

1.2 Organic Solid State Photochemistry: Origins and the Topochemical Postulate

The discovery of the first organic solid state photochemical reaction in 1834 by Hermann Trommsdorff marked the beginning of the field that inspired many, including our research group, to endeavor to understand the factors that control chemical reactivity in the solid state.[10,11] Trommsdorff observed that crystals of α-santonin turned yellow and burst when exposed to sunlight, and it was not until 1988 that the X-ray crystal structure of the photoproduct was determined to be an α-santonin dimer (Scheme 1.2.1).[12] Prior to the crystal structure of the α-santonin dimer being identified, Matsuura et al. studied the crystalline state photochemical reaction of α-santonin, proposed the dimer as the photoproduct, and suggested a mechanism for the photodimerization.[13] The crystal structure of the dimer species showed that α-santonin molecules crystallize in pairs with a distance of 4.54 Å between molecules and in an orientation that favors photocyclodimerization.[12]

Scheme 1.2.1

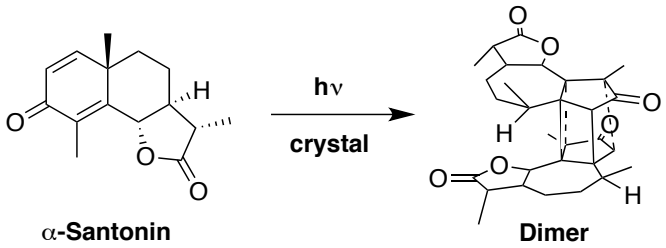

However, before X-ray crystallography became widely available, solid state photochemical reactions were studied and rationalized through product analysis, which involves dissolving the crystals in solvent and determining the molecular structure by other spectroscopic methods, such as nuclear magnetic resonance (NMR). One of the greatest advantages in studying solid state reactions is knowing the precise arrangement of atoms in space, and so dissolving a crystal in solvent results in the loss of extremely important spatial information encoded in the lattice that would enable the rationalization of chemical reactivity to crystal packing. Performing reactions in crystals has led to the observation that unique and otherwise unattainable products can be formed.[8,14–18] First suggested in 1918 by Kohlshutter[19] and experimentally confirmed by Cohen and Schmidt[20–23] in 1964 is the cornerstone idea of solid state organic photochemistry: the topochemical postulate.

Schmidt and Cohen studied the solid state [2+2] photodimerization reaction of *trans*-cinnamic acid (Scheme 1.2.2), which was known to crystallize in three different polymorphs (α, β, and γ).[20–22] Using X-ray crystallography, the α, β, and γ polymorphs were shown to differ in the distances as well as the molecular positions between nearest neighbors. In spite of these differences, the three polymorphs all packed in one-dimensional stacks with adjacent stacks being paired by hydrogen bonds. In the α-polymorph, molecules between adjacent stacks had intermolecular double bond distances of 4.2 Å and distances of 5.5 Å between molecules in the same stack. Upon UV light irradiation, the centrosymmetric [2+2] cycloadduct, α-truxillic acid, is formed between closest neighbors. Molecules of *trans*-cinnamic acid in the β-polymorph have close intermolecular double distances of 4.1 Å between neighbors with UV irradiation resulting the formation of β-truxillic acid, which contained mirror symmetry. Lastly, in the γ-polymorph, neighboring molecules are 4.8 Å apart and no reaction was observed, suggesting that 4.8 Å is too

great of a distance for dimerization to occur. This work clearly demonstrated that the way molecules pack in crystals directly affects their photochemical reactivity and thus helped to define the topochemical postulate, which consists of two key points: (1) solid state reactions occur with a minimal amount of molecular motion, and (2) molecular geometry and crystal packing have a greater impact on the photochemical reaction than does the intrinsic reactivity of the molecule.[24,25] The field of organic solid state photochemistry has built upon the foundation that the topochemical postulate provided and has led to the limitations of this idea being tested, with a few key studies more clearly describing what can or cannot occur in the crystalline environment.[26–30]

Scheme 1.2.2

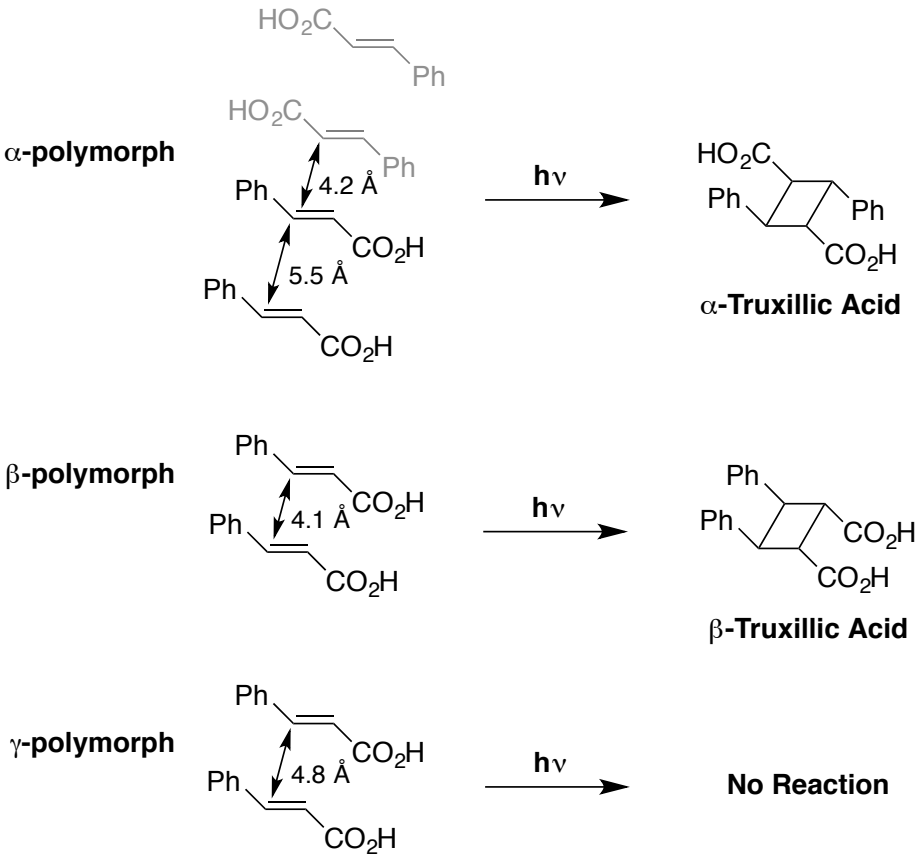

1.3 Observing Reactive Intermediates in Crystals

Understanding how a chemical reaction proceeds from reactant to product is a very important step in learning how to control chemical reactivity and design more efficient photoactive molecules. In solution state photochemistry, transmission spectroscopic techniques are used to gain insight into the electronic structure of reactive intermediates (i.e. biradicals, radical pairs, zwitterions, charge-transfer complexes, singlet/triplet states, etc.) as well as the kinetics of the associated photoprocesses (i.e. intersystem crossing, fluorescence, isomerization, bond cleavages, bond formations, etc.). One of the most commonly used methods for observing reactive intermediates in solution is transient absorption spectroscopy. Specifically, this method uses laser flash photolysis to generate and detect excited state species, which Manfred Eigen, George Porter, and Ronald Norrish won the 1967 Nobel Prize in chemistry for their work in developing instrumentation to study chemical reactions in the microsecond time scale.[31] As the name suggests, laser flash photolysis is a pump-probe spectroscopic technique in which a short laser pulse (nanosecond, picosecond, or femtosecond pulse width) is used to excite the molecules in a sample and another delayed pulse from a different source (commonly a continuous wave xenon lamp) is used to probe the now excited sample. This technique allows us to monitor how the absorption spectrum of the sample changes over time, and thus measure the lifetimes of excited state species. Being able to directly detect transient species and measure their lifetimes means that we can better understand the mechanisms of photochemical reactions.

Using laser flash photolysis to observe transients in crystals or bulk powders is much more difficult due to optical effects such as dichroism, birefringence, and light scattering that prevent the transmission of light through the sample and thus the detection of any meaningful signal.[32,33] Another issue with studying photochemical reactions in crystals is that excitation can

produce excitons that can then transfer energy to surrounding molecules in the crystal and induce other events to occur that will complicate the interpretation of any collected data. In spite of these complications, McBride and coworkers were able to detect free radicals in crystals for several diacyl peroxide and azoalkane species at cryogenic temperatures.[34] They used electron paramagnetic resonance (EPR) spectroscopy, X-ray diffraction, and infrared (IR) spectroscopy to detect the methyl-benzoyloxyl radical pairs initially formed upon photolysis of acetyl benzoyl peroxide (Scheme 1.3.1),[35] with continued photolysis resulting in methy-phenyl radical pairs being generated. The sharpness of their EPR spectra indicates that a high degree of structural uniformity exists among the radical pairs, otherwise a spectrum with broader peaks would have been observed if the radical pair structures varied throughout the sample. However, this technique is limited to studying photochemical reactions that produce radicals as intermediates.

Scheme 1.3.1

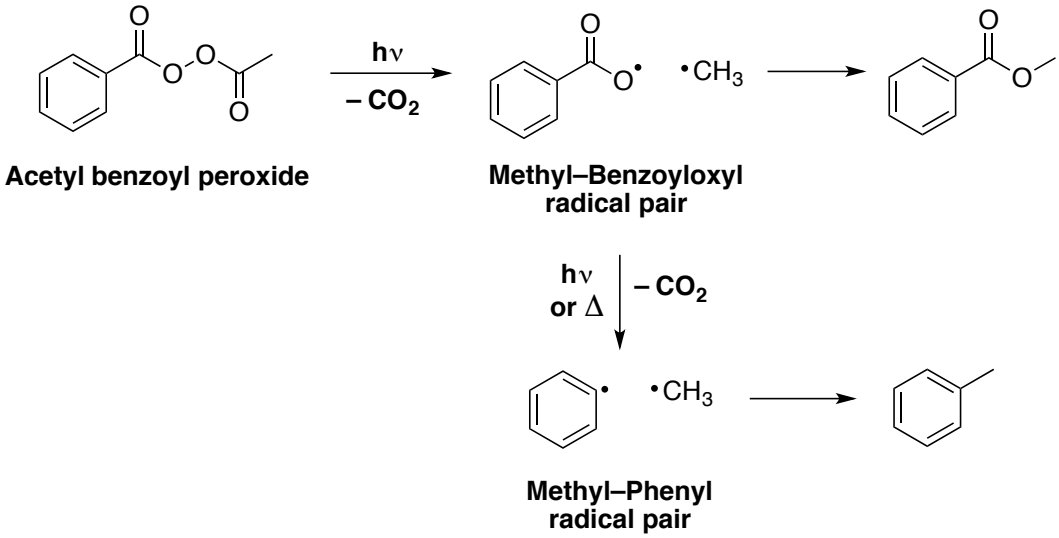

Another technique that can be used to study transient species of opaque materials is diffuse reflectance flash photolysis spectroscopy. Francis Wilkinson[36,37] has pioneered the development of this method in order to study the kinetics of optically dense and opaque samples including organic microcrystals,[38,39] semiconductor powders,[40,41] and dyes chemically bound to a

polymer substrate.[42] Although Wilkinson has reported that data obtained using his diffuse reflectance flash photolysis setup for studying solids is comparable in terms of its signal-to-noise ratio to that obtained in solution using transmission flash photolysis, he does mention that excitation light penetration depth into solids results in the production of very small concentrations of transient species that are confined mostly to the surface,[37] and so no information can be gathered on the reactivity of molecules within the bulk of the solid or crystal. These examples demonstrate the technical difficulty associated with studying photochemical reactions in the solid state, and so there exists a general need for the development of additional methods of observing excited state species and measuring their kinetics.

1.4 Aqueous Nanocrystalline Suspensions

As mentioned in the previous section, optical effects such as light scattering, birefringence, and dichroism make studying reactions in crystals quite difficult. However, these effects are dependent on the size of the crystal or solid particle, with larger particles resulting in more of the incident light being scattered, refracted, or more or less strongly absorbed based on polarization direction. Another issue that arises with larger crystals and bulk solids is that laser excitation can produce a high density of excited state species that can then interact with each other via different energy transfer mechanisms, thus resulting in more complicated kinetic data that is difficult to interpret. We have proposed that one way to address this problem is to use nanocrystalline (NC) solids suspended in a nondissolving fluid such as water.[43–50] Aqueous NC suspensions with nanocrystal sizes below 500 nm can be prepared using the reprecipitation, or solvent shift method, which was first reported by Kasai et al.[51] Crystals that are tens to hundreds of nanometers in size approach the size of supramolecular complexes such that it should be possible to excite them in a homogeneous manner and reduce complications from mulitphotonic

processes, light scattering, and birefringence (Figure 1.4.1). Furthermore, the loading of NC suspensions can be easily adjusted so that it should be possible to use the same transmission spectroscopic methods that are commonly used for solution state photochemical studies.

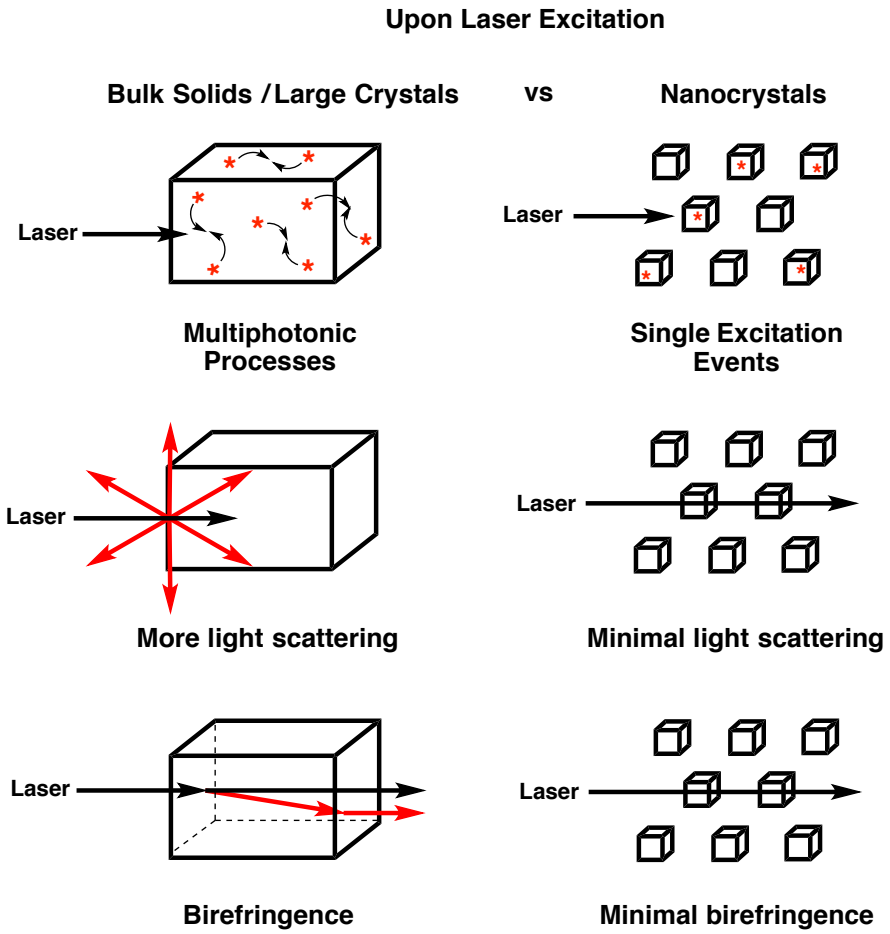

Figure 1.4.1. Differences between how bulk solids/large crystals and nanocrystals interact with incident laser beam.

One common issue found when making NC suspensions is that the conditions for making stable suspensions can vary significantly from compound to compound. The experimental variable that usually requires the most optimization is whether or not a surfactant, such as cetyltrimethylammonium bromide (CTAB) or sodium dodecyl sulfate (SDS), is needed and in what concentration to prevent the nanocrystals from aggregating and precipitating out of the

suspension. Once conditions for making stable NC suspensions are found, the crystallinity and size of the nanocrystals can be characterized using powder X-ray diffraction (PXRD) and dynamic light scattering (DLS), respectively. Sharp peaks like the ones shown in the diffractograms in Figure 1.4.2 for a spiropyran (**SP1**) indicate that both the bulk crystals (bottom blue line) and the nanocrystals (top red line) are indeed crystalline, and the similar peak positions between the bulk crystals and the nanocrystals suggest that the two samples belong to the same crystal polymorph. This allows us to draw conclusions on the solid state photochemical reactivity in nanocrystals based on the single crystal packing information determined for the bulk crystals.

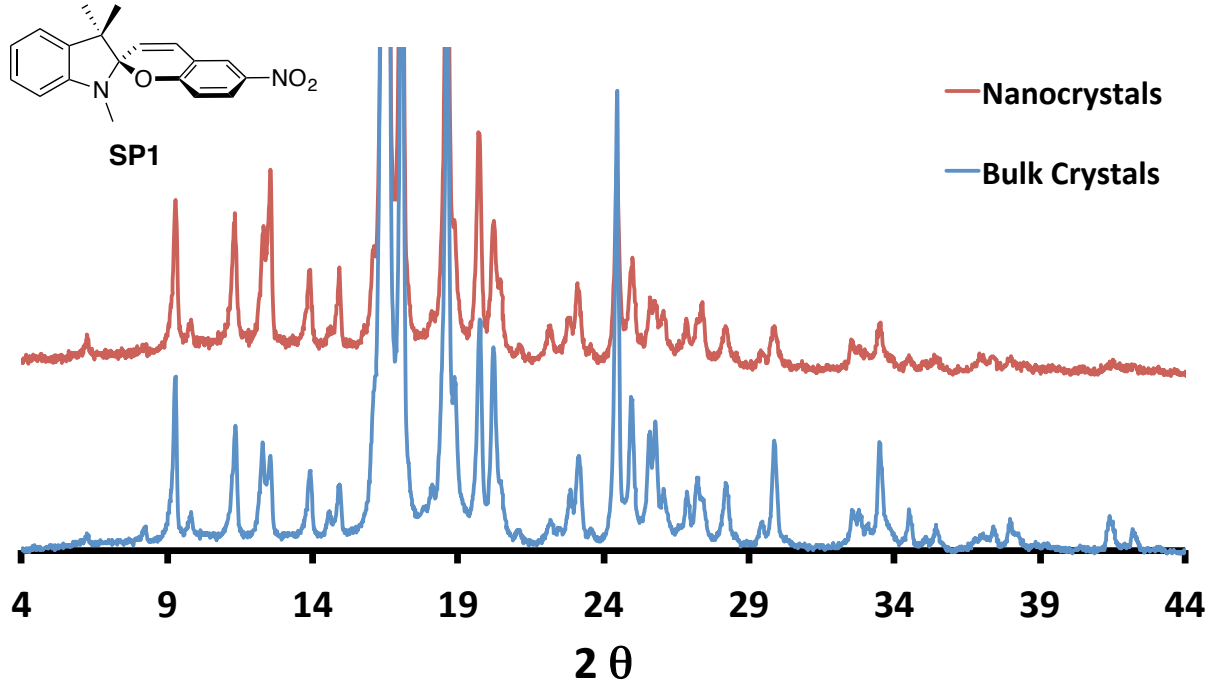

Figure 1.4.2. Powder X-ray diffraction (PXRD) patterns of bulk crystals (bottom blue line) and nanocrystals (top red line) of **SP1**.

Similarly, DLS analysis of the NC suspensions provides information on the average particle size as well as the size range of the nanocrystals in order to verify that they are of suitable size to minimize the optical effects shown in Figure 1.4.1 so as to study their

photochemistry via transmission spectroscopy (i.e. UV-vis, fluorescence, and transient absorption spectroscopies). Using this methodology to study the absolute kinetics in solid state photochemical reactions, we have developed a flow system in which NC suspensions are flowed continuously, but only once, through a quartz cell to ensure that pristine nanocrystals are available for each laser excitation pulse. Chapters 2, 3, and 4 of this dissertation will further discuss how aqueous NC suspensions were used to gain insight into the solid state photochemical reaction mechanisms and kinetics of several 6-nitroindolinospiropyrans and a 1,1'-biphenyl-2-phenyl carbene.

1.5 Photochromism in the Solid State

Scheme 1.5.1

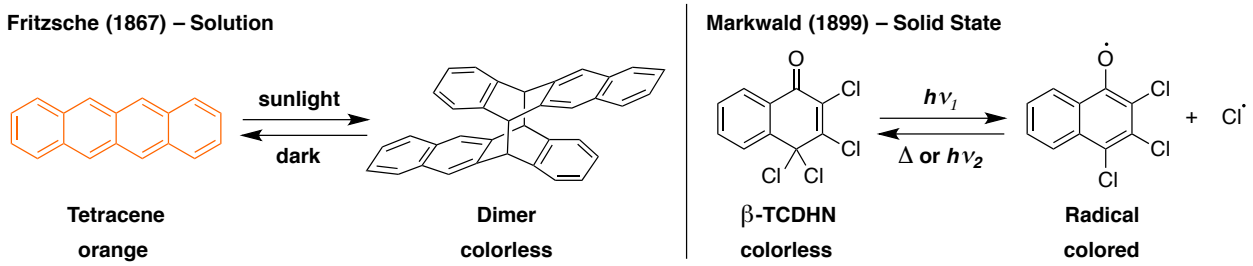

In 1867, Fritzsche first reported that an orange solution of tetracene became colorless when exposed to sunlight and then returned to orange overnight.[52] This color-changing phenomenon was a result of the photodimerization of tetracene molecules to generate the higher energy dimer product (colorless), which then regenerates tetracene (orange) in the dark (Scheme 1.5.1). The photodimerization of tetracene is a unique reaction for two reasons: (1) the reaction proceeds with a visible color change, and (2) the reaction is reversible. Since Fritzsche's initial report on tetracene, others soon found that a number of other compounds had similar color-changing behavior. In particular, Markwald discovered in 1899 that 2,3,4,4-

tetrachloronaphthalen-1-(4*H*)-one (β-TCDHN) reversibly changed color in the solid state (Scheme 1.5.1).[53,54] Thinking that this was purely a physical phenomenon, Markwald named it phototropy.[54] However, this term implies that what Fritzsche, Markwald, and others observed was somehow related to the biological term phototropism, which refers to how a plant or other organism orients itself either toward or away from a light source. Therefore, in 1950 Hirshberg coined the term photochromism to describe these reversible reactions and to avoid confusion.[55] Specifically, photochromism is defined as a reversible transformation between two distinct species have different absorption spectra that is induced in one or both directions by electromagnetic radiation.[56,57] Since Fritzsche's and Markwald's discoveries, a variety of molecular systems have been found to be photochromic in solution and the solid state, such as diarylethenes, spiropyrans, azobenzenes, fulgides, and *N*-salicylideneanilines (Schiff bases) to name a few (Figure 1.5.1). These compounds are of great interest to researchers because of their applications as optical memories and switches,[58–60] with one of the first commercial products being ophthalmic lenses, which used an indolinospironaphthoxazine as the photochromic component (Scheme 1.5.2).[61]

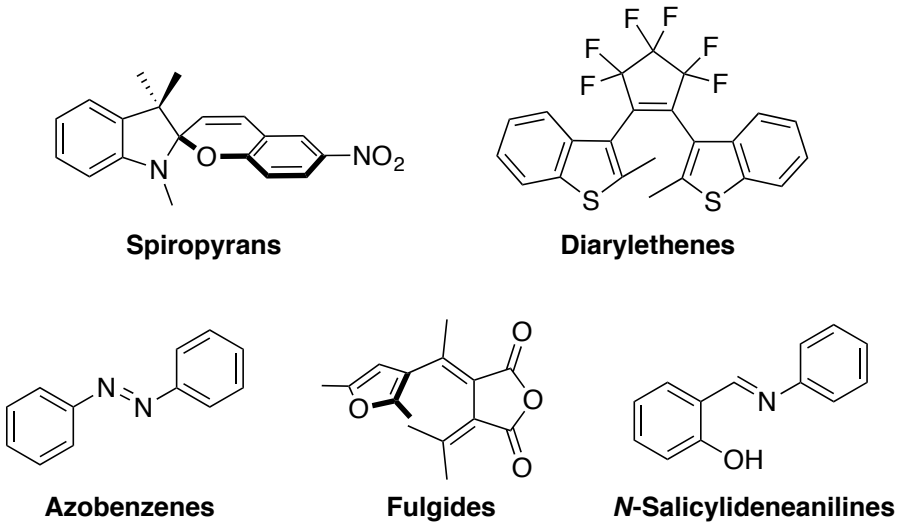

Figure 1.5.1. Representative examples of common photochromic molecules.

Scheme 1.5.2

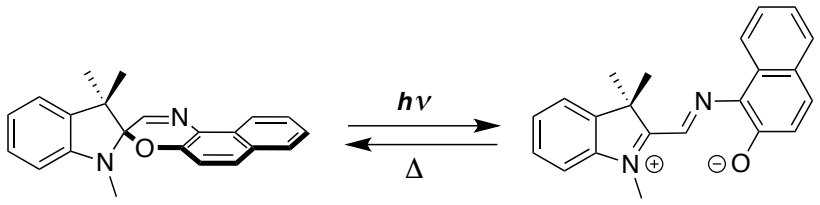

Spironaphthoxazine

colorless

Oxazine Derived Merocyanine

colored

Initially, it was thought that crystalline state photochromism was unusual due to the idea set forth in the topochemical postulate that solid state reactions occur with a minimal amount of molecular motion.[62,63] Thus, out of the many known photochromic systems in solution, only a small subset, such as diarylethenes,[63–67] N-salicylideneanilines,[68,69] and paracyclophanes,[70] were originally found to be photochromic in the solid state presumably because of the small structural differences between the pre- and post irradiated forms. On the other hand, the large geometrical changes required for spiropyrans, spiroxazines, and azobenzenes to isomerize were considered too great to be tolerated by the crystal lattice and therefore little effort was invested in studying these compounds in the solid state.[71] However, Masuhara and coworkers,[72] Bénard and Yu,[73,74] and Eichen and coworkers[75] were not deterred by these notions and each reported on the solid state photochromism of a neutral spiropyran induced by laser excitation, a cationic spiropyran and a spirooxazine under steady-state irradiation, and a neutral spiropyran under steady-state irradiation, respectively (Figure 1.5.2). A common idea expressed in each article was that the crystal lattice appears to have enough free volume between adjacent molecules to allow the spiropyrans and spirooxazines to ring-open and at least partially isomerize to a more planar merocyanine structure. It then follows that although crystals are very ordered and rigid, the molecules they are comprised of cannot be regarded as static and immobile, but rather as free to move within the cavities they occupy in the crystal. The idea that crystals can have varying

degrees of flexibility, such that molecules can twist, rotate, etc., was a key motivational factor in choosing to study the solid state photochemical reactivity of spiropyrans as part of my dissertation research.

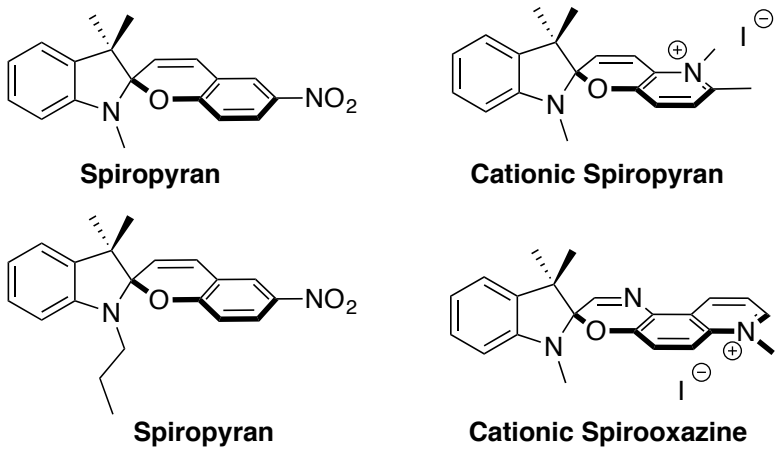

Figure 1.5.2. Representative structures for some of the first spiropyran and spirooxazine molecules reported to be photochromic in the solid state.

In order to fully realize the potential of photochromic molecules for the development of optically switchable devices, understanding the kinetics and mechanism of both the forward and reverse reactions in a variety of media (i.e. solution, polymer matrices, crystals) is crucial. Although a wealth of information exists on the solution state kinetics for many different photochromic molecules, the same cannot be said of the solid state, most likely because of the difficulty involved in overcoming the optical complications associated with studying solids spectroscopically as was discussed in Section 1.4. In particular, a systematic comparison of the kinetics of these photochromic reactions in solution and in crystals would allow for both substituent and packing effects to be documented, which would greatly enhance our understanding of how photochromic molecules behave in the solid state. As a result, Chapters 2 and 3 of this dissertation are dedicated to studying the solution and solid state kinetics of the

spiropyran-merocyanine photochromic system with transmission spectroscopic methods (Scheme 1.5.3).

Scheme 1.5.3

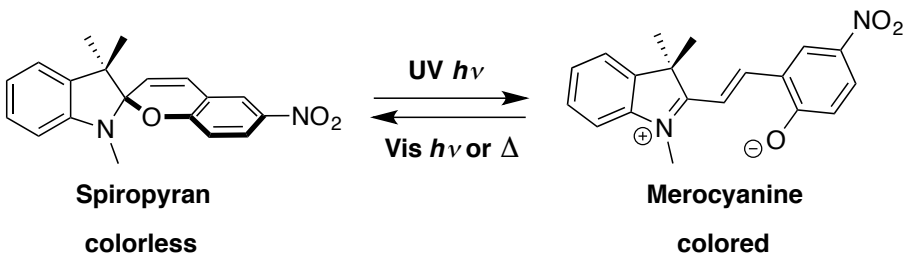

1.6 Conclusions

Studying the photochemical mechanism and kinetics of molecules in the solid state spectroscopically is very challenging due to optical complications, such as dichroism, birefringence, and light scattering, that prevent the transmission of light through large crystals and bulk powders. However, these effects are size dependent and so can be overcome by using dilute aqueous suspensions of nanocrystals, which then allows common transmission spectroscopic methods to be utilized for detecting reactive intermediates and ultimately leading to a better understanding of chemical reactivity in the solid state. The work described in this dissertation expands our understanding of organic solid state photochemical reactions through studying the mechanism and kinetics of both the spiropyran-merocyanine photochromic system and a 1,1'-biphenyl-2-phenyl carbene in nanocrystalline suspensions. Additionally, we wanted to explore the nature of the topochemical postulate on the photochemical reactions of spiropyrans and diarylcarbenes in order to test whether the crystalline lattice could tolerate the molecular motion required for the detection of photoproducts.

1.7 References

1. Chung, T. S.; Xue, Y.; Caranza, A.; Garcia-Garibay, M. A. *Photochem. Photobiol. Sci.* **2017**, *16*, 1458–1463.

2. Chung, T. S.; Lopez, S. A.; Houk, K. N.; Garcia-Garibay, M. A. *Org. Lett.* **2015**, *17*, 4568–4571.

3. Hernández-Linares, M. G.; Guerrero-Luna, G.; Pérez-Estrada, S.; Ellison, M.; Ortin, M.-M.; Garcia-Garibay, M. A. *J. Am. Chem. Soc.* **2015**, *137*, 1679–1684.

4. Shiraki, S.; Natarajan, A.; Garcia-Garibay, M. A. *Photochem. Photobiol. Sci.* **2011**, *10*, 1480–1487.

5. Resendiz, M. J. E.; Natarajan, A.; Garcia-Garibay, M. A. *Chem. Commun.* **2008**, 193–195.

6. Natarajan, A.; Ng, D.; Yang, Z.; Garcia-Garibay, M. A. *Angew. Chem. Int. Ed.* **2007**, *46*, 6485–6487.

7. Mortko, C. J.; Garcia-Garibay, M. A. *J. Am. Chem. Soc.* **2005**, *127*, 7994–7995.

8. Ng, D.; Yang, Z.; Garcia-Garibay, M. A. *Org. Lett.* **2004**, *6*, 645–647.

9. Ellison, M. E.; Ng, D.; Dang, H.; Garcia-Garibay, M. A. *Org. Lett.* **2003**, *5*, 2531–2534.

10. Trommsdorff, H. *Ann. Chem. Pharm.* **1834**, *11*, 190–208.

11. Roth, H. D. *Angew. Chem. Int. Ed.* **1989**, *28*, 1193–1207.

12. Reisch, J.; Henkel, G.; Topaloglu, Y.; Simon, G. *Pharmazie* **1988**, *43*, 15–17.

13. Matsuura, T.; Sata, Y.; Ogura, K.; Mori, M. *Tet. Lett.* **1968**, *9*, 4627–4630.

14. Campos, L. M.; Dang, H.; Ng, D.; Yang, Z.; Martinez, H. L.; Garcia-Garibay, M. A. *J. Org. Chem.* **2002**, *67*, 3749–3754.

15. Sharma, C. V. K.; Panneerselvam, K.; Shimoni, L.; Katz, H.; Carrell, H. L.; Desiraju, G. R. *Chem. Mater*. **1994**, *6*, 1282–1292.

16. Kuzmanich, G.; Gard, M. N.; Garcia-Garibay, M. A. *J. Am. Chem. Soc.* **2009**, *131*, 11606–11614.

17. Chung, J. W.; You, Y.; Huh, H. S.; An, B.-K.; Yoon, S.-J.; Kim, S. H.; Lee, S. W.; Park, S. Y. *J. Am. Chem. Soc*. **2009**, *131*, 8163–8172.

18. Odani, T.; Matsumoto, A. *Cryst. Eng. Comm*. **2002**, *4*, 467–471.

19. Kohlshutter, H. W. *Anorg. Allg. Chem.* **1918**, *105*, 121.

20. Cohen, M. D.; Schmidt, G. M. J. *J. Chem. Soc*. **1964**, 1996–2000.

21. Cohen, M. D.; Schmidt, G. M. J.; Sonntag, F. I. *J. Chem. Soc.* **1964**, 2000–2013.

22. Schmidt, G. M. J. *J. Chem. Soc.* **1964**, 2014–2021.

23. Schmidt, G. M. J. in *Reactivity of the Photoexcited Organic Molecule*. Ginsburg, D., Ed.; Wiley Interscience: New York, 1967, p 227.

24. Cohen, M. D. *Angew. Chem. Int. Ed*. **1975**, *14*, 386–393.

25. Schmidt, G. M. J. *Pure Appl. Chem*. **1971**, *27*, 647–678.

26. Scheffer, J. R.; Scott, C. *Science*, **2001**, *291*, 1712–1713.

27. Gnanaguru, K.; Ramasubbu, N.; Venkatesan, K.; Ramamurthy, V. *J. Photochem.* **1984**, *27*, 355–362.

28. Ramasubbu, N.; Guru Row, N. T.; Venkatesan, K.; Ramamurthy, V.; Ramachandra Rao, C. N. *J. Chem. Soc. Chem. Commun*. **1982**, 178–179.

29. Ramasubbu, N.; Gnanaguru, K.; Venkatesan, K.; Ramamurthy, V. *Can. J. Chem*. **1982**, *60*, 2159–2161.

30. Gudmundsdottir, A. D.; Lewis, T. J.; Randall, L. H.; Scheffer, J. R.; Rettig, S. J.; Trotter, J.; Wu, C.-H. *J. Am. Chem. Soc*. **1996**, *118*, 6167–6184.

31. Vullev, V. I.; Jones II, G. *J. Applied. Sci.* **2005**, *5*, 517–526.

32. Wood, E. A. *Crystals and Light: An Introduction to Optical Crystallography, 2nd Ed.*; Dover Publications: New York, 1977.

33. Swenbergy, C. E.; Gaecintov, N. E. in *Organic Molecular Photophysics*, Vol. 1, Ch. 10, J. B. Birks, Ed., John Wiley & Sons, London, 1973.

34. McBride, J. M. *Acc. Chem. Res.* **1983**, *16*, 304–312.

35. Karch, N. J.; Koh, E. T.; Whitsel, B. L.; McBride, J. M. *J. Am. Chem. Soc.* **1975**, *97*, 6729–6743.

36. Kessler, R. W.; Wilkinson, F. *J. Chem. Soc., Faraday Trans. 1* **1981**, *77*, 309–320.

37. Wilkinson, F. *J. Chem. Soc., Faraday Trans. 2* **1986**, *82*, 2073–2081.

38. Wilkinson, F.; Willsher, C. J. *Chem. Phys. Lett.* **1984**, *104*, 272–276.

39. Wilkinson, F.; Willsher, C. J. *Appl. Spectrosc.* **1984**, *38*, 897–901.

40. Wilkinson, F.; Willsher, C. J. *J. Chem. Soc., Chem. Commun.* **1985**, 142–143.

41. Pouliquen, J.; Fichou, D.; Valat, P.; Kossanyi, J.; Wilkinson, F.; Willsher, C. J. *J. Photochem.* **1986**, *35*, 381–388.

42. Wilkinson, F.; Willsher, C. J.; Pritchard, R. B. *Eur. Polym. J.* **1985**, *21*, 333–341.

43. Chin, K. K.; Natarajan, A.; Gard, M. N.; Campos, L. M.; Shepard, H.; Johansson, E.; Garcia-Garibay, M. A. *Chem. Commun.* **2007**, 4266–4268.

44. Kuzmanich, G.; Simoncelli, S.; Gard, M. N.; Spänig, F.; Henderson, B. L.; Guldi, D. M.; Garcia-Garibay, M. A. *J. Am. Chem. Soc.* **2011**, *133*, 17296−17306.

45. Kuzmanich, G.; Vogelsberg, C. S.; Maverick, E. F.; Netto-Ferreira, J. C.; Scaiano, J. C.; Garcia-Garibay, M. A. *J. Am. Chem. Soc.* **2012**, *134*, 1115−1123.

46. Doan, S. C.; Kuzmanich, G.; Gard, M. N.; Garcia-Garibay, M. A.; Schwartz, B. J. *J. Phys. Chem. Lett.* **2012**, *3*, 81–86.

47. Ayitou, A. J.-L.; Flynn, K.; Jockusch, S.; Khan, S. I.; Garcia-Garibay, M. A. *J. Am. Chem. Soc.* **2016**, *138*, 2644−2648.

48. Breslin, V. M.; Garcia-Garibay, M. A. *Cryst. Growth Des.* **2017**, *17*, 637–642.

49. Chung, T. S.; Park. J. H.; Garcia-Garibay, M. A. *J. Org. Chem.* **2017**, *82*, 12128–12133.

50. Park, J. H.; Hughs, M.; Chung, T. S.; Ayitou, A. J.-L.; Breslin, V. M.; Garcia-Garibay, M. A. *J. Am. Chem. Soc.* **2017**, *139*, 13312–13317.

51. Kasai, H.; Nalwa, H. S.; Oikawa, H.; Okada, S.; Matsuda, H.; Minami, N.; Kakuta, A.; Ono, K.; Mukoh, A.; Nakanishi, H. *Jpn. J. Appl. Phys.* **1992**, *31*, L1132−L1134.

52. Fritzsche, J. *Compt. Rend. Acad. Sci.* **1867**, *69*, 1035–1037.

53. Markwald, W. *Z. Physik. Chem.* **1899**, *30*, 140–145.

54. Bouas-Laurent, H.; Dürr, H. *Pure Appl. Chem.* **2001**, *73*, 639–665.

55. Hirshberg, Y. *Compt. Rend. Acad. Sci.* **1950**, *231*, 903–904.

56. Irie, M. *Chem. Rev.* **2000**, *100*, 1683–1684.

57. Irie, M.; Yokoyama, Y.; Seki, T.; Eds. *New Frontiers in Photochromism*; Springer: Tokyo, 2013.

58. Irie, M. *Chem. Rev.* **2000**, *100*, 1685–1716.

59. Yokoyama, Y. *Chem. Rev.* **2000**, *100*, 1717–1739.

60. Berkovic, G.; Krongauz, V.; Weiss, V. *Chem. Rev.* **2000**, *100*, 1741–1754.

61. Crano, J. C.; Flood, T.; Knowles, D.; Kumar, A.; Van Gemert, B. *Pure Appl. Chem.* **1996**, *68*, 1395–1398.

62. Scheffer, J. R.; Pokkuluri, P. R. In *Photochemistry in Organized & Constrained Media*; Ramamurthy, V., Ed.; VCH Publ.: New York, 1990; p 185.

63. Kobatake, S.; Yamada, T.; Uchida, K.; Kato, N.; Irie, M. *J. Am. Chem. Soc.* **1999**, *121*,

2380–2386.

64. Irie, M.; Uchida, K. *Bull. Chem. Soc. Jpn.* **1998**, *71*, 985–996.

65. Irie, M.; Uchida, K.; Eriguchi, T.; Tsuzuki, H. *Chem. Lett.* **1995**, *24*, 899–900.

66. Irie, M. *Pure Appl. Chem.* **1996**, *68*, 1367–1371.

67. Miyasaka, H.; Nobuto, T.; Itaya, A.; Tamai, N.; Irie, M. *Chem. Phys. Lett.* **1997**, *269*, 281–285.

68. Hadjoudis, E.; Vittorakis, M.; Moustakali-Mavridis, I. *Tetrahedron* **1987**, *43*, 1345–1360.

69. Hadjoudis, E. *Mol. Eng.* **1995**, *5*, 301–337.

70. Golden, J. H. *J. Chem. Soc.* **1961**, 3741–3748.

71. Kobatake, S.; Irie, M. *Chem. Lett.* **2004**, *33*, 904–905.

72. Suzuki, M.; Asahi, T.; Masuhara, H. *Mol. Cryst. Liq. Cryst.* **2000**, *345*, 51–56.

73. Bénard, S.; Yu, P. *Chem. Commun.* **2000**, 65–66.

74. Bénard, S.; Yu, P. *Adv. Mater.* **2000**, *12*, 48–50.

75. Godsi, O.; Peskin, U.; Kapon, M.; Natan, E.; Eichen, Y. *Chem. Commun.* **2001**, 2132–2133.

CHAPTER 2

Transmission Spectroscopy and Kinetics in Crystalline Solids Using Aqueous Nanocrystalline Suspensions: The Spiropyran-Merocyanine Photochromic System

2.1 Abstract

A comparison of the solution and solid state thermal decay kinetics of five photochromic spiropyrans with different *N*-alkyl groups (**SP1–SP5**) was carried out in acetonitrile and nanocrystalline suspensions at 298 K. The change in absorbance at ca. 550 nm was measured as a function of time for the merocyanine (MC) using transmission UV-vis spectroscopy. We found that the thermal decay kinetics are slower and follow a biexponential decay in the solid state compared to a faster, monoexponential decay that was measured in solution. We observed that, while the kinetic range measured in solution varies by a factor of 13, the decay kinetics in the solid state cover a range of ca. 150, indicating that crystal packing has an influence much greater than that of the effects of *N*-alkyl substitution. A fluorescence analysis of irradiated samples of **SP1** in solution could be used to determine the formation of the MC species and its subsequent decay. By contrast, a similar analysis of nanocrystalline suspensions displayed changes as a function of time that are consistent with self-quenching.

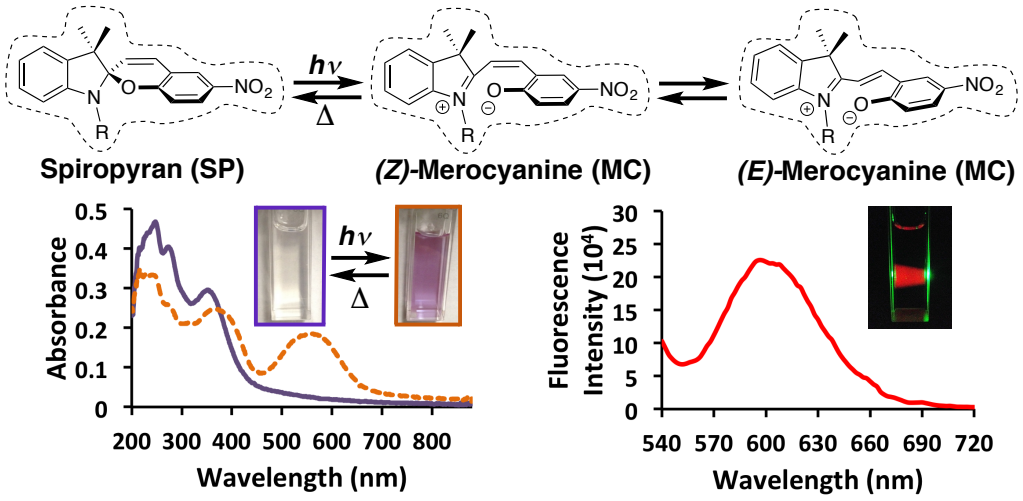

Figure 2.1.1. The spiropyran–*Z*-merocyanine–*E*-merocyanine photochromic reaction in the solid state under stead-state irradiation conditions along with corresponding UV-vis and fluorescence spectra.

2.2 Introduction

Spiropyrans (SPs) are one of several classes of photochromic molecules that have gained widespread interest from researchers because of their potential applications as optical memories and switches.[1] In particular, spiropyrans have been extensively studied with regards to molecular switching applications because of the vastly different properties between their two main isomers (Scheme 2.2.1), which make spiropyrans more responsive to a variety of stimuli (i.e. light, pressure, pH, and solvent polarity) compared to other photochromic systems.[2–6] Photochromism can be defined as the reversible, light-induced isomerization between two distinct species having different absorption spectra that proceeds with a visible color change.[7,8] The photochromic reactions of spiropyrans shown in Scheme 2.2.1 begins with the colorless or lightly colored SP being irradiated with ultraviolet (UV) light. This causes the heterolytic cleavage of the C_{spiro}–O bond, which results in the formation of the colored merocyanine (MC) isomer until the reaction reaches a photostationary state that depends on the excitation wavelength. However, because the merocyanine is thermally unstable, removal of the sample from the UV irradiation source results in its thermal decay back to the SP. Furthermore, selective excitation of the MC using visible light (>500 nm) can also be used to accelerate the recovery of the SP.

Scheme 2.2.1

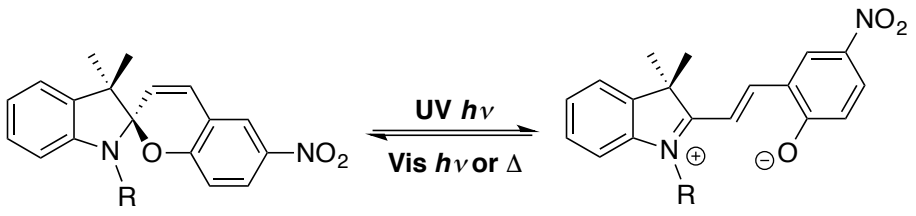

Spiropyran (SP)
colorless
λ_{max} ~ 355 nm

Merocyanine (MC)
deeply colored
λ_{max} ~ 550 nm

In 1952, Fischer and Hirshberg[9] first reported the photochromism of spiropyrans in solution, and it was not until 2000 that Bénard and Yu[10] first described the photochromism of SPs using steady UV irradiation in the crystalline state. Although Masuhara and co-workers showed in 1997 that intense femtosecond laser excitation could induce the photochromism of a spirooxazine in microcrystalline powder,[11] they reported that their spiropyran and spirooxazine crystals do not exhibit any photochromic behavior under steady UV irradiation.[12–15] A subsequent study by Harada et al. provided an explanation for Masuhara's observations. They suggested that the photochemical ring opening reaction to the colored MC may not be observable in the crystalline state at ambient temperature because the thermal ring closing reaction might occur at a rate that is much larger than its rate of formation, and thus prevent the accumulation of the merocyanine.[16] Harada et al. then showed that several compounds became visibly colored upon exposure to steady UV light irradiation by decreasing the rate of ring closure at lower temperatures.

While several examples of photochromic spiropyrans in crystals have been documented in the literature,[10,16–18] a systematic comparison of their thermal decay kinetics in solution and the crystalline state has not been explored, most likely due to complications arising from the use of large single crystals or dry powders, which have high optical densities and intense light scattering. We recently proposed[19–22] that one way to address this problem is to use nanocrystalline (NC) solids suspended in a nondissolving fluid such as water.[23] Crystals that are tens to hundreds of nanometers in size approach the size of supramolecular complexes such that it should be possible to excite them in a homogeneous manner, reducing complications from light scattering and other optical effects like birefringence and dichroism. Furthermore, the loading of nanocrystalline suspensions can be easily adjusted so that it should be possible to use

the same UV-vis transmission spectroscopic methods that are commonly used for solution studies. Under these conditions, one should be able to compare directly solution and crystalline state reaction kinetics and be able to document both substituent and crystal packing effects.

Scheme 2.2.2

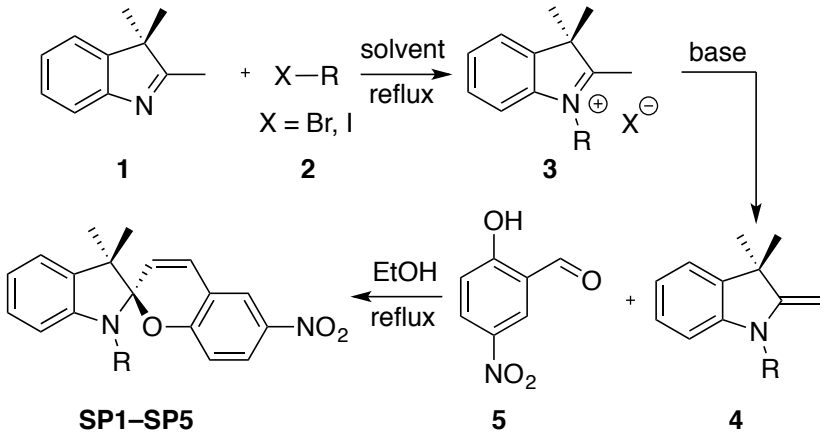

Table 2.2.1. Compound Information for **SP1–SP5**

Name	R	mp (°C)	Space group [Z']^{a}	NC size^{b}
SP1	CH_3	182–183	$P2_1/n[2]^{(24)}$	230
SP2	CH_2Ph	162–163	$P1[1]^{(25)}$	220
SP3	$(CH_2)_2CH_3$	150–151	$P1[2]^{(17)}$	185
SP4	$(CH_2)_3CO_2Et$	122–123	$P2_1/c[4]^{(26)}$	170
SP5	$(CH_2)_2OH$	156–157	$I2/a[1]^{(27)}$	240

[a]Molecules per asymmetric unit; [b]Determined by dynamic light scattering in nm.

To test our hypothesis, we compared the thermal decay kinetics for the MC→SP reaction for a set of structurally related spiropyrans (**SP1–SP5**, Scheme 2.2.2 and Table 2.2.1) in solution and in NC suspensions. We selected a homologous set based on a nitro-substituted chromophore with different *N*-alkyl substituents. While they are expected to have minor electronic and steric perturbations in solution, they are likely to have a substantial effect on the corresponding crystal packing. Our results showed that **SP1–SP5** with *N*-methyl, *N*-benzyl, *N*-propyl, *N*-(3-carboxyethyl)propyl, and *N*-(2-hydroxy)ethyl groups, respectively, are indeed photochromic in

the two media. As described below, we were able to measure the photochromic reaction and the MC thermal decays both in solution and in the solid state, and we discovered that solid state MC lifetimes are biexponential with long-lived components that are 10–100 times longer than the single exponential decays measured in solution.

2.3 Results and Discussion

Samples of **SP2–SP5** were obtained from the three-step sequence shown in Scheme 2.2.2 with minor modifications to experimental procedures reported in the literature.[26–29] The *N*-methyl **SP1** was made in a single step from commercially available **4** (R = CH_3) and 2-hydroxy-5-nitrobenzaldehyde **5** as illustrated in the final step of the scheme.[30] For **SP2–SP5**, commercially available 2,3,3-trimethylindolenine **1** was reacted with the desired alkyl halide **2** to produce iminium **3**, which was then treated with base to afford the *N*-substituted-3,3-dimethyl-2-methyleneindoline product **4**. Subsequent condensation of **4** with **5** yielded the desired *N*-substituted spiropyrans **SP2–SP5**. The identities of all the spiropyrans were confirmed by comparison of their physical and spectroscopic data with those reported in the literature.

UV-vis spectroscopic studies were carried out in acetonitrile solutions and in the solid state using aqueous NC suspensions prepared by the solvent shift, or reprecipitation method.[23] In a simple and general protocol, 10 μL of a 15 mM acetonitrile solution of the SP (**SP1–SP5**) was added into 3 mL of vortexing Millipore water. For solution studies, samples were made by adding 15 μL of a 10 mM acetonitrile solution of the SP (**SP1–SP5**) into a 1 cm quartz cuvette containing 2.5 mL of pure acetonitrile.

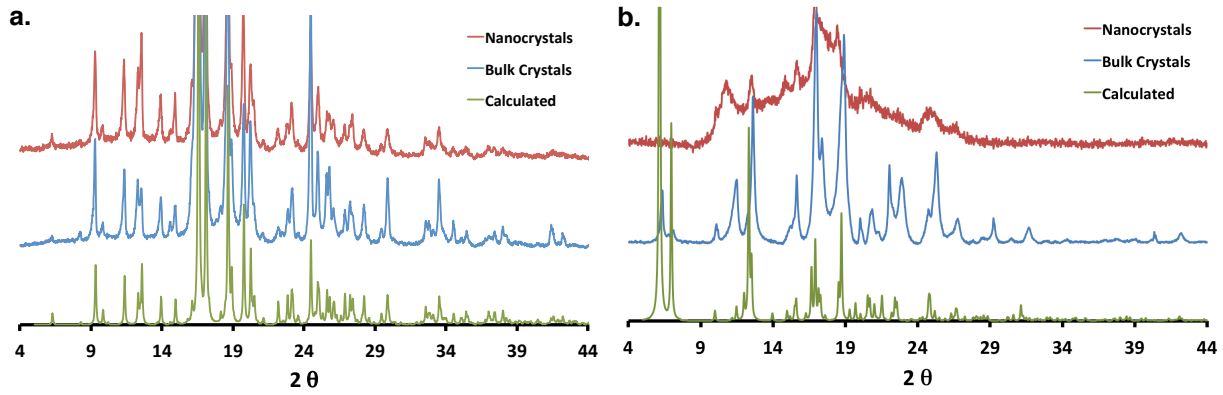

Figure 2.3.1. Comparison of PXRD from nanocrystals (top, red) and bulk powders (middle, blue) with the one calculated from data available from the Cambridge Crystallographic Data Centre (bottom, green) for (a) **SP1** and (b) **SP5**. High quality nanocrystals were obtained in the case of **SP1–SP4** (Appendix 2.6.4), but only semicrystalline samples could be obtained in the case of **SP5**.

To prove that our NC suspensions were crystalline and that they formed the same polymorph as the bulk crystals, we used powder X-ray diffraction (PXRD). We compared data from collected nanocrystals and bulk crystals of **SP1–SP5** to each other and to diffractograms obtained by simulations from structural data available at the Cambridge Crystallographic Data Centre (CCDC). The PXRD comparison for **SP1** in Figure 2.3.1.a shows that the NCs, the bulk crystal sample, and the calculated diffractogram match each other very well, meaning that they belong to the same crystal polymorph. The same can be said of the bulk crystals and NCs for **SP2–SP4** (Appendix 2.6.4, Figures 2.6.4.1–2.6.4.3). However, the PXRD comparison for **SP5** in Figure 2.3.1.b shows broad peaks over a very broad baseline for the NCs, suggesting that these samples have a largely amorphous character. On that basis, the solid state kinetic data discussed below for **SP5** cannot be correlated to differences in its crystal lattice in the same way as for samples of **SP1–SP4**.

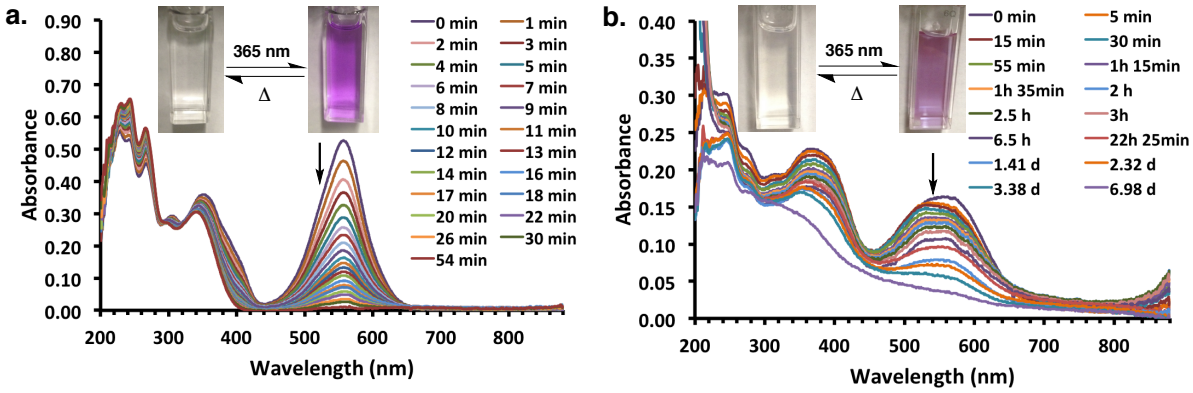

Figure 2.3.2. UV-vis absorption spectra showing the MC thermal decay for **MC1** in (a) MeCN and (b) in NC suspension. Insets: pictures of the cuvettes before and after irradiation at 365 nm (see Appendix 2.6.3 for **SP1–SP5** absorption spectra and decay plots).

For the ensuing UV-vis studies in solution and in NC suspensions, absorption spectra were recorded before and after samples were irradiated at 365 nm for 1 min intervals until the photostationary state (PSS) was reached. A color change was observed after the first minute of irradiation, which resulted in the growth of a band in the visible region with a $\lambda_{max} \approx 550$ nm, indicating that the photochemical ring opening reaction was producing the colored MC. In the case of **SP1**, it took ca. 6 min of irradiation with four 365 nm lamps in a Rayonet reactor for the PSS to be attained both in solution and in nanocrystals. Once the PSS had been reached, the colored sample was left to decay thermally under ambient light conditions. The absorption spectra were recorded in regular intervals until the visible band decayed back to baseline (Figure 2.3.2). As can be seen in Figure 2.3.2, the visible band is much sharper at the PSS in solution than in NC suspension, which has been observed by others studying spiropyrans in the solid state.[4,31,32] Specifically for **MC1** in a polystyrene matrix thin film, Whelan et al. reported a λ_{max} of 596 nm, which is red-shifted by almost 50 nm compared to that for **MC1** in NC suspension (Figure 2.3.2.b).[32] Corval and co-workers observed a similar spectral shift from $\lambda_{max} = 570$ nm of

SP microcrystals embedded in a KBr pellet to λ_{max} = 535 nm for a sol-gel film doped with SP nanocrystals.[33] Further analysis of Figure 2.3.2 shows that the spectral decay in solution (Figure 2.3.2.a) occurs in a homogeneous manner, indicating that there is a single, average MC structure responsible for the spectra observed at all times. By contrast, the spectral decay in the NC suspension in Figure 2.3.2.b shows a blue shift within the first 5 min followed by a more homogeneous decay until ca. 2 days. After that, the spectra begin to lose intensity, suggesting the occurrence of nanocrystal aggregation and precipitation. Observations similar to those made with **SP1** could also be made with samples of **SP2–SP5**, revealing that all of the compounds are photochromic at ambient temperature both in solution and in NC suspensions. In addition to this, the absorption spectra obtained for the NC suspensions for **SP1–SP5** all have similarly detailed spectral features compared to those of their solution counterparts, whereas studies by Masuhara and co-workers using microcrystalline dry powders show broad, featureless spectral profiles in the UV region.[13,15] Therefore, much more spectral detail can be observed in the solid state using NC suspensions rather than microcrystalline powders.

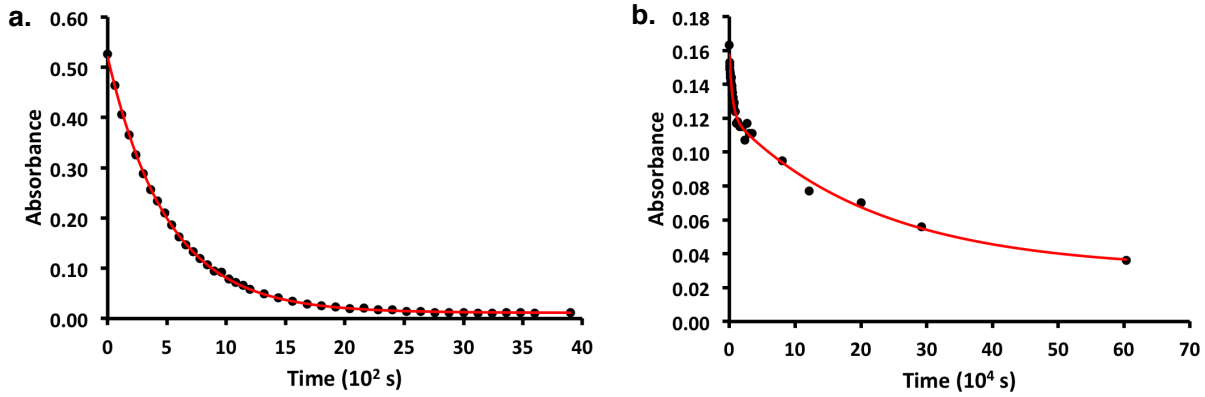

Figure 2.3.3. Thermal decay kinetic plots with trendline (red line) for **MC1** at 557 nm (a) in MeCN and (b) in NC suspension.

Table 2.3.1. Thermal Decay Lifetimes for **SP1–SP5**

	Solution	Nanocrystalline Suspensions			
Compound	**MeCN τ (s)**	**NC τ_1 (10^3 s)**	**NC I_1**	**NC τ_2 (10^3 s)**	**NC I_2**
SP1	504 ± 2.4	4.9 ± 0.54	2.4 ± 0.12	222 ± 27	5.4 ± 0.24
SP2	39 ± 0.6	9.8 ± 0.84	7.2 ± 0.3	407 ± 22	23 ± 0.36
SP3	480 ± 3.0	5.1 ± 0.66	2.4 ± 0.18	135 ± 6.6	11 ± 0.18
SP4	264 ± 4.8	0.19 ± 0.06	1.8 ± 0.18	3.2 ± 0.06	14 ± 0.12
SP5	318 ± 4.8	11 ± 4.8	31 ± 7.2	499 ± 227	140 ± 29

Using the experimental absorption values at 550 nm for **MC1–MC5** to generate decay plots (Figure 2.3.3, **MC1**), we were able to calculate the MC lifetimes in solution and in NC suspensions (Table 2.3.1). We found that the solution kinetics for **MC1–MC5** are all monoexponential. By contrast, the thermal decays in NC suspension were all complex and much longer than those in solution, consistent with the rigidity of the crystal lattice, which restricts structural changes that the MC must undergo to return to the SP (Scheme 2.3.1). While reasonable fits were obtained using a biexponential function, the use of more complex fitting functions was not attempted given that precise measurements could not be obtained as a result of sample precipitation over a few days.

Scheme 2.3.1

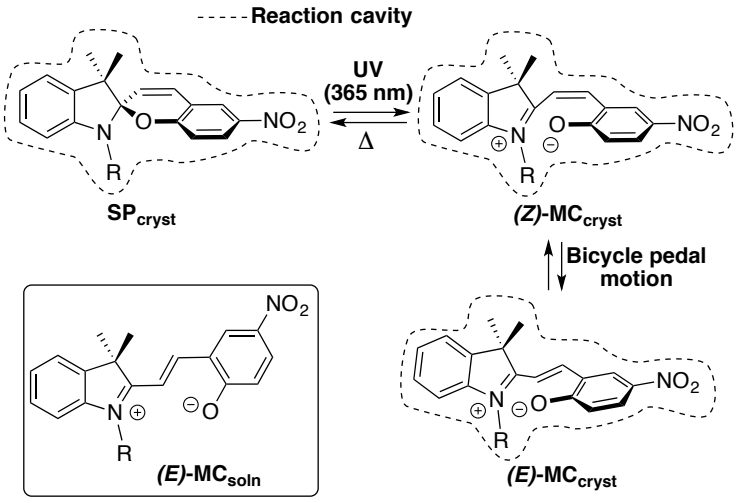

In spite of the eventual sample precipitation, our biexponential decay results compare favorably with those reported by Bénard et al.[31] and Gentili et al.[4] with microcrystalline dry powders. The former authors interpret the results as MC molecules located at the crystal's surface being next to mostly other MC molecules, whereas MC molecules deeper in the crystal will be surrounded by mostly ring closed SP molecules. Thus, the two different environments within the crystal lead to two different MC decay rates. On the other hand, Gentili et al. suggest that localized heating from rapid ring closure after the initial C_{spiro}–O cleavage event results in areas of more and less disorder, which correspond to different ring closure rates. Although these hypotheses are reasonable when considering crystals around 10 μm in size, the same logic does not translate to NC suspensions because, due to the nanocrystals being smaller in size than the wavelength of incident UV irradiation, the entire crystal is homogeneously excited, meaning that there should be no difference in the extent of photochemical reaction on the surface and within the crystal's interior.

A report by Eichen and co-workers that describes the crystalline state photochromism of **SP3** microcrystals found that the thermal decay of the visible band (λ_{max} = 600 nm) for **MC3** followed a biexponential curve with lifetimes of τ_1 = 3095 s and τ_2 = 19040 s at 304.5 K and τ_1 = 875 s and τ_2 = 5910 s at 315 K.[17] In comparison, we describe the decay of **MC3** nanocrystals (λ_{max} = 550 nm) also as being biexponential but with lifetimes of τ_1 = 5100 s and τ_2 = 135000 s at 298 K (Table 2.3.1). It is reasonable that our decay lifetimes are longer than those reported by Eichen and co-workers as it is expected that decreasing the temperature should slow down the thermal decay process of the MC.[16] On the basis of crystallographic data, Eichen and co-workers suggested that two nonequivalent SP structures in the crystal lattice are responsible for the two components of the decay. However, while we also observe biexponential kinetics, and our

nanocrystals of **SP3** are identical to those reported by Eichen and co-workers (Appendix 2.6.4 Figure 2.6.4.2), we observed biexponentiality for all SP samples even when they have only a single type of molecule in the crystal. Given our observations, we propose that the *(E)*- and *(Z)*-configurations of the MC may be responsible for the different lifetimes (Scheme 2.3.1), as discussed in more detail below.

As illustrated in Scheme 2.2.1 (and in the box in Scheme 2.3.1), the photochromic SP ring opening reaction in solution leads to an electronically delocalized MC with several conformational degrees of freedom that can adopt an extended conformation with a formal *(E)*-configuration at the central double bond. By contrast, it is unlikely that extended conformations can be formed in the solid state with the reasonable expectation that shape and volume will be conserved within the reaction cavity, as shown in Scheme 2.3.1. Single exponential decays for **MC1–MC5** in solution are consistent with a single merocyanine species or a mixture of isomers that exist under rapid equilibrium. The range of time constants in solution is relatively small, as expected from the similar nature of the *N*-alkyl substituents. There is a factor of 13 in going from the shortest-lived benzyl compound **SP2** with τ = 39 s to the longest-lived methyl derivative **SP1** with τ = 504 s (Table 2.3.1). At a first approximation, there appears to be a weak dependence on the electron withdrawing ability of the alkyl group, which would destabilize the positive charge on nitrogen, as judged by the expected acidity of the corresponding R-**H** hydrocarbon, following the order: $PhCH_2$-**H** > $EtO_2C(CH_2)_2CH_2$-**H** > $HOCH_2CH_2$-**H** > $CH_3CH_2CH_2$-**H** > CH_3-**H**. However, other factors may also play a role. For example, Roxburgh et al.[30] found that an *N*-hexyl substituted MC had a thermal decay that is about 5 times faster than that of the analogous *N*-methyl derivative (**MC1**) in methanol. The relatively large difference observed in this case was assigned to differences in solvation, which may also play a role in the case of **MC1–MC5**.

While results in solution indicate the decay of a single species for **MC1–MC5**, kinetics in NC suspensions reveal a biexponential decay for the same set of MC derivatives. This suggests that at least two different populations exist, with one of them being able to revert rapidly to the closed form and the second one taking much longer. On the basis of topochemical considerations that require reactions in crystals to occur with a minimum of atomic and molecular motions, one may speculate about potential candidates for the short- and long-lived MC species. It is reasonable that the short-lived MC may relate to species that have a close resemblance to the original structure, as indicated by *(Z)*-$\mathbf{MC}_{\mathbf{cryst}}$ in Scheme 2.3.1. Structures that depart further from the local atomic configuration, which may help explain the long-lived components, are also possible. On the basis of observations made with *trans*-stilbenes, *trans*-azobenzenes, and salicylidene anilines,[34,35] we suggest that longer-lived species may correlate with structures that undergo a *cis*-to-*trans* isomerization by a volume-conserving bicycle-pedal motion, as in the isomerization of *(Z)*- to *(E)*-$\mathbf{MC}_{\mathbf{cryst}}$ (Scheme 2.3.1). Notably, when the decay lifetimes of **MC1–MC5** in solution and in NC suspensions are compared, there is no apparent trend (Table 2.3.1). For example, *N*-benzyl **MC2** decayed the fastest in solution but is the second slowest in the solid state. Similarly, **MC1** decays the slowest in solution but is second fastest in NC suspension. On that basis, we conclude that the crystal packing of **SP1–SP4** and the amorphous nature of **SP5** have a determinant influence on the decay kinetics in the solid state.

To further probe the differences in the properties and kinetics of the photochromic system in solution and in NC suspensions, we also explored changes in the fluorescence intensity of **MC1** as a function of time. We showed that the emission of **MC1** has a maximum at ca. 615 nm in acetonitrile solution and at ca. 600 nm in NC suspension (Appendix 2.6.6, Figures 2.6.6.1 and 2.6.6.3). By contrast, a slightly red-shifted emission maximum (625 to 635 nm) was reported for

MC1 in a toluene solution[36] and a PMMA film,[37] respectively. It is well-established that increasing the solvent polarity causes a blue shift in the absorption maximum due to the stabilization of the ground state MC such that a similar shift in the emission spectrum is expected.[38–40] Figure 2.3.4.a shows an experiment where changes in the fluorescence intensity of **MC1** are detected in acetonitrile as a function of irradiation of **SP1** at λ = 365 nm light for ca. 9 min (540 s), followed by a dark period where the thermal decay of **MC1** can occur. As expected, the growth and decay of the fluorescence signal in Figure 2.3.4.a matches the growth and decay of the absorption signal in solution shown in Figure 2.3.3.a. However, the results from a similar experiment carried out with a NC suspension were quite different. Changes in the fluorescence intensity shown in Figure 2.3.4.b correspond to three different stages. The first stage takes place as the sample is illuminated with UV light, which results in an increase in the amount of MC formed. The second stage illustrates the changes in fluorescence intensity that occurs as the concentration of the MC decreases thermally in the dark. The third stage occurs when the sample is exposed to visible white light, which results in a rapid decrease in the MC concentration. The first section of the plot shows that excitation using UV light at 365 nm for 2 min results in an initial increase in MC fluorescence intensity, but continued irradiation for three additional 2 min intervals showed a noticeable decrease in the signal intensity, suggesting that an increase in the concentration of the MC beyond a certain point results in self-quenching. This hypothesis was readily confirmed by removal of the UV irradiation source, which resulted in the thermal recover of the SP, a decrease in the concentration of the MC, and a remarkable increase in the fluorescence signal over a 2 h period followed by a plateau, indicating a decrease in the extent of self-quenching (Figure 2.3.4.b). After about 6 h in the dark, when the signal intensity remains relatively stable, exposure to visible light accelerates the decay of the MC with the consequent

decrease in the fluorescence intensity. One can see that a complex relation between self-quenching and thermal decay would make it impossible to determine the kinetics of the latter via emission studies. In fact, it is likely that this behavior is a property of the crystalline material where excited state energy delocalization may assist in efficient self-quenching, an effect that was not observed based on fluorescence lifetime measurements by Kinashi et al. for **MC5** in PMMA films.[41]

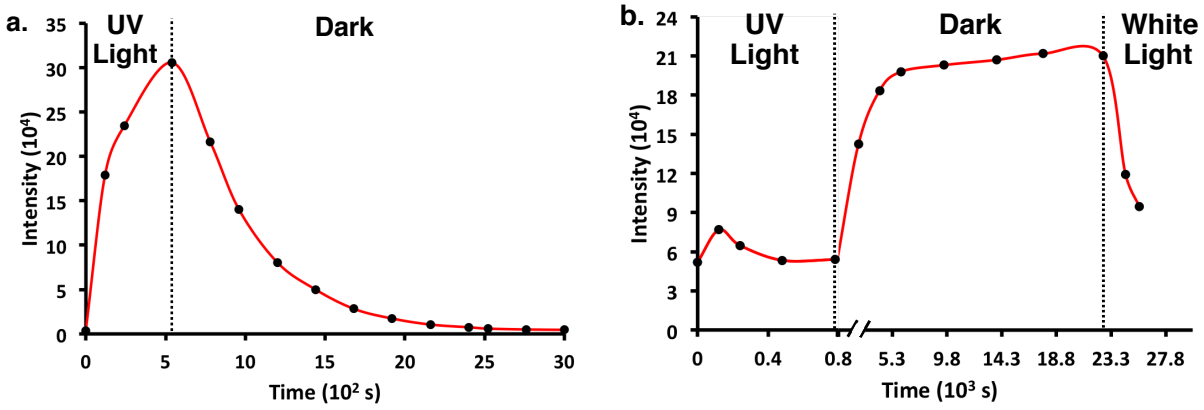

Figure 2.3.4. Fluorescence intensity at 614 nm vs. time with excitation at 530 nm for **SP1** (a) in MeCN with UV irradiation (365 nm) for 540 s and in the dark for 3000 s and (b) in NC suspension upon UV irradiation (365 nm) for 780 s and in the dark after UV irradiation followed with white light irradiation. Note: in panel b, the *x*-axis scale changes between 0.8 and 5.3 x 10^3 s.

2.4 Conclusions

Our results demonstrate that NC suspensions can be used to study the kinetics of the photochromic reaction of spiropyrans in the solid state using common transmission spectroscopic methods which cannot be done easily with single crystals or bulk powders due to their high optical densities, dichroism, birefringence, and strong light scattering.[42] After documenting the thermal decay for **MC1–MC5** in solution and the solid state, we found that the MC has a lifetime

10–100 times longer in NC suspensions than in solution. However, the decay kinetics in solution can be fit to a monoexponential decay compared to the biexponential decay that is required in the solid state. This indicates that the crystal lattice impedes potentially different MC structures form interconverting rapidly enough to have a single kinetic signature. Another difference in the photochromic behavior of SPs in solution and in NC suspensions was found when analyzing the change in MC fluorescence over time for **SP1**. While the fluorescence results obtained in solution were consistent with those obtained using absorption data, the results in NC suspension gave strong indications of self-quenching. We feel that this report strongly validates the use of transmission spectroscopy with NC suspensions as a valuable tool to study the kinetics of reactions in crystalline solids.

Author's note: Chapter 2 is adapted with permission from the following publication: Breslin, V. M.; Garcia-Garibay, M. A. "Transmission Spectroscopy and Kinetics in Crystalline Solids Using Aqueous Nanocrystalline Suspensions: The Spiropyran-Merocyanine Photochromic System." *Cryst. Growth Des.* **2017**, *17*, 637–642. Copyright 2017 American Chemical Society (**DOI**: 10.1021/acs.cgd.6b01476).

2.5 Experimental

2.5.1 General Information for Synthetic Procedures

All commercially obtained reagents/solvents were used as received without further purification. Unless stated otherwise, reactions were conducted in oven-dried glassware under argon atmosphere. ^{1}H and ^{13}C NMR spectra were acquired on a Bruker Avance spectrometer at 500 MHz (^{1}H) and 125 MHz (^{13}C). All chemical shifts are reported in ppm on the δ-scale relative

to the residual solvent signal as reference ($CDCl_3$ δ 7.26 and δ 77.16 for proton and carbon, respectively, CD_3CN δ 1.94 for proton and δ 1.32, 118.26 for carbon). Coupling constants (*J*) are reported in hertz (Hz). Standard abbreviations indicating multiplicity were used as follows: s (singlet), b (broad), d (doublet), t (triplet), q (quartet), m (multiplet), dd (doublet of doublets), dt (doublet of triplets), and td (triplet of doublets). High-resolution mass spectrum data was recorded on a DART spectrometer in positive (ESI+) ion mode. Melting point values were recorded on a Melt-Point II® apparatus. Infrared spectra were recorded on a PerkinElmer® Spectrum 100 spectrometer equipped with a universal ATR sampling accessory.

2.5.2 Synthetic Procedures

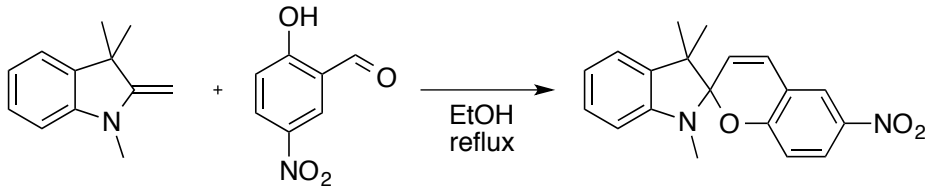

4a **5** **SP1**

Synthesis of 1',3',3'-Trimethyl-6-nitrospiro[chromene-2,2'-indoline] (SP1): SP1 was prepared with minor modifications to the experimental procedure in reference 30. 1,3,3-Trimethyl-2-methylene-indoline (**4a**) (0.275 mL, 1.55 mmol) was added dropwise to a solution containing 2-hydroxy-5-nitrobenzaldehyde (**5**) (0.2593 g, 1.55 mmol) in 8.5 mL of freshly distilled ethanol followed by refluxing for 16 h under argon. Once cooled to room temperature, the mixture was concentrated and filtered using ice cold ethanol to afford **SP1** as a yellow solid. Recrystallized from DCM/EtOH (1:1) to obtain yellow crystals (0.377 g, 75% yield). m.p. 181.7–182.7 °C (lit. 178–179 °C).[30] IR (film): 3067, 2963, 2865, 1609, 1509, 1488, 1476, 1466, 1329, 1299, 1268, 1183, 1122, 1088, 1021, 1015, 948, 916, 806,782, 750 cm^{-1}. ^1H NMR ($CDCl_3$, 500 MHz): δ 8.02 (dd, *J* = 8.71, 2.72 Hz, 1H) 8.00 (s, 1H), 7.21 (td, *J* = 7.62, 1.26 Hz, 1H), 7.09 (dd, *J* = 7.30, 0.81 Hz, 1H), 6.92 (d, *J* = 9.65 Hz, 1H), 6.89 (td, *J* = 7.39, 0.90 Hz, 1H), 6.77 (d, *J*

= 9.38 Hz, 1H), 6.56 (d, *J* = 7.75 Hz, 1H), 5.86 (d, *J* = 10.37 Hz, 1H), 2.74 (s, 3H), 1.30 (s, 3H), 1.19 (s, 3H) ppm. ^{13}C NMR ($CDCl_3$, 125 MHz): δ 160.0, 147.8, 141.1, 136.2, 128.4, 128.0, 126.0, 122.8, 121.8, 121.7, 119.9, 118.8, 115.6, 107.2, 106.5, 52.4, 29.0, 26.0, 20.1 ppm. HRMS (ESI-TOF) m/z: $[M]^{\bullet+}$ calcd. for $C_{19}H_{18}N_2O_3$: 322.13119, found: 322.13180.

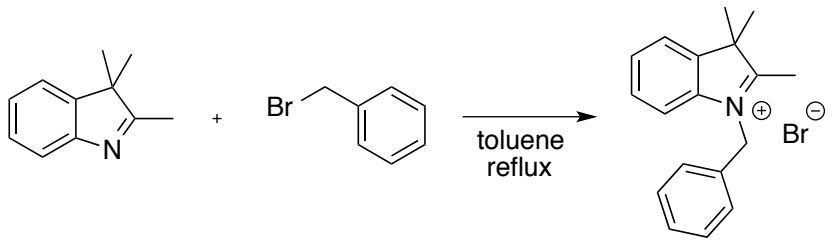

1 **2a** **3a**

Synthesis of 1-Benzyl-2,3,3-trimethylindolenium bromide (3a): Compound **3a** was prepared with minor modifications to the experimental procedure in reference 29. 2,3,3-Trimethylindolenine (**1**) (1.0 mL, 6.23 mmol) was added dropwise to a solution containing benzyl bromide (**2a**) (1.50 mL, 12.6 mmol) in 6 mL of dry toluene followed by refluxing for 22 h under argon. Let cool to room temperature, removed solvent under reduced pressure, and washed 3 x 5 mL with hexanes. Dried red solid **3a** under vacuum and stored in a desiccator (2.013 g, 97% yield).

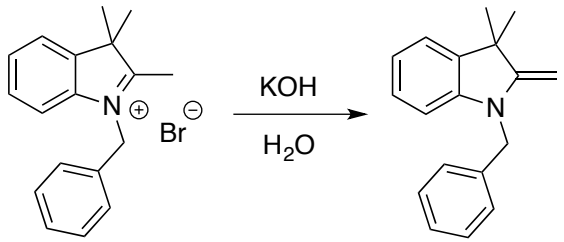

3a **4b**

Synthesis of 1-Benzyl-3,3-dimethyl-2-methyleneindoline (4b): Compound **4b** was prepared with minor modifications to the experimental procedure in reference 27. To a solution of 1-benzyl-2,3,3-trimethylindolenium bromide (**3a**)(2.0135 g, 6.1 mmol) dissolved in 23 mL of DI

H_2O was added a solution of KOH (1.061 g, 18.9 mmol) dissolved in 23 mL of DI H_2O under argon. After 1 h at room temperature, extracted 3 x 40 mL with DCM, washed the combined organic layers 1 x 125 mL brine, dried over $MgSO_4$, filtered and removed solvent under reduced pressure to obtain **4b** as a red-orange oil. Crude product used in next step without further purification.

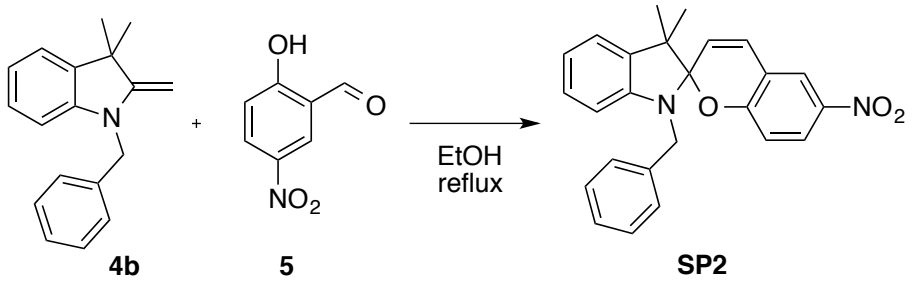

4b **5** **SP2**

Synthesis of 1'-Benzyl-3',3'-dimethyl-6-nitrospiro[chromene-2,2'-indoline] (SP2): SP2 was prepared with minor modifications to the experimental procedure in reference 27. To a solution containing 2-hydroxy-5-nitrobenzaldehyde (**5**) (1.018 g, 6.1 mmol) in 20 mL of freshly distilled ethanol was added crude 1-benzyl-3,3-dimethyl-2-methylenindoline (**4b**) dissolved in 15 mL of ethanol followed by refluxing for 18 h under argon. After cooling to room temperature, removed solvent under reduced pressure and purified by flash chromatography on silica with hexanes/DCM as eluent (2:1→1:1) to afford **SP2** as a yellow solid. Recrystallized from ethanol to obtain yellow crystals (1.0231 g, 42% yield over 2 steps). m.p. 161.5–162.8 °C (lit. 162 °C).[43] IR (film): 3030, 2966, 1611, 1518, 1481, 1458, 1336, 1273, 1090, 949, 810, 745 cm^{-1}. ^1H NMR ($CDCl_3$, 500 MHz): δ 8.03 (dd, *J* = 8.99, 2.78 Hz, 1H), 7.98 (d, *J* = 2.68 Hz, 1H), 7.33–7.23 (m, 5H), 7.12 (dd, *J* = 7.24, 0.82 Hz, 1H), 7.08 (td, *J* = 7.70, 1.30 Hz, 1H), 6.88 (dd, *J* = 14.76, 0.91 Hz, 1H), 6.87 (d, *J* = 10.19Hz, 1H), 6.78 (d, *J* = 8.98 Hz, 1H), 6.35 (d, *J* = 7.72 Hz, 1H), 5.92 (d, *J* = 10.39 Hz, 1H), 4.51 (d, *J* = 16.54 Hz, 1H), 4.21 (d, *J* = 16.54 Hz, 1H), 1.34 (s, 3H), 1.31 (s,

3H) ppm. ^{13}C NMR ($CDCl_3$, 125 MHz): δ 159.7, 147.2, 141.2, 138.7, 136.2, 128.8, 128.6, 127.9, 127.2, 126.7, 126.1, 122.9, 121.9, 121.8, 120.1, 118.7, 115.7, 108.1, 106.9, 52.9, 47.8, 26.3, 20.1 ppm. HRMS (ESI-TOF) m/z: $[M]^{\bullet+}$ calcd. for $C_{25}H_{22}N_2O_3$: 398.16249, found 398.16092.

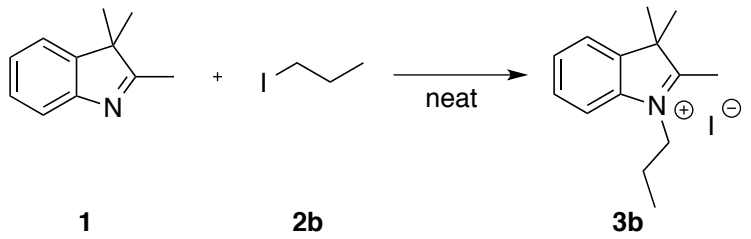

Synthesis of 2,3,3-Trimethyl-1-propylindolenium iodide (3b): Compound **3b** was prepared with minor modifications to the experimental procedure in reference 28. 2,3,3-Trimethylindolenine (**1**) (0.24 mL, 1.5 mmol) was dissolved in 1-iodopropane (**2b**) (0.40 mL, 4.10 mmol) and heated to 95 °C for 7 h under argon. The resulting viscous oil (**3b**) was cooled to room temperature, rinsed with hexanes, and stored in a desiccator. Crude product used in next step without further purification.

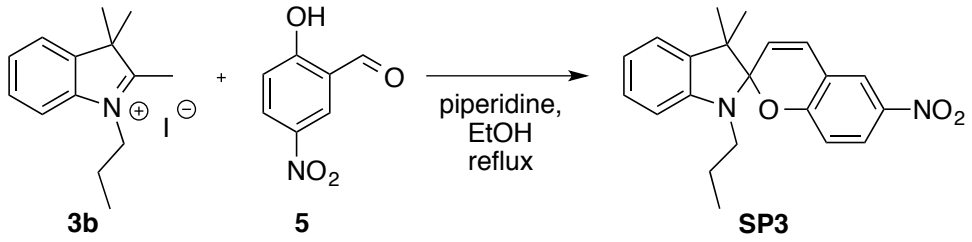

Synthesis of 3,3'-Dimethyl-6-nitro-1'-propylspiro[chromene-2,2'-indoline] (SP3): SP3 was prepared with minor modifications to the experimental procedure in reference 28. To a solution containing crude 2,3,3-trimethyl-1-propylindolenium iodide (**3b**) in 5 mL of freshly distilled ethanol was added dropwise piperidine (0.18 mL, 1.82 mmol) under argon. After 25 min, a solution of 2-hydroxy-5-nitrobenzaldehyde (**5**) (0.2542 g, 1.52 mmol) in 7 mL of ethanol was

added followed by refluxing for 18 h. The mixture was cooled to room temperature and purified by flash chromatography on silica with hexanes/DCM as eluent (1.5:1) to afford **SP3** as a yellow solid. Recrystallized from DCM/ethanol (1:1) to obtain yellow crystals (0.4321 g, 82% yield over 2 steps). m.p. 150.2–151.2 °C. IR (film): 3057, 2964, 1610, 1514, 1481, 1335, 1275, 1089, 957, 807, 748 cm^{-1}. ^{1}H NMR ($CDCl_3$, 500 MHz): δ 8.01 (dd, *J* = 10.3, 2.71 Hz, 1H), 7.99 (s, 1H), 7.18 (td, *J* = 7.65, 1.25 Hz, 1H), 7.08 (dd, *J* = 7.25, 0.94 Hz, 1H), 6.89 (d, *J* = 10.34 Hz, 1H), 6.86 (td, *J* = 7.43, 0.88 Hz, 1H), 6.74 (d, *J* = 8.33 Hz, 1H), 6.57 (d, *J* = 7.70 Hz, 1H), 5.87 (d, *J* = 10.41 Hz, 1H), 3.15–3.09 (m, 2H), 1.71–1.55 (m, 2H), 1.28 (s, 3H), 1.19 (s, 3H), 0.90 (t, *J* = 7.39, 3H) ppm. ^{13}C NMR ($CDCl_3$, 125 MHz): δ 159.9, 147.3, 141.0, 136.0, 128.1, 127.8, 126.0, 122.8, 122.2, 121.8, 119.4, 118.6, 115.6, 106.9, 106.8, 52.8, 45.6, 26.1, 22.3, 20.0, 11.9 ppm. HRMS (ESI-TOF) m/z: $[M]^{\bullet+}$ calcd. for $C_{21}H_{22}N_2O_3$: 350.16249, found: 350.16220.

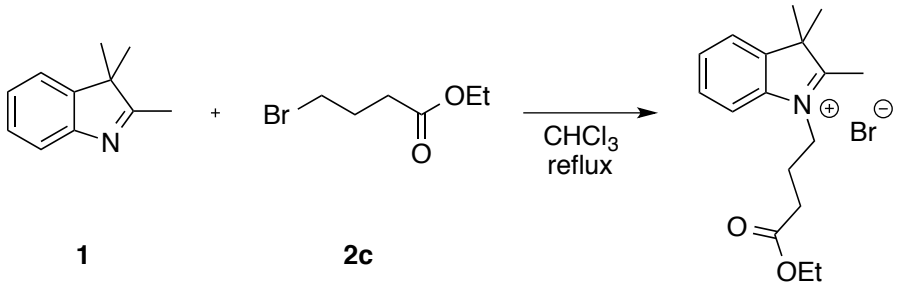

1 **2c** **3c**

Synthesis of 1-(4-ethoxy-4-oxobutyl)-2,3,3-trimethylindolium bromide (3c): Compound **3c** was prepared with minor modifications to the experimental procedure in reference 26. To a solution containing 2,3,3-trimethylindolenine (**1**) (0.32 mL, 1.99 mmol) in 5 mL of $CHCl_3$ was added ethyl-4-bromobutyrate (**2c**) (0.93 mL, 6.5 mmol) dropwise under argon followed by refluxing for 3 days. The crude mixture was cooled to room temperature and the solvent was removed under reduced pressure. The crude mixture was dissolved in methanol (2 mL) and then

diethyl ether (10 mL) was added to precipitate out the product. Subsequent filtration afforded **3c** (0.360 g, 51% yield), which was used in the next step without further purification.

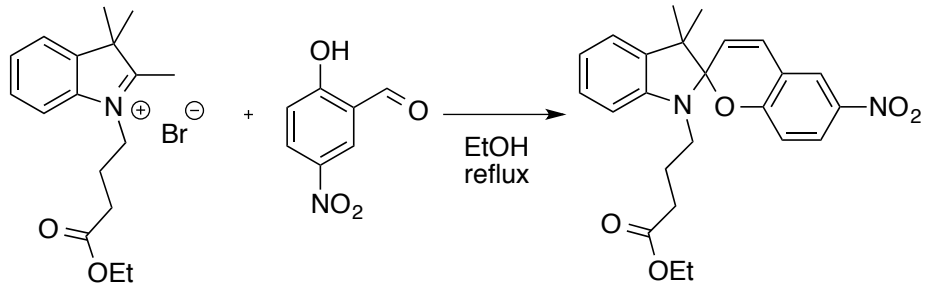

3c **5** **SP4**

Synthesis of Ethyl 4-(3',3'-dimethyl-6-nitrospiro[chromene-2,2'-indolin]-1'-yl)butanoate (SP4): SP4 was prepared with minor modifications to the experimental procedure in reference 26. To a solution of **3c** (0.3412 g, 0.963 mmol) in 12 mL of freshly distilled ethanol was added 2-hydroxy-5-nitrobenzaldehyde (**5**) (0.1933 g, 1.16 mmol) under argon followed by refluxing for 18 h. After cooling to room temperature, removed solvent under reduced pressure. Dissolved the crude mixture in DCM, washed 3 x 10 mL with saturated Na_2CO_3, dried over Na_2SO_4, and concentrated. Purified by flash chromatography on silica with DCM/hexanes as eluent (2:1) to afford **SP4** as a golden yellow solid. Recrystallized from ethanol to obtain yellow needles (0.118 g, 29% yield). m.p. 122.0–123.2 °C (lit. 116 °C).[26] IR (film): 3054, 2966, 1729, 1609, 1518, 1480, 1335, 1273, 1089, 954, 808, 747 cm^{-1}. ^1H NMR ($CDCl_3$, 500 MHz): δ 8.01 (dd, *J* = 11.46, 2.72 Hz, 1H), 7.99 (s, 1H), 7.19 (td, *J* = 7.66, 1.24 Hz, 1H), 7.08 (dd, *J* = 7.22, 1.03 Hz, 1H), 6.89 (d, *J* = 9.99 Hz, 1H), 6.88 (td, *J* = 7.81, 0.77 Hz, 1H), 6.74 (d, *J* = 8.58 Hz, 1H), 6.64 (d, *J* = 7.78 Hz, 1H), 5.87 (d, *J* = 10.36 Hz, 1H), 4.09 (qd, *J* = 7.13, 1.41 Hz, 2H), 3.24–3.17 (m, 2H), 2.34 (td, *J* = 7.20, 1.69 Hz, 2H), 2.01–1.80 (m, 2H), 1.28 (s, 3H), 1.23 (t, *J* = 7.15 Hz, 3H), 1.18 (s, 3H) ppm. ^{13}C NMR ($CDCl_3$, 125 MHz): δ 173.2, 159.7, 147.2, 141.1, 136.1, 128.4, 128.0,

126.1, 122.9, 122.0, 121.9, 119.8, 118.6, 115.7, 107.0, 106.8, 60.6, 52.8, 43.2, 31.9, 26.1, 24.3, 20.0, 14.3 ppm. HRMS (ESI-TOF) m/z: $[M]^{\bullet+}$ calcd. for $C_{24}H_{26}N_2O_5$: 422.18362, found: 422.18276.

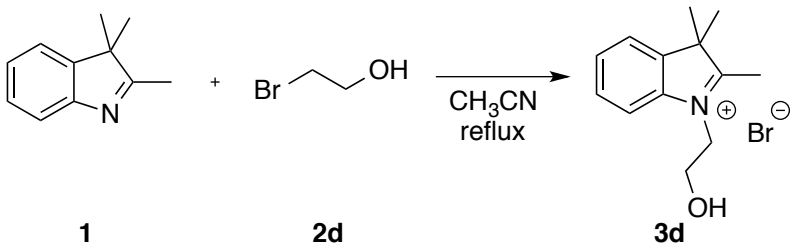

1 **2d** **3d**

Synthesis of 1-(2-Hydroxyethyl)-2,3,3-trimethylindolium bromide (3d): Compound **3d** was prepared with minor modifications to the experimental procedure in reference 27. To a solution of 2,3,3-trimethylindolenine (**1**) (1.0 mL, 6.23 mmol) in 8 mL of acetonitrile was added 2-bromoethanol (**2d**) (0.55 mL, 7.78 mmol) followed by heating to reflux for 24 h. After cooling to room temperature, concentrated the reaction mixture and then sonicated and filtered using hexanes to obtain **3d** as a purple solid, which was used in the next step without further purification.

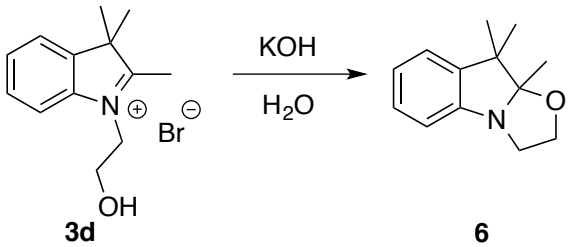

3d **6**

Synthesis of 9,9,9a-Trimethyl-2,3,9,9a-tetrahydrooxazolo[2,3-*a*]indole (6): Compound **6** was prepared with minor modifications to the experimental procedure in reference 27. To a solution of **3d** in 10 mL of DI H_2O was added a solution of KOH (0.46 g, 8.2 mmol) dissolved in 15 mL of DI H_2O. Let stir for 10 min., then extracted the reaction mixture 3 x 40 mL of diethyl ether,

dried over Na_2SO_4, filtered and concentrated under reduced pressure. Purified by flash chromatography on silica with hexanes/ethyl acetate as eluent (3:0.5) to obtain **6** (0.636 g, 50% yield over 2 steps) as a yellow-orange oil.

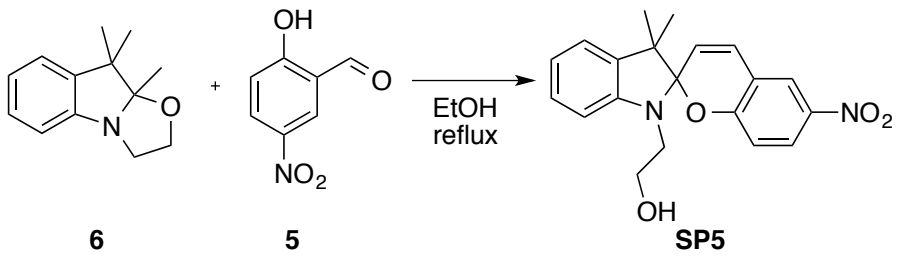

6 **5** **SP5**

Synthesis of 2-(3',3'-Dimethyl-6-nitrospiro[chromene-2,2'-indolin]-1'-yl)ethanol (SP5): SP5 was prepared with minor modifications to the experimental procedure in reference 27. To a solution of **6** (0.636 g, 3.13 mmol) in 10 mL of freshly distilled ethanol was added 2-hydroxy-5-nitrobenzaldehyde (0.654 g, 3.91 mmol) followed by refluxing for 6 h. After cooling to room temperature, removed solvent under reduced pressure. Recrystallized from DCM/ethanol (1:1) to obtain dark purple plates (0.90 g, 81% yield). m.p. 155.5–157.0 °C (lit. 171 °C).[27] IR (film): 3411 (broad), 3069, 2964, 2924, 1610, 1517, 1481, 1459, 1336, 1273, 1089, 1026, 953, 807, 746 cm^{-1}. ^1H NMR (CD_3CN, 500 MHz): δ 8.07 (d, J = 2.75 Hz, 1H), 7.99 (dd, J = 9.00, 2.80 Hz,1H), 7.14 (td, J = 7.69, 1.27 Hz, 1H), 7.11 (dd, J = 7.30, 0.85 Hz, 1H), 7.02 (d, J = 10.40 Hz, 1H), 6.83 (td, J = 7.41, 0.85 Hz, 1H), 6.71 (dd, J = 8.98, 0.23 Hz, 1H), 6.66 (d, J = 7.75 Hz, 1H), 5.99 (d, J = 10.40 Hz, 1H), 3.68–3.63 (m, 1H), 3.58–3.53 (m, 1H), 3.32 (dt, J = 14.75, 6.84 Hz, 1H), 3.24–3.19 (m, 1H), 1.25 (s, 3H), 1.15 (s, 3H) ppm. ^{13}C NMR (CD_3CN, 125 MHz): δ 160.4, 148.3, 142.0, 136.9, 128.7, 128.6, 126.5, 123.6, 123.2, 122.7, 120.3, 120.0, 116.2, 108.0, 107.7, 60.8, 53.4, 46.8, 26.1, 20.0 ppm. HRMS (ESI-TOF) m/z: $[M]^{\bullet+}$ calcd. for $C_{20}H_{20}N_2O_4$: 352.14176, found 352.14017.

2.5.3 Sample Preparation for UV-vis and Fluorescence Experiments

General preparation of solutions for UV-Vis absorption experiments (SP1–SP5)

15 μL of a stock solution (~10 mM) in acetonitrile was added to a quartz cuvette containing 2.5 mL of pure acetonitrile to give a final sample concentration of ~6 x 10^{-5} M.

General preparation of nanocrystalline suspensions for UV-Vis absorption experiments (SP1–SP5)

10 μL of a stock solution (~15 mM) in acetonitrile was injected via a micropipette into a culture tube containing 3 mL of vortexing Millipore water. Vortexing continued for 30 seconds after injection. Then the newly created suspension was transferred via pipette to a quartz cuvette.

General preparation of solutions for fluorescence experiments (SP1)

10 μL of a stock solution (6.51 mM) in acetonitrile was added to a quartz cuvette containing 2.5 mL of pure acetonitrile to give a final sample concentration of 2.6 x 10^{-5} M.

General preparation of nanocrystalline suspensions for fluorescence experiments (SP1)

15 μL of a stock solution (6.51 mM) in acetonitrile was injected via a micropipette into a culture tube containing 3 mL of vortexing Millipore water. Vortexing continued for 30 seconds after injection. Then the newly created suspension was transferred via pipette to a quartz cuvette.

2.5.4 Experimental Methods for UV-vis and Fluorescence Studies

General method for UV-Vis absorption experiments in solution and nanocrystalline suspensions (SP1–SP5)

An initial absorption spectrum was recorded, and then the sample was irradiated at 365 nm in a Rayonet photochemical reactor (4 bulbs) in 1 minute intervals until the photostationary state (PSS) was reached (as determined by monitoring the band growing in at ca. 550 nm). Absorption

spectra were recorded after every irradiation interval. Once the PSS was reached, the sample was left to thermally decay under ambient light conditions, and the absorbance spectrum was recorded in regular time intervals until the absorbance of the visible band at ca. 550 nm remained constant.

General method for fluorescence experiments in solution and nanocrystalline suspensions (SP1)

An initial emission spectrum was recorded with excitation at 530 nm and scanning from 540–720 nm, and then the sample was irradiated at 365 nm in a Rayonet photochemical reactor (4 bulbs) in 2 minute intervals for a total of 4–8 minutes irradiation, followed by a final irradiation interval of 5 minutes. Emission spectra were recorded after every irradiation interval. The samples were then allowed to thermally decay inside the fluorometer, and emission spectra were recorded in regular time intervals.

2.6 Appendix

Characterization and Supplemental Information for Chapter 2

2.6.1 General Information.....48

2.6.2 ^{1}H and ^{13}C NMR Spectra for **SP1–SP5**.....49

2.6.3 UV-vis Spectra and Thermal Decay Kinetic Plots for **SP1–SP5**.....54

2.6.4 Powder X-ray Diffraction Analysis of **SP2–SP4**.....59

2.6.5 Dynamic Light Scattering Analysis for **SP1–SP5**.....60

2.6.6 Fluorescence Spectra for **SP1**.....63

2.6.1 General Information

^{1}H and ^{13}C NMR spectra were acquired on a Bruker Avance spectrometer at 500 MHz (^{1}H) and 125 MHz (^{13}C). All chemical shifts are reported in ppm on the δ-scale relative to the residual solvent signal as reference ($CDCl_3$ δ 7.26 and δ 77.16 for proton and carbon, respectively, CD_3CN δ 1.94 for proton and δ 1.32, 118.26 for carbon). UV-Vis absorption and transmission spectra were recorded on Ocean Optics spectrometer (DT-MINI-2-GS UV-VIS-NIR LightSource and USB2000+ using SpectraSuite software package). Dynamic Light Scattering (DLS) data were recorded using a Beckman-Coulter N4 Plus particle analyzer with a 10 mW helium-neon laser at 632.8 nm. The particle size was determined using the 62.6° detection angle and was calculated using the size distribution processor (SDP) analysis package provided by the manufacturer. Powder X-ray diffraction measurements were performed on a flat stage using a PANalytical Inc. X'Pert Pro Cu K-a = 1.5406 Å radiation at power settings of 45 kV and 40 mA and a slit width of 0.5°. Data were collected at room temperature in the range of 2θ = 4–45°. All samples were irradiated using a Rayonet photochemical reactor with four 12 inch 8W (BLE-8T365) 365 nm bulbs. Fluorescence spectra were acquired using an Edinburgh Instruments FLSP920 spectrometer equipped with a 450 W xenon arc lamp (Xe900) as the light source, a single photon counting PMT as the detector, and the F900 software program.

2.6.2 ^{1}H and ^{13}C NMR Spectra for SP1–SP5

^{1}H NMR of **SP1** in $CDCl_3$ at 500 MHz

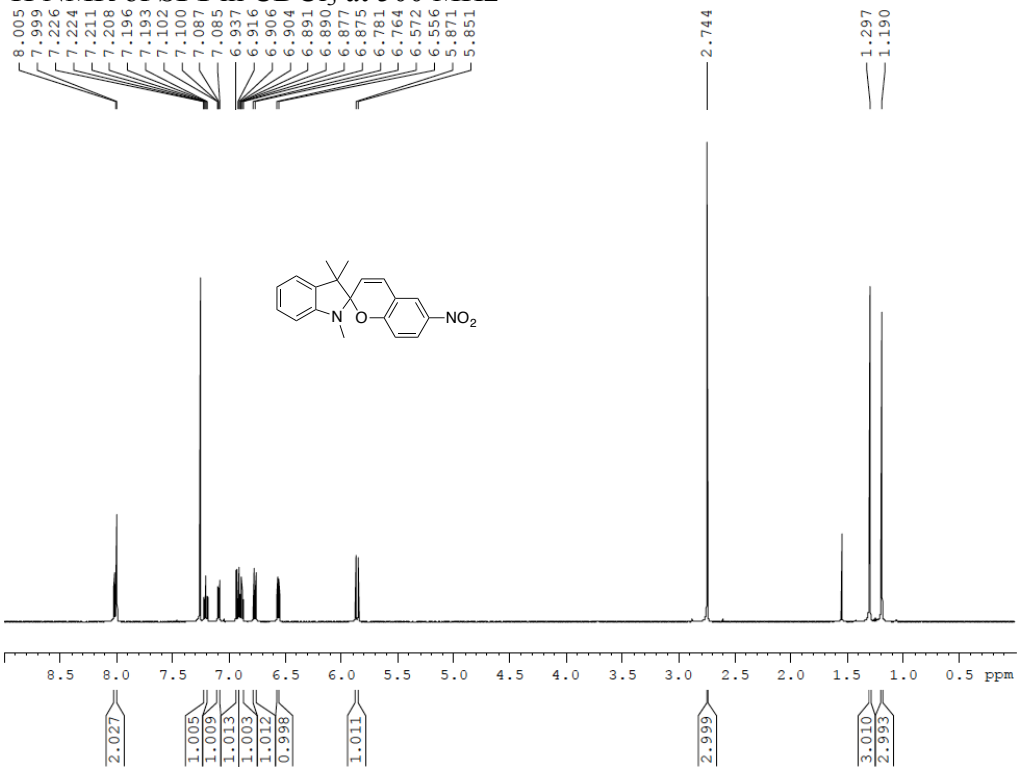

^{13}C NMR of **SP1** in $CDCl_3$ at 125 MHz

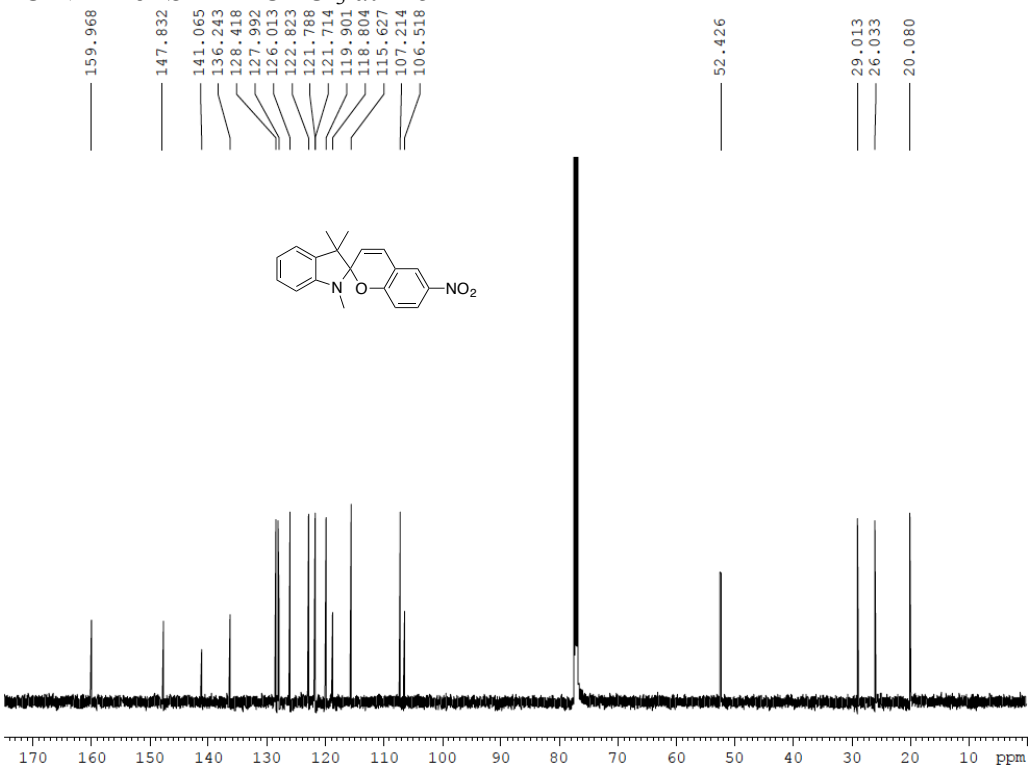

^{1}H NMR of **SP2** in $CDCl_3$ at 500 MHz

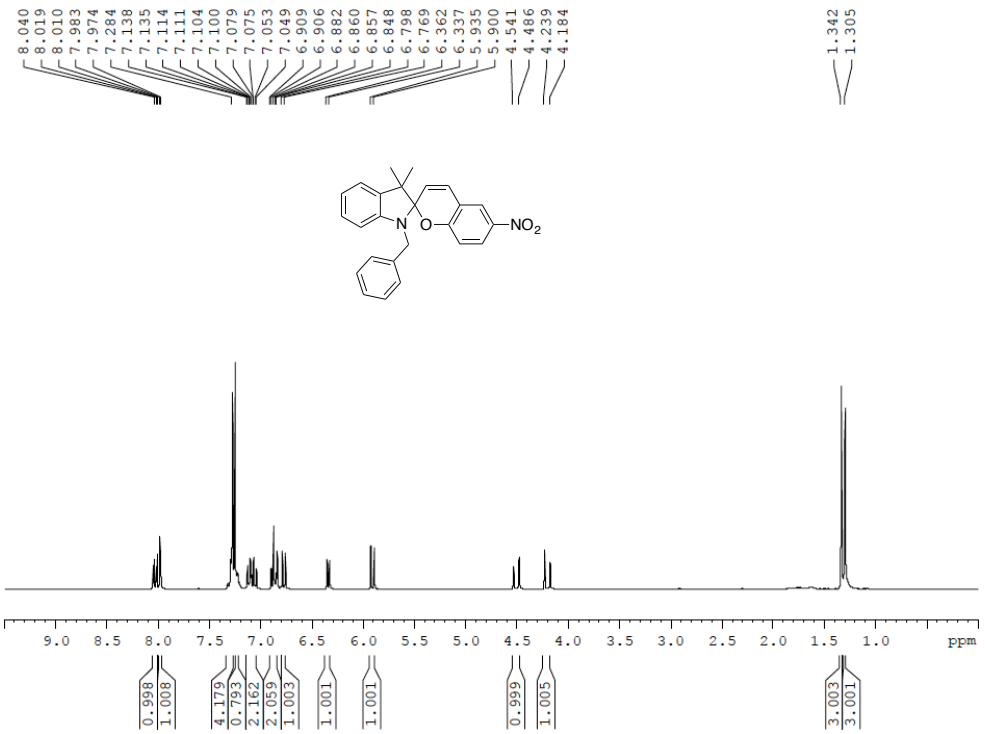

^{13}C NMR of **SP2** in $CDCl_3$ at 125 MHz

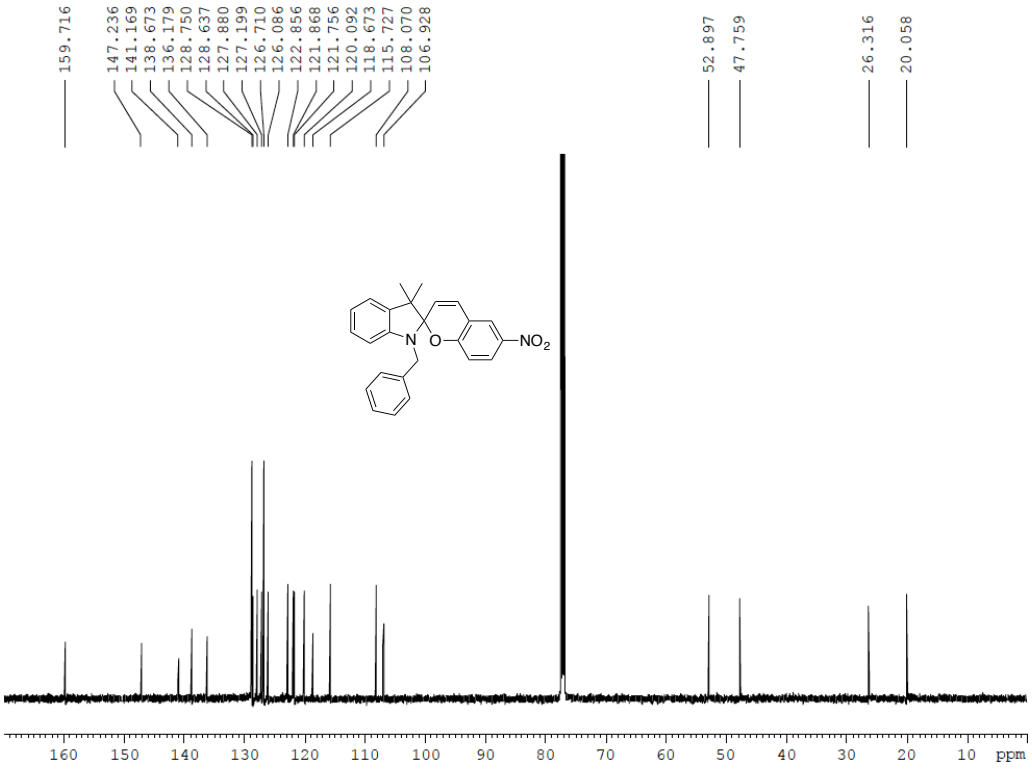

^{1}H NMR of **SP3** in $CDCl_3$ at 500 MHz

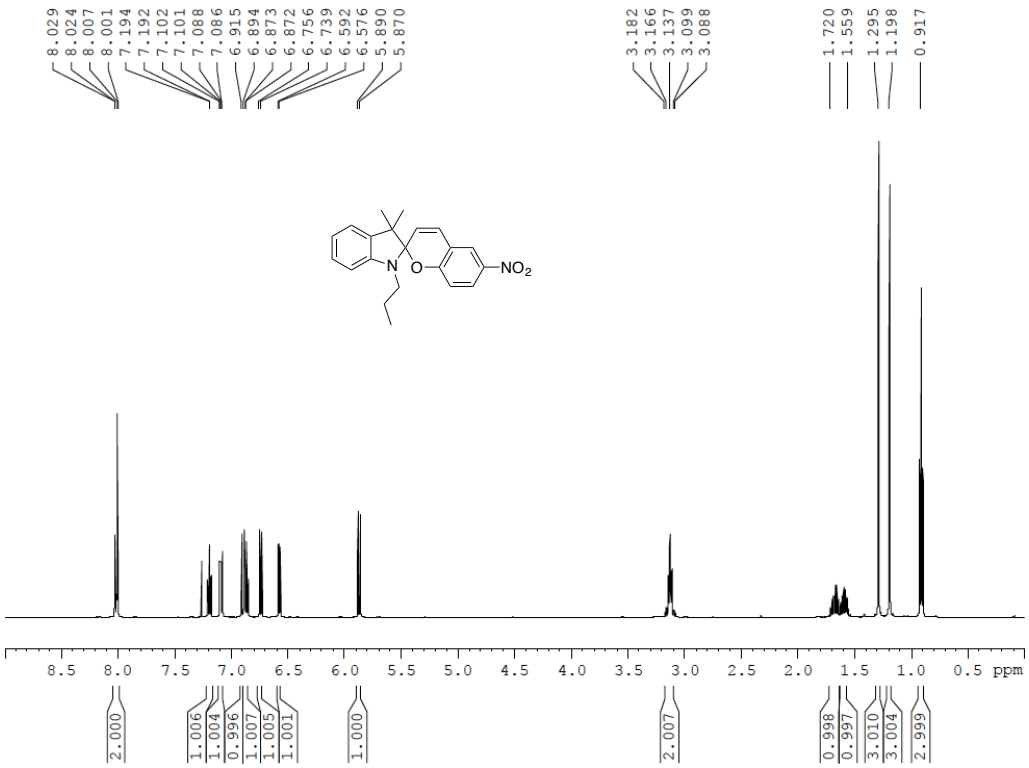

^{13}C NMR of **SP3** in $CDCl_3$ at 125 MHz

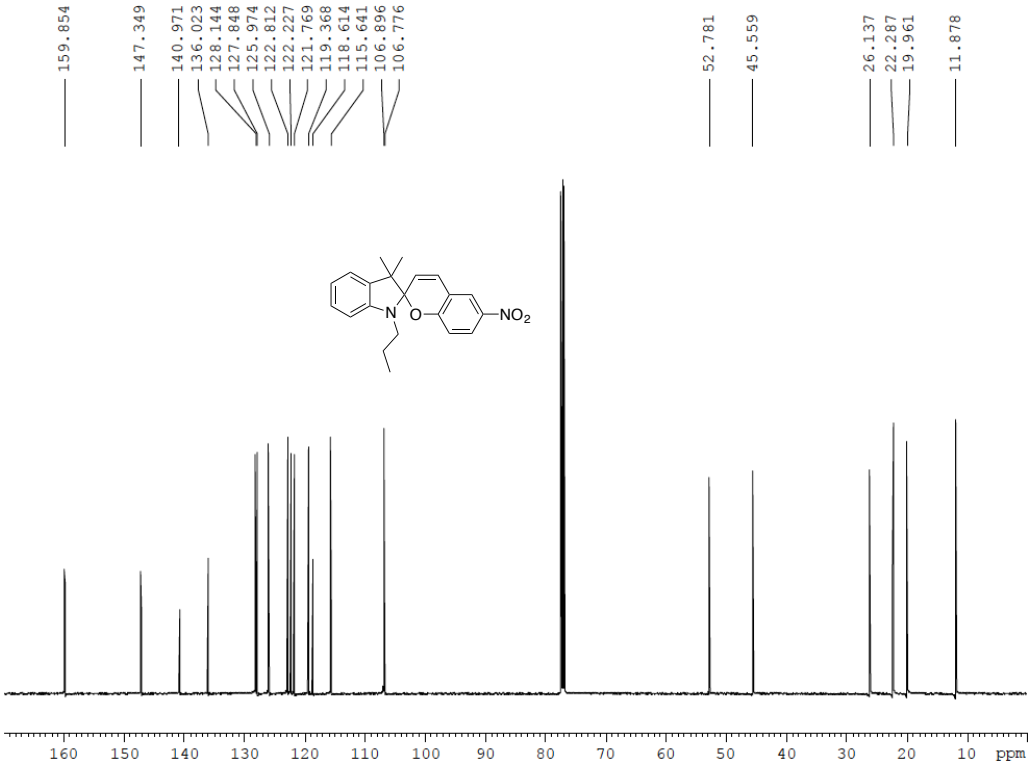

^{1}H NMR of **SP4** in $CDCl_3$ at 500 MHz

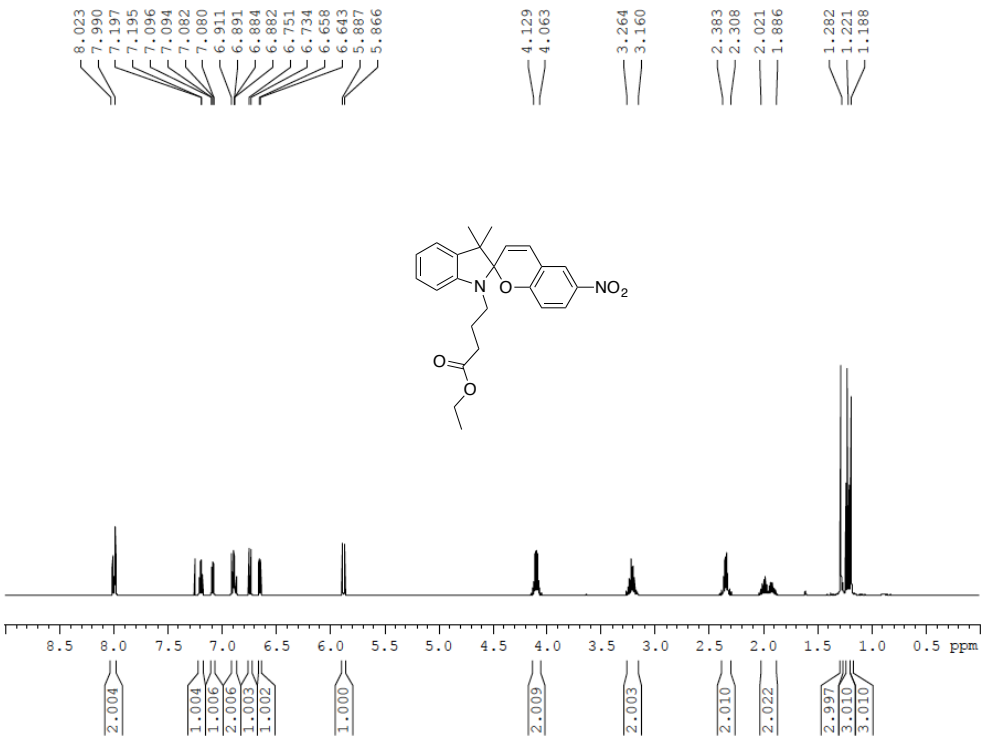

^{13}C NMR of **SP4** in $CDCl_3$ at 125 MHz

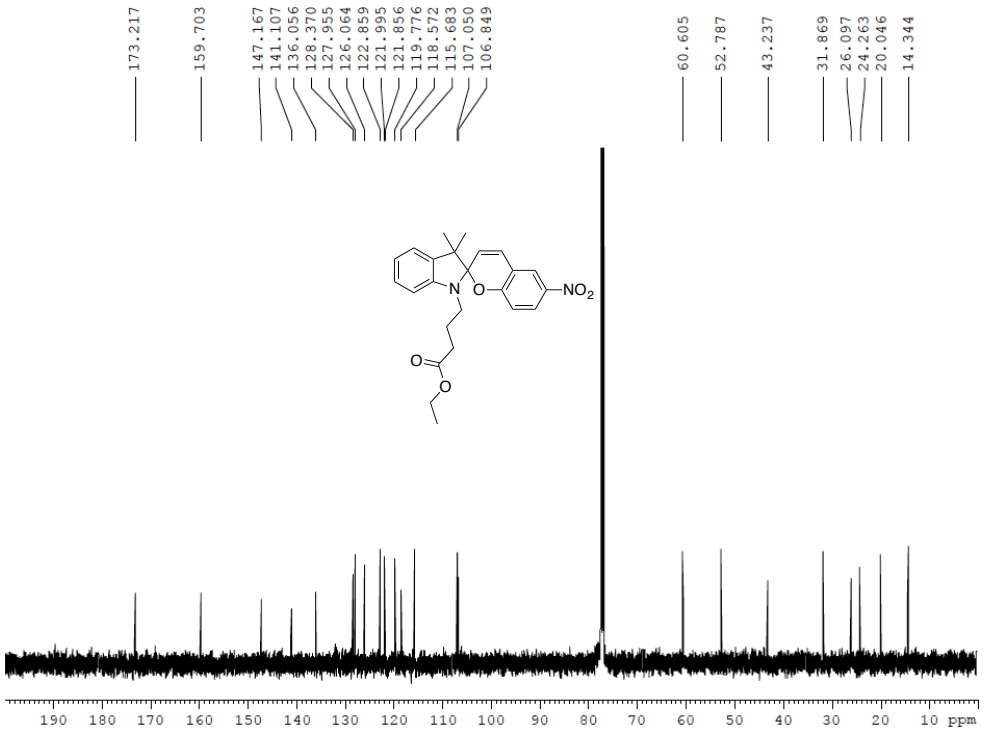

^{1}H NMR of **SP5** in CD_3CN at 500 MHz

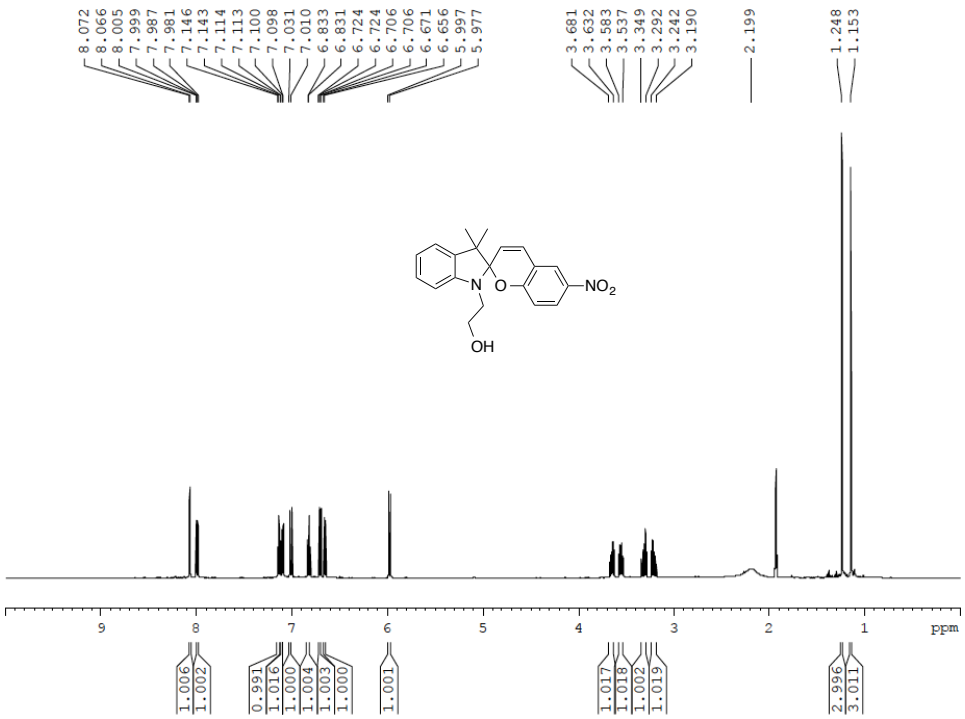

^{13}C NMR of **SP5** in CD_3CN at 125 MHz

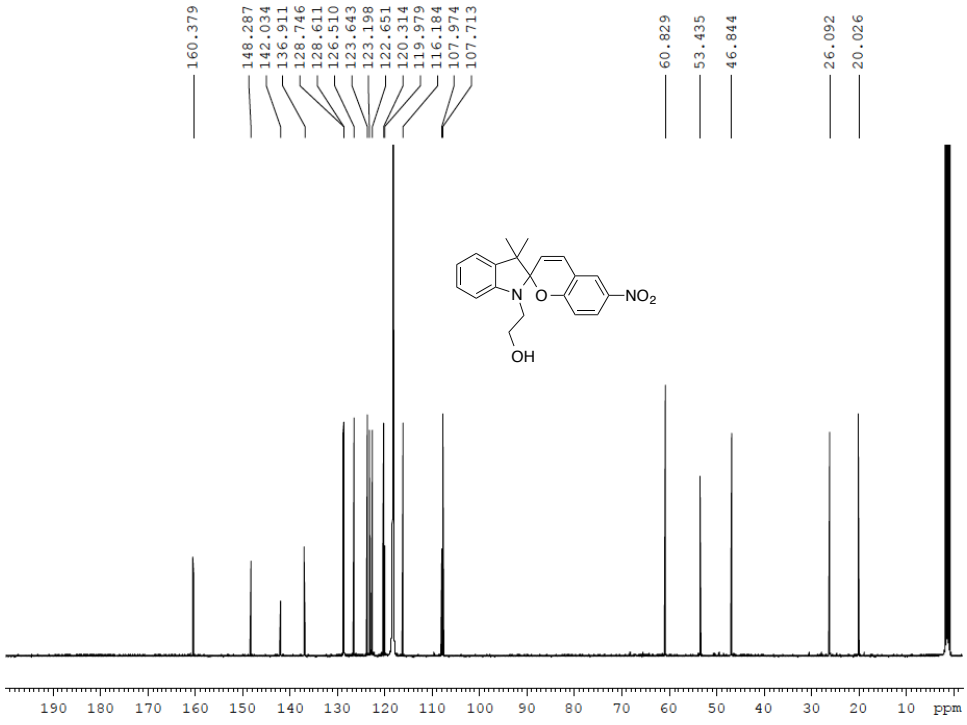

2.6.3 UV-vis Spectra and Thermal Decay Kinetic Plots for SP1–SP5

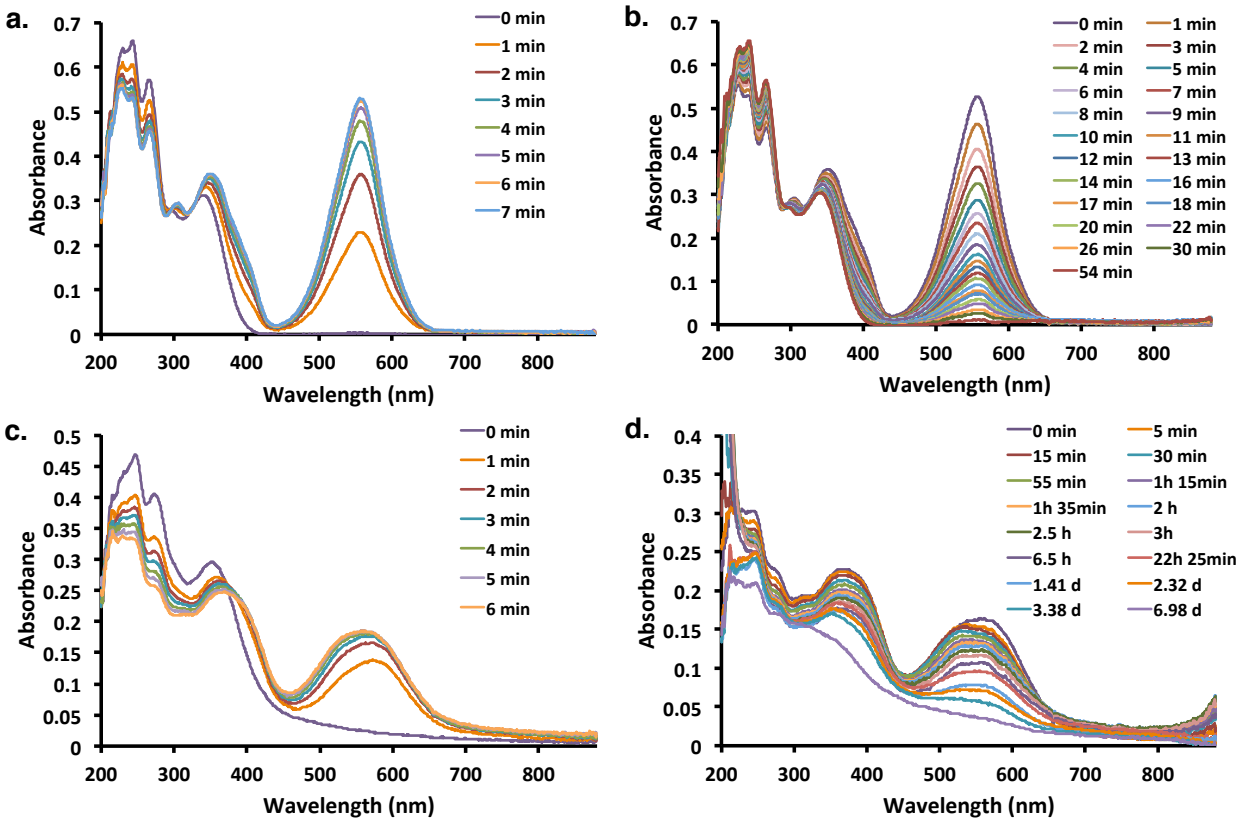

Figure 2.6.3.1. UV-vis absorption spectra for **SP1** a) irradiation at 365 nm in MeCN, b) thermal decay at 557 nm in MeCN, c) irradiation at 365 nm in nanocrystalline suspension, and d) thermal decay at 557 nm in nanocrystalline suspension.

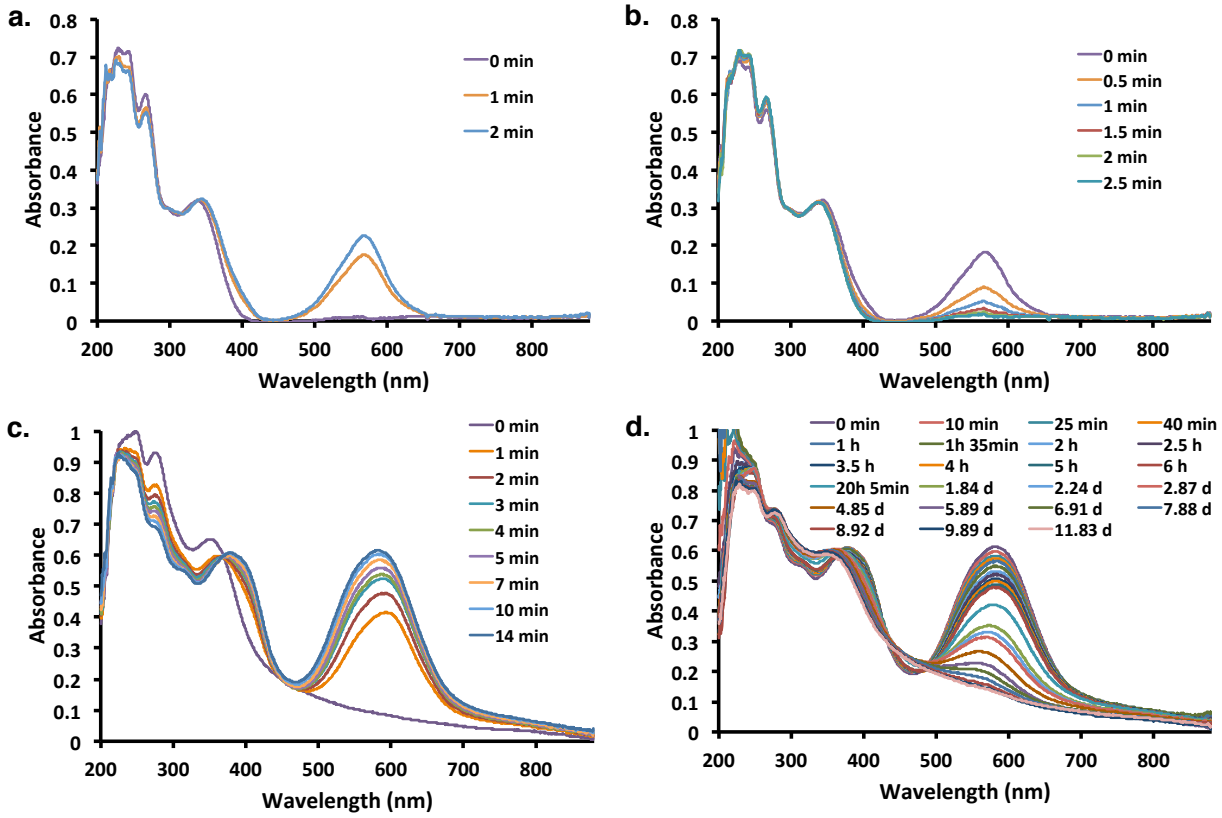

Figure 2.6.3.2. UV-vis absorption spectra for **SP2** a) irradiation at 365 nm in MeCN, b) thermal decay at 566 nm in MeCN, c) irradiation at 365 nm in nanocrystalline suspension, and d) thermal decay at 582 nm in nanocrystalline suspension.

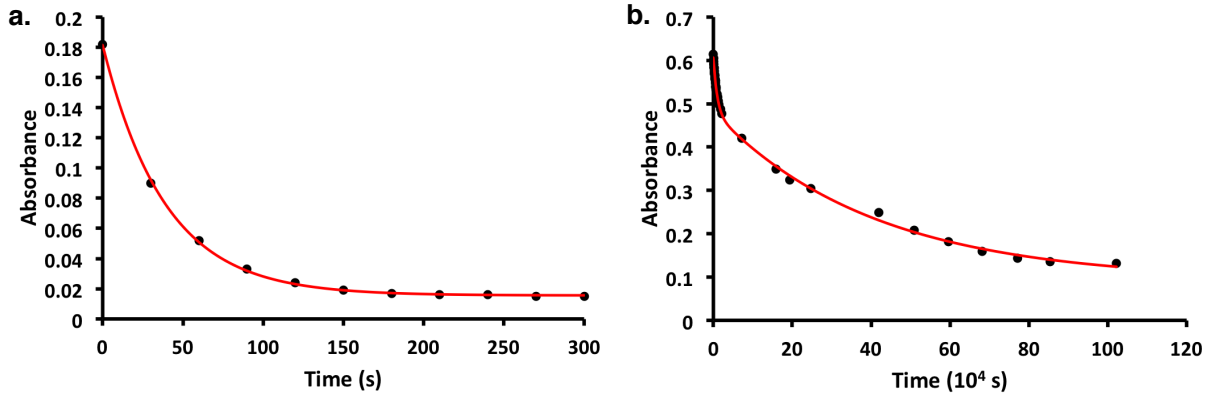

Figure 2.6.3.3. Thermal decay kinetic plots with trendline (red line) for **SP2** a) at 566 nm in MeCN and b) at 582 nm in NC suspension.

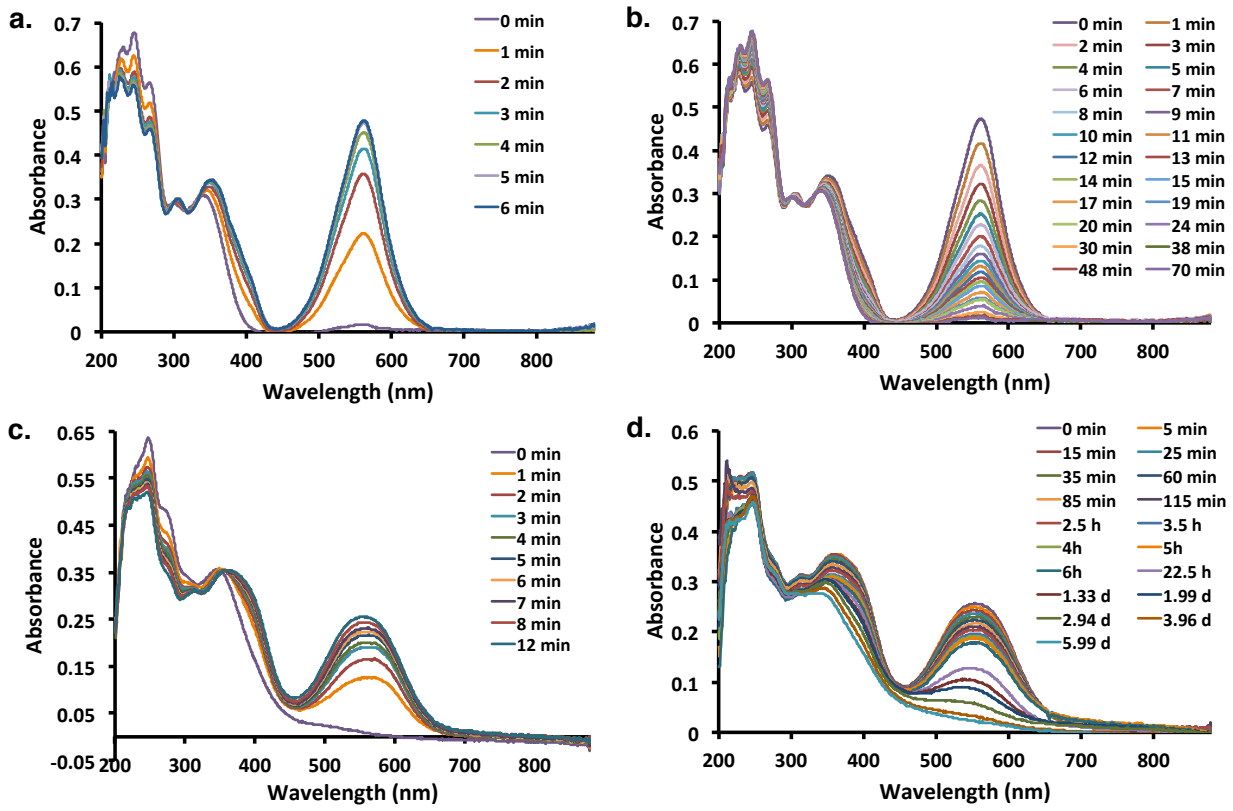

Figure 2.6.3.4. UV-Vis absorption spectra for **SP3** a) irradiation at 365 nm in MeCN, b) thermal decay at 561 nm in MeCN, c) irradiation at 365 nm in nanocrystalline suspension, and d) thermal decay at 554 nm in nanocrystalline suspension.

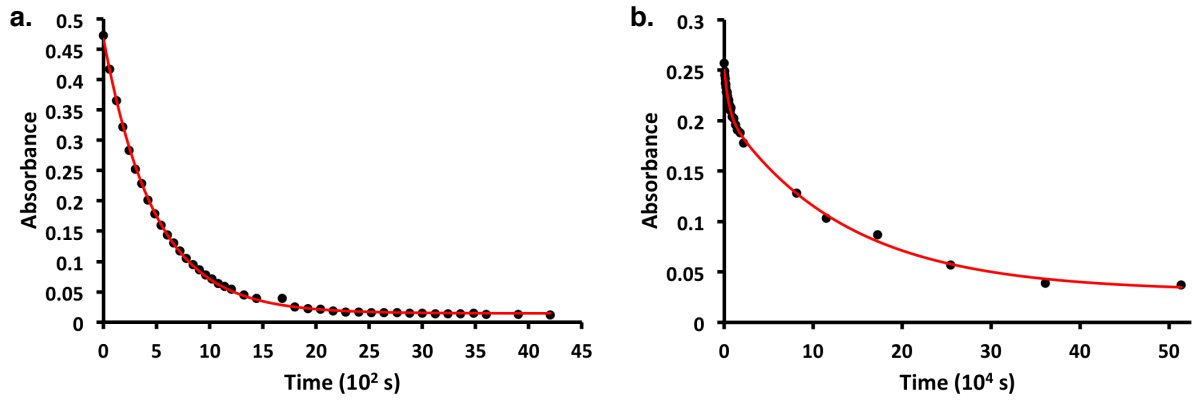

Figure 2.6.3.5. Thermal decay kinetic plots with trendline (red line) for **SP3** a) at 561 nm in MeCN and b) at 554 nm in NC suspension.

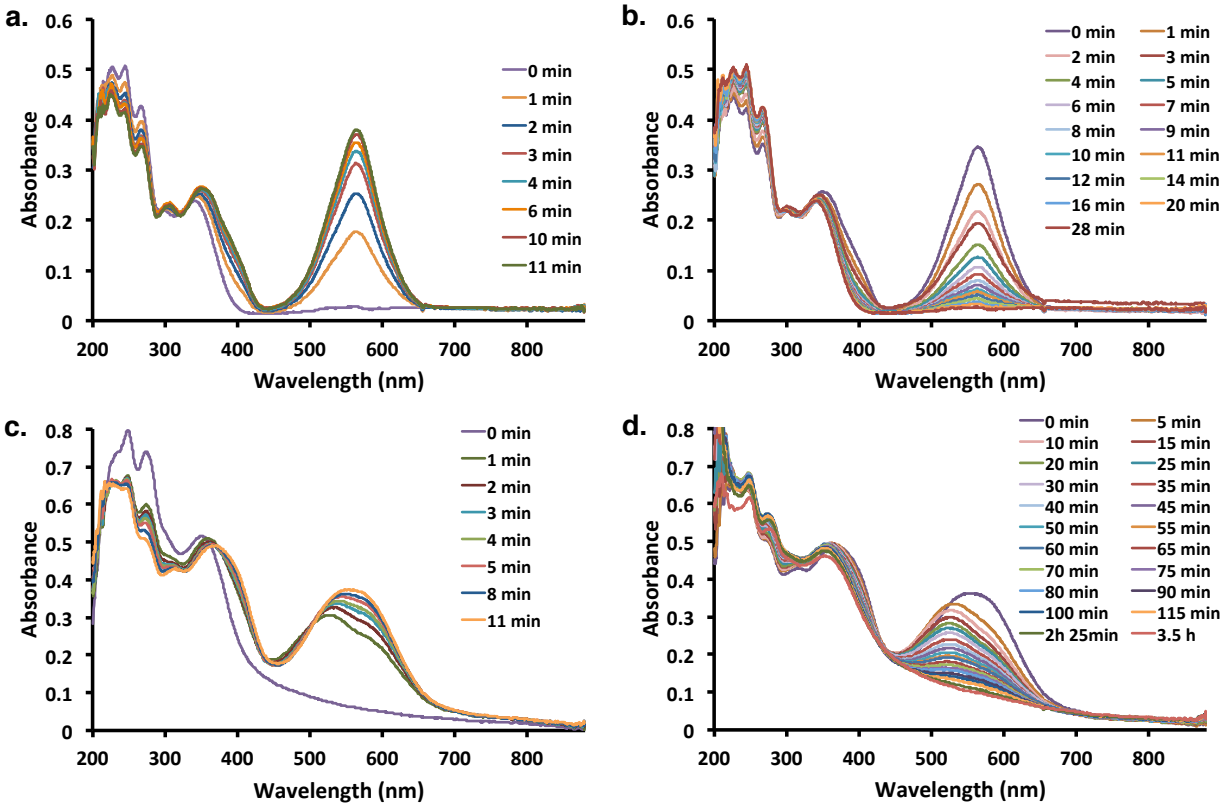

Figure 2.6.3.6. UV-Vis absorption spectra for **SP4** a) irradiation at 365 nm in MeCN, b) thermal decay at 564 nm in MeCN, c) irradiation at 365 nm in nanocrystalline suspension, and d) thermal decay at 552 nm in nanocrystalline suspension.

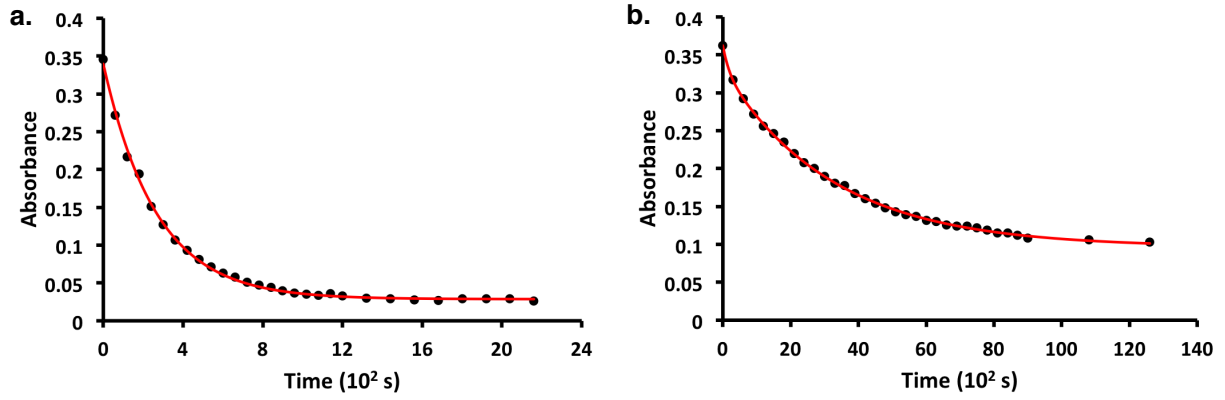

Figure 2.6.3.7. Thermal decay kinetic plots with trendline (red line) for **SP4** a) at 564 nm in MeCN and b) at 552 nm in NC suspension.

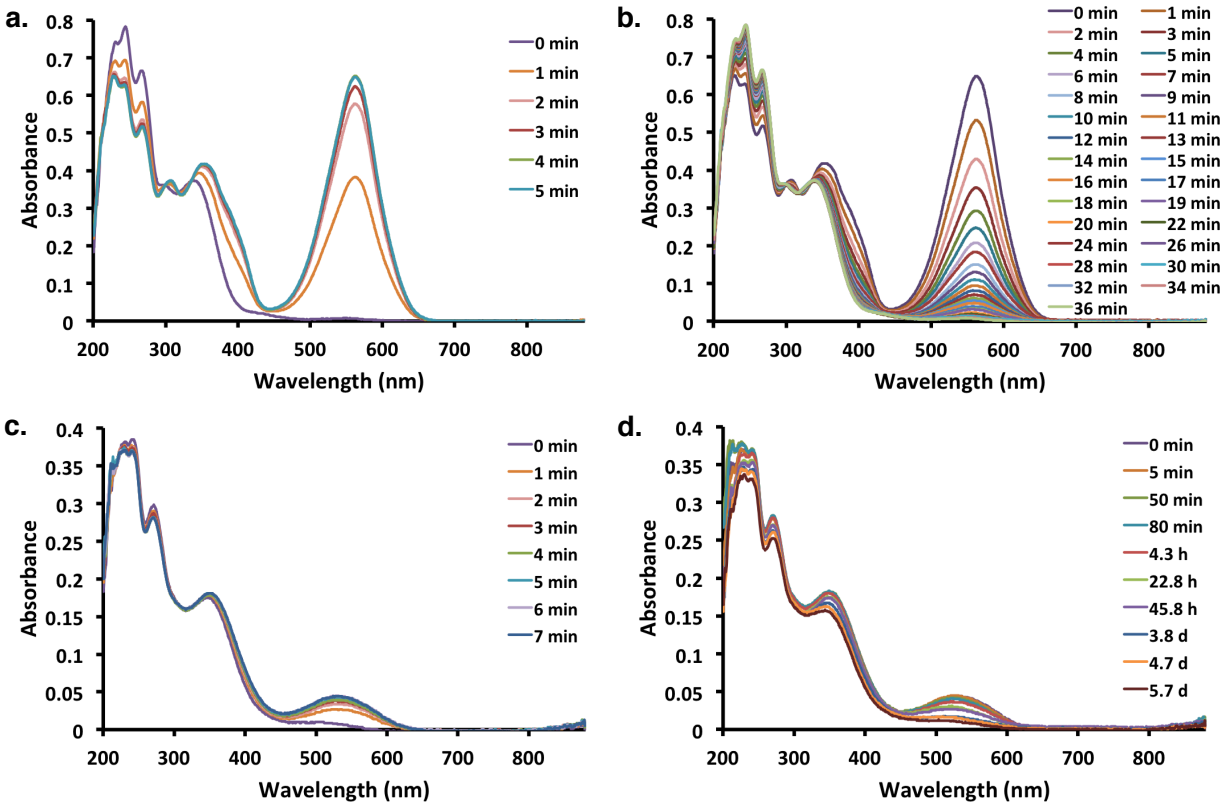

Figure 2.6.3.8. UV-Vis absorption spectra for **SP5** a) irradiation at 365 nm in MeCN, b) thermal decay at 562 nm in MeCN, and c) irradiation at 365 nm in nanocrystalline suspension, and d) thermal decay at 531 nm in nanocrystalline suspension.

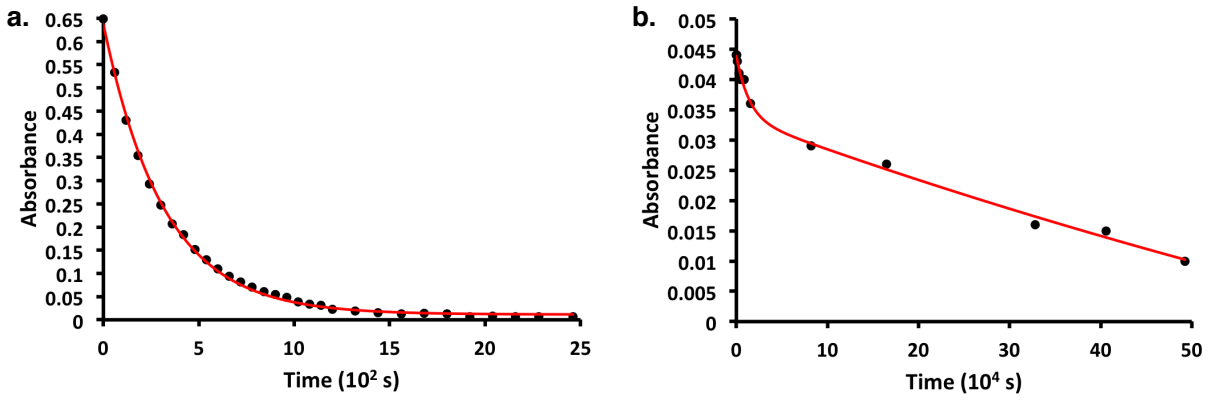

Figure 2.6.3.9. Thermal decay kinetic plots with trendline (red line) for **SP5** a) at 562 nm in MeCN and b) at 531 nm in NC suspension.

2.6.4 Powder X-ray Diffraction Analysis of SP2–SP4

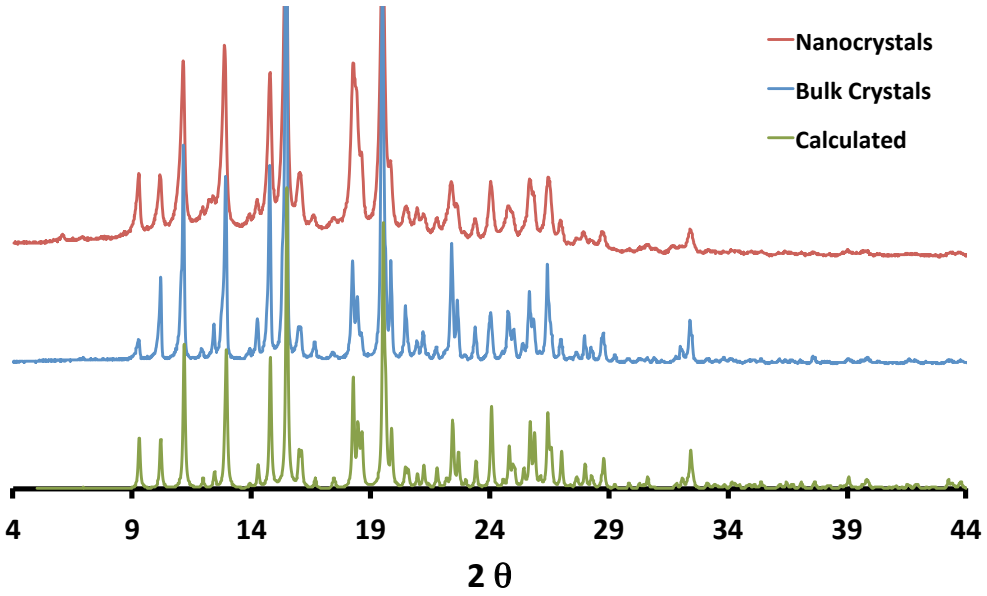

Figure 2.6.4.1. PXRD comparison of experimentally obtained nanocrystals (top, red) and bulk crystals (middle, blue) to the calculated (bottom, green) diffractogram from the CSD for **SP2**.

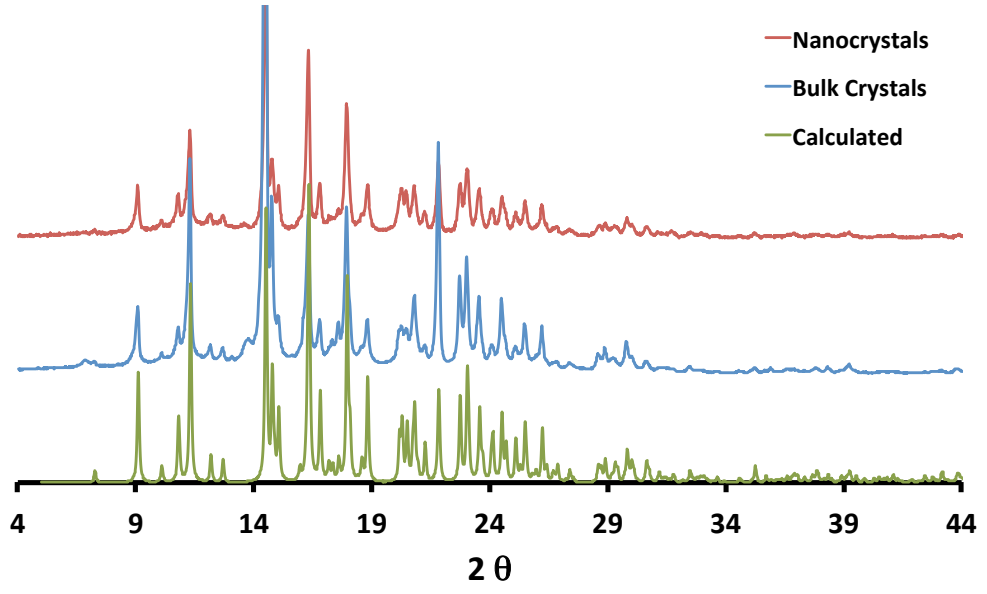

Figure 2.6.4.2. PXRD comparison of experimentally obtained nanocrystals (top, red) and bulk crystals (middle, blue) to the calculated (bottom, green) diffractogram from the CSD for **SP3**.

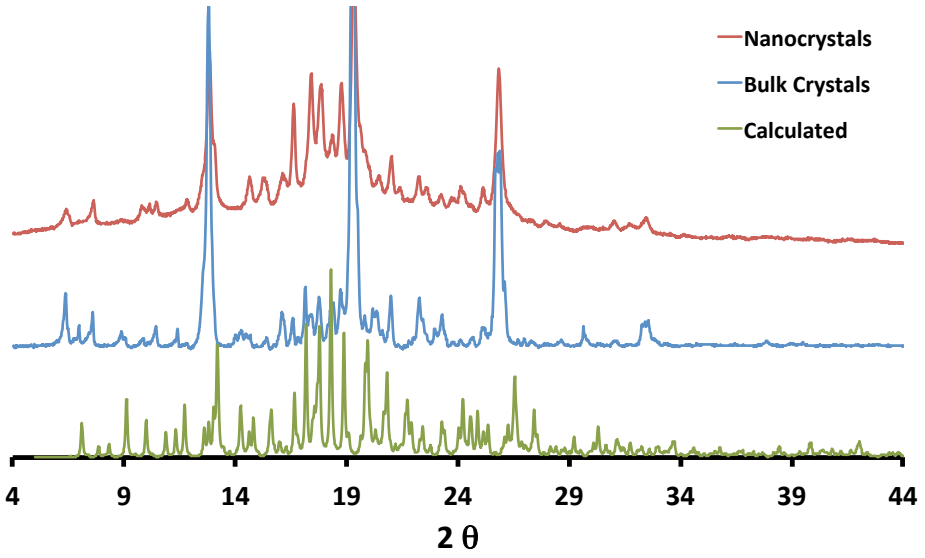

Figure 2.6.4.3. PXRD comparison of experimentally obtained nanocrystals (top, red) and bulk crystals (middle, blue) to the calculated (bottom, green) diffractogram from the CSD for **SP4**.

2.6.5 Dynamic Light Scattering Analysis for SP1–SP5

Unimodal Results Summary

Rept#.	Mean (nm)	Std.Dev (nm)	Baseline Error	P.I.	Counts/s	Diff.Coef (m^2/s)	Overflow
Rept.1	224.5	87.0	0.02%	0.188	3.77e+05	2.02e-12	0
Rept.2	234.6	77.5	0.01%	0.097	3.69e+05	1.93e-12	0
Rept.3	236.8	86.2	0.04%	0.141	3.55e+05	1.91e-12	0
Average	232.0	83.54		0.142			

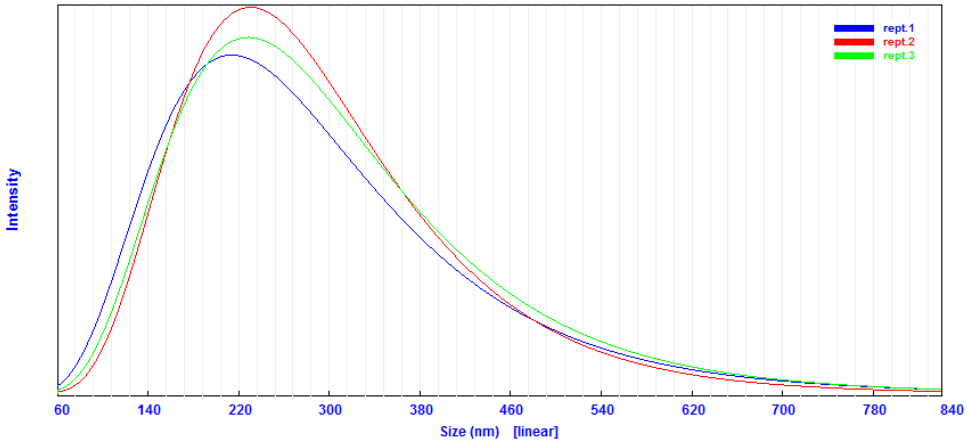

Figure 2.6.5.1. Dynamic light scattering results for the nanocrystals of **SP1** dispersed in water showing the average particle size to be 232 nm.

Unimodal Results Summary

Rept#.	Mean (nm)	Std.Dev (nm)	Baseline Error	P.I.	Counts/s	Diff.Coef (m^2/s)	Overflow
Rept.1	223.4	88.6	-0.00%	0.212	1.59e+06	2.03e-12	0
Rept.2	223.6	90.6	0.00%	0.239	1.58e+06	2.02e-12	0
Rept.3	224.9	87.4	0.00%	0.190	1.58e+06	2.01e-12	0
Average	224.0	88.86		0.214			

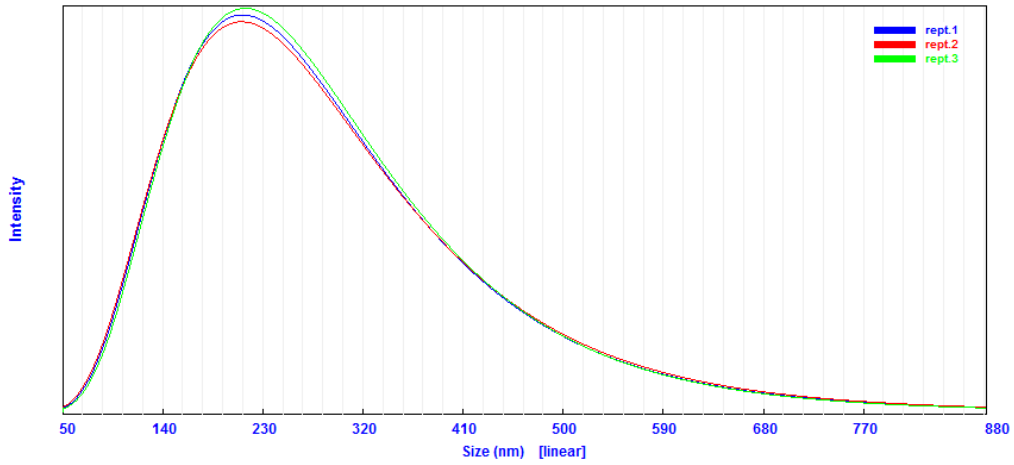

Figure 2.6.5.2. Dynamic light scattering results for the nanocrystals of **SP2** dispersed in water showing the average particle size to be 224 nm.

Unimodal Results Summary

Rept#.	Mean (nm)	Std.Dev (nm)	Baseline Error	P.I.	Counts/s	Diff.Coef (m^2/s)	Overflow
Rept.1	181.7	63.5	0.00%	-0.119	6.59e+05	2.49e-12	0
Rept.2	182.0	68.7	0.01%	0.165	6.85e+05	2.49e-12	0
Rept.3	189.9	60.8	0.01%	0.087	7.17e+05	2.38e-12	0
Average	184.5	64.32		0.044			

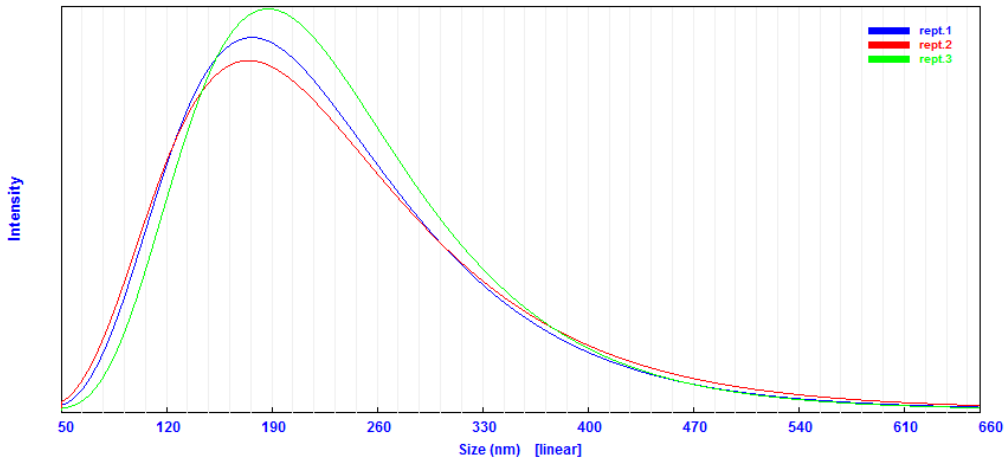

Figure 2.6.5.3. Dynamic light scattering results for the nanocrystals of **SP3** dispersed in water showing the average particle size to be 184 nm.

Unimodal Results Summary

Rept#.	Mean (nm)	Std.Dev (nm)	Baseline Error	P.I.	Counts/s	Diff.Coef (m^2/s)	Overflow
Rept.1	160.8	56.3	0.14%	0.121	4.46e+05	2.82e-12	0
Rept.2	171.2	54.0	0.06%	0.083	5.04e+05	2.64e-12	0
Rept.3	178.8	43.2	0.03%	0.038	5.46e+05	2.53e-12	0
Average	170.2	51.17		0.080			

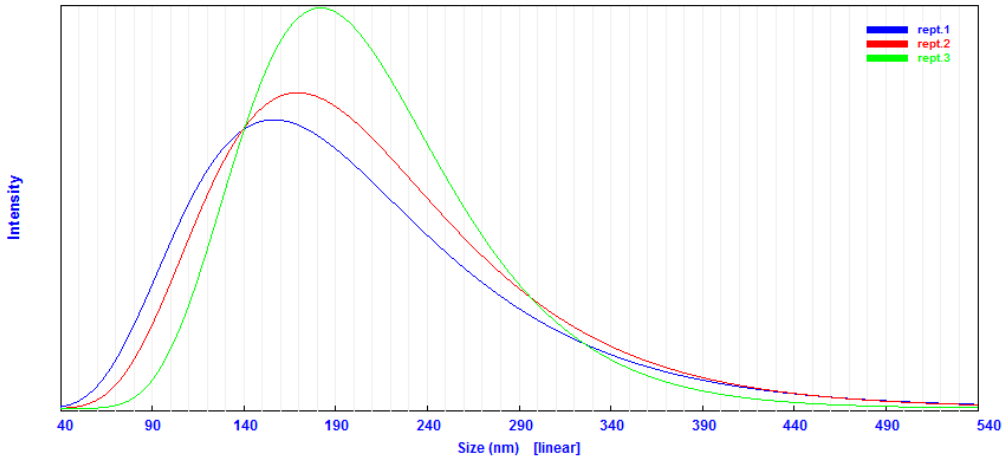

Figure 2.6.5.4. Dynamic light scattering results for the nanocrystals of **SP4** dispersed in water showing the average particle size to be 170 nm.

Unimodal Results Summary

Rept#.	Mean (nm)	Std.Dev (nm)	Baseline Error	P.I.	Counts/s	Diff.Coef (m^2/s)	Overflow
Rept.1	238.3	103.0	4.13%	0.371	2.27e+05	1.90e-12	0
Rept.2	246.9	109.5	3.33%	0.463	2.22e+05	1.83e-12	0
Rept.3	225.4	100.5	0.27%	0.486	2.04e+05	2.01e-12	0
Average	236.9	104.37		0.440			

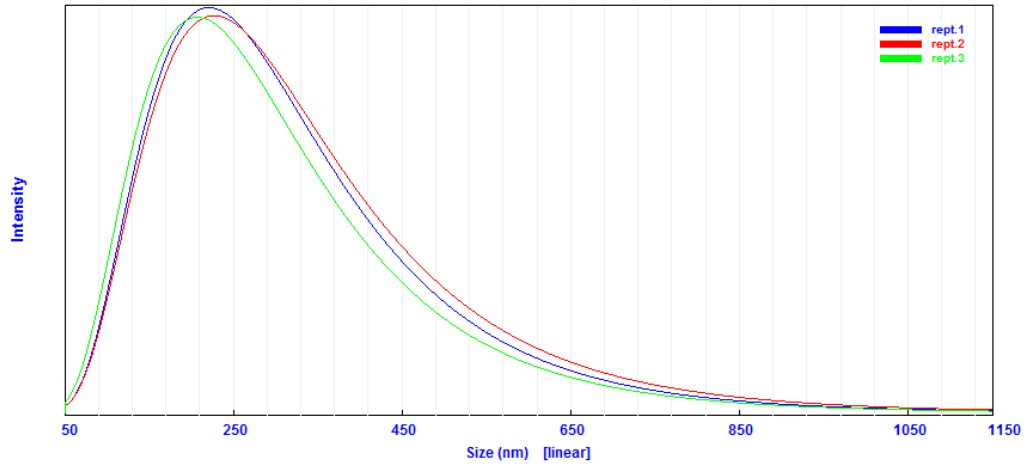

Figure 2.6.5.5. Dynamic light scattering results for the nanocrystals of **SP5** dispersed in water showing the average particle size to be 237 nm.

2.6.6 Fluorescence Spectra for SP1

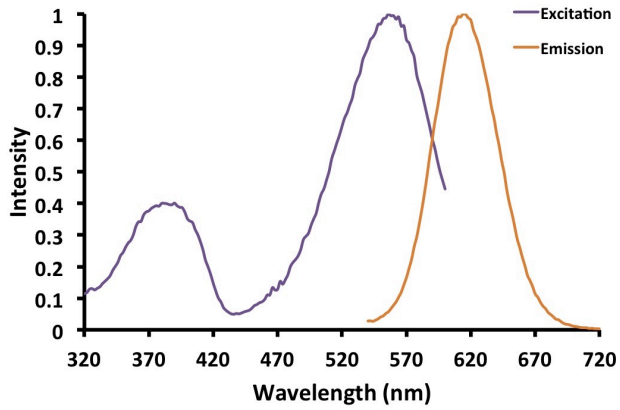

Figure 2.6.6.1. Normalized excitation and emission spectra for **SP1** in acetonitrile post 365 nm irradiation. Excitation and emission spectra were acquired using an emission wavelength of 612 nm and an excitation wavelength of 530 nm, respectively.

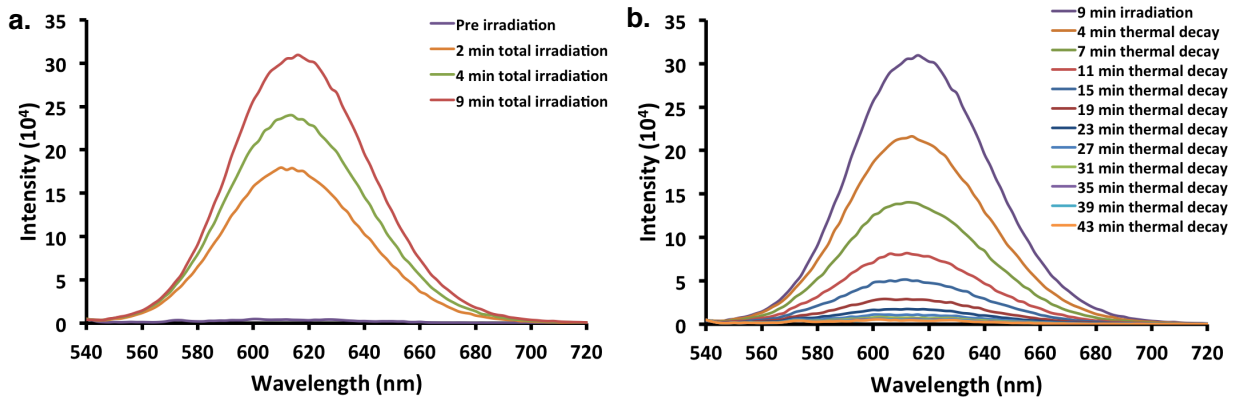

Figure 2.6.6.2. Emission spectra for **SP1** in acetonitrile using an excitation wavelength of 530 nm a) pre irradiation and post 2, 4, and 9 min irradiations at 365 nm and b) thermal decay of the merocyanine over time.

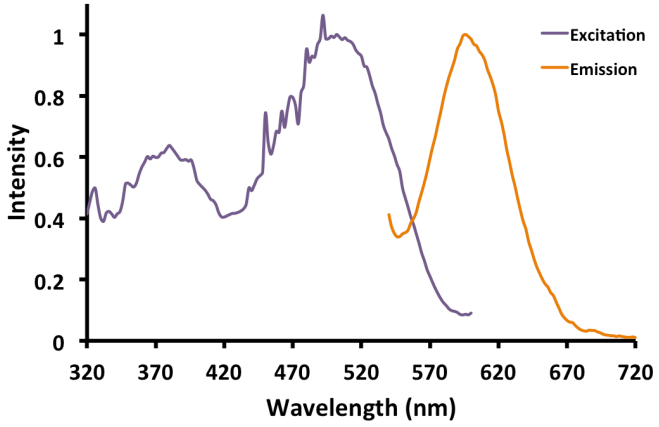

Figure 2.6.6.3. Normalized excitation and emission spectra for **SP1** in nanocrystalline suspension post 365 nm irradiation. Excitation and emission spectra were acquired using an emission wavelength of 612 nm and an excitation wavelength of 530 nm, respectively.

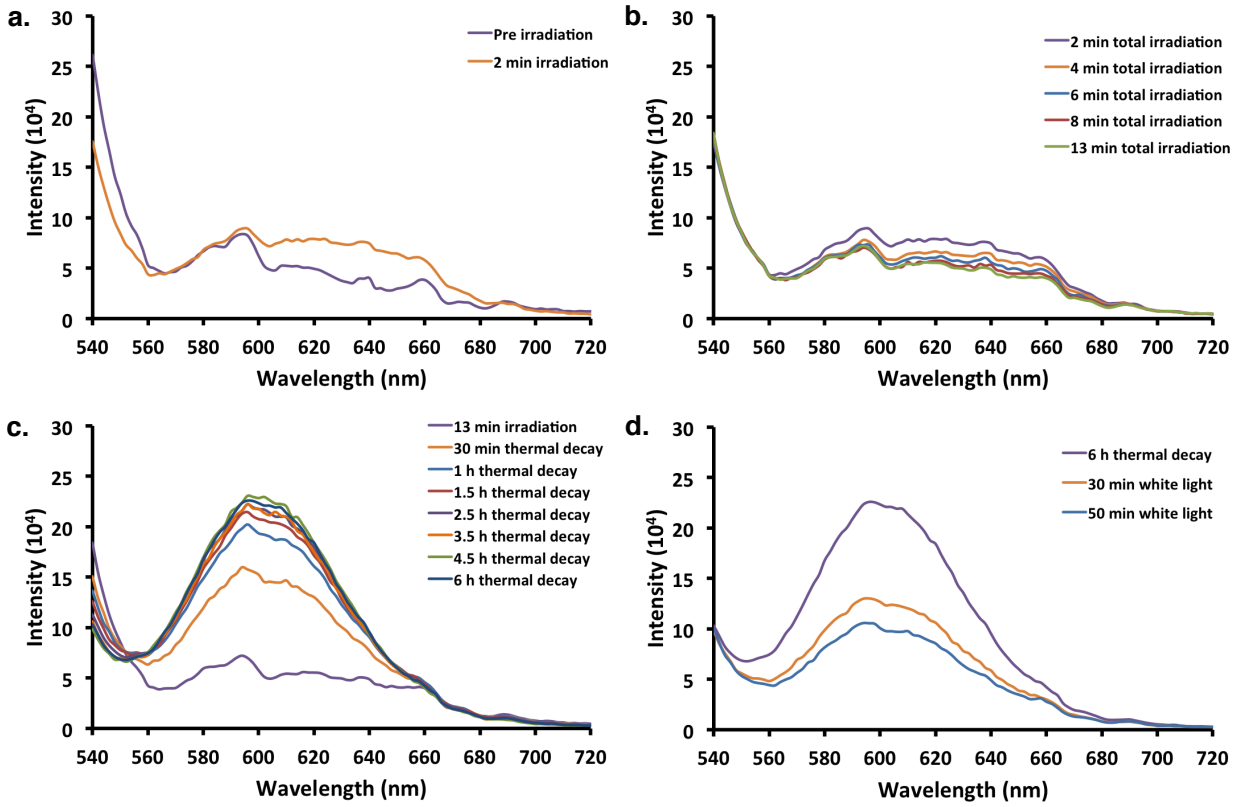

Figure 2.6.6.4. Emission spectra for **SP1** in nanocrystalline suspension using an excitation wavelength of 530 nm a) pre irradiation and post 2 min irradiation at 365 nm, b) repeated

irradiations at 365 nm, c) fluorescence signal intensity increase during the thermal decay of the merocyanine over time, and d) white light induced decay of the merocyanine.

2.7 References

1. Berkovic, F.; Krogauz, V.; Weiss, V. *Chem. Rev.* **2000**, *100*, 1741–1753.

2. Klajn, R. *Chem. Soc. Rev.* **2014**, *43*, 148–184.

3. Meng, X.; Qi, G.; Zhang, C.; Wang, K.; Zou, B.; Ma, Y. *Chem. Commun.* **2015**, *51*, 9320–9323.

4. Gentili, P. L.; Nocchetti, M.; Miliani, C.; Favaro, G. *New J. Chem.* **2004**, *28*, 379–386.

5. Wojtyk, J. T. C.; Wasey, A.; Xiao, N.-N.; Kazmaier, P. M.; Hoz, S.; Yu, C.; Lemieux, R. P.; Buncel, E. *J. Phys. Chem. A* **2007**, *111*, 2511–2516.

6. Guglielmetti, R. 4n+2 Systems: Spiropyrans. In *Photochromism: Molecules and Systems*; Dürr, H.; Bouas-Laurent, H., Eds.; Elsevier: Amsterdam, 2003; p 314.

7. Irie, M *Chem. Rev.* **2000**, *100*, 1683–1684.

8. Irie, M.; Yokoyama, Y.; Seki, T., Eds.; *New Frontiers in Photochromism*; Springer: Tokyo, 2013.

9. Fischer, E.; Hirshberg, Y. *J. Chem. Soc.* **1952**, 4522–4524.

10. Bénard, S.; Yu, P. *Adv. Mater.* **2000**, *12*, 48–50.

11. Asahi, T.; Masuhara, H. *Chem. Lett.* **1997**, *26*, 1165–1166.

12. Suzuki, M.; Asahi, T.; Masuhara, H. *Mol. Cryst. Liq. Cryst.* **2000**, *345*, 51–56.

13. Suzuki, M.; Asahi, T.; Masuhara, H. *Phys. Chem. Chem. Phys.* **2002**, *4*, 185–192.

14. Asahi, T.; Suzuki, M.; Masuhara, H. *J. Phys. Chem. A* **2002**, *106*, 2335–2340.

15. Suzuki, M.; Asahi, T.; Masuhara, H. *Chem. Phys. Chem.* **2005**, *6*, 2396–2403.

16. Harada, J.; Kawazoe, Y.; Ogawa, K. *Chem. Commun.* **2010**, *46*, 2593–2595.

17. Godsi, O.; Peskin, U.; Kapon, M.; Natan, E.; Eichen, Y. *Chem. Commun.* **2001**, 2132–2133.

18. Naumov, P.; Yu, P.; Sakurai, K. *J. Phys. Chem. A* **2008**, *112*, 5810–5814.

19. Chin, K. K.; Natarajan, A.; Gard, M. N.; Campos, L. M.; Shepard, H.; Johansson, E.; Garcia-Garibay, M. A. *Chem. Commun.* **2007**, 4266–4268.

20. Kuzmanich, G.; Simoncelli, S.; Gard, M. N.; Spänig, F.; Henderson, B. L.; Guldi, D. M.; Garcia-Garibay, M. A. *J. Am. Chem. Soc.* **2011**, *133*, 17296–17306.

21. Kuzmanich, G.; Vogelsberg, C. S.; Maverick, E. F.; Netto-Ferreira, J. C.; Scaiano, J. C.; Garcia-Garibay, M. A. *J. Am. Chem. Soc.* **2012**, *134*, 1115–1123.

22. Ayitou, A. J.-L.; Flynn, K.; Jockusch, S.; Khan, S. I.; Garcia-Garibay, M. A. *J. Am. Chem. Soc.* **2016**, *138*, 2644–2648.

23. Kasai, H.; Nalwa, H. S.; Oikawa, H.; Okada, S.; Matsuda, H.; Minami, N.; Kakuta, A.; Ono, K.; Mukoh, A.; Nakanishi, H. *Jpn. J. Appl. Phys.* **1992**, *31*, L1132–L1134.

24. Clegg, W.; Norman, N. C.; Flood, T.; Sallans, L.; Kwak, W. S.; Kwiatkowski, P. L.; Lasch, J. G. *Acta Cryst.* **1991**, *C47*, 817–824.

25. Karaev, K. S.; Furmanova, N. G. *Zh. Strukt. Khim.* **1984**, *25*, 185–188.

26. Aakeröy, C. B.; Hurley, E. P.; Desper, J.; Natali, M.; Douglawi, A.; Giordani, S. *Cryst. Eng. Comm.* **2010**, *12*, 1027–1033.

27. Raymo, F. M.; Giordani, S.; White, A. J. P.; Williams, D. J. *J. Org. Chem.* **2003**, *68*, 4158–4169.

28. Wu, Y.; Sasaki, T.; Kazushi, K.; Seo, T.; Sakurai, K. *J. Phys. Chem. B* **2008**, *112*, 7530–7536.

29. Oushiki, D.; Kojima, H.; Terai, T.; Arita, M.; Hanaoka, K.; Urano, Y.; Nagano, T. *J. Am. Chem. Soc.* **2010**, *132*, 2795–2801.

30. Roxburgh, C. J.; Sammes, P. G.; Abdullah, A. *Dyes and Pigments* **2011**, *90*, 146–162.

31. Bénard, S.; Yu, P. *Chem. Commun.* **2000**, 65–66.

32. Whelan, J.; Abdallah, D.; Wojtyk, J.; Buncel, E. *J. Mater. Chem.* **2010**, *20*, 5727–5735.

33. Spagnoli, S.; Block, D.; Botzung-Appert, E.; Colombier, I.; Baldeck, P. L.; Ibanez, A.; Corval, A. *J. Phys. Chem. B* **2005**, *109*, 8587–8591.

34. Harada, J.; Ogawa, K. *J. Am. Chem. Soc.* **2001**, *123*, 10884–10888.

35. Staehle, I. O.; Rodríguez-Molina, B.; Khan, S. I.; Garcia-Garibay, M. A. *Cryst. Growth Des*. **2014**, *14*, 3667–3673.

36. Wohl, C. J.; Kuciauskas, D. *J. Phys. Chem. B* **2005**, *109*, 22186–22191.

37. Horie, K.; Hirao, K.; Mita, I.; Takubo, Y.; Okamoto, T.; Washio, M.; Tagawa, S.; Tabata, Y. *Chem. Phys. Lett.* **1985**, *119*, 499–502.

38. Arul Murugan, N.; Chakrabarti, S.; Ågren, H. *J. Phys. Chem. B* **2011**, *115*, 4025–4032.

39. Nadolski, B.; Uznański, P.; Kryszewski, M. *Makromol. Chem., Rapid Commun.* **1984**, *5*, 327–331.

40. Zhou, J.; Li, Y.; Tang, Y.; Zhao, F.; Song, X.; Li, E. *J. Photochem. Photobiol. A: Chem.* **1995**, *90*, 117–123.

41. Kinashi, K.; Ono, Y.; Naitoh, Y.; Otomo, A.; Ueda, Y. *J. Photochem. Photobiol. A: Chem.* **2011**, *217*, 35–39.

42. Wood, E.A. *Crystals and Light: An Introduction to Optical Crystallography*, 2nd Ed.; Dover Publications: New York, 1977.

43. Lazarenko, I. B. *Khimiya Geterotsiklicheskikh Soedinenii* **1982**, 10.

CHAPTER 3

Nanosecond Laser Flash Photolysis of a 6-Nitroindolinospiropyran in Solution and in Nanocrystalline Suspension Under Single Excitation Conditions

3.1 Abstract

Nanosecond transient absorption spectroscopy was used to study the photochemical ring-opening reaction for a 6-nitroindolinospiropyran (**SP1**) in solution and in nanocrystalline (NC) suspension at 298 K. We measured the kinetics in argon-purged and air-saturated acetonitrile and found that the presence of oxygen affected two out of the three components of the kinetic decay at 440 nm. These are assigned to the triplet excited states of the *Z*- and *E*-merocyanines (**^{3}*Z*-MC*** and **^{3}*E*-MC***). In contrast, a long-lived growth component at 550 nm and the decay of a band centered at 590 nm showed no dependence on oxygen and are assigned, respectively, to the ground state *Z*- and *E*-merocyanines (***Z*-MC$_0$** and ***E*-MC$_0$**). Laser flash photolysis studies performed in NC suspensions initially showed a very broad, featureless absorption spectrum that decayed uniformly for ca. 70 ns before revealing a more defined spectrum that persisted for greater than 4 ms and is consistent with a mixture of the more stable ***Z*-** and ***E*-MC$_0$** structures. We performed quantum mechanical calculations on the interconversion of ***E*-** and ***Z*-MC**s on the **S$_0$** and **S$_1$** potential energy surfaces. The computed UV-vis spectra for a scan along the *Z* → *E* interconversion reaction coordinate show substantial absorptivity from 300–600 nm, which suggests that the broad, featureless transient absorption spectrum results from the contribution of the transition structure and other high-energy species during the *Z* to *E* isomerization.

3.2 Introduction

The photochromic reaction of the spiropyran-merocyanine system (**SP-MC**, Scheme 3.2.1) has been studied extensively in solution and polymer matrices.[1–5] However, fewer reports exist that describe the crystalline state photochromism of these compounds,[6–9] which have applications as molecular switches due to their ability to respond to a variety of stimuli such as light, solvent polarity, pressure, temperature, and pH.[1,2,4,10–14] Scheme 3.2.1 shows the

photochromic reaction for the 6-nitroindolinospiropyran (**SP1**) studied in this work with UV light irradiation causing the cleavage of the C_{spiro}–O bond to produce the colored ***Z*-** and ***E*-MC** ring-opened isomers. The **MC** species can then return back to the spiro form either thermally or photochemically.

Scheme 3.2.1

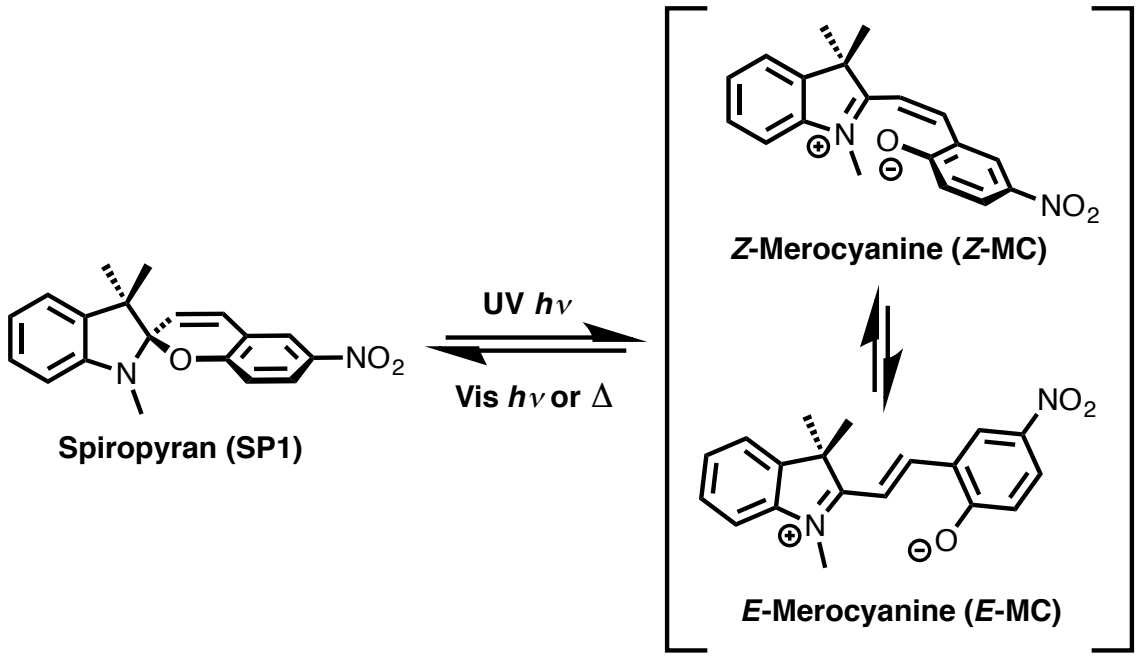

Although the photochromism of spiropyrans is generally well-documented in solution and more recently in crystals, the photochemical mechanism for the **SP** → **MC** ring-opening process remains a source of some debate.[15–17] While nanosecond, picosecond, and even femtosecond laser flash photolysis have been used in elucidating the photochemical mechanism of **SP**s in solution, polymer films, and crystalline solids, different interpretations of the similar spectral and kinetic data have been reported.[10,15,16,18–26] Several reasons may account for the different suggestions, including the spectral overlap of multiple transient species, the potential involvement of side reactions, and differences in experimental conditions.[15]

For example, in a study carried out in hexane solution by Lenoble et al.,[16] a transient

absorption band at 630 nm was assigned to a merocyanine dimer species. A similar study reported by Krysanov and Alfimov in benzene did not describe any absorption bands maximizing above 600 nm, suggesting that dimers were not produced in their experiments.[27] Subsequent studies based on these observations found that dimer complexes or higher aggregates involving **SP** and **MC** species would be preferentially formed in saturated aliphatic hydrocarbons with more concentrated samples resulting in more aggregate formation upon irradiation.[28–30] Variations in the reported excited state kinetic data have also resulted in different species being assigned to the transient observed between 420–450 nm in almost every kinetic study involving nitro-substituted spiropyrans, such as **SP1**.[10,15–18,28] These discrepancies and our interest in exploring the reaction in the solid state have served as motivation for our present work. Here we intend to shed more light on the mechanism for the photochemical ring-opening of **SP1** in solution and the crystalline state. A key aspect of our investigation in the solid state is the use of transient absorption analysis using nanosecond pump-probe spectroscopy with nanocrystals (NC) suspended in water. Nanocrystals that are smaller than the wavelength of incident light make it possible to use conventional transmission methods by diminishing complications that arise from dichroism, birefringence, and light scattering.[31] An additional advantage of paramount importance for this work, which has been shown in previous studies,[32–34] is that suspended nanocrystals make it possible to study photochemical reactions under single excitation conditions, thus avoiding multiphotonic processes that are commonly observed in bulk solids.[35] We are therefore interested in using NC suspensions to study how the nanocrystal environment affects the kinetics of photochemical reactions in order to compare to solution and bulk solid studies.

In fact, a limited number of studies describing the photochromic reaction of spiropyrans and spirooxazines in crystals using pulsed laser excitation have been reported, with the majority

being described by Masuhara and coworkers.[22–26] In their first study, they showed that weak laser excitation (< 1 mJ/cm^2) of their spirooxazine microcrystalline powders never resulted in the color changes indicative of a stable merocyanine species.[23] However, increasing the laser intensity to a few mJ/cm^2 resulted in the expected coloration of the powder samples, which was attributed to the formation of an ***E*-MC** species (Scheme 3.2.1). They suggested that the excess light energy not used to break the C_{spiro}–O bond would still be absorbed by the crystal as heat and would result in rapid local heating, which could produce enough flexibility in the crystal lattice to allow for the formation of a stable ***E*-MC**. However, it is also possible that their observations were the result of multiphotonic interactions from the intense excitation pulses. They then went on to perform "double pulse excitation" experiments, which involved using a half mirror to divide a femtosecond excitation pulse into two, and then reintroducing the two pulses to the sample with an optical delay varied from 40 ps to 5 ns.[25] The laser fluence of each pulse was held constant at 1.7 mJ/cm^2. The authors found that when the time interval between the two pulses was less than 3 ns the observed **MC** absorption at ca. 600 nm was greater than that observed in the single pulse experiments at the same laser fluence of 1.7 mJ/cm^2, whereas at delays greater than 3 ns the observed **MC** absorption was the same as that in the single pulse experiments. This suggested that the photoprocesses induced by the first pulse are correlated to those induced by the second pulse at short delay times (< 3 ns) and not correlated at longer delay times (> 3 ns). The authors noted that these results, however, cannot be well explained by the photothermal model described above where local heating of a crystal from laser excitation can induce enough lattice disorder to allow the ***E*-MC** to form. This is because thermal diffusion is estimated to occur on the microsecond time scale, meaning that the amount of **MC** produced between two excitation pulses separated by delays of more than 10 ns should still be correlated,

which is not what the double pulse experimental data shows. Therefore, Masuhara and coworkers proposed a new model, which they call the cooperative photochemical reaction model. In this model, the authors suggest that intense pulsed laser excitation should produce a high density of ***Z*-MC** excited states, resulting in the sites containing multiple transient species having enough local lattice disorder to create the free volume necessary for isomerization to a long-lived planar ***E*-MC** to occur. Consequently, the number of lattice sites containing plural transient species at shorter delay times (< 3 ns) between pulses increases with the laser fluence to produce a greater number of ***E*-MC** species and results in a greater **MC** absorbance. Additional studies by the same group found similar results for spiropyrans in microcrystalline powders as well.[22,24]

Although Masuhara and coworkers reported that they did not observe any photocoloration of their microcrystalline powders of spiropyrans or spirooxazines with weak laser excitation or steady-state irradiation, we and others have shown that weak, continuous light sources work well,[1,6–9,13,36,37] perhaps highlighting the intensity-dependence of the photochromic reaction. Our previous work focused on the thermal decay kinetics for a set of structurally analogous nitro-substituted spiropyrans in solution and in the solid state.[1] Specifically, we used nanocrystals suspended in water to study the solid state photochromism of spiropyrans using transmission spectroscopy.[1] We showed that a set of five *N*-alkyl substituted 6-nitroindolinospiropyrans underwent rapid coloration with thermal recovery kinetics that are very similar in solution but varied widely in the crystalline state. Based on that study, and knowing that large single crystals and dry powders can exhibit complex kinetics as a result of mulitphotonic interactions, we have shown that NC suspensions can be used to explore absolute kinetics in the solid state.[38–41] Here we compare the excited state ring-opening reaction for a 6-nitroindolinospiropyran (**SP1**) in solution and in NC suspension using nanosecond transient

absorption spectroscopy. Specifically, we set out to study how the nanocrystal environment affects the kinetics of the photoreaction of **SP1** upon pulsed laser excitation. By choosing conditions known to disfavor dimer and aggregate formation in solution, we identified what we hypothesize to be the *E* and *Z* ground state merocyanine species and also propose the presence of a triplet excited state species whose identity will be discussed in the next section. Our results in NC suspension showed a very broad transient spectrum immediately after the laser pulse, which after about 70 ns transforms into the spectrum of a long-lived **MC** isomer, suggesting that spiropyrans in NCs behave more similarly to **SP**s in solution than they do to **SP**s in microcrystalline powders.

3.3 General Methods

3.3.1 Synthesis of SP1

SP1 was synthesized as previously reported in a single step from the condensation of commercially available 1,3,3-trimethyl-2-methyleneindoline with 2-hydroxy-5-nitrobenzaldehyde.[1]

3.3.2 Solution Sample Preparation

730 μL of a stock solution (17.2 mM) of **SP1** in acetonitrile was diluted to 500 mL to give a final sample concentration of 0.025 mM with an optical density of ca. 0.25 at 355 nm.

3.3.3 NC Suspension Sample Preparation

15 μL of a stock solution (~50 mM) of **SP1** in acetonitrile was injected via a micropipette into a graduated cylinder containing a vigorously stirring solution of 16 mL of Millipore water and 4 mL of a CTAB (cetyltrimethylammonium bromide) solution (0.193 mM). The newly created suspension was gently poured into a large culture tube and sonicated for 2 minutes. The

suspension was then immediately used for LFP studies and new suspensions were made as needed. NC suspensions had an optical density of ca. 0.365 at 355 nm.

3.3.4 Transient Absorption Measurements

Nanosecond laser flash photolysis experiments were performed using a Brilliant b Quantel Q-switched Nd:YAG laser operating at 355 nm with a repetition rate of 1 Hz and a pulse width of ca. 8 ns. Samples were flowed continuously through a 1 cm quartz flow cell mounted on a home-built sample holder with all measurements carried out in single pass experiments. Degassed solutions were purged with argon for 3 hours prior to and throughout the course of the transient absorption experiments. Air-saturated solutions were allowed to equilibrate overnight under standard atmospheric conditions prior to transient absorption experiments.

3.4 Results and Discussion

3.4.1 Sample Characterization and Flash Photolysis Setup

In order to study the transient kinetics of **SP1** via laser flash photolysis, we prepared and analyzed the stability of **SP1** in acetonitrile solutions (0.025 mM) and aqueous nanocrystalline (NC) suspensions (See Appendix 3.7.1, Figures 3.7.1.1 and 3.7.1.2). NC suspensions of **SP1** were prepared by the solvent shift, or reprecipitation method,[42] and their crystallinity was established by powder X-ray diffraction (PXRD) (Appendix 3.7.2, Figure 3.7.2.1). Although small amounts of amorphous materials cannot be rigorously excluded, we assume that our observations are representative of the much greater crystalline component. Using dynamic light scattering (DLS), we determined the size of our nanocrystals averaged between 200–365 nm (Appendix 3.7.2, Figure 3.7.2.2), which is smaller than the excitation wavelength. Under these conditions, optical effects such as scattering and birefringence are reduced as compared to those of bulk solids, thus making them amenable to transmission spectroscopy measurements.[31] UV-

vis spectra were obtained for NC suspensions of **SP1**, which showed significant scattering and broader peaks compared to those collected in acetonitrile solutions (Figure 3.4.1.1). However, the spectral features for **SP1** in NC suspensions are clearly visible, rendering our suspensions suitable for analysis via transmission spectroscopic methods.

Laser flash photolysis (LFP) spectroscopic studies of **SP1** were carried out in argon degassed and air-saturated acetonitrile solutions as well as in NC suspensions. The solutions and suspensions were flowed continuously, but only once through the quartz cell, to ensure that pristine sample was available for each laser excitation pulse. All LFP data was reproduced in triplicate (see Appendix 3.7.3 for additional spectra).

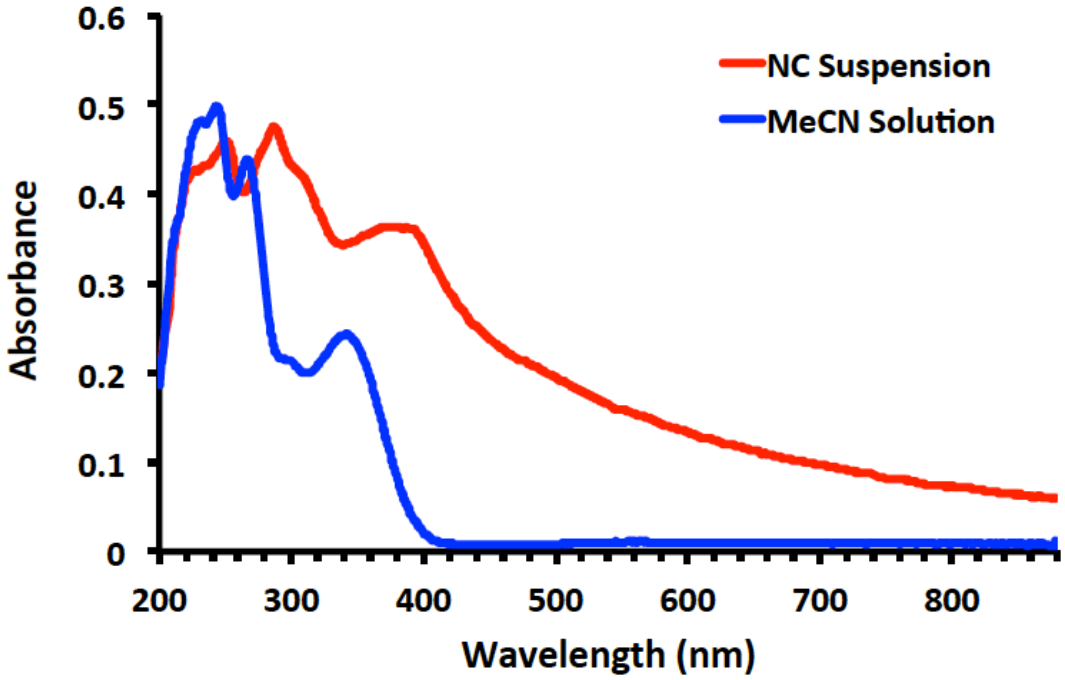

Figure 3.4.1.1. UV-vis absorption spectra of **SP1** in acetonitrile (blue) and in nanocrystalline (NC) suspension (red).

3.4.2 Solution Photochemical Studies

Figure 3.4.2.1a shows how the transient absorption spectrum for **SP1** in argon degassed

acetonitrile evolves over time starting immediately after the laser pulse (0 μs) and continuing until 262 μs after the laser pulse. The end-of-pulse spectrum is characterized by three absorption bands with maxima at 410, 440, and 590 nm. Over time, the band at 440 nm decays while the bands at 410 and 590 nm appear to undergo a growth and shift to 380 and 550 nm, respectively. While these multiple absorption bands are known in the literature, the identities and kinetics for the absorbing species are ambiguous.[15,16,18–21] To address that, we collected kinetic data at the different absorption maxima identified in Figure 3.4.2.1a for an argon degassed sample of **SP1** in acetonitrile. The kinetic data obtained at 440 nm revealed three decay components with lifetimes of 31 ns, 495 ns, and 5.7 μs (Figure 3.4.2.1b). Subsequent analysis of the absorption at 590 nm showed a very rapid growth within the laser pulse (lifetime could not be measured) with a slower monoexponential growth component of 2.9 μs followed by a monoexponential decay of 22.9 μs (Figure 3.4.2.1d). Finally, the kinetic data collected at 550 nm also revealed a very rapid growth within the laser pulse (lifetime could not be measured) followed by a biexponential growth with lifetimes of 3.1 μs and 22.0 μs (Figure 3.4.2.1c). The absorption bands observed at 380 and 410 nm were found to have the same transient kinetics as those at 550 and 590 nm, respectively, which suggests that one transient species absorbs at both 380 and 550 nm and another at 410 and 590 nm. In the work of Lenoble and Becker, very similar transient absorptions at 370, 430, 530, and 570 nm were identified for solutions of **SP1** in hexane.[16] Specifically, they assigned the absorptions at 370 and 570 nm to a single species, namely the ***E*-MC**. Another report by Görner states that the ***E*-** and ***Z*-MC** ground state isomers both have absorptions between 390–410 nm and 560–620 nm,[10] which supports our experimental observations.

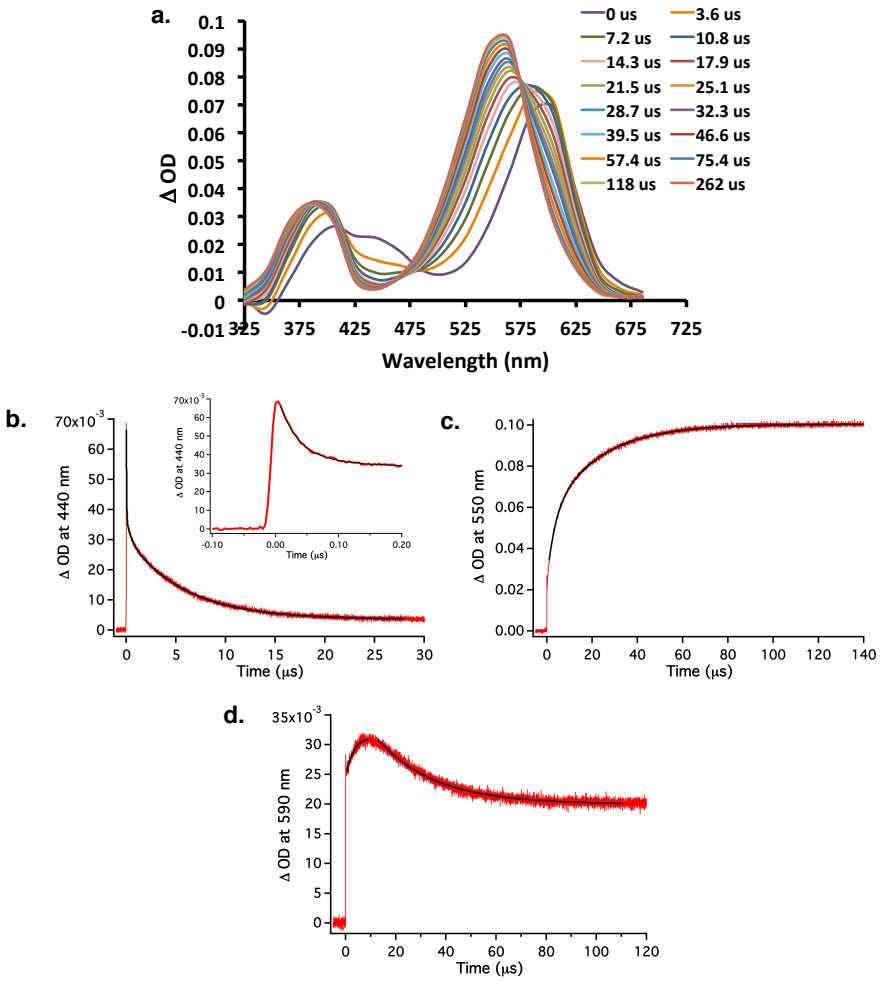

Figure 3.4.2.1. (a) Transient absorption spectrum for **SP1** at various time points in argon degassed acetonitrile along with the corresponding transient kinetic plots showing (b) a decay at 440 nm with the earliest portion of the decay shown in the inset, (c) a growth at 550 nm, and (d) a growth followed by a decay at 590 nm. Fit lines are shown in black.

In order to compare the different transient species we observed upon the excitation of **SP1** in argon degassed acetonitrile to those assignments reported in the literature, we gathered a similar transient absorption spectrum of **SP1** in air-saturated acetonitrile to establish the effects of oxygen as a triplet quencher. Figure 3.4.2.2a shows how the transient absorption spectrum for **SP1** in air-saturated acetonitrile evolves over time starting immediately after the laser pulse (0 ns) and continuing until 3.49 μs after the laser pulse. The end-of-pulse spectrum is characterized

by two absorption bands with maxima at 430 and 590 nm. Over time, the band at 430 nm decays and splits into two bands with maxima at 410 and 440 nm, which then follow the same spectral progression seen in Figure 3.4.2.1a for the argon degassed sample. The bands at 410 and 590 nm appear to undergo a similar growth and shift to 380 and 550 nm, respectively, just as in the argon degassed sample. However, transient lifetimes were found to be different. The kinetic data obtained at 440 nm revealed a biexponential decay with lifetimes of 24 ns and 186 ns (Figure 3.4.2.2b), which is different than the three component decay observed at 440 nm in the argon degassed sample. The short decay component in both cases is similar (31 and 24 ns), suggesting a short-lived transient with a limited opportunity to interact with and be quenched by oxygen. The second component in air-saturated acetonitrile with a lifetime of 186 ns correlates with the intermediate-lived component in argon degassed solution (495 ns), while the long-lived component (5.7 μs) seems to be efficiently quenched so that it merges with the intermediate one. This data suggests that multiple triplet species absorb at 440 nm, as expected for a conformationally heterogeneous system. Continuing our data analysis, the kinetics at 590 nm revealed one very rapid growth within the laser pulse, for which a lifetime could not be calculated, followed by a monoexponential decay with a lifetime of 21.5 μs (Figure 3.4.2.2d). The kinetics at 550 nm showed an initial growth within the laser pulse followed by a biexponential growth with lifetimes of 156 ns and 20.4 μs (Figure 3.4.2.2c). The decay lifetime at 590 nm remains essentially constant both in the presence and absence of oxygen. This suggests that the absorbing species is not a triplet, but rather a ground state. The same can be said of the longer-lived portion of the kinetic growth at 550 nm, implying that this species is also a ground state. A final observation we made concerning our solution transient data (argon degassed and air-saturated) is that the decays at 440 and 590 nm never return to the original

baseline value, as others have also observed.[10,15,16,18] The reason for this is most likely due to the fact that the long-lived species at 550 nm absorbs at both of these wavelengths, and thus makes it appear as if the transients at 440 and 590 nm have an extremely long-lived component of their own or decompose.

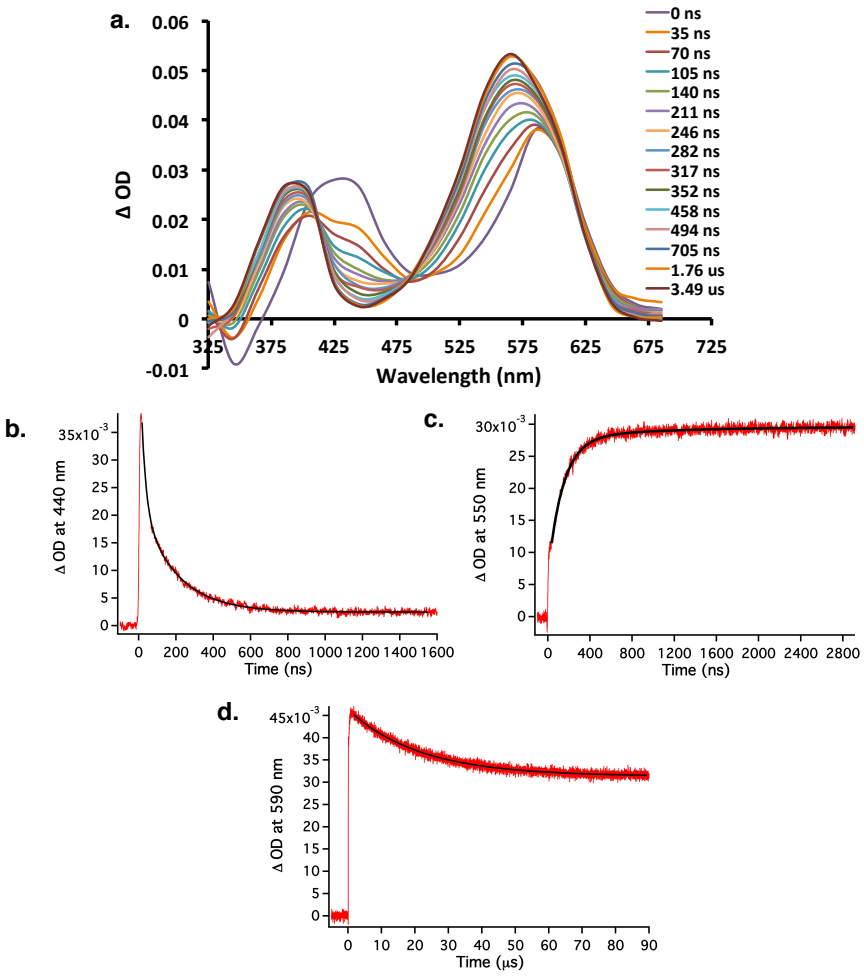

Figure 3.4.2.2. (a) Transient absorption spectrum for **SP1** at various time points in air-saturated acetonitrile along with the corresponding transient kinetic plots showing (b) a decay at 440 nm, (c) a growth at 550 nm, and (d) a decay at 590 nm. Fit lines are shown in black.

3.4.3 Mechanistic Analysis

With our transient kinetic results in solution now in hand, we can put our data in the context of a photochemical mechanism from spiropyran to merocyanine. Our proposed

mechanism is shown in Scheme 3.4.3.1 with observable transient species shown between braces and their absorbance maxima indicated below, with the final product being ***E*-MC$_0$**. For nitro-substituted spiropyrans such as **SP1**, it has been established that UV irradiation excites the ground state spiropyran (**SP$_0$**) to its first excited singlet state (^{1}**SP***), which then intersystem crosses (ISC) to the excited triplet state (^{3}**SP***).[15,16,43–45] The ^{3}**SP*** then undergoes rapid ring-opening to a triplet merocyanine species, the identity of which the literature still does not agree on. What the literature does agree on is that the photochemical processes just mentioned occur on a sub-nanosecond time scale, which is shorter than our laser pulse, such that our analysis begins with the triplet merocyanine species (^{3}***Z*-MC***). The decay we measured at 440 nm has previously been assigned to several different triplet species, such as the triplet spiropyran (^{3}**SP***),[17,28] triplet *Z*-merocyanine (^{3}***Z*-MC***),[16] the triplet *E*-merocyanine (^{3}***E*-MC***),[15,18] or a somewhat ambiguous triplet perpendicular merocyanine conformer (^{3}**perp***),[10,15,18] which is described as a merocyanine isomer that maintains the same orthogonal orientation of its two ring systems as in the spiropyran form. We propose that the band at 440 nm is largely determined by overlapping absorptions for both ^{3}***Z*-MC*** and ^{3}***E*-MC***. In fact, the experimentally determined decay lifetimes do not correlate in a simple manner with any of the growth lifetimes at 550 or 590 nm, suggesting that the species responsible for the kinetics measured at 440 nm may exist under competing pre-equilibrium and with various decay channels. Although the ^{3}**perp*** has been proposed previously as the species that gives rise to the absorption at 440 nm, calculations discussed below suggest that the ^{3}**perp*** species should be considered more like a transition state between the ^{3}***E*-** and ^{3}***Z*-MC*** species, and therefore may not be an observable transient species in solution. However, different rotational isomers should indeed be possible. As for the possibility that the ^{3}**SP*** is the triplet species absorbing at 440 nm, Chibisov and Görner observed

a transient at 440 nm with a decay lifetime in the microsecond time regime.[15,18] However, in oxygen saturated solution, the decay at 440 nm was almost completely quenched. If we make the assumption that **^{3}SP*** is long-lived enough and efficiently populated at room temperature, then quenching by oxygen should result in ISC to the **SP_0** with almost no ***Z*-** or ***E*-MC_0** being produced. Since their experimental evidence shows significant ***Z*-** and ***E*-MC_0** formation in both argon and oxygen saturated solutions just as we observe in argon degassed and air-saturated solutions, this suggests that the **^{3}SP*** is probably too short-lived to interact with and be quenched by oxygen, which is why we do not favor the assignment of the band at 440 nm to **^{3}SP***. Chibisov and Görner have also determined the rate constants for triplet quenching by oxygen in several solvents, which ranged between 0.5 – 2 x 10^9 M^{-1} s^{-1} and gives a benchmark for how fast the spiropyran ring-opening occurs.[18,46]

Scheme 3.4.3.1

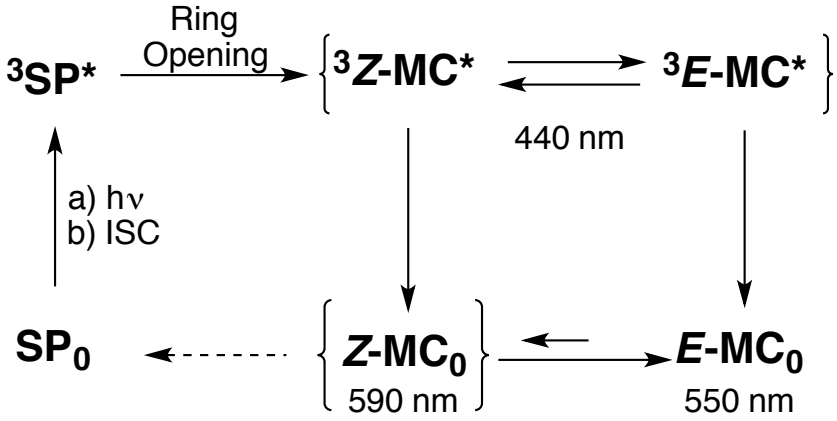

Turning our attention now to the absorption bands at 550 and 590 nm, previous reports have described them as either one broad absorption from 500–650 nm or as one absorption band with a maximum at 570 nm and a shoulder at 630 nm, and assigned them as a mixture of the *E* and *Z* ground state merocyanine species (***E/Z*-MC_0**).[16,18–20] Our results in argon degassed

acetonitrile (Figure 3.4.2.1a) show two absorption bands that appear to evolve from one to the other with no clear isosbestic point, suggesting a combination of spectral relaxation and equilibration. From Figure 3.4.2.2 (in air-saturated acetonitrile) we found that as the absorption band at 590 nm decreases with a lifetime of 21.5 μs, the long-lived portion of growth at 550 nm has a lifetime of 20.4 μs. Since these long lifetimes are quite similar to those observed in argon degassed solution, we propose that these transients are not affected by oxygen, meaning that neither of these bands correspond to a triplet species. From the transient absorption spectra in Figures 3.4.2.1a and 3.4.2.2a, we observe an apparent shift from 590 nm to 550 nm, which we measured as a decay at 590 nm and a growth at 550 nm. In our previous steady-state solution studies we found that the ***E*-MC$_0$** absorbs at ca. 550 nm in acetonitrile,[1] and so we assign the band at 590 nm to the ***Z*-MC$_0$** and the one at 550 nm to the ***E*-MC$_0$**. The ***E*-** and ***Z*-MC$_0$** are shown in Scheme 3.4.3.1 to be in an equilibrium that favors ***E*-MC$_0$**, which is in agreement with previous steady-state studies involving the **SP-MC** system.[1,2,11,47–49]

DFT calculations also support our ***E/Z*-MC$_0$** assignments as the **$S_0 \rightarrow S_1$** 0-0 transition energy ($E_{0\text{-}0}$) computed for the ***Z*-MC** is lower than that for the ***E*-MC**, which is consistent with our experimental observation of the ***E*-MC$_0$** being blue-shifted relative to the ***Z*-MC$_0$** (Figure 3.4.3.1). These computations were performed at the CAM-B3LYP-(D3BJ)/6-311++G(d,p)[50–53] IEFPCM-(CH_3CN) level of theory with time-dependent (TD) considerations for the excited states in Gaussian 16[54]. Additionally, our computational methods were able to predict that the ***E*-MC** has a higher absorptivity than does the ***Z*-MC** (Appendix 3.7.4, Figure 3.7.4.2), as observed in our solution experiments (Figure 3.4.2.1a).

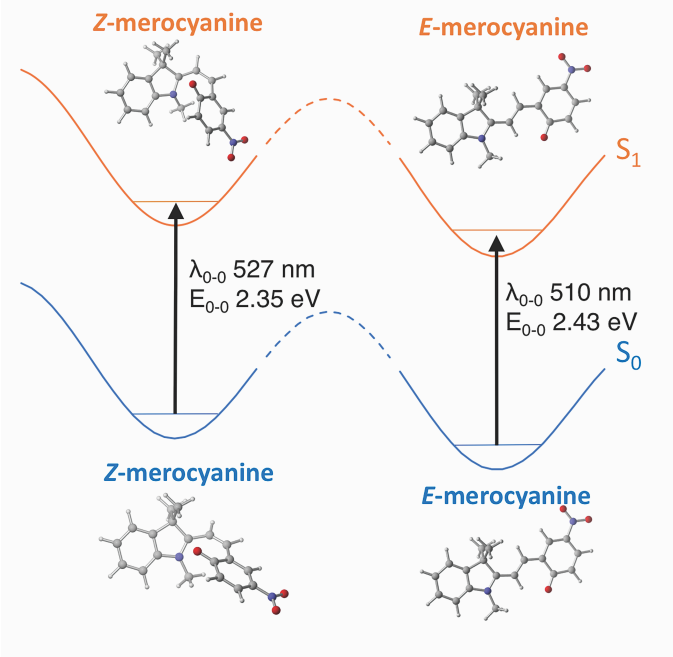

Figure 3.4.3.1. Calculated 0-0 transitions for the ***Z***- and ***E*-MC** from $\mathbf{S_0}$ → $\mathbf{S_1}$ with transition energies provided in nm and eV following a procedure reported by Adamo and Jacquemin[55] using (TD)-CAM-B3LYP-(D3BJ)/6-311++G(d,p) IEFPCM-(CH_3CN).

Using our suggested assignments for the observed transient absorption bands, we can interpret the rest of our kinetic data to complete our proposed mechanism from ^{3}***E*-MC*** and ^{3}***Z*-MC*** to ***E*-$\mathbf{MC_0}$** and ***Z*-$\mathbf{MC_0}$**. The kinetic growth we observe at 590 nm has a lifetime of 2.9 μs in argon degassed acetonitrile, but in air-saturated acetonitrile this growth appears to be contained within the laser pulse and so the kinetics could not be measured with our nanosecond laser system. Since this lifetime is affected by the presence of oxygen, it implies that a triplet species immediately precedes the ***Z*-$\mathbf{MC_0}$** along the photochemical pathway. The same observation was made with the short-lived portion of the kinetic growth at 550 nm, which had a lifetime of 3.1 μs in argon degassed acetonitrile and a much shorter lifetime of 156 ns in air-saturated acetonitrile, thus indicating that a triplet state immediately precedes the ***E*-$\mathbf{MC_0}$** as well. With the kinetic growth lifetimes at 550 and 590 nm being essentially identical in argon degassed and air-

saturated acetonitrile, we postulate that either the same triplet species, i.e. the ^{3}***E*-MC*** or ^{3}***Z*-MC***, could be responsible for populating both the ***E*-** and ***Z*-MC** ground states, or the ^{3}***E*-MC*** and ^{3}***Z*-MC*** could be in rapid equilibrium with each other and then decay with similar rates to their respective ground states. Others have argued that the ^{3}***E*-MC*** does not directly intersystem cross to the ***E*-MC$_0$** because only fluorescence, not phosphorescence, was observed upon excitation of the ***E*-MC$_0$** to the ^{1}***E*-MC*** in acetonitrile.[10,18] However, this argument is questionable as it compares two different mechanisms to access the ^{3}***E*-MC***.

3.4.4 Solid State Photochemical Studies

With a detailed investigation of the nanosecond transient kinetics of **SP1** in acetonitrile experimentally characterized, we began studying the same spiropyran model in the solid state. As mentioned in the introduction, we chose to use aqueous nanocrystalline suspensions in order to increase the probability of observing single excitation photoprocesses. Regarding the excitation of our nanocrystals, the power of our laser (ca. 8 x 10^6 W) is three to four orders or magnitude smaller than the one used by Masuhara and coworkers[22] (ca. 3 x 10^9 – 2 x 10^{10} W), which supports our expectation that the signals observed upon laser flash photolysis of **SP1** in NC suspensions are the result of single excitation events. Figure 3.4.4.1 shows the transient absorption spectrum for an NC suspension of **SP1** from 0–310 ns, with the bottom portion expanded from 78–310 ns. The observed spectrum can be described as very broad, featureless, and appears to decay uniformly over all wavelengths from 325–675 nm with a maximum near 330 nm. However, the expanded bottom portion of the spectrum shows some spectral definition with two noisy absorptions, one below 400 nm and the other between 500–685 nm, which looks similar to the final absorption spectrum for **SP1** in solution under both argon degassed and air-saturated conditions (Figures 3.4.2.1a and 3.4.2.2a), suggesting that both ***E*-** and ***Z*-**like **MC$_0$**

isomers are produced in NC suspension. This data also implies that in the solid state we are unable to observe other excited state species after the ca. 8 ns laser pulse.

To analyze our results, we recall that Masuhara and coworkers have described the solid state transient kinetics of **SP1** in microcrystalline powders and PMMA films using a femtosecond diffuse reflectance experimental setup.[22] An observation they made was that the growth they observed between 550–650 nm with a maximum at ca. 630 nm was assigned to a merocyanine species in both microcrystalline powders and PMMA films and that it reached its maximum absorption after ca. 5 ns. However, in the powder sample they found that this species decayed biexponentially with lifetimes of 20 and 150 μs, whereas in the PMMA films the decay of this absorption was shown to take several tens of minutes.[22] In agreement with our previous steady-state excitation studies which revealed merocyanine lifetimes of minutes to hours,[1] we do not observe a decay of the absorption band between 550–650 nm in our NC suspensions at timescales up to 4 ms (Figure 3.4.4.1, inset), suggesting that **SP1** is capable of attaining a stable ***E*-**like **MC** configuration in the crystalline environment even when using a weaker excitation pulse. One may consider the possibility that the original broad transient and the subsequent long-lived ***E*-**like **MC** signal may be due to merocyanine formed on the surface of the nanocrystals. However, one can estimate that surface sites account for no more than ca. 2–3% of the total molecules in each (200–400 nm) nanocrystal. Furthermore, considering that crystals of this size are able to transmit light, it is unlikely that excitation can only occur on the surface. Therefore, we suggest that it is reasonable to conclude that MC molecules are mainly generated in the bulk of the nanocrystals, as it is likely that the evolution of surface transients under significantly lower constraints should approach the evolution of those observed in solution.

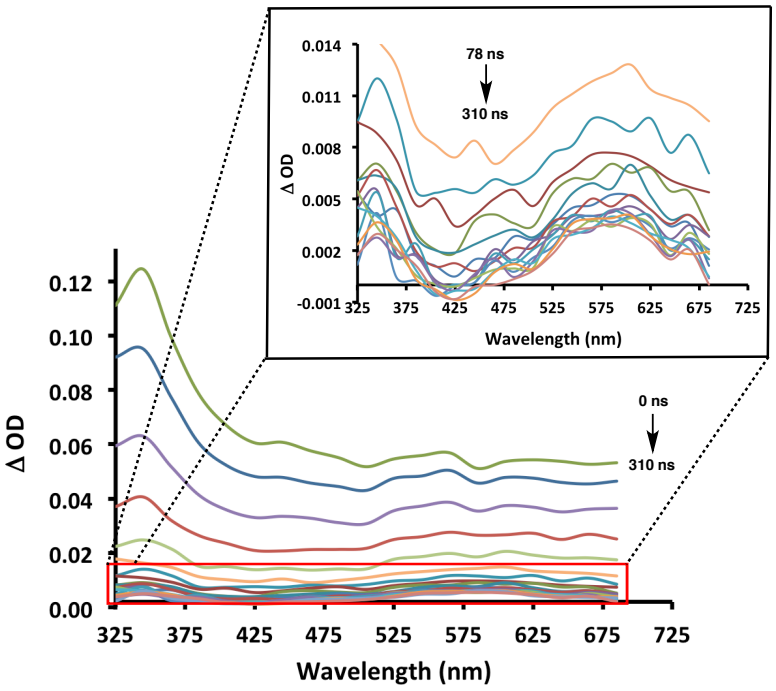

Figure 3.4.4.1. Transient absorption spectrum for **SP1** at various time points in NC suspension. Red box: expansion of spectrum at longer times. Laser output (λ=355 nm, 36–40 mJ/pulse, 5–8 ns, 10 Hz).

The extremely broad and featureless absorption we observe in NC suspensions using laser flash photolysis is quite different from the one in solution. Since the solid state spectrum did not resolve on the nanosecond timescale, we can only speculate as to the nature of the solid state photochemical mechanism. We start our analysis by considering that the absorption spectra of linearly conjugated chromophores tend to be highly sensitive to conformational changes that have an effect on the extent of conjugation. Based on that, it is reasonable to postulate that the broad spectrum in Figure 3.4.4.1 may be the result of multiple absorbing species, rather than arising from a single chromophore that absorbs over all wavelengths. A plausible scenario involved a ring-opening reaction from ^{3}**SP*** to the *cisoid* configuration *of* ^{3}***Z*-MC**, where the bonds between the indoline imminium and phenolate groups begin to evolve towards the

transoid configuration of ^{3}***E*-MC***. One may expect that the crystal lattice can slow down the kinetics of this process, such that multiple structures may co-exist along the ^{3}***E*-MC** and ^{3}***Z*-MC*** energy surface before going to the ground state chromophore. Subsequent decay of the hypothetical ^{3}***E*-MC*** and ^{3}***Z*-MC*** species to the long-lived ground state ***E*-MC$_0$** would result in the more defined final spectrum in the expanded portion of Figure 5. As we do not observe a growth of ***Z*-MC$_0$** as we do in solution, this interpretation would require that ^{3}***E*-MC*** and ^{3}***Z*-MC*** have a greater extinction coefficient than the ***E*-MC$_0$**, so that the growth of the ground state **MC**s can be obscured by the absorption of the triplet species.

In order to gain support qualitative for the suggested mechanism, we calculated the absorption profiles for numerous **MC** structures along the torsional reaction coordinate between the two rings, as shown in Figure 3.4.4.2. Specifically, we evaluated the torsional potential about the central C=C π-bond (highlighted in green in Figure 3.4.4.2) at the B3LYP/6-31+G(d,p) level of theory to explore relatively high-energy constrained structures and their absorbance properties. While the intermediate structures along the torsional potential are not local minima in solution, we propose that the solid state may sufficiently augment their lifetimes such that they may contribute to the observed absorption. Thus, we use their structures to approximate possible high-energy conformations stabilized by the nanocrystal and their corresponding absorbance profiles. The torsional potential in Figure 3.4.4.2 shows the optimized structures along the scanned coordinate between the ***Z*-** and ***E*-MC** configurations at regular 20° intervals (see Appendix 3.7.4 for complete computational results). We then performed single-point energy calculations on each structure with the (TD)-CAM-B3LYP/6-311++G(d,p) method to obtain vertical excitations to the **S$_1$** surface and predict the UV-vis absorbance spectra for each structure as shown in Figure 3.4.4.3. The normalized absorbance curves in Figure 3.4.4.3 are color-coded

by their structural similarity to either the ***Z*-MC** or the ***E*-MC**. ***Z***-like merocyanines (θ_{dih} = 0°–90°) correspond to the yellow, orange, and red solid curves, while ***E***-like merocyanines (θ_{dih} = 90°–180°) correspond to the green and blue dashed curves. The solid black curve represents the structure closest to the transition state geometry between ***Z*-MC** and ***E*-MC**. The calculated UV-vis spectra in Figure 3.4.4.3 for intermediate points along the ***Z*-** to ***E*-MC** reaction coordinate show significant absorptivity ranging from 300–600 nm. This suggests that the broad and featureless transient absorption spectrum initially observed in NC suspension (Figure 3.4.4.1) could result from the simultaneous contribution of the ***E*-** and ***Z*-MC** with numerous ***E*-** and ***Z*-**like **MC** intermediate structures.

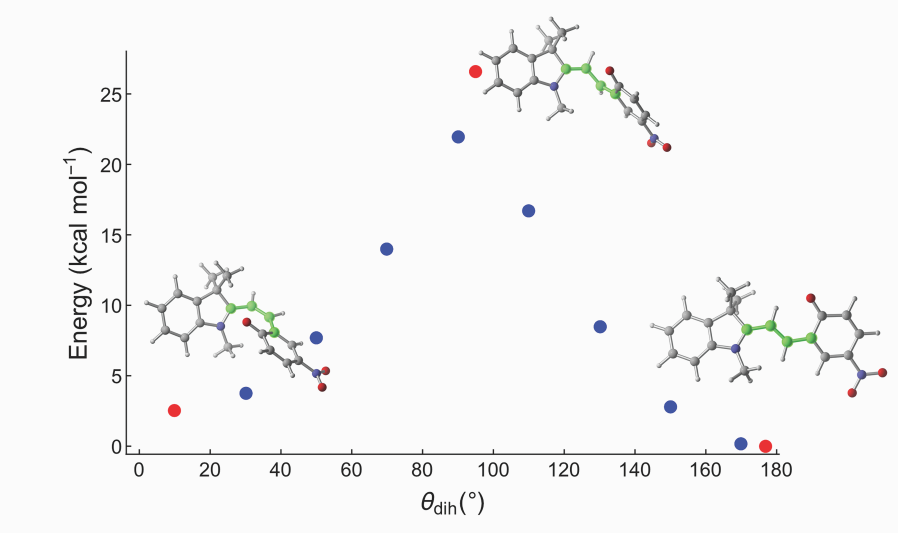

Figure 3.4.4.2. Calculated energies for each geometry along the scanned coordinate based on the dihedral angle highlighted in green. Energies are relative to the optimized ***E*-MC** isomer (0 kcal mol^{-1}, θ_{dih} = 178°). The red plot points correspond to the structures shown, which are the optimized stationary points for the ***Z*-MC**, ***E*-MC**, and transition state structures. Calculations were done at the CAM-B3LYP-(D3BJ)/6-31+G(d,p) IEFPCM-(CH_3CN) level of theory.

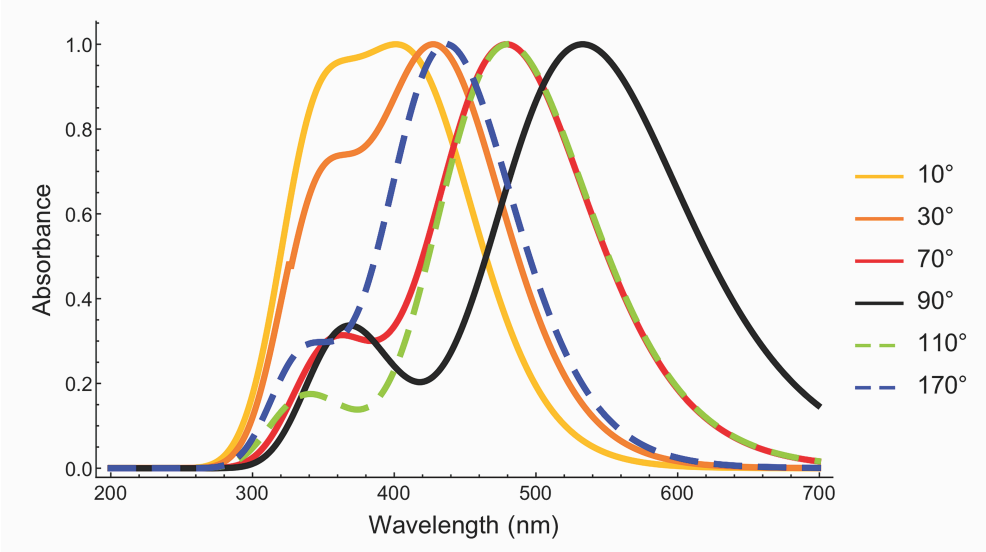

Figure 3.4.4.3. Calculated UV-vis absorbance spectra (normalized) for selected merocyanine geometries from Figure 3.4.4.2. Spectra were predicted using the (TD)-CAM-B3LYP/6-311++G(d,p) method. The solid black line corresponds to the structure closest to the transition state between ***Z***- and ***E***-**MC**. The yellow, orange, and red solid lines correspond to ***Z***-like **MC**s, and the green and blue dashed lines correspond to ***E***-like **MC**s.

3.5 Conclusions

Using nanosecond transient absorption spectroscopy, we were able to measure the kinetics of the ***Z***-$\mathbf{MC_0}$ and the ***E***-$\mathbf{MC_0}$ in solution and suggest a model that includes the formation of the relatively stable ***E***-$\mathbf{MC_0}$ from rapid contributions of what appears to be equilibrated or spectrally overlapping ^{3}***Z***-**MC*** and ^{3}***E***-**MC*** and slower contributions from ***Z***-$\mathbf{MC_0}$, which appears to also form from the two triplet **MC**s. Subsequent studies in NC suspension revealed an initially broad, featureless transient spectrum that appeared to decay uniformly in ca. 70 ns before becoming a more defined spectrum that persisted for greater than 4 ms. DFT calculations helped to rationalize our solid state results by exploring how the absorption profiles for numerous ***E***- and ***Z***-like **MC** isomers change as a function of structure about the

central C=C π-bond. The predicted UV-vis absorbance profiles showed that relatively high-energy ***E*-** and ***Z*-**like **MC** conformers potentially accessible in the constrained environment of nanocrystals are represented by intermediate structures along the torsional potential, and have significant absorptivity over the range of 300–600 nm. This suggests that the initially broad and featureless transient absorption spectrum observed in NC suspension could be a sum of the absorbance profiles for numerous ***E*-** and ***Z*-**like **MC** transient structures. Eventually only the more stable ***E*-** and ***Z*-MC** isomers persist giving rise to the more defined spectrum observed at longer times. As we compare our steady state and transient studies with those of Masuhara and coworkers,[22–26] our results show that ring-opening of the spiropyran to relatively stable MC species can occur even when using a weaker excitation laser pulse than that used by Masuhara and coworkers. This leads us to propose that the differences observed between our work and Masuhara's may arise from the limited number of multiphotonic interactions that occur in nanocrystalline solids as compared to dry powders. This report demonstrates that NC suspensions provide a simple medium for studying kinetics in solid state photochemical reactions by reducing challenges arising from optical effects and by reducing the probability of multiphotonic processes.

3.6 Experimental

3.6.1 General Information

All commercially obtained reagents/solvents were used as received without further purification. UV-vis absorption spectra were recorded on an Ocean Optics spectrometer (DT-MINI-2-GS UV-VIS-NIR LightSource and USB2000+ using SpectraSuite software package). Dynamic Light Scattering (DLS) data were recorded using a Beckman-Coulter N4 Plus particle

analyzer with a 10 mW helium-neon laser at 632.8 nm. The particle size was determined using the 62.6° detection angle and was calculated using the size distribution processor (SDP) analysis package provided by the manufacturer. Powder X-ray diffraction measurements were performed on a flat stage using a PANalytical Inc. X'Pert Pro Cu K-α = 1.5406 Å radiation source at power settings of 45 kV and 40 mA and a slit width of 0.5°. Data were collected at room temperature in the range of 2θ = 4–45°. Nanosecond transient absorption experiments were performed using a laser flash photolysis (LFP) instrument from Edinburgh Instruments in conjunction with a Q-switched Nd:YAG laser (Brilliant b, Quantel®) with a 355 nm output wavelength, 5–8 ns pulse width, 1 Hz repetition rate, and 36–40 mJ pulse energy. The optical detection is based on a pulsed Xenon arc lamp (450 W), a monochromator (TMS300, Czerny-Turner), a photomultiplier detector (Hamamatsu R928), and a digital oscilloscope (TDS3012C, 100 MHz and 1.25 GS/s from Tektronix). Transient absorption data was processed using the L900 software package provided by Edinburgh Instruments. Laser flash photolysis experiments were performed with a 1 cm quartz flow cell mounted on a home-built sample holder that is placed at the cross-section of the laser incident beam and the probe flashlamp. Samples were flowed through a Masterflex L/S peristaltic pump at a rate of 15 mL/min for acetonitrile solutions and at a rate of 1.9 mL/min for nanocrystalline suspension samples.

3.6.2 Laser Flash Photolysis of SP1 in solution (argon degassed and air-saturated)

Degassed acetonitrile solutions of **SP1** were purged with argon for 3 hours prior to conducting laser flash photolysis experiments, and a continuous flow of argon was maintained for the duration of data collection. Air-saturated acetonitrile solutions of **SP1** were allowed to equilibrate overnight under normal atmospheric conditions prior to conducting laser flash photolysis experiments.

Time-resolved transient absorption maps were then recorded from 325–685 nm in 20 nm steps while continuously flowing the sample solutions through the quartz cell at 15 mL/min. Absorption bands with λ_{max} values of 370, 440, 550, and 590 nm were observed, and the kinetics at 440, 550, and 590 nm were then measured with a 1.5 nm bandwidth and 20–30 scans averaged together. Flashlamp settings were set where the frequency was 10 Hz, width at 40 μs, and delay at 4000 μs. Q-switch settings were set where the frequency was at 1.0 Hz, width at 20 μs, and delay at 280 μs. All transient data was reproduced in triplicate.

3.6.3 Laser Flash Photolysis of SP1 in Nanocrystalline (NC) Suspensions

Suspensions were prepared immediately prior to performing kinetic measurements as described in section 3.3.3. Time-resolved transient absorption maps were then recorded from 325–685 nm in 20 nm steps while continuously flowing the sample suspensions through a quartz cell at 1.9 mL/min. Kinetic measurements were made at the same wavelengths, same bandwidth, and same number of averaged scans as in solution due to no real absorption bands being observed in nanocrystalline suspension. Flashlamp settings were set where the frequency was 10 Hz, width at 40 μs, and delay at 4000 μs. Q-switch settings were set where the frequency was at 1.0 Hz, width at 20 μs, and delay at 300 μs. All transient data was reproduced in triplicate.

3.7 Appendix

Supplemental Information for Chapter 3

3.7.1 UV-vis spectra in solution and NC suspension.....95

3.7.2 PXRD diffractogram of nanocrystals and DLS analysis of NC suspensions.....96

3.7.3 Laser flash photolysis kinetic plots in degassed and air-saturated acetonitrile.....97

3.7.4 Computational methods and calculated energies for *E*- and *Z*-merocyanines.....100

3.7.1 UV-vis Spectra in Solution and NC Suspension

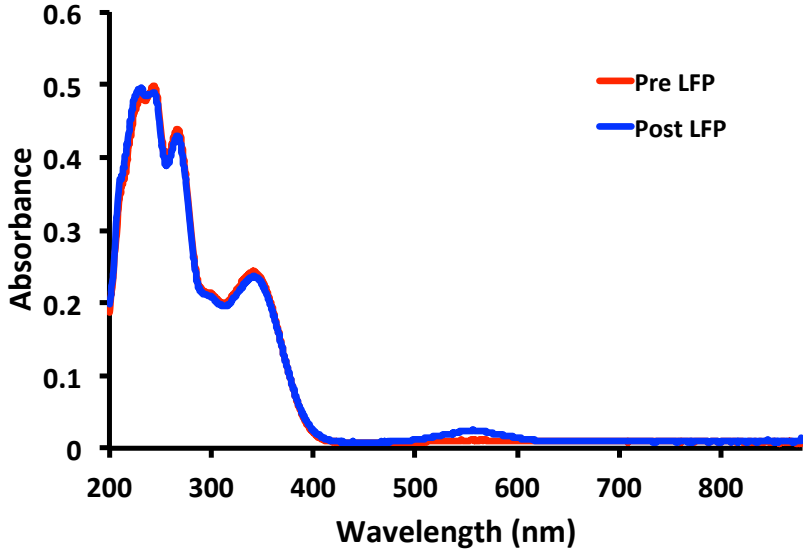

Figure 3.7.1.1. UV-vis absorption spectra of **SP1** in acetonitrile pre-laser flash photolysis (LFP) irradiation (red) and post-LFP irradiation.

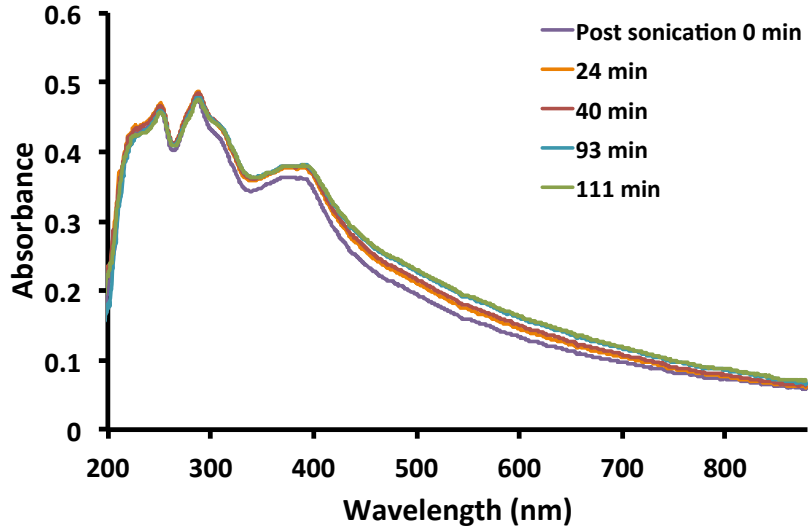

Figure 3.7.1.2. UV-vis absorption spectra of **SP1** in nanocrystalline suspension over time.

3.7.2 PXRD Diffractogram of Nanocrystals and DLS Analysis of NC Suspensions

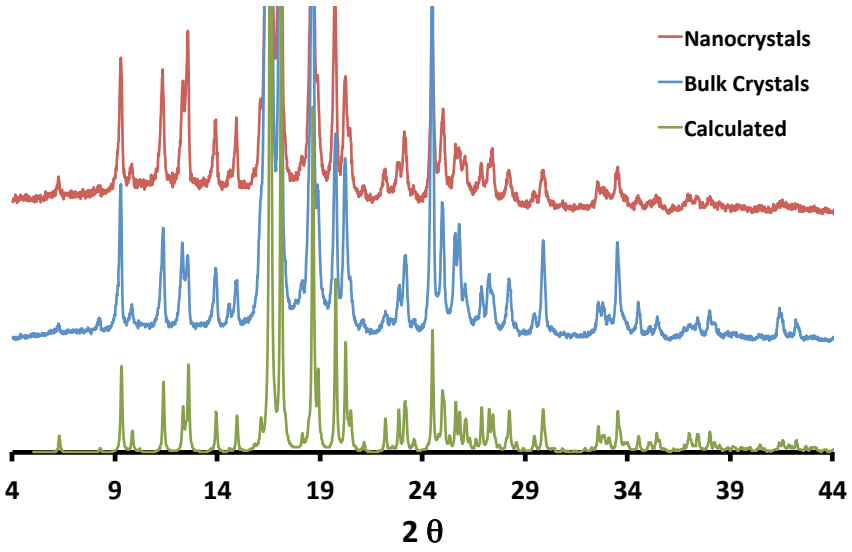

Figure 3.7.2.1. PXRD comparison of experimentally obtained nanocrystals (top) and bulk crystals (middle) to the calculated (bottom) diffractogram from the CSD for **SP1**.

Unimodal Results Summary

Rept#.	Mean (nm)	Std.Dev (nm)	Baseline Error	P.I.	Counts/s	Diff.Coef (m^2/s)	Overflow
Rept.1	365.8	178.9	-0.00%	-2.763	1.15e+05	1.24e-12	0
Rept.2	234.8	114.2	0.00%	2.170	1.15e+05	1.93e-12	0
Rept.3	206.0	100.4	0.00%	2.343	1.15e+05	2.20e-12	1
Average	268.9	131.16		0.583			

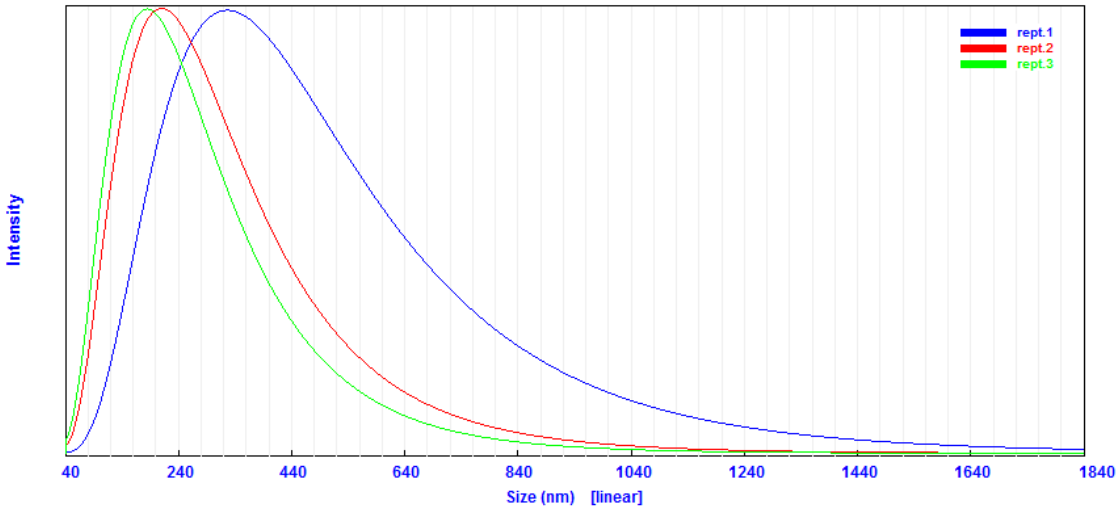

Figure 3.7.2.2. Dynamic light scattering (DLS) results for the nanocrystalline suspensions of **SP1** showing the average particle size to be 269 nm.

3.7.3 Laser Flash Photolysis Kinetic Plots in Degassed and Air-Saturated Acetonitrile

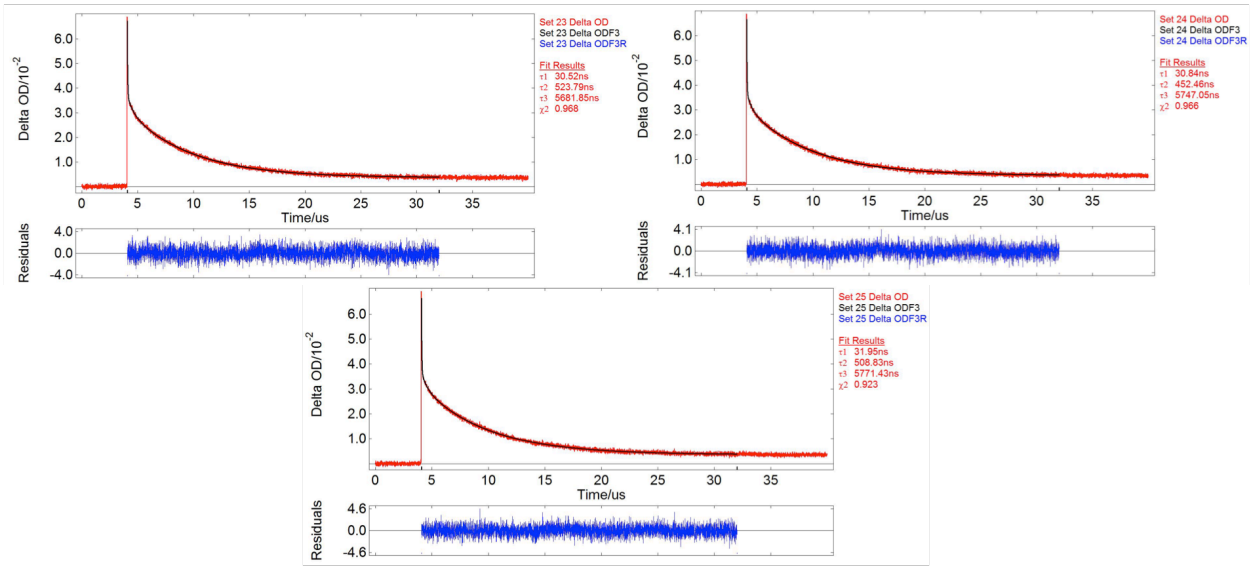

Figure 3.7.3.1. Laser flash photolysis transient kinetic decay plots at 440 nm in argon degassed acetonitrile with the kinetic trace (red), fit line (black), residual (blue), and lifetimes shown.

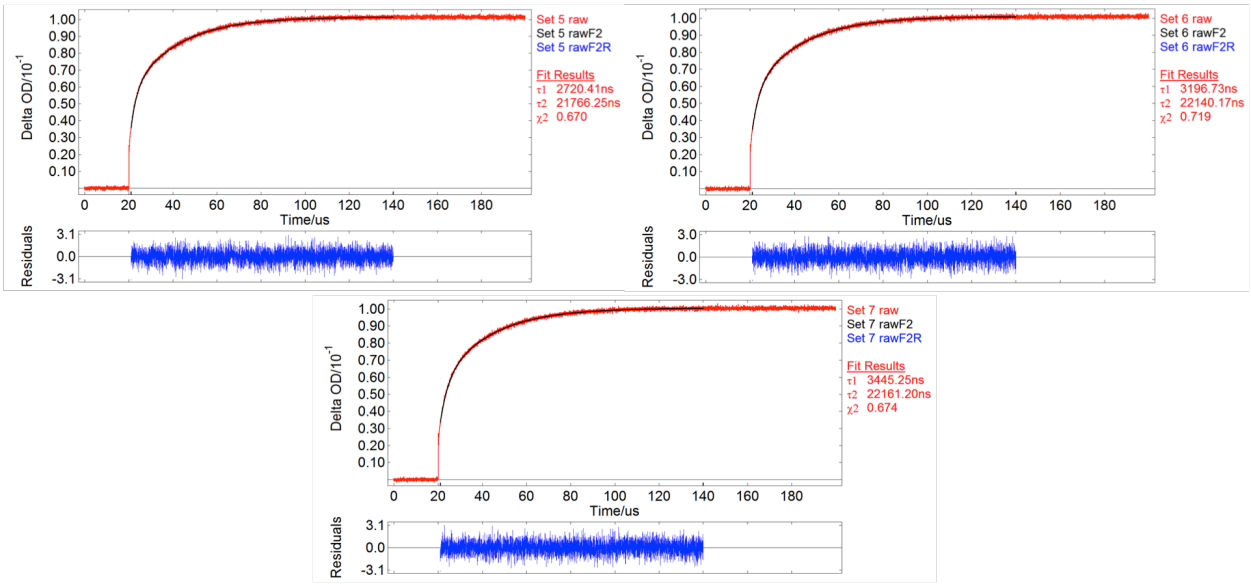

Figure 3.7.3.2. Laser flash photolysis transient kinetic growth plots at 550 nm in argon degassed acetonitrile with the kinetic trace (red), fit line (black), residual (blue), and lifetimes shown.

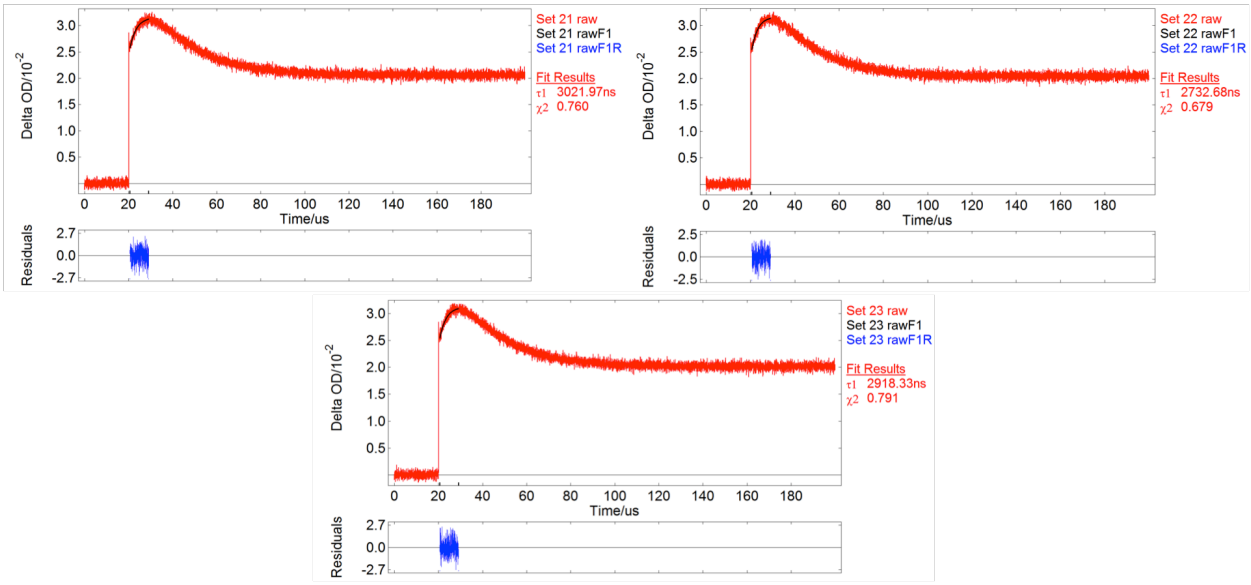

Figure 3.7.3.3. Laser flash photolysis transient kinetic growth plots at 590 nm in argon degassed acetonitrile with the kinetic trace (red), fit line (black), residual (blue), and lifetime shown.

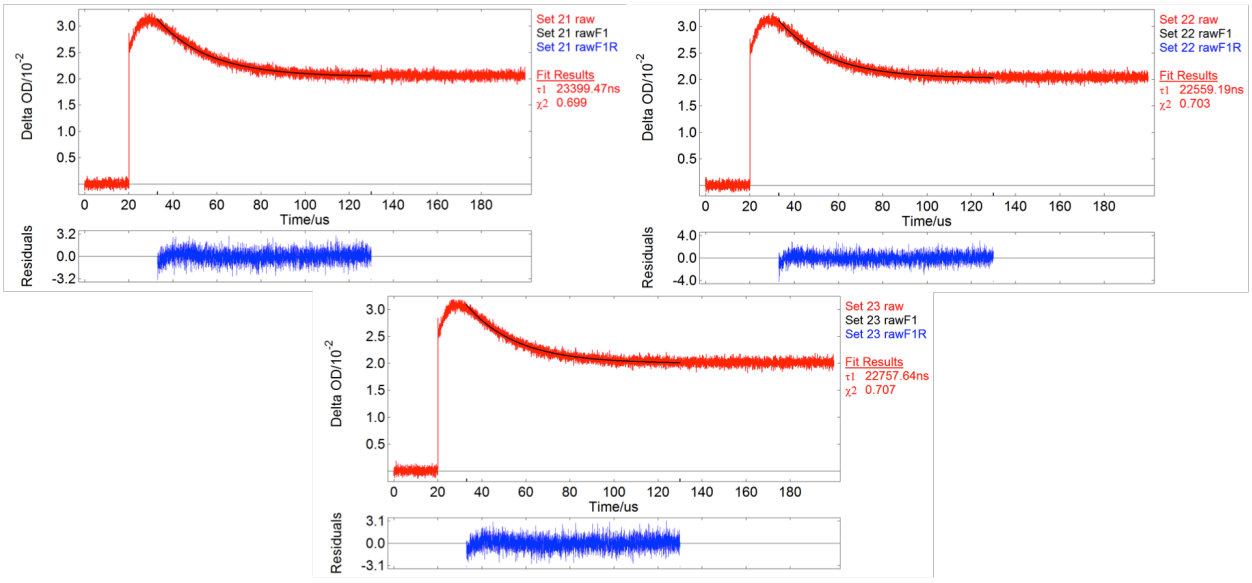

Figure 3.7.3.4. Laser flash photolysis transient kinetic decay plots at 590 nm in argon degassed acetonitrile with the kinetic trace (red), fit line (black), residual (blue), and lifetime shown.

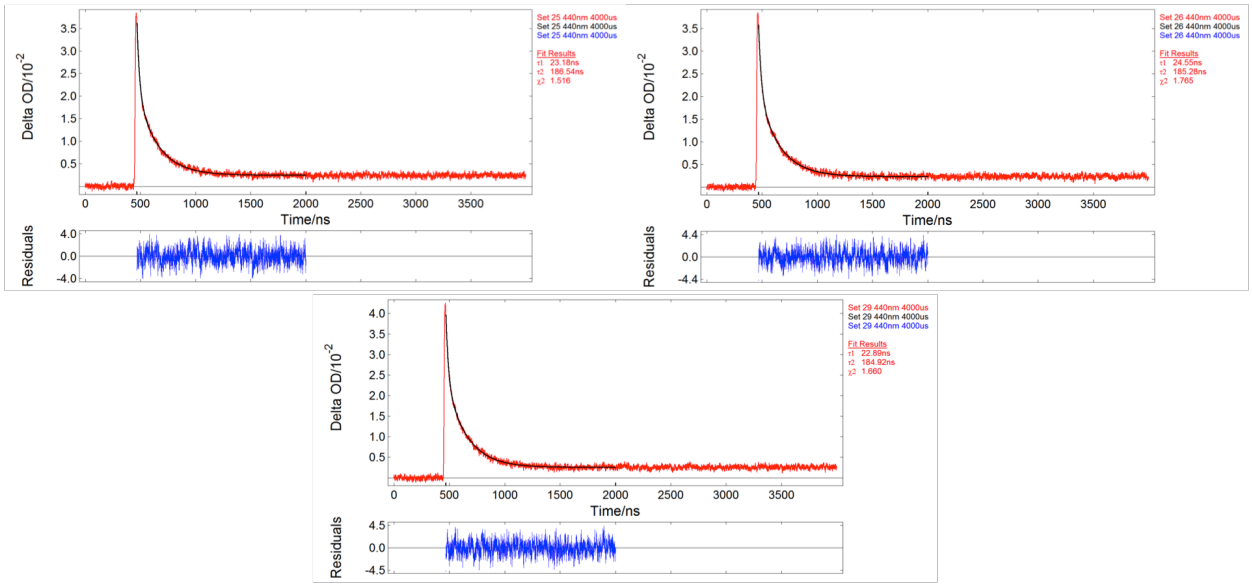

Figure 3.7.3.5. Laser flash photolysis transient kinetic decay plots at 440 nm in air-saturated acetonitrile with the kinetic trace (red), fit line (black), residual (blue), and lifetimes shown.

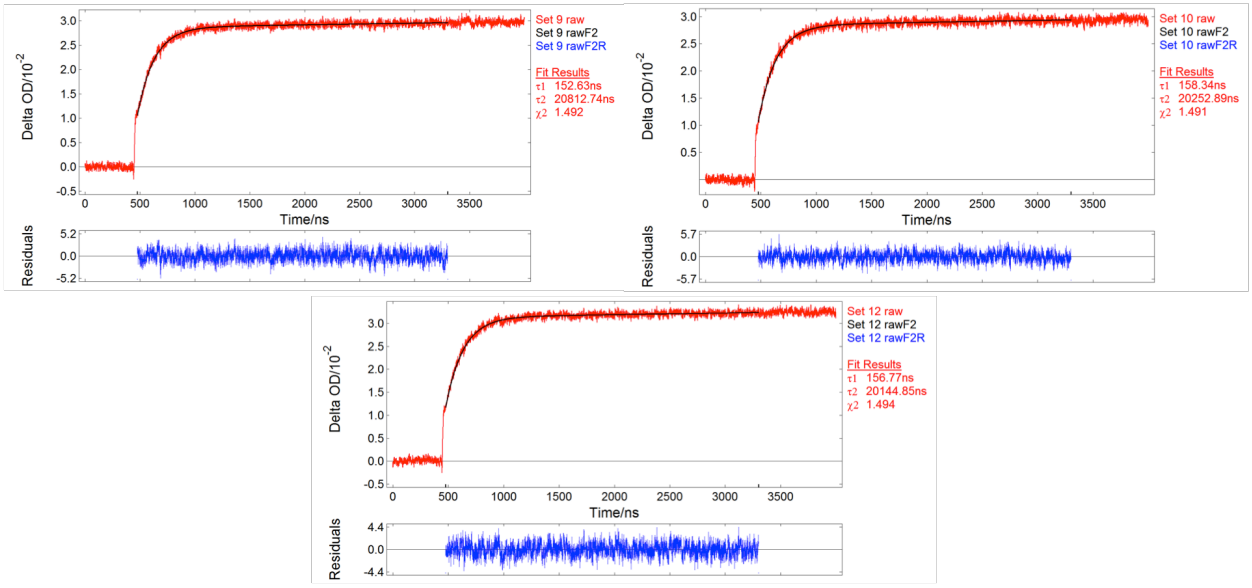

Figure 3.7.3.6. Laser flash photolysis transient kinetic growth plots at 550 nm in air-saturated acetonitrile with the kinetic trace (red), fit line (black), residual (blue), and lifetimes shown.

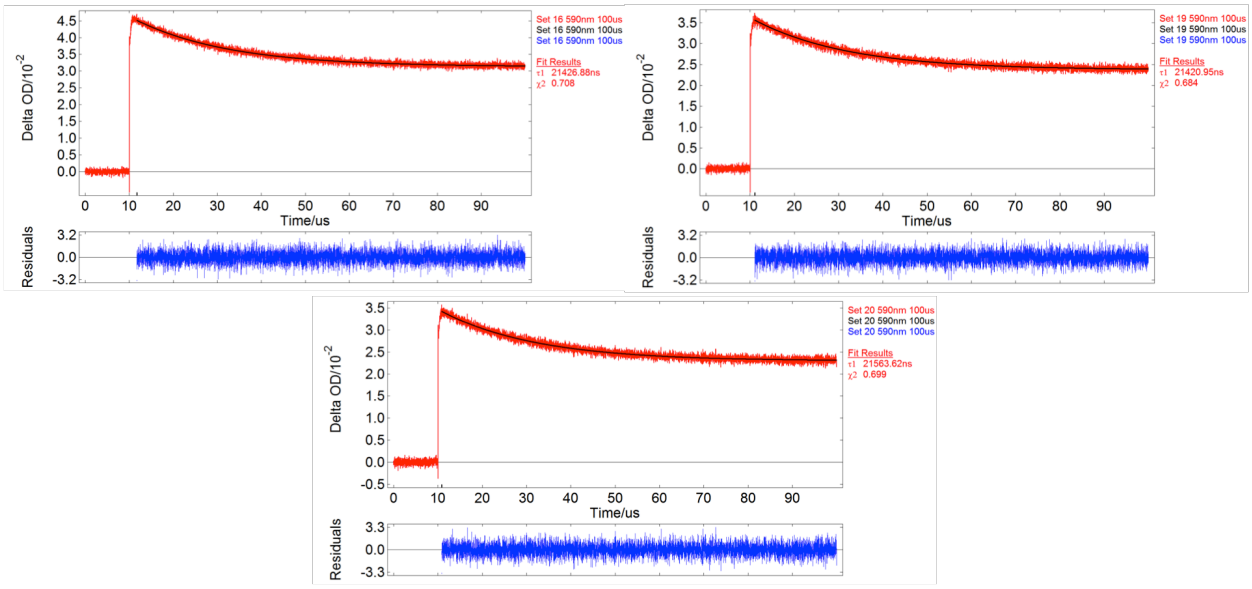

Figure 3.7.3.7. Laser flash photolysis transient kinetic decay plots at 590 nm in air-saturated acetonitrile with the kinetic trace (red), fit line (black), residual (blue), and lifetime shown.

3.7.4 Computational Methods and Calculated Energies for *E*- and *Z*-merocyanines

We used density functional theory (DFT) and TD-DFT calculations to explain the blue shift we observed from 590 to 550 nm in our transient absorption spectra (Figures 3.4.2.1a and 3.4.2.2a above). To understand the origin of this shift and the molar absorptivity difference between the bands at 550 and 590 nm we performed a conformational search to identify the lowest energy conformer for the spiropyran (**SP1**), *Z*-merocyanine (***Z*-MC**), and *E*-merocyanine (***E*-MC**) on the ground state ($\mathbf{S_0}$) and first excited singlet state ($\mathbf{S_1}$) potential energy surfaces (PESs). The conformational search on **SP1** and ***E*-** and ***Z*-MC** isomers was performed with the MMFF94[56] force field using Maestro/Macromodel[57,58] in the Schrödinger Suite of Programs (energy cutoff and other information). Each of the resulting conformers were optimized to their ground state geometries ($\mathbf{S_0}$) and excited state geometries ($\mathbf{S_1}$) using the (TD)-CAM-B3LYP[50] density functional at the 6-311++G(d,p) level of theory utilizing the IEFPCM-(CH_3CN)

continuum solvent method[51,52] and D3 empirical dispersion with Becke-Johnson damping[53] within Gaussian16 Revision A[54]. Upon vibrational analysis, each optimized structure only had positive frequencies, indicating a local minimum. A transition state between **MCZ-a$_0$** and **MCE-c$_0$** was also optimized and confirmed to be a transition state with one imaginary frequency along the calculated intrinsic reaction coordinate (IRC). Single point energies, corrections to thermal free energies, and free energies are provided below for each stationary point.

We computed a full torsional potential about the central C=C π-bond ($C_2C_3C_4C_5$– highlighted in green in Figure 3.7.4.1) to explore relatively high-energy structures and their absorbance properties. We obtained the torsional potentials with the IEFPCM-(CH_3CN) solvation model instead of with multiscale (QM/MM) modeling to maintain reasonable computational cost. The key stationary points **MCZ-a$_0$**, **TS(MCZ$_0$→MCE$_0$)**, and **MCE-c$_0$** are shown in Figure 3.7.4.1.

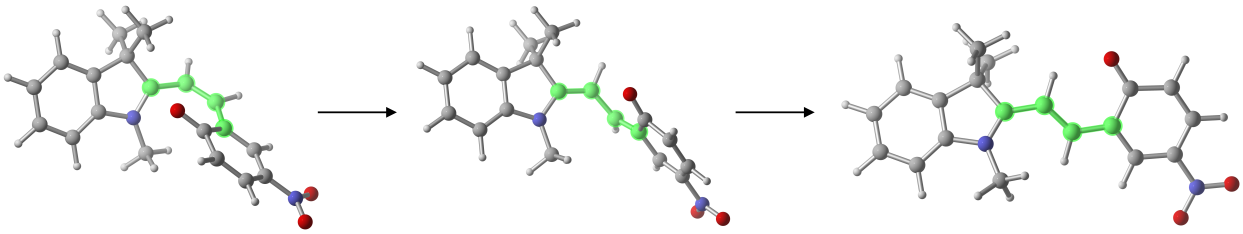

Figure 3.7.4.1. Key stationary points from the torsional potential of the *E*- and *Z*-MCs: **MCZ-a$_0$**, **TS(MCZ$_0$→MCE$_0$)**, and **MCE-c$_0$**. Computed with CAM-B3LYP-(D3BJ)/6-31+G(d,p)/IEFPCM-(CH_3CN) level of theory.

In aiming to understand how the absorption profile varies as a function of structure, we performed single-point calculations on each structure along the torsional potential shown in

Figure 3.4.4.2 above using the TD-CAM-B3LYP method and 6-311++G(d,p) basis set. From this we obtained vertical excitations in order to generate predicted UV-vis absorbance spectra, as shown below in Figure 3.7.4.2. The spectra show that the *E*-like MC structures have a higher absorptivity compared to the ***Z***-like **MC**s, which is in agreement with our solution experimental results shown in Figures 3.4.2.1a and 3.4.2.2a above.

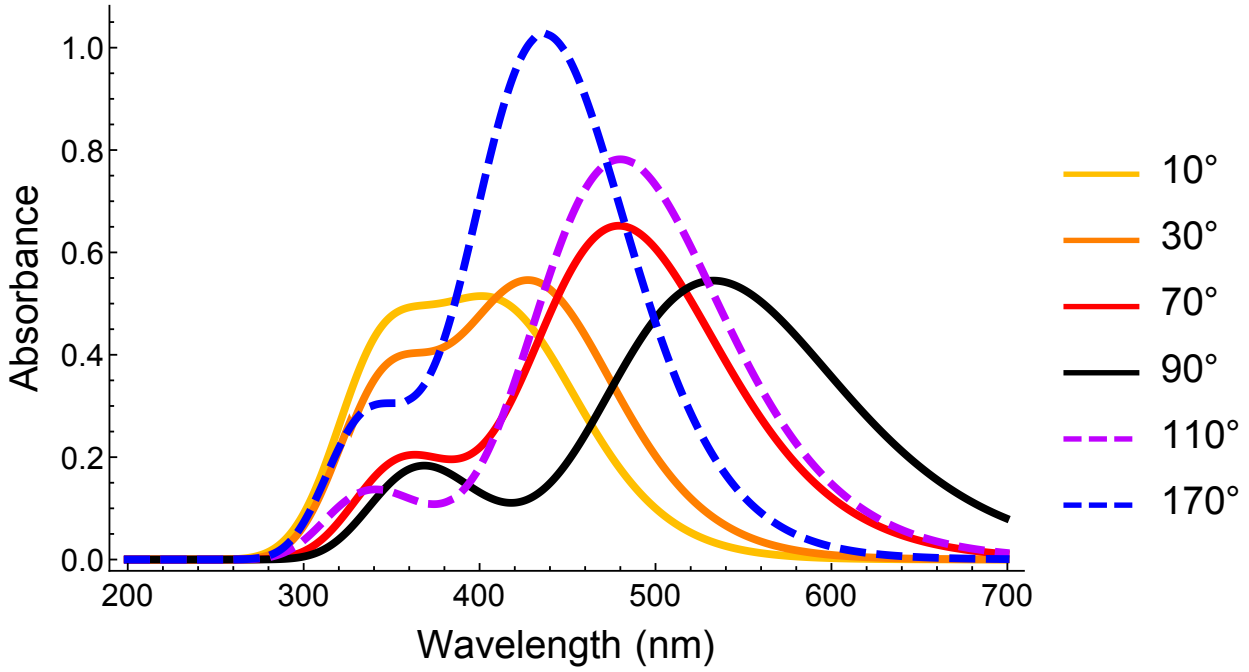

Figure 3.7.4.2. Calculated UV-vis spectra for **MC** geometries along the relaxed scan about the central π-bond (highlighted in green in Figure 3.7.4.1). **MC** geometries were computed at the CAM-B3LYP-(D3BJ)/6-31+G(d,p) IEFPCM-(CH_3CN) level of theory. Absorbance spectra were predicted with the 6-311++G(d,p) basis set. The thick black line indicates the structure closest to the transition state between ***Z***- and ***E***-**MC**. The yellow, orange, and red solid lines correlate to ***Z***-like **MC**s, and the purple and blue dashed lines correlate to ***E***-like **MC**s.

MCZ-a_0

C	-3.87129	0.95369	4.58200
C	-4.78398	0.58700	3.59809
C	-4.50436	0.78731	2.24905
C	-3.28612	1.36141	1.94757
C	-2.36013	1.73021	2.91023
C	-2.64838	1.53184	4.24587
N	-2.75558	1.67817	0.66616
C	-1.53727	2.14844	0.76370
C	-1.15801	2.32830	2.22270
C	-1.03054	3.83007	2.54501
C	0.14762	1.59232	2.54704
C	-0.70678	2.57605	-0.32289
C	-0.44084	1.94944	-1.49026
C	-0.72424	0.60724	-1.94055
C	-3.51831	1.47393	-0.55275
C	-0.97690	-0.49999	-1.02641
C	-1.18881	-1.79279	-1.63670
C	-1.15179	-1.98415	-2.98056
C	-0.87187	-0.89347	-3.83271
C	-0.64262	0.36643	-3.30638
O	-0.99724	-0.36127	0.21696
N	-0.80772	-1.09121	-5.24074
O	-0.55539	-0.13263	-5.97170
O	-1.00873	-2.21986	-5.69023
H	-4.11395	0.78460	5.62359
H	-5.72620	0.13576	3.88198
H	-5.21089	0.49501	1.48410
H	-1.94398	1.81328	5.01915
H	-0.85902	3.94844	3.61529
H	-1.93808	4.37416	2.27956
H	-0.18491	4.27147	2.01659
H	0.36314	1.69204	3.61172
H	0.06881	0.53837	2.28784
H	0.97598	2.02785	1.98605
H	-0.20962	3.52362	-0.14596
H	0.13881	2.53761	-2.19648
H	-3.49885	0.42044	-0.83105
H	-4.54456	1.78940	-0.37660
H	-3.08442	2.06988	-1.34916

H	-1.38918	-2.61953	-0.96627
H	-1.32431	-2.96090	-3.41085
H	-0.41009	1.17980	-3.98132

Single Point Energy: -1069.73029003
Thermal Correction to Free Energy: 0.287682
Free Energy: -1069.442609

MCZ-b_0

C	-4.75358	0.61117	3.49062
C	-5.38293	0.96891	2.30215
C	-4.65042	1.42664	1.21110
C	-3.28175	1.50350	1.37429
C	-2.63327	1.14515	2.54482
C	-3.36938	0.69686	3.62360
N	-2.30500	1.93617	0.43081
C	-1.09078	1.81672	0.91827
C	-1.14990	1.34017	2.35954
C	-0.59649	2.42341	3.30258
C	-0.36602	0.02828	2.51838
C	0.13316	2.14534	0.25368
C	0.49392	1.88981	-1.02596
C	-0.13931	1.04155	-2.00399
C	-2.68020	2.49372	-0.85899
C	0.10016	1.35194	-3.40953
C	-0.49937	0.45084	-4.36775
C	-1.23925	-0.62370	-3.98867
C	-1.43061	-0.89923	-2.61567
C	-0.87474	-0.07541	-1.64918
O	0.76573	2.34934	-3.75966
N	-2.17440	-2.04150	-2.21508
O	-2.32749	-2.26841	-1.01297
O	-2.65391	-2.77222	-3.08319
H	-5.34898	0.25735	4.32276
H	-6.45930	0.88867	2.22024
H	-5.13923	1.69849	0.28562
H	-2.88855	0.41325	4.55174
H	0.47102	2.57403	3.13987
H	-0.73883	2.09955	4.33376
H	-1.11432	3.37332	3.16460
H	-0.76025	-0.75432	1.86869

H	0.68831	0.18086	2.28528
H	-0.44610	-0.31530	3.55024
H	0.87016	2.61220	0.89757
H	1.41945	2.34561	-1.36425
H	-1.86793	3.11158	-1.22942
H	-3.57206	3.10048	-0.72149
H	-2.88077	1.69291	-1.57053
H	-0.33765	0.66744	-5.41656
H	-1.68052	-1.28333	-4.72309
H	-1.00120	-0.34882	-0.61136

Single Point Energy: -1069.72748733
Thermal Correction to Free Energy: 0.287097
Free Energy: -1069.440390

MCE-a_0

C	-5.14503	-2.95148	0.34428
C	-5.55224	-2.12711	1.38777
C	-4.75650	-1.07192	1.82466
C	-3.55067	-0.88504	1.17532
C	-3.12865	-1.69641	0.13377
C	-3.92405	-2.74054	-0.29308
N	-2.55514	0.09648	1.40744
C	-1.52611	-0.04082	0.57753
C	-1.77669	-1.22593	-0.35193
C	-0.72674	-2.33296	-0.15393
C	-1.86551	-0.78337	-1.82277
C	-0.42540	0.83322	0.63772
C	0.66393	0.74697	-0.18611
C	1.81235	1.58402	-0.19287
C	-2.65606	1.12651	2.43287
C	1.99301	2.70846	0.72804
C	3.22613	3.45647	0.58072
C	4.16276	3.14602	-0.34712
C	3.95216	2.04957	-1.22158
C	2.80385	1.29627	-1.13708
O	1.15200	3.02144	1.59285
N	4.94078	1.72343	-2.19949
O	5.95897	2.40975	-2.25706
O	4.74739	0.77059	-2.95204
H	-5.78349	-3.76517	0.02434

H	-6.50404	-2.30506	1.87205
H	-5.08445	-0.43829	2.63689
H	-3.61142	-3.38553	-1.10543
H	0.25936	-2.02298	-0.49568
H	-1.02371	-3.21087	-0.72877
H	-0.65481	-2.61965	0.89586
H	-2.18460	-1.63121	-2.42998
H	-2.59386	0.01899	-1.94581
H	-0.90478	-0.43888	-2.20173
H	-0.43214	1.62122	1.37401
H	0.68774	-0.03813	-0.93147
H	-2.63040	2.11385	1.97327
H	-3.59366	1.00888	2.96458
H	-1.83293	1.03047	3.13995
H	3.37125	4.29047	1.25613
H	5.07411	3.72099	-0.43543
H	2.66908	0.46501	-1.81704

Single Point Energy: -1069.73666717
Thermal Correction to Free Energy: 0.284413
Free Energy: -1069.452254

MCE-b_0

C	-5.51347	-2.21629	0.81435
C	-4.75595	-3.19674	1.44567
C	-3.37317	-3.07970	1.55465
C	-2.79407	-1.94932	1.00912
C	-3.53271	-0.96342	0.37371
C	-4.90357	-1.08745	0.27092
N	-1.42803	-1.57480	0.97713
C	-1.25169	-0.41349	0.35239
C	-2.60334	0.12530	-0.11261
C	-2.66957	0.23249	-1.64614
C	-2.94910	1.46163	0.56751
C	0.02560	0.14559	0.18604
C	0.26018	1.34028	-0.43840
C	1.50883	1.97252	-0.66124
C	-0.35688	-2.37653	1.55348
C	1.48284	3.26808	-1.34763
C	2.77109	3.89585	-1.56929

C	3.93056	3.32307	-1.16876
C	3.91059	2.06602	-0.50767
C	2.72536	1.41349	-0.26360
O	0.42236	3.80287	-1.71967
N	5.14163	1.46920	-0.09205
O	6.19043	2.06788	-0.32041
O	5.11675	0.38071	0.47879
H	-6.58754	-2.33207	0.74363
H	-5.24534	-4.06861	1.86099
H	-2.79565	-3.85056	2.04557
H	-5.49868	-0.32753	-0.22095
H	-2.40529	-0.71620	-2.11527
H	-2.00276	1.00411	-2.02739
H	-3.68774	0.48795	-1.94189
H	-2.30183	2.26940	0.22992
H	-2.86570	1.38075	1.65210
H	-3.97789	1.72877	0.32311
H	0.85926	-0.41976	0.57895
H	-0.57330	1.91096	-0.82533
H	0.20336	-1.78558	2.27658
H	0.31172	-2.73053	0.76904
H	-0.78731	-3.23161	2.06267
H	2.77204	4.85361	-2.07451
H	4.88145	3.80695	-1.34363
H	2.75809	0.45739	0.24031

Single Point Energy: -1069.73517504
Thermal Correction to Free Energy: 0.285232
Free Energy: -1069.449944

MCE-c_0

C	-5.32628	-2.72142	0.77067
C	-4.38636	-3.41702	1.52342
C	-3.08417	-2.94430	1.66344
C	-2.77826	-1.75906	1.02334
C	-3.69806	-1.05551	0.26182
C	-4.98756	-1.53039	0.13100
N	-1.54008	-1.05860	1.00740
C	-1.61232	0.01924	0.23935
C	-3.02893	0.17409	-0.29622
C	-3.02576	0.18253	-1.83183

C	-3.66525	1.46092	0.25650
C	-0.60291	0.94945	-0.08341
C	0.74600	0.73618	-0.02269
C	1.78113	1.63956	-0.39988
C	-0.41125	-1.48403	1.82095
C	1.52736	3.00234	-0.86955
C	2.69842	3.77931	-1.22285
C	3.95821	3.29062	-1.12133
C	4.16445	1.96769	-0.65700
C	3.09483	1.17215	-0.30985
O	0.38197	3.48570	-0.96822
N	5.49139	1.45359	-0.54924
O	6.43175	2.18120	-0.86354
O	5.65802	0.30315	-0.14697
H	-6.33168	-3.11216	0.67764
H	-4.66638	-4.34371	2.00807
H	-2.35597	-3.49556	2.24228
H	-5.72360	-0.99492	-0.45627
H	-2.56287	-0.72146	-2.22987
H	-2.48310	1.04902	-2.21107
H	-4.05269	0.23378	-2.19588
H	-3.64792	1.47328	1.34705
H	-4.70371	1.51483	-0.07241
H	-3.14388	2.34398	-0.11398
H	-0.93963	1.88621	-0.50178
H	1.10737	-0.23422	0.29443
H	0.25171	-2.14000	1.25644
H	-0.79134	-2.01913	2.68694
H	0.13464	-0.60834	2.16349
H	2.52319	4.78800	-1.57597
H	4.81475	3.89347	-1.38937
H	3.28117	0.16484	0.03943

Single Point Energy: -1069.73399849
Thermal Correction to Free Energy: 0.286866
Free Energy: -1069.447133

MCE-d_0

C	-5.38596	-2.58000	0.49432
C	-5.29088	-2.02674	1.76652
C	-4.18929	-1.26044	2.13800

C	-3.20283	-1.08087	1.18744
C	-3.28413	-1.61660	-0.08819
C	-4.37855	-2.37718	-0.44712
N	-1.98250	-0.35912	1.30424
C	-1.30982	-0.37200	0.15997
C	-2.05662	-1.21620	-0.86513
C	-1.21851	-2.44219	-1.26433
C	-2.41327	-0.37250	-2.09834
C	-0.09028	0.25299	-0.15818
C	0.52930	1.25980	0.52973
C	1.74350	1.91392	0.19015
C	-1.55877	0.23362	2.56285
C	2.17723	3.00144	1.07173
C	3.41884	3.65624	0.70987
C	4.14008	3.28608	-0.37494
C	3.68544	2.22433	-1.20056
C	2.51443	1.55961	-0.91744
O	1.52410	3.34638	2.07433
N	4.45483	1.83977	-2.34168
O	5.49809	2.44547	-2.57814
O	4.05451	0.91911	-3.05163
H	-6.25397	-3.17134	0.23162
H	-6.08578	-2.18943	2.48327
H	-4.12926	-0.82688	3.12664
H	-4.45904	-2.80767	-1.43796
H	-1.80675	-3.07474	-1.93021
H	-0.93704	-3.03029	-0.38997
H	-0.31302	-2.14354	-1.79352
H	-3.00537	-0.97465	-2.78848
H	-2.99632	0.50604	-1.81922
H	-1.51289	-0.04338	-2.61811
H	0.33887	-0.08151	-1.09375
H	0.07142	1.67047	1.41884
H	-2.07035	-0.27315	3.37559
H	-0.48696	0.09373	2.68612
H	-1.80129	1.29619	2.59423
H	3.75392	4.46372	1.34889
H	5.06449	3.78655	-0.62781
H	2.20797	0.75603	-1.57267

Single Point Energy: -1069.73263546
Thermal Correction to Free Energy: 0.285975
Free Energy: -1069.446661

MCZ-a_1

C	-4.05394	-2.45596	0.28126
C	-2.94305	-3.08266	-0.27573
C	-1.83571	-2.34896	-0.69018
C	-1.88224	-0.97422	-0.51740
C	-2.99406	-0.33003	0.02282
C	-4.08731	-1.06851	0.42653
N	-0.89963	-0.03177	-0.84154
C	-1.30716	1.21661	-0.44269
C	-2.76574	1.16530	-0.01362
C	-3.64538	1.80716	-1.10859
C	-3.02251	1.84517	1.33233
C	-0.50621	2.36435	-0.42312
C	0.87357	2.37900	-0.27124
C	1.60840	1.27422	0.25143
C	0.10749	-0.33841	-1.85084
C	0.99086	0.42804	1.29421
C	1.62311	-0.83249	1.58448
C	2.84954	-1.14325	1.08080
C	3.48423	-0.22419	0.21850
C	2.89326	0.95313	-0.18922
O	-0.01121	0.81292	1.92433
N	4.80652	-0.55155	-0.29048
O	5.39005	0.28049	-0.96887
O	5.27666	-1.64643	-0.01788
H	-4.90138	-3.05023	0.59956
H	-2.93541	-4.16017	-0.38560
H	-0.97049	-2.83948	-1.11658
H	-4.96223	-0.58438	0.84458
H	-4.69983	1.69792	-0.84675
H	-3.47823	1.33101	-2.07597
H	-3.42413	2.87231	-1.20048
H	-4.06890	1.72096	1.61838
H	-2.38515	1.41893	2.10466
H	-2.81729	2.91545	1.26619
H	-1.02230	3.31517	-0.51821
H	1.42607	3.26185	-0.57552

H	0.87157	-1.00846	-1.45655
H	-0.37996	-0.81887	-2.70200
H	0.57748	0.58090	-2.18345
H	1.12598	-1.48355	2.29179
H	3.35223	-2.06360	1.33917
H	3.40168	1.59114	-0.89843

Single Point Energy: -1069.70648460
Thermal Correction to Free Energy: 0.284504
Free Energy: -1069.356709

MCZ-b_1

C	-4.69103	0.48073	3.47121
C	-5.30565	0.75044	2.24922
C	-4.56985	1.18692	1.15591
C	-3.20005	1.33341	1.33389
C	-2.57159	1.07789	2.55257
C	-3.31577	0.64767	3.63121
N	-2.25424	1.75324	0.39859
C	-1.00293	1.73892	0.94214
C	-1.09951	1.38170	2.42059
C	-0.70766	2.59350	3.28927
C	-0.22622	0.16935	2.77254
C	0.20112	1.97735	0.28632
C	0.52005	1.86311	-1.07238
C	-0.09986	1.02299	-2.02206
C	-2.67810	2.43135	-0.81921
C	0.25801	1.23469	-3.44873
C	-0.42667	0.42601	-4.43495
C	-1.32132	-0.52792	-4.07585
C	-1.59064	-0.75143	-2.70202
C	-0.98424	-0.01787	-1.69865
O	1.09885	2.08376	-3.76789
N	-2.52100	-1.77921	-2.33883
O	-2.77778	-1.94401	-1.14626
O	-3.03061	-2.46215	-3.22811
H	-5.29039	0.14108	4.30653
H	-6.37517	0.61495	2.14790
H	-5.04707	1.38822	0.20628
H	-2.84853	0.44667	4.58788
H	0.34356	2.84747	3.14388

H	-0.85683	2.34993	4.34265
H	-1.31595	3.46531	3.04555
H	-0.49091	-0.69598	2.16355
H	0.82869	0.39673	2.61230
H	-0.36251	-0.09341	3.82306
H	1.01271	2.28159	0.94124
H	1.39334	2.39827	-1.42497
H	-1.82297	2.90072	-1.29192
H	-3.41048	3.19588	-0.55314
H	-3.13218	1.72633	-1.51571
H	-0.18767	0.61048	-5.47437
H	-1.83178	-1.12935	-4.81430
H	-1.20178	-0.26233	-0.67203

Single Point Energy: -1069.71891541
Thermal Correction to Free Energy: 0.284637
Free Energy: -1069.359141

MCE-a_1

C	-5.16892	-2.94979	0.39871
C	-5.56095	-2.11162	1.44267
C	-4.76075	-1.06022	1.86361
C	-3.54826	-0.87330	1.20210
C	-3.14505	-1.70763	0.15307
C	-3.95227	-2.74833	-0.25247
N	-2.57300	0.08451	1.41611
C	-1.52199	-0.06632	0.54934
C	-1.79664	-1.25645	-0.35823
C	-0.75504	-2.37683	-0.17280
C	-1.89848	-0.84143	-1.83848
C	-0.43079	0.79310	0.58296
C	0.68641	0.72171	-0.25076
C	1.81597	1.57517	-0.24956
C	-2.64735	1.11814	2.43017
C	1.96549	2.75028	0.65233
C	3.19164	3.51909	0.54861
C	4.17053	3.21097	-0.33764
C	3.99622	2.09631	-1.19169
C	2.85966	1.30575	-1.14888
O	1.08788	3.07381	1.46203
N	5.03442	1.77947	-2.12848

O	6.04533	2.48327	-2.15743
O	4.87751	0.81161	-2.87311
H	-5.81542	-3.76247	0.09252
H	-6.50928	-2.28264	1.93676
H	-5.07958	-0.41972	2.67415
H	-3.65216	-3.40195	-1.06298
H	0.23107	-2.06897	-0.51802
H	-1.05796	-3.25209	-0.74985
H	-0.67892	-2.66606	0.87606
H	-2.20756	-1.70106	-2.43533
H	-2.63624	-0.04882	-1.96922
H	-0.94209	-0.48871	-2.22220
H	-0.43853	1.58765	1.31400
H	0.73184	-0.07036	-0.98620
H	-2.62144	2.10565	1.96671
H	-3.57463	1.01539	2.98360
H	-1.81079	1.02615	3.12476
H	3.28461	4.36588	1.21661
H	5.07664	3.79488	-0.40826
H	2.78068	0.46366	-1.82168

Single Point Energy: -1069.73291353
Thermal Correction to Free Energy: 0.281359
Free Energy: -1069.363542

MCE-b_1

C	-5.49533	-2.27652	0.88274
C	-4.69794	-3.24796	1.49373
C	-3.31516	-3.11050	1.56256
C	-2.75832	-1.96422	0.99677
C	-3.54568	-0.98285	0.38270
C	-4.91780	-1.13372	0.32219
N	-1.42311	-1.57998	0.92575
C	-1.28266	-0.37871	0.29183
C	-2.65657	0.12865	-0.12715
C	-2.77882	0.25532	-1.65941
C	-3.01045	1.46083	0.56468
C	-0.03499	0.21138	0.10808
C	0.21472	1.43185	-0.52967
C	1.50359	1.99171	-0.68801
C	-0.31839	-2.35448	1.45812

C	1.58048	3.29722	-1.39737
C	2.88580	3.89779	-1.57538
C	4.01532	3.29546	-1.11167
C	3.91286	2.05109	-0.43910
C	2.69679	1.40969	-0.22868
O	0.54628	3.84515	-1.82009
N	5.11195	1.43554	0.03855
O	6.19690	2.00710	-0.14287
O	5.02501	0.34556	0.62111
H	-6.57075	-2.41094	0.84414
H	-5.16250	-4.12831	1.92467
H	-2.71155	-3.87178	2.04108
H	-5.54098	-0.38145	-0.15072
H	-2.52755	-0.68825	-2.14929
H	-2.12266	1.03371	-2.05083
H	-3.80776	0.51529	-1.91997
H	-2.36150	2.27080	0.22938
H	-2.92102	1.37195	1.64989
H	-4.04200	1.73013	0.32501
H	0.81499	-0.33472	0.50020
H	-0.59353	2.01727	-0.94239
H	0.19938	-1.79045	2.23850
H	0.38799	-2.60098	0.66143
H	-0.69713	-3.27806	1.88614
H	2.92538	4.84869	-2.09432
H	4.99123	3.74347	-1.24441
H	2.69709	0.46296	0.29226

Single Point Energy: -1069.73075115
Thermal Correction to Free Energy: 0.284852
Free Energy: -1069.364736

MCE-c_1

C	-6.16975	-0.48944	-0.32602
C	-5.74633	-1.78058	-0.01343
C	-4.40785	-2.06445	0.21824
C	-3.50558	-1.00796	0.12579
C	-3.91715	0.28990	-0.19228
C	-5.25081	0.55590	-0.41685
N	-2.12936	-1.02227	0.31624
C	-1.59012	0.21388	0.08452

C	-2.71402	1.19770	-0.20932
C	-2.53365	1.87370	-1.57769
C	-2.80734	2.26179	0.90113
C	-0.25192	0.58533	0.07277
C	0.89208	-0.21679	0.10229
C	2.23512	0.23114	0.12849
C	-1.42444	-2.19371	0.80475
C	2.61984	1.64935	0.35996
C	4.02752	1.98288	0.26245
C	4.98213	1.04235	0.05220
C	4.59249	-0.30873	-0.10228
C	3.26467	-0.70221	-0.06620
O	1.78442	2.51664	0.64560
N	5.61003	-1.29674	-0.31478
O	6.78805	-0.93845	-0.35568
O	5.26826	-2.47180	-0.44923
H	-7.22092	-0.29844	-0.50154
H	-6.47341	-2.58082	0.04734
H	-4.09156	-3.07249	0.44862
H	-5.58501	1.55763	-0.65955
H	-2.45683	1.13212	-2.37388
H	-1.63284	2.48904	-1.58772
H	-3.38846	2.51938	-1.78706
H	-2.93465	1.79603	1.87924
H	-3.66189	2.91468	0.71363
H	-1.90536	2.87542	0.92162
H	-0.08743	1.64984	-0.01514
H	0.78437	-1.28978	0.02712
H	-0.96650	-2.75183	-0.01482
H	-2.13074	-2.84085	1.31799
H	-0.65949	-1.89016	1.51516
H	4.28638	3.02427	0.40501
H	6.03038	1.29919	0.00532
H	3.02199	-1.74561	-0.20879

Single Point Energy: -1069.72890487
Thermal Correction to Free Energy: 0.283182
Free Energy: -1069.358619

MCE-d_1

C	-6.07092	-0.60598	-0.13457

C	-5.99369	0.76499	0.10288
C	-4.76934	1.40450	0.24482
C	-3.62565	0.62052	0.14050
C	-3.68891	-0.75280	-0.10222
C	-4.91177	-1.37444	-0.23893
N	-2.29084	1.00914	0.24747
C	-1.45729	-0.04679	0.03942
C	-2.28861	-1.30815	-0.15593
C	-2.04353	-2.30375	0.99354
C	-1.99471	-1.97428	-1.50931
C	-0.06955	-0.04879	-0.01643
C	0.82685	1.02131	-0.07572
C	2.23096	0.86459	-0.07705
C	-1.90176	2.35615	0.62764
C	3.03832	2.10300	-0.23620
C	4.47810	1.97184	-0.25566
C	5.08355	0.76295	-0.12742
C	4.28960	-0.39698	0.03187
C	2.90322	-0.35664	0.06438
O	2.48188	3.20279	-0.34896
N	4.95063	-1.66288	0.17073
O	6.18195	-1.69764	0.15995
O	4.25905	-2.67362	0.29685
H	-7.03985	-1.07722	-0.24106
H	-6.90404	1.34687	0.17556
H	-4.72296	2.47079	0.41805
H	-4.97695	-2.44000	-0.42417
H	-2.70391	-3.16510	0.87789
H	-2.24272	-1.84205	1.96138
H	-1.01250	-2.66059	0.98229
H	-2.65495	-2.83213	-1.64806
H	-2.15487	-1.27727	-2.33278
H	-0.96391	-2.32938	-1.54961
H	0.34948	-1.04686	-0.07034
H	0.48300	2.03893	-0.16174
H	-2.73189	2.82830	1.14581
H	-1.05351	2.31358	1.30582
H	-1.64463	2.95444	-0.24862
H	5.05390	2.88048	-0.37529
H	6.15930	0.66509	-0.14223

H	2.36542	-1.28134	0.20511

Single Point Energy: -1069.72873385
Thermal Correction to Free Energy: 0.283462
Free Energy: -1069.363493

TS-MCE-MCZ-S_0

C	-3.31430	3.29944	-0.26816
C	-3.88385	4.42817	0.30184
C	-3.14765	5.60040	0.47678
C	-1.82497	5.65586	0.09687
C	-1.23019	4.52598	-0.47227
C	-1.97399	3.36792	-0.65018
C	-4.03081	6.65694	1.10581
C	-5.37324	5.91751	1.20410
N	-5.18221	4.60912	0.77590
O	-7.89641	7.10051	-0.84203
C	-8.84356	6.45806	-0.41340
C	-8.88200	5.89050	0.96836
C	-7.83187	5.91225	1.82466
C	-6.50074	6.49401	1.63118
C	-10.02740	6.21559	-1.24169
C	-11.11260	5.58173	-0.77234
C	-11.13730	5.09944	0.58559
C	-10.09160	5.24335	1.41688
C	-3.52253	7.03832	2.50269
C	-4.13346	7.90022	0.21679
C	-6.21084	3.59817	0.69799
N	-12.33810	4.42817	1.06459
O	-13.27010	4.31064	0.28573
O	-12.36020	4.01641	2.21227
H	-3.87898	2.38988	-0.42365
H	-1.24885	6.56431	0.23351
H	-0.19192	4.55626	-0.77805
H	-1.51104	2.49644	-1.09782
H	-8.02940	5.48079	2.80639
H	-6.43737	7.53921	1.92201
H	-9.99166	6.59258	-2.25551
H	-11.98340	5.42277	-1.39264
H	-10.14060	4.85970	2.42717
H	-4.19590	7.75863	2.97176

H	-3.45491	6.15985	3.14679
H	-2.53106	7.49079	2.43227
H	-4.81711	8.63241	0.65050
H	-3.15286	8.37010	0.11586
H	-4.49477	7.64042	-0.77909
H	-5.74630	2.61704	0.62699
H	-6.81732	3.60316	1.60241
H	-6.86298	3.74070	-0.16871

Single Point Energy: -1069.69279642
Thermal Correction to Free Energy: 0.282639
Free Energy: -1069.410158
Imaginary frequency of transition state: -278.7828 cm^{-1}

Scans

MCZ 10.0°

C	-5.03462	-1.69553	0.30435
C	-4.22300	-2.54146	-0.45154
C	-2.98023	-2.11537	-0.92241
C	-2.60394	-0.82399	-0.59947
C	-3.39323	0.03434	0.15516
C	-4.62612	-0.39563	0.61362
N	-1.40506	-0.14297	-0.95148
C	-1.36404	1.05152	-0.40825
C	-2.67372	1.35298	0.30124
C	-3.42444	2.47858	-0.44057
C	-2.42730	1.74337	1.76586
C	-0.31069	2.01423	-0.56055
C	1.02995	1.84567	-0.44671
C	1.82051	0.73859	0.04290
C	-0.39808	-0.75140	-1.80332
C	1.29108	-0.28428	0.93970
C	2.22739	-1.29503	1.38210
C	3.53527	-1.30070	1.00302
C	4.02202	-0.27210	0.16147
C	3.17364	0.73285	-0.28439
O	0.09520	-0.29483	1.32732
N	5.38904	-0.25694	-0.21916
O	5.80597	0.65372	-0.94860
O	6.13365	-1.15891	0.18890
H	-5.99510	-2.05320	0.65909

H	-4.55804	-3.54798	-0.67651
H	-2.34696	-2.77568	-1.50260
H	-5.26359	0.25532	1.20289
H	-4.40612	2.61144	0.01909
H	-3.56829	2.23624	-1.49615
H	-2.88402	3.42453	-0.36353
H	-3.38695	1.89659	2.26492
H	-1.86759	0.96409	2.28333
H	-1.85811	2.67464	1.81819
H	-0.66463	3.02074	-0.76469
H	1.61782	2.71968	-0.71977
H	0.20209	-1.45554	-1.22439
H	-0.90039	-1.27526	-2.61591
H	0.24247	0.02665	-2.21026
H	1.83713	-2.06641	2.03739
H	4.21308	-2.07426	1.34187
H	3.57805	1.51802	-0.91279

Single Point Energy: -1069.72991001

MCZ 30.0°

C	-5.13661	-1.63334	0.25718
C	-4.32251	-2.50618	-0.46426
C	-3.05570	-2.11526	-0.90066
C	-2.65603	-0.82955	-0.58085
C	-3.44765	0.05351	0.14253
C	-4.70440	-0.34103	0.56618
N	-1.43187	-0.18191	-0.90470
C	-1.38038	1.02399	-0.37438
C	-2.69993	1.35371	0.30617
C	-3.41371	2.50423	-0.43044
C	-2.46528	1.71829	1.78035
C	-0.31154	1.95795	-0.49316
C	1.03185	1.73502	-0.57358
C	1.84761	0.68461	-0.02567
C	-0.42744	-0.81450	-1.73980
C	1.35395	-0.27516	0.95997
C	2.33024	-1.20091	1.49717
C	3.63193	-1.20644	1.10178
C	4.07653	-0.25542	0.14967

C	3.19810	0.67426	-0.38096
O	0.15851	-0.30279	1.34241
N	5.44026	-0.24348	-0.25359
O	5.81909	0.59215	-1.08457
O	6.21439	-1.07377	0.23947
H	-6.11619	-1.96352	0.58536
H	-4.67429	-3.50701	-0.68936
H	-2.42230	-2.79862	-1.45314
H	-5.34232	0.33237	1.12932
H	-4.39795	2.65690	0.01783
H	-3.54918	2.27668	-1.49041
H	-2.85171	3.43614	-0.33672
H	-3.42794	1.87791	2.27173
H	-1.92391	0.92272	2.29355
H	-1.88175	2.63922	1.85412
H	-0.64595	2.97599	-0.67413
H	1.60599	2.57943	-0.95091
H	0.21786	-1.45593	-1.13708
H	-0.93226	-1.40818	-2.50050
H	0.17313	-0.04511	-2.21958
H	1.97066	-1.91504	2.23017
H	4.33776	-1.92055	1.50715
H	3.57147	1.40293	-1.09128

Single Point Energy: -1069.72782629

MCZ 50.0°

C	-5.32006	-1.48735	0.20075
C	-4.51714	-2.42578	-0.44643
C	-3.21076	-2.11616	-0.82861
C	-2.75780	-0.84137	-0.53413
C	-3.53853	0.10477	0.11913
C	-4.83427	-0.20910	0.48871
N	-1.48803	-0.27053	-0.81710
C	-1.40269	0.96097	-0.33310
C	-2.73213	1.36880	0.28810
C	-3.36497	2.54546	-0.47659
C	-2.52661	1.73189	1.76789
C	-0.29572	1.83215	-0.41655
C	1.02795	1.55498	-0.67766

C	1.89987	0.59152	-0.08426
C	-0.49012	-0.96649	-1.60645
C	1.46775	-0.30227	0.99112
C	2.50334	-1.10785	1.60962
C	3.79432	-1.08924	1.18567
C	4.17109	-0.22641	0.12234
C	3.24354	0.59781	-0.48209
O	0.27764	-0.36755	1.37649
N	5.52809	-0.19646	-0.31442
O	5.84852	0.55792	-1.24024
O	6.34807	-0.93089	0.24831
H	-6.33131	-1.75432	0.48779
H	-4.90882	-3.41527	-0.65553
H	-2.58817	-2.85274	-1.32169
H	-5.46277	0.51637	0.99515
H	-4.35470	2.75125	-0.06252
H	-3.47647	2.31571	-1.53881
H	-2.76109	3.44973	-0.37190
H	-3.49416	1.94357	2.22914
H	-2.04595	0.91324	2.30617
H	-1.89791	2.62118	1.85638
H	-0.59379	2.86498	-0.58434
H	1.56160	2.36243	-1.17787
H	0.17685	-1.54531	-0.96604
H	-0.99859	-1.62763	-2.30609
H	0.09329	-0.23542	-2.16410
H	2.19450	-1.75811	2.42096
H	4.54544	-1.71753	1.64765
H	3.56539	1.26293	-1.27507

Single Point Energy: -1069.72154366

MCZ 70.0°

C	-5.54326	-1.29134	0.10476
C	-4.76461	-2.31179	-0.43837
C	-3.41521	-2.11049	-0.73568
C	-2.89125	-0.85636	-0.46803
C	-3.65045	0.17108	0.08232
C	-4.98755	-0.03613	0.36901
N	-1.56891	-0.39158	-0.67782

C	-1.43214	0.86823	-0.25105
C	-2.77553	1.38981	0.25198
C	-3.27699	2.55903	-0.61410
C	-2.65889	1.81704	1.72347
C	-0.27669	1.64922	-0.27181
C	1.01806	1.33493	-0.69125
C	1.97096	0.47705	-0.09504
C	-0.57438	-1.17139	-1.38797
C	1.63367	-0.36405	1.05778
C	2.74526	-1.03555	1.70849
C	4.01248	-0.97004	1.22728
C	4.29066	-0.18553	0.07132
C	3.29748	0.52078	-0.56405
O	0.46156	-0.48772	1.47047
N	5.63079	-0.11518	-0.42465
O	5.86758	0.57025	-1.42388
O	6.51133	-0.74736	0.16619
H	-6.58853	-1.47437	0.32877
H	-5.20890	-3.28228	-0.63127
H	-2.81450	-2.91290	-1.14630
H	-5.59679	0.75496	0.79454
H	-4.27950	2.84705	-0.28912
H	-3.32391	2.27882	-1.66909
H	-2.62540	3.42990	-0.51052
H	-3.63912	2.12491	2.09558
H	-2.29276	0.99530	2.34240
H	-1.97079	2.65999	1.82312
H	-0.52256	2.70203	-0.41043
H	1.47436	2.10369	-1.31586
H	0.08280	-1.69892	-0.69643
H	-1.08328	-1.88427	-2.03433
H	0.02308	-0.49982	-2.00578
H	2.51265	-1.63086	2.58464
H	4.82329	-1.50249	1.70823
H	3.54313	1.12807	-1.42740

Single Point Energy: -1069.71152376

MCZ 90.0°

C	-5.77338	-1.03860	0.00247

C	-5.05582	-2.14749	-0.44009
C	-3.67661	-2.07992	-0.65290
C	-3.05411	-0.86530	-0.40914
C	-3.75613	0.25073	0.04149
C	-5.12100	0.17454	0.24659
N	-1.69059	-0.53172	-0.54669
C	-1.46714	0.75150	-0.17863
C	-2.79372	1.40367	0.21471
C	-3.14569	2.56387	-0.73120
C	-2.73918	1.89302	1.66967
C	-0.26202	1.41243	-0.14160
C	1.00729	1.05487	-0.67848
C	2.04267	0.33567	-0.08404
C	-0.70858	-1.41965	-1.13384
C	1.82949	-0.41891	1.16202
C	3.02725	-0.91190	1.82697
C	4.25448	-0.80105	1.26553
C	4.40814	-0.13888	0.00658
C	3.34200	0.41113	-0.64668
O	0.69307	-0.61634	1.62515
N	5.71979	-0.03086	-0.57197
O	5.85086	0.54445	-1.65353
O	6.66960	-0.52275	0.03954
H	-6.84313	-1.11732	0.16301
H	-5.57163	-3.08481	-0.61993
H	-3.12799	-2.95317	-0.98478
H	-5.68086	1.03744	0.59384
H	-4.13919	2.94774	-0.48649
H	-3.15004	2.23634	-1.77369
H	-2.43050	3.38360	-0.62547
H	-3.71153	2.29880	1.96058
H	-2.48652	1.07591	2.34928
H	-1.98992	2.68080	1.78126
H	-0.42265	2.48817	-0.24201
H	1.35472	1.73691	-1.45701
H	-0.08079	-1.88127	-0.37128
H	-1.22084	-2.18920	-1.70876
H	-0.07523	-0.84572	-1.81462
H	2.89049	-1.41992	2.77511
H	5.13257	-1.20610	1.75239

H	3.49267	0.92860	-1.58687

Single Point Energy: -1069.69913102

MCZ 110.0°

C	-5.51681	-0.70122	1.34872
C	-5.07030	-1.99042	1.06479
C	-3.86693	-2.20676	0.38999
C	-3.14337	-1.08651	0.01546
C	-3.56973	0.20779	0.29663
C	-4.76265	0.41183	0.96606
N	-1.91215	-1.02041	-0.68203
C	-1.50165	0.24854	-0.82144
C	-2.54253	1.18927	-0.21627
C	-3.11499	2.11843	-1.29875
C	-1.93674	2.00715	0.93763
C	-0.31755	0.72962	-1.38125
C	0.92374	0.08007	-1.36193
C	2.08037	0.44910	-0.64484
C	-1.24307	-2.17924	-1.24149
C	2.23674	1.74735	0.02667
C	3.40551	1.88979	0.87955
C	4.35055	0.92295	0.98322
C	4.20068	-0.29516	0.25762
C	3.10353	-0.51597	-0.53694
O	1.42282	2.68265	-0.11295
N	5.20422	-1.30868	0.36783
O	5.06347	-2.36476	-0.25575
O	6.18405	-1.09048	1.08608
H	-6.45538	-0.56053	1.87360
H	-5.66318	-2.84487	1.37289
H	-3.52639	-3.21377	0.18163
H	-5.11046	1.41474	1.19242
H	-3.90068	2.74105	-0.86394
H	-3.54431	1.54667	-2.12479
H	-2.33781	2.77671	-1.69408
H	-2.71672	2.62118	1.39437
H	-1.52160	1.35029	1.70617
H	-1.13923	2.65922	0.57601
H	-0.23477	1.80084	-1.24080
H	0.95502	-0.95873	-1.68404

H	-0.37664	-2.45823	-0.63544
H	-1.93766	-3.01547	-1.27017
H	-0.92772	-1.96130	-2.26281
H	3.50674	2.82757	1.41466
H	5.22383	1.05721	1.60905
H	3.01088	-1.45780	-1.06499

Single Point Energy: -1069.70748315

MCZ 130.0°

C	-5.68318	-0.59674	1.25394
C	-5.35115	-1.86935	0.79172
C	-4.15592	-2.09990	0.10786
C	-3.32678	-1.00886	-0.08761
C	-3.63599	0.26648	0.37090
C	-4.82288	0.48507	1.04699
N	-2.07210	-0.96197	-0.75206
C	-1.54290	0.25709	-0.69252
C	-2.51172	1.20569	0.00563
C	-2.97124	2.30236	-0.97148
C	-1.86242	1.82628	1.25421
C	-0.28372	0.69846	-1.14498
C	0.87593	-0.04948	-1.08287
C	2.14091	0.35646	-0.57194
C	-1.51539	-2.10348	-1.45809
C	2.46348	1.74680	-0.23688
C	3.74284	1.96682	0.41128
C	4.62781	0.96153	0.63841
C	4.30128	-0.36676	0.25164
C	3.08884	-0.65076	-0.34235
O	1.69250	2.70128	-0.48602
N	5.23106	-1.41974	0.48926
O	4.93646	-2.57327	0.15448
O	6.31144	-1.14679	1.02500
H	-6.61775	-0.44543	1.78294
H	-6.02817	-2.69834	0.96665
H	-3.89950	-3.09309	-0.24057
H	-5.08449	1.47287	1.41229
H	-3.71136	2.93635	-0.47783
H	-3.42722	1.87080	-1.86539

H	-2.13058	2.93133	-1.27275
H	-2.60064	2.43634	1.77989
H	-1.50495	1.05268	1.93797
H	-1.01977	2.46253	0.97576
H	-0.14179	1.76701	-1.04551
H	0.79313	-1.12905	-1.17986
H	-0.86596	-2.68817	-0.80200
H	-2.33191	-2.73336	-1.80691
H	-0.95464	-1.75217	-2.32349
H	3.97741	2.98773	0.69245
H	5.58325	1.15280	1.11066
H	2.86239	-1.67493	-0.61556

Single Point Energy: -1069.72027101

MCZ 150.0°

C	-5.93155	-0.56130	0.92540
C	-5.57015	-1.82779	0.46779
C	-4.30534	-2.06580	-0.07276
C	-3.43866	-0.98808	-0.13094
C	-3.77622	0.28013	0.32581
C	-5.03303	0.50672	0.85805
N	-2.10990	-0.95136	-0.63728
C	-1.57101	0.25114	-0.47766
C	-2.59904	1.20231	0.12240
C	-2.92158	2.32808	-0.87777
C	-2.08849	1.78482	1.45090
C	-0.25698	0.67823	-0.77638
C	0.86472	-0.10772	-0.68470
C	2.19673	0.31662	-0.39430
C	-1.50701	-2.09212	-1.30909
C	2.59277	1.72469	-0.31482
C	3.96443	1.98032	0.08079
C	4.85374	0.98170	0.32428
C	4.44225	-0.37213	0.20485
C	3.14320	-0.68445	-0.14882
O	1.80784	2.66813	-0.57020
N	5.37283	-1.41815	0.45737
O	5.00345	-2.59486	0.35511
O	6.53127	-1.11977	0.77298

H	-6.92075	-0.40422	1.34128
H	-6.27932	-2.64561	0.53345
H	-4.02724	-3.05396	-0.41872
H	-5.31989	1.48946	1.21781
H	-3.71462	2.95597	-0.46528
H	-3.26302	1.92416	-1.83362
H	-2.04530	2.95594	-1.05278
H	-2.86765	2.40725	1.89649
H	-1.83349	0.99171	2.15766
H	-1.20439	2.40428	1.28636
H	-0.09947	1.74823	-0.74348
H	0.74142	-1.18591	-0.64752
H	-0.98450	-2.73252	-0.59497
H	-2.29421	-2.66554	-1.79561
H	-0.81336	-1.73580	-2.06916
H	4.26165	3.02022	0.16256
H	5.87563	1.19922	0.60886
H	2.85491	-1.72662	-0.22510

Single Point Energy: -1069.72927072

MCZ 170.0°

C	-6.10480	-0.56388	0.51806
C	-5.67722	-1.83641	0.14111
C	-4.34583	-2.07826	-0.20091
C	-3.48158	-0.99797	-0.14834
C	-3.88545	0.27572	0.23221
C	-5.20794	0.50620	0.56723
N	-2.09091	-0.96501	-0.45007
C	-1.58463	0.24288	-0.23290
C	-2.69288	1.19821	0.19084
C	-2.86831	2.30759	-0.86341
C	-2.38460	1.80554	1.56964
C	-0.24427	0.67598	-0.35819
C	0.86914	-0.11424	-0.24667
C	2.23003	0.31465	-0.17868
C	-1.40017	-2.11856	-1.00750
C	2.64103	1.71394	-0.31565
C	4.06216	1.97643	-0.19321
C	4.97349	0.99067	0.01999

C	4.53901	-0.35591	0.13620
C	3.19693	-0.67290	0.03785
O	1.82908	2.64570	-0.52743
N	5.49092	-1.38902	0.35812
O	5.10184	-2.55981	0.45723
O	6.68755	-1.08649	0.44600
H	-7.14505	-0.40413	0.77975
H	-6.38677	-2.65607	0.11490
H	-4.01861	-3.07163	-0.48261
H	-5.54610	1.49347	0.86428
H	-3.71672	2.93564	-0.58256
H	-3.06204	1.88808	-1.85322
H	-1.97907	2.93938	-0.91567
H	-3.22048	2.43542	1.88267
H	-2.23875	1.02629	2.32122
H	-1.48501	2.42317	1.52629
H	-0.09121	1.74622	-0.39246
H	0.74101	-1.18284	-0.10973
H	-0.96649	-2.73393	-0.21653
H	-2.11665	-2.71261	-1.57167
H	-0.61932	-1.77637	-1.68491
H	4.37570	3.01064	-0.28594
H	6.02992	1.21334	0.10337
H	2.89337	-1.70909	0.13414

Single Point Energy: -1069.73337853

3.8 References

1. Breslin, V. M.; Garcia-Garibay, M. A. *Cryst. Growth Des.* **2017**, *17*, 637–642.

2. Klajn, R. *Chem. Soc. Rev.* **2014**, *43*, 148–184.

3. Rad, J. K.; Mahdavian, A. R. *J. Phys. Chem. C* **2016**, *120*, 9985–9991.

4. Berkovic, F.; Krongauz, V.; Weiss, V. *Chem. Rev.* **2000**, *100*, 1741–1754.

5. Balmond, E. I.; Tautges, B. K.; Faulkner, A. L.; Or, V. W.; Hodur, B. M.; Shaw, J. T.; Louie, A. Y. *J. Org. Chem.* **2016**, *81*, 8744–8758.

6. Bénard, S.; Yu, P. *Adv. Mater.* **2000**, *12*, 48–50.

7. Harada, J.; Kawazoe, Y.; Ogawa, K. *Chem. Commun.* **2010**, *46*, 2593–2595.

8. Godsi, O.; Peskin, U.; Kapon, M.; Natan, E.; Eichen, Y. *Chem. Commun.* **2001**, 2132–2133.

9. Naumov, P.; Yu, P.; Sakurai, K. *J. Phys. Chem. A* **2008**, *112*, 5810–5814.

10. Görner, H. *Chem. Phys.* **1997**, *222*, 315–329.

11. Wojtyk, J. T. C.; Wasey, A.; Xiao, N.-N.; Kazmaier, P. M.; Hoz, S.; Yu, C.; Lemieux, R. P.; Buncel, E. *J. Phys. Chem. A* **2007**, *111*, 2511–2516.

12. Meng, X.; Qi, G.; Zhang, C.; Wang, K.; Zou, B.; Ma, Y. *Chem. Commun.* **2015**, *51*, 9320–9323.

13. Gentili, P. L.; Nocchetti, M.; Miliani, C.; Favaro, G. *New J. Chem.* **2004**, *28*, 379–386.

14. Guglielmetti, R. 4n+2 Systems: Spiropyrans. In *Photochromism: Molecules and Systems*; Dürr, H., Bouas-Laurent, H., Eds.; Elsevier: Amsterdam, 2003; p 314.

15. Görner, H.; Atabekyan, L. S.; Chibisov, A. K. *Chem. Phys. Lett.* **1996**, *260*, 59–64.

16. Lenoble, C.; Becker, R. S. *J. Phys. Chem.* **1986**, *90*, 62–65.

17. Bercovici, T.; Heiligman-Rim, R.; Fischer, E. *Mol. Photochem.* **1969**, *1*, 23–55.

18. Chibisov, A. K.; Görner, H. *J. Phys. Chem. A* **1997**, *101*, 4305–4312.

19. Görner, H. *Chem. Phys. Lett.* **1998**, *282*, 381–390.

20. Holm, A.-K.; Mohammed, O. F.; Rini, M.; Mukhtar, E.; Nibbering, E. T. J.; Fidder, H. *J. Phys. Chem. A* **2005**, *109*, 8962–8968.

21. Holm, A.-K.; Rini, M.; Nibbering, E. T. J.; Fidder, H. *Chem. Phys. Lett.* **2003**, *376*, 214–219.

22. Suzuki, M.; Asahi, T.; Masuhara, H. *Mol. Cryst. and Liq. Cryst.* **2000**, *345*, 51–56.

23. Asahi, T.; Masuhara, H. *Chem. Lett.* **1997**, *26*, 1165–1166.

24. Suzuki, M.; Asahi, T.; Masuhara, H. *Phys. Chem. Chem. Phys.* **2002**, *4*, 185–192.

25. Suzuki, M.; Asahi, T.; Masuhara, H. *Chem. Phys. Chem.* **2005**, *6*, 2396–2403.

26. Asahi, T.; Suzuki, M.; Masuhara, H. *J. Phys. Chem A* **2002**, *106*, 2335–2340.

27. Krysanov, S. A.; Alfimov, M. V. *Chem. Phys. Lett.* **1982**, *91*, 77–80.

28. Krongauz, V.; Kiwi, J.; Gratzel, M. *J. Photochem.* **1980**, *13*, 89–97.

29. Barachevskii, V. A.; Karpov, R. E. *High Energy Chem.* **2007**, *41*, 188–199.

30. Kalisky, Y.; Orlowski, T. E.; Williams, D. J. *J. Phys. Chem.* **1983**, *87*, 5333–5338.

31. Wood, E. A. Crystals and Light: An Introduction to Optical Crystallography, 2nd ed.; Dover Publications: New York, 1977.

32. Chin, K. K.; Natarajan, A.; Gard, M. N.; Campos, L. M.; Shepard, H.; Johansson, E.; Garcia-Garibay, M. A. *Chem. Commun.* **2007**, 4266–4268.

33. Kuzmanich, G.; Simoncelli, S.; Gard, M. N.; Spänig, F.; Henderson, B. L.; Guldi, D. M.; Garcia-Garibay, M. A. *J. Am. Chem. Soc.* **2011**, *133*, 17296–17306.

34. Simocelli, S.; Kuzmanich, G.; Gard, M. N.; Garcia-Garibay, M. A. *J. Phys. Org. Chem.,* 2010, **23**, 376–381.

35. Swenbergy, C. E.; Gaecintov, N. E. in Organic Molecular Photophysics, Vol. 1, Ch. 10, J. B. Birks, Ed., John Wiley & Sons, London, 1973.

36. Bénard, S.; Yu, P. *Chem. Commun.* **2000**, 65–66.

37. Spagnoli, S.; Block, D.; Botzung-Appert, E.; Colombier, L.; Baldeck, P. L.; Ibanez, A.; Corval, A. *J. Phys. Chem. B* **2005**, *109*, 8587–8591.

38. Chung, T. S.; Park, J. H.; Garcia-Garibay, M. A. *J. Org. Chem.* **2017**, *82*, 12128–12133.

39. Park, J. H.; Hughs, M.; Chung, T. S.; Ayitou, A. J.-L.; Breslin, V. M. *J. Am. Chem. Soc.* **2017**, *139*, 13312–13317.

40. Ayitou, A. J.-L.; Flynn, K.; Jockusch, S.; Khan, S. I.; Garcia-Garibay, M. A. *J. Am. Chem. Soc.* **2016**, *138*, 2644–2648.

41. Kuzmanich, G.; Vogelsberg, C. S.; Maverick, E. F.; Netto-Ferreira, J. C.; Scaiano, J. C.; Garcia-Garibay, M. A. *J. Am. Chem. Soc.* **2012**, *134*, 1115–1123.

42. Kasai, H.; Nalwa, H. S.; Oikawa, H.; Okada, S.; Matsuda, H.; Minami, N.; Kakuta, A.; Ono, K.; Mukoh, A.; Nakanishi, H. *Jpn. J. Appl. Phys.* **1992**, *31*, L1132–L1134.

43. Sheng, Y.; Leszczynski, J.; Garcia, A. A.; Rosario, R.; Gust, D.; Springer, J. *J. Phys. Chem. B* **2004**, *108*, 16233–16243.

44. Rini, M.; Holm, A.-K.; Nibbering, E. T. J.; Fidder, H. *J. Am. Chem. Soc.* **2003**, *125*, 3028–3034.

45. Ernsting, N. P.; Arthes-Engeland, T. *J. Phys. Chem.* **1991**, *95*, 5502–5509.

46. Chibisov, A. K.; Görner, H. *J. Photochem. Photobiol. A* **1997**, *105*, 261–267.

47. Wojtyk, J. T. C.; Kazmaier, P. M.; Buncel, E. *Chem. Mater.* **2001**, *13*, 2547–2551.

48. Raymo, F. M.; Giordani, S.; White, A. J. P.; Williams, D. J. *J. Org. Chem.* **2003**, *68*, 4158–4169.

49. Wojtyk, J. T. C.; Wasey, A.; Kazmaier, P. M.; Hoz, S.; Buncel, E. *J. Phys. Chem. A* **2000**, *104*, 9046–9055.

50. Yanai, T.; Tew, D. P.; Handy, N. C. *Chem. Phys. Lett.* **2004**, *393*, 51–57.

51. Miertuš, S.; Scrocco, E.; Tomasi, J. *Chem. Phys.* **1981**, *55*, 117–129.

52. Scalmani, G.; Frisch, M. J. *J. Chem. Phys.* **2010**, *132*, 114110-1–114110-15.

53. Grimme, S.; Ehrlich, S.; Goerigk, L. *J. Comput. Chem.* **2011**, *32*, 1456–1465.

54. Frisch, M. J.; Trucks, G. W.; Schlegel, H. B.; Scuseria, G. E.; Robb, M. A.; Cheeseman, J. R.; Scalmani, G.; Barone, V.; Petersson, G. A.; Nakatsuji, H.; Li, X.; Caricato, M.; Marenich, A. V.; Bloino, J.; Janesko, B. G.; Gomperts, R.; Mennucci, B.; Hratchian, H. P.; Ortiz, J. V.; Izmaylov, A. F.; Sonnenberg, J. L.; Williams-Young, D.; Ding, F.; Lipparini, F.; Egidi, F.; Goings, J.; Peng, B.; Petrone, A.; Henderson, T.; Ranasinghe, D.; Zakrzewski, V. G.; Gao, J.; Rega, N.; Zheng, G.; Liang, W.; Hada, M.; Ehara, M.; Toyota, K.; Fukuda, R.; Hasegawa, J.; Ishida, M.; Nakajima, T.; Honda, Y.; Kitao, O.; Nakai, H.; Vreven, T.; Throssell, K.; Montgomery Jr., J. A.; Peralta, J. E.; Ogliaro, F.; Bearpark, M. J.; Heyd, J. J.; Brothers, E. N.; Kudin, K. N.; Staroverov, V. N.; Keith, T. A.; Kobayashi, R.; Normand, J.; Raghavachari, K.; Rendell, A. P.; Burant, J. C.; Iyengar, S. S.; Tomasi, J.; Cossi, M.; Millam, J. M.; Klene, M.; Adamo, C.; Cammi, R.; Ochterski, J. W.; Martin, R. L.; Morokuma, K.; Farkas, O.; Foresman, J. B.; Fox, D. J. *Gaussian 16*, Wallingford, CT, 2016.

55. Adamo, C.; Jacquemin, D. *Chem. Soc. Rev.* **2013**, *42*, 845–856.

56. Halgren, T. A. *J. Comput. Chem.* **1996**, *17*, 490–519.

57. *Schrödinger Release 2015-3: MacroModel*, version 10.9; Schrödinger, LLC: New York, 2015.

58. Banks, J. L.; Beard, H. S.; Cao, Y.; Cho, A. E.; Damm, W.; Farid, R.; Felts, A. K.; Halgren, T. A.; Mainz, D. T.; Maple, J. R.; Murphy, R.; Philipp, D. M.; Repasky, M. P.; Zhang, L. Y.;

Berne, B. J.; Friesner, R. A.; Gallicchio, E.; Levy, R. M. *J. Comput. Chem.* **2005**, *26*, 1752–1780.

CHAPTER 4

Nanosecond Transient Absorption Spectroscopic Investigation of a 1,1'-Biphenyl-2-Phenyl Diazomethane in Solution and in the Solid State

4.1 Introduction

The photochemical generation and reactivity of carbenes has been an area of interest to researchers for many decades, with the multiplicity of the carbene being a particularly important topic of discussion.[1–3] Carbenes are unique in that they can exist as both a ground state singlet or a ground state triplet species, with the experimental evidence suggesting that arylcarbenes are ground state triplets.[4,5] However, O–H insertion products from supposedly triplet arylcarbenes reacting with methanol and ethanol have been observed,[6–10] which appears to violate the Skell-Woodworth rules[11] that are based on the principle of spin conservation, and so molecules of different spin states, such as a ground state triplet carbene and a ground state singlet molecule of methanol, should not react with each other. In order to resolve this conflict, it was proposed that the singlet and triplet states of arylcarbenes are actually in rapid equilibrium with each other.[8–10,12] This means that the kinetics for these systems can be quite complicated because reactions from both the singlet and triplet carbene will occur, thus making it difficult to determine the actual rate constants for these reactions.

Interestingly, Eisenthal and coworkers observed that in polar solvents where the singlet-triplet energy gaps of arylcarbenes are small, the rate of intersystem crossing (ISC) actually decreases, which appears to violate Fermi's golden rule of radiationless transitions.[13–16] Intuition says that a smaller energy gap between two states should result in a faster transition,[17–19] nonetheless, Eisenthal and coworkers observed the exact opposite. They hypothesized that the small singlet-triplet energy gap results from polar solvents preferentially stabilizing the singlet arylcarbene over the triplet; however, since the rate of ISC is slow they suggested that the vibrational wavefunction of the singlet carbene overlaps with the triplet carbene's in a region where its vibrational levels are sparse resulting in poor vibronic coupling and hence slow ISC.[16]

Similarly, in nonpolar solvents, Eisenthal and coworkers observed faster rates of ISC for arylcarbenes, which correlated to a larger singlet-triplet energy gap that they postulated resulted from the vibrational wavefunction of the singlet carbene overlapping with a larger number of the triplet carbene's vibrational levels thus giving rise to greater vibronic coupling and fast ISC. This argument fails when the singlet-triplet energy gap of arylcarbenes becomes too large and returns to following the golden rule of radiationless transitions.[5]

Experimental and computational evidence supporting Eisenthal and coworkers' claims that polar solvents reduce the singlet-triplet gap of arylcarbenes and that nonpolar solvents increase it have been reported by Toscano, Hadad, and Platz.[20–24] Furthermore, Kohler,[25] Platz,[24,26] and Schuster[27] have determined the lifetimes for several singlet arylcarbenes in both polar and nonpolar solvents, and their results reveal shorter lifetimes in nonpolar solvents, which correlates to faster ISC rates in nonpolar solvents, thus validating the Fermi's golden rule violation proposed by Eisenthal and coworkers. An understanding of this violation to Fermi's golden rule provides the potential for experiments to be designed in which the reactivity of the singlet carbene can be isolated from the triplet carbene and vice versa in order to directly measure the kinetics of their subsequent reactions.

In this study we report the nanosecond laser flash photolysis of a 1,1'-biphenyl-2-phenyldiazomethane (**1**) as shown in Scheme 4.1.1 both in solution and in the solid state. Although Kirmse and coworkers have previously described the transient kinetics of the parent biphenyl-2-phenyldiazomethane in solution,[12] to the best of our knowledge there have been no reports describing the transient kinetics of a triplet diarylcarbene in the solid state. Since diarylcarbenes are known to react with solvents such as methanol and cyclohexane via O–H insertion and H-atom abstraction to form methylethers[6–10] and benzhydryl radicals[28–31] (Scheme

4.1.1, compounds **2**, **3b**, **3c**), we chose diaryldiazomethane **1** as our model system because Kirmse[12] and others[32,33] have described the preference for derivatives of **1** to undergo intramolecular cyclization to fluorenyl derivatives such as **4** with minimal formation of solvent-derived products. Therefore, our kinetic data both in solution and the solid state should be quite simple to interpret. A key aspect of our investigation in the solid state is the use of nanosecond pump-probe transient absorption spectroscopy with nanocrystals (NC) suspended in water. Nanocrystals that are between 50–500 nm make it possible to use conventional transmission spectroscopic methods to study photochemical reactions in the solid state by diminishing complications that arise from dichroism, birefringence, and light scattering,[34] which has been discussed previously.[35–37] Our results showed the presence of a single transient species both in solution and in NC suspension that we hypothesize to be the triplet excited state of the 9-phenylfluorenyl product (**4**).

Scheme 4.1.1

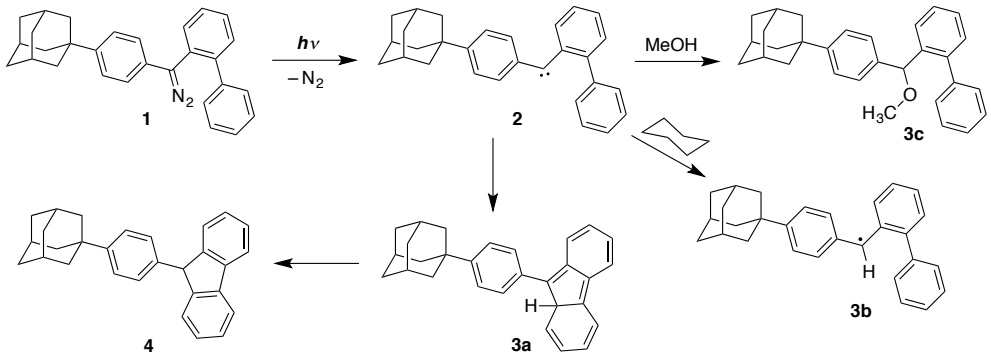

4.2 Results and Discussion

The diaryldiazomethane compound (**1**) used to study the transient kinetics of a triplet carbene both in solution and in the solid state was synthesized via the reaction sequence shown in parts a, b, and c of Scheme 4.2.1. In part a, Friedel-Crafts alkylation of benzene with commercially available 1-bromoadamantane (**5**) and $FeCl_3$ as a Lewis acid catalyst produced 1-

phenyladamantane (**6**), which was then brominated using Br_2 to give arylbromide **7** as the only product. Next Weinreb amide **11** was synthesized in two steps as illustrated in part b of Scheme 4.2.1 starting from commercially available [1,1'-biphenyl]-2-carboxylic acid (**8**), which was reacted with oxalyl chloride and catalytic DMF to yield acid chloride **9**. Subsequent nucleophilic acyl substitution of acid chloride **9** with *N,O*-dimethyldydroxylamine produced Weinreb amide **11** in excellent yield. ^{1}H and ^{13}C NMR spectra were recorded for Weinreb amide **11** in $CDCl_3$ (see Appendix 4.5.2), however, they did not match the literature[38] and so further analysis was required. Variable temperature ^{1}H and ^{13}C NMR spectra were collected for Weinreb amide **11** in C_6D_6 at room temperature (298 K) and at elevated temperatures and showed that the broader peaks observed at room temperature became much sharper and more defined at higher temperatures (Figures 4.2.1 and 4.4.2), suggesting the presence of rotamers.

Scheme 4.2.1

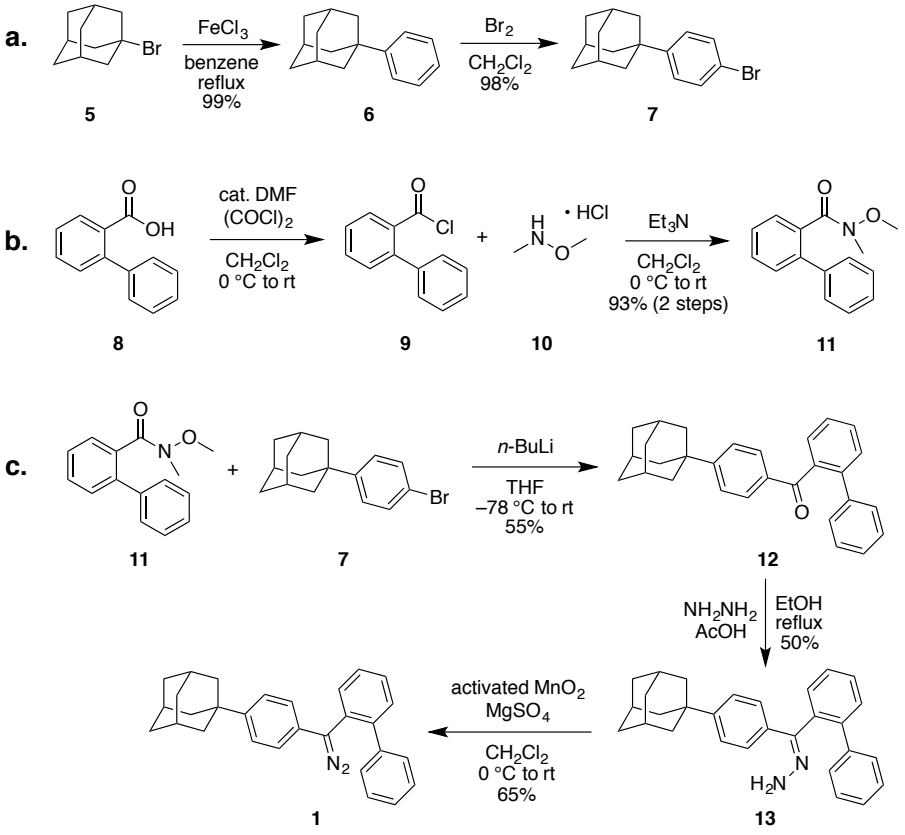

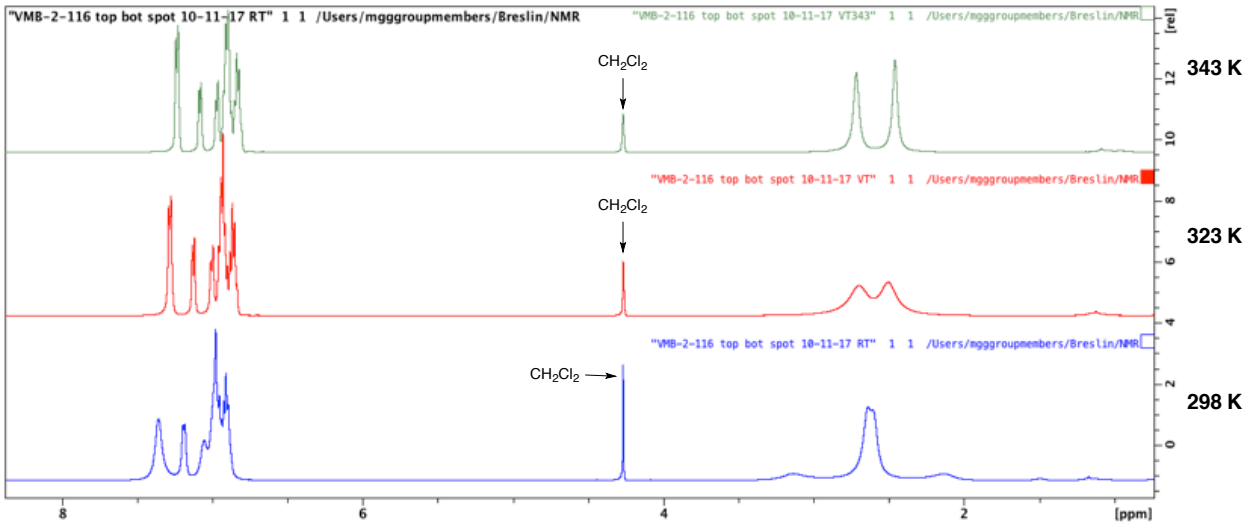

Figure 4.2.1. Variable temperature (VT) ^{1}H NMR spectra of Weinreb amide **11** in C_6D_6 collected at 298 K, 323 K, and 343 K.

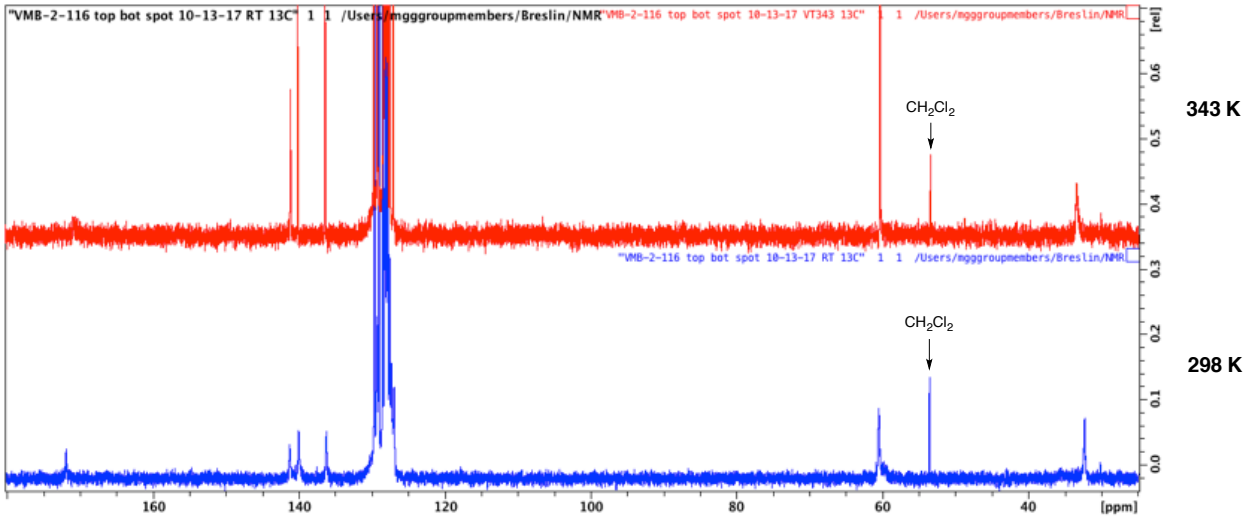

Figure 4.2.2. Variable temperature (VT) ^{13}C NMR spectra of Weinreb amide **11** in C_6D_6 collected at 298 K and 343 K.

In the final reaction sequence shown in part c of Scheme 4.2.1, lithium-halogen exchange of arylbromide **7** with *n*-butyllithium affords the corresponding aryllithium species that then undergoes another nucleophilic acyl substitution reaction with Weinreb amide **11** to produce ketone **12**. Hydrazine was then used to convert ketone **12** to hydrazone **13**, followed by oxidation

with activated MnO_2 to yield the desired diaryldiazomethane **1**, which was fully characterized by spectroscopic methods. Diaryldiazomethane **1** was shown to be a crystalline solid by obtaining a powder X-ray diffraction (PXRD) pattern (Figure 4.2.3), and was also found to have a melting point of 137 °C, which is well above room temperature (see section 4.4.2 Synthetic Procedures), thus making **1** suitable for solid state photochemical studies at room temperature.

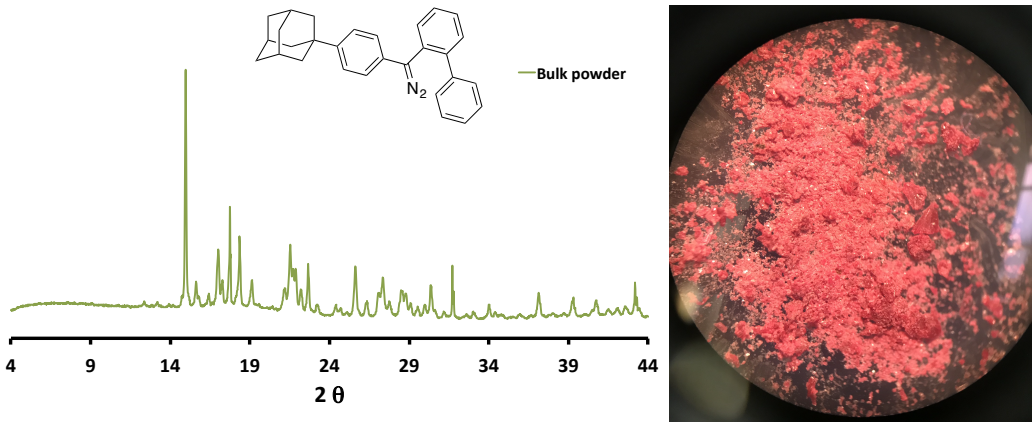

Figure 4.2.3. PXRD of the bulk powder for diaryldiazomethane **1** along with a microscope image of the dark pink powder.

Solid state spectroscopic studies of diaryldiazomethane **1** were carried out in aqueous nanocrystalline (NC) suspensions prepared by the solvent shift, or reprecipitation method.[39] Using dynamic light scattering (DLS), we determined the size of our nanocrystals averaged between 130–300 nm (see Appendix 4.5.4, Figure 4.5.1), which is very close to the excitation wavelength of 266 nm used in our laser flash photolysis experiments. Under these conditions, optical effects such as scattering and birefringence are reduced as compared to those of bulk solids, thus making them amenable to transmission spectroscopy measurements.[34] UV-vis spectra were recorded for NC suspensions of diaryldiazomethane **1** and showed minimal scattering over a period of 30 minutes (Figure 4.2.4), which again confirms that our NC suspensions are suitable for transmission spectroscopic studies.

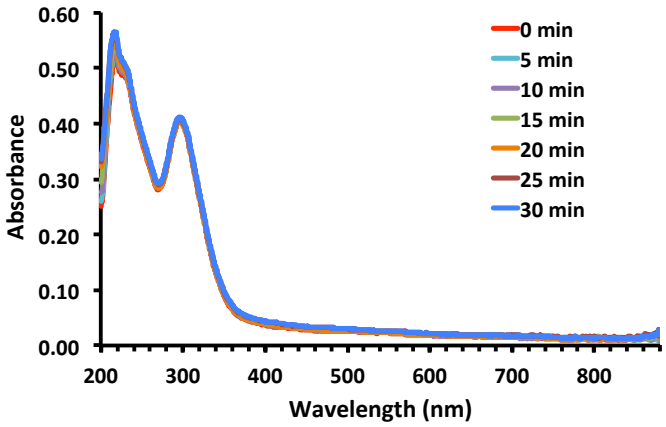

Figure 4.2.4. UV-vis spectra for diaryldiazomethane **1** in NC suspension recorded every 5 min for 30 min.

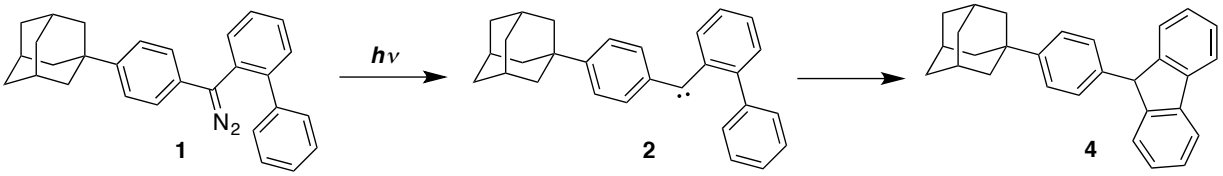

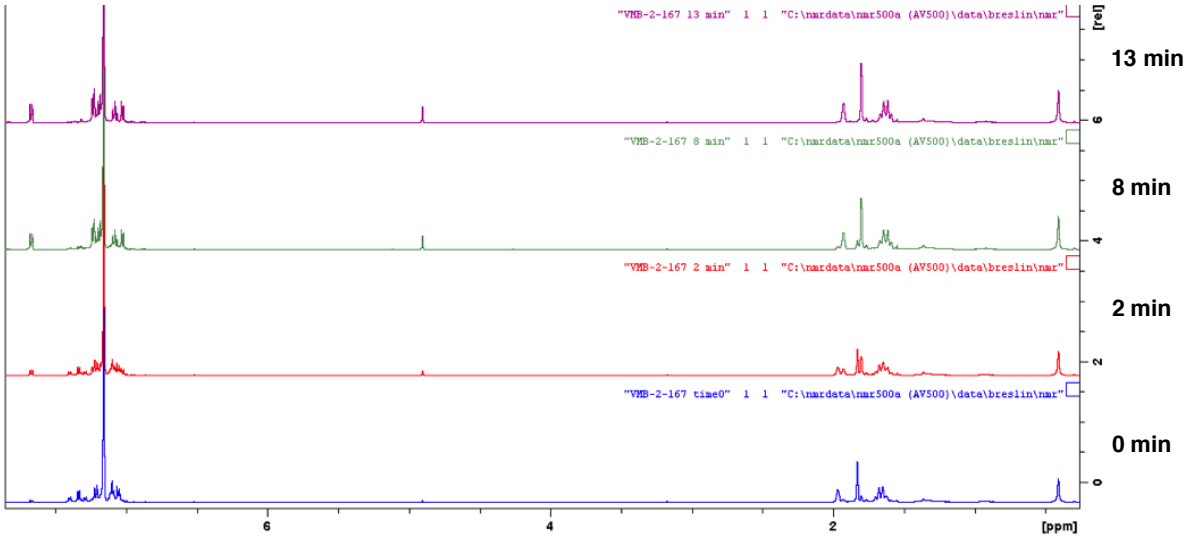

Figure 4.2.5. ^{1}H NMR analysis for the photolysis of **1** in C_6D_6 before irradiation (0 min) and 2 min, 8 min, and 13 min post irradiation (λ_{ex} > 290 nm).

Before beginning our transient absorption studies, we followed the progress of the photochemical reaction in solution (C_6D_6) from diaryldiazomethane **1** to 9-phenylfluorenyl **4** via product analysis using ^{1}H NMR (Figure 4.2.5). Photolysis was performed in a Hanovia photochemical reactor (450 W medium pressure Hg arc lamp) with a Pyrex filter (cutoff $\lambda < 290$ nm), and reaction progress was monitored at various time points (0 min, 2 min, 8 min, and 13 min) until no more starting material was observed. Our results showed that only the 9-phenylfluorenyl product **4** was formed as evidenced by the peak that grows in at 4.91 ppm, which corresponds to the triply benzylic proton of **4**, as well as the changes observed in the aromatic and adamantyl proton regions, thus indicating that the intramolecular cyclization is very efficient.

Nanosecond laser flash photolysis (LFP) spectroscopic studies of diaryldiazomethane **1** were carried out in argon degassed and air-saturated *n*-hexane solutions as well as in NC suspensions using an excitation wavelength of 266 nm. To avoid the potential interference from transients originating from the excitation of accumulating photoproducts, all pump-probe measurements were carried out in a single pass flow system that ensures the presence of pristine sample in the excitation volume.

The time-dependent transient absorption spectrum for **1** in *n*-hexane reveals a single transient species absorbing between 330–420 nm with a $\lambda_{max} = 370$ nm that decays over time (Figure 4.2.6). Another feature of the solution transient absorption spectrum is the presence of a negative absorbance between 300–330 nm, which most likely correlates to the disappearance of the diaryldiazomethane starting compound **1** as it is converted to product. The UV-vis spectrum obtained prior to pulsed laser excitation supports this hypothesis as it shows that **1** has a significant absorption band between 260–340 nm with a $\lambda_{max} \sim 310$ nm (Figure 4.2.7, red line).

A UV-vis spectrum was also collected after pulsed laser excitation of **1**, and it shows that the band at λ_{max} = 310 nm undergoes a blue shift to λ_{max} = 270 nm as well as decreases significantly in intensity (Figure 4.2.7, blue line). Interestingly, the post photolysis absorbance spectrum matches exactly with the spectrum for a pure sample of fluorene,[40] indicating that pulsed laser irradiation of **1** seems to produce 9-phenylfluorenyl **4** almost exclusively. In order to reveal more about the nature of the transient that absorbs at 370 nm, we wanted to study the effects of oxygen as a triplet quencher and so we collected kinetic data at 370 nm in both argon degassed and air-saturated samples of diaryldiazomethane **1** in *n*-hexane. The kinetic data revealed a single decay component with a lifetime of 1.3 μs in argon degassed solution and 250 ns in air-saturated solution (Figures 4.2.8 and 4.2.9), suggesting that the transient absorbing at 370 nm is a triplet species and is at least partially quenched in the presence of oxygen.

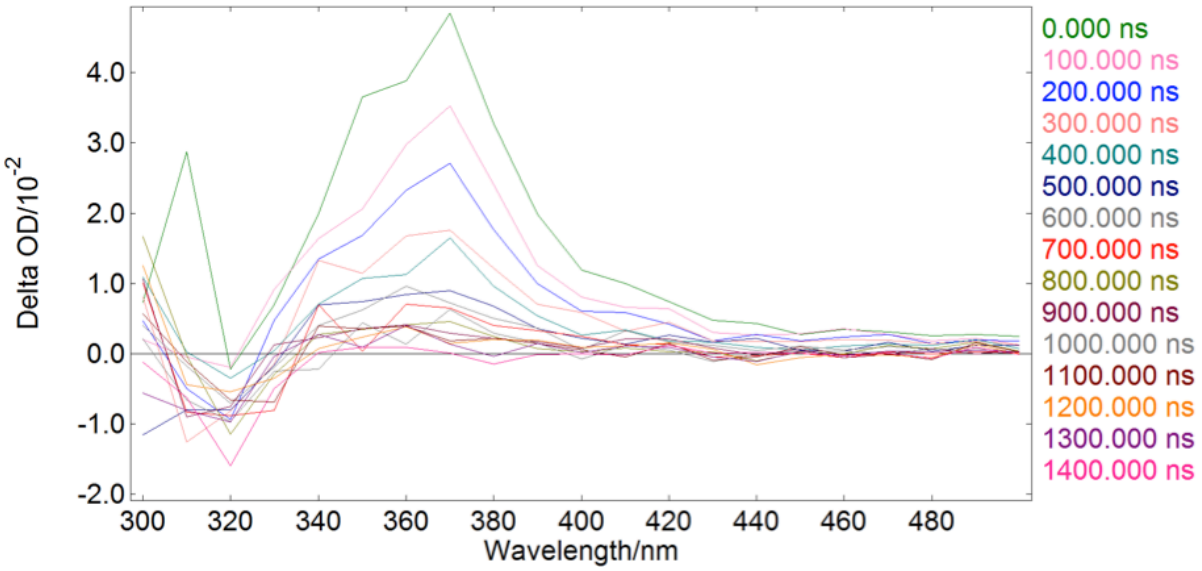

Figure 4.2.6. Time-dependent transient absorption spectrum for **1** at various time points in *n*-hexane solution collected between 0 and 1.4 μs.

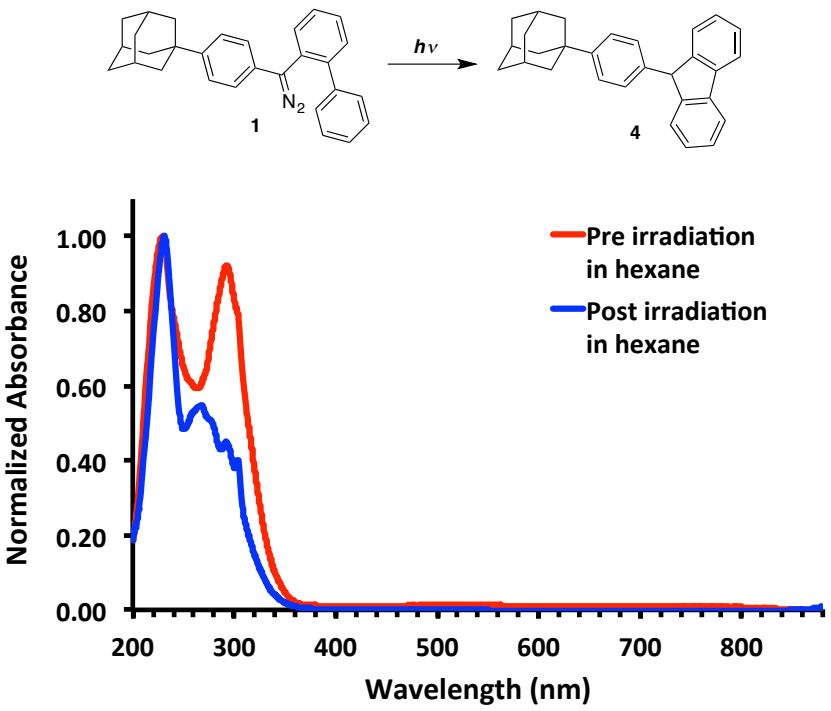

Figure 4.2.7. UV-vis spectra for **1** pre (red line) and post (blue line) pulsed laser irradiation in *n*-hexane solution.

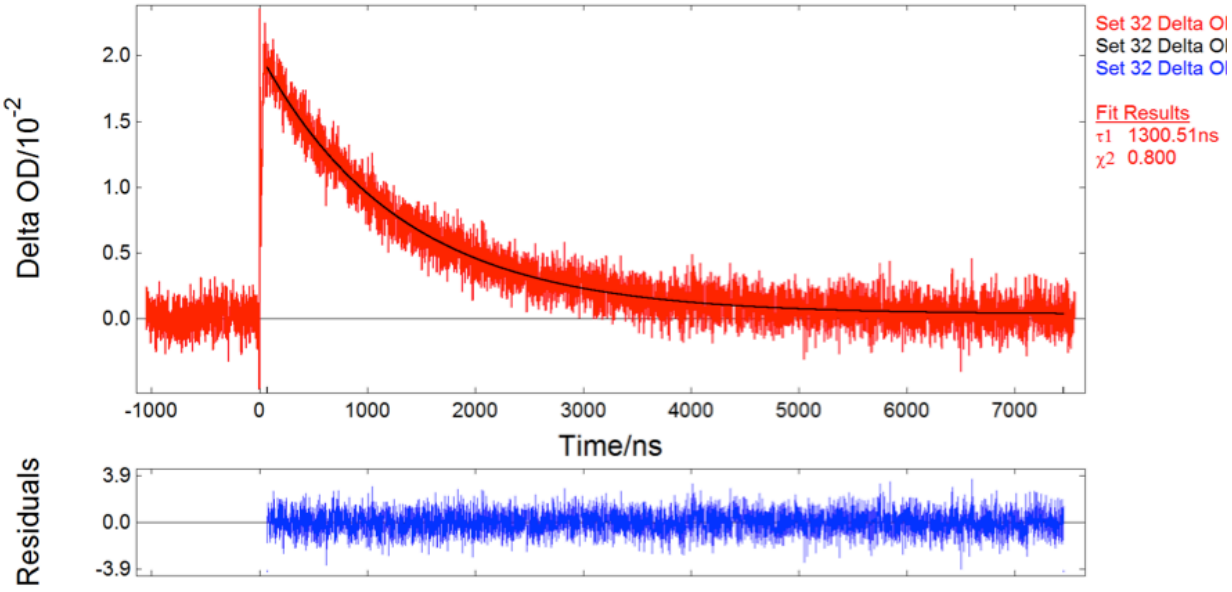

Figure 4.2.8. Transient decay at 370 nm for **1** measured in argon degassed *n*-hexane at 298 K. Fit line is shown in black.

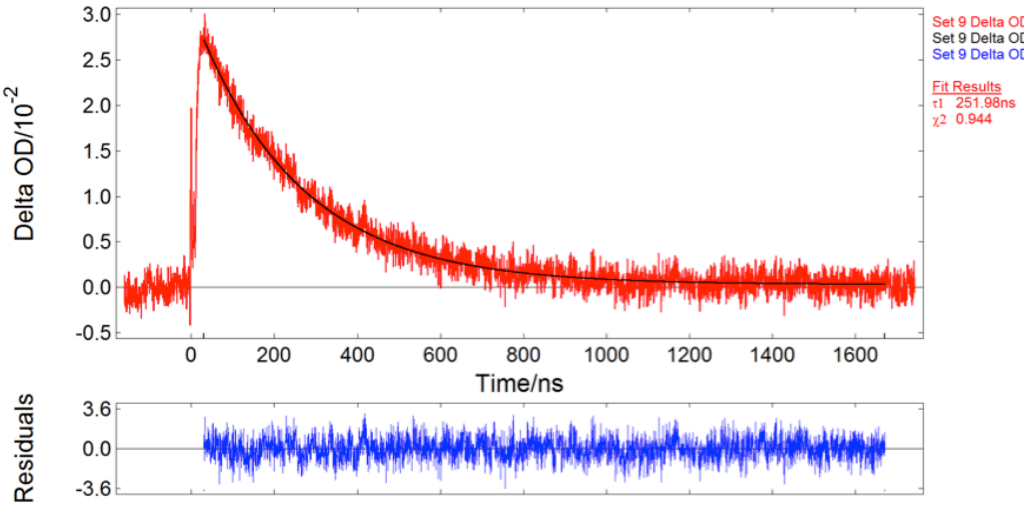

Figure 4.2.9. Transient decay at 370 nm for **1** measured in air-saturated *n*-hexane at 298 K. Fit line is shown in black.

These observations have also been reported by Kirmse and coworkers in their study of the same diaryldiazomethane system as ours minus the adamantyl group (Scheme 4.1.1), suggesting that the photochemical reaction of **1** is very similar to that of its adamantyl-less counterpart, which we expected.[12] Kirmse and coworkers detected only a single transient at 370 nm that decayed at a rate of 2.4 x 10^5 s^{-1} in argon-saturated cyclohexane, which is a lifetime of ca. 2.9 μs. Although they observe a longer lifetime than we do, these results are for a different molecule and so some minor differences in the kinetic data is not unexpected. In another experiment, Kirmse and coworkers also found that the presence of oxygen accelerates the decay of this transient at 370 nm, suggesting that this transient is a triplet species, which matches well with our results. Subsequent laser excitation of 9-phenylfluorene revealed the same transient absorption band at 370 nm, which they assigned to the triplet 9-phenylfluorene. They hypothesized that 9-phenylfluorene is formed and excited during their 20 ns laser pulse, which is why they are only able to detect the triplet excited state of the cyclized product. Furthermore, this

suggests that the intramolecular cyclization of their diaryldiazomethane to the isofluorene followed by the [1,5]-H shift to form the final product is extremely fast (Scheme 4.1.1).

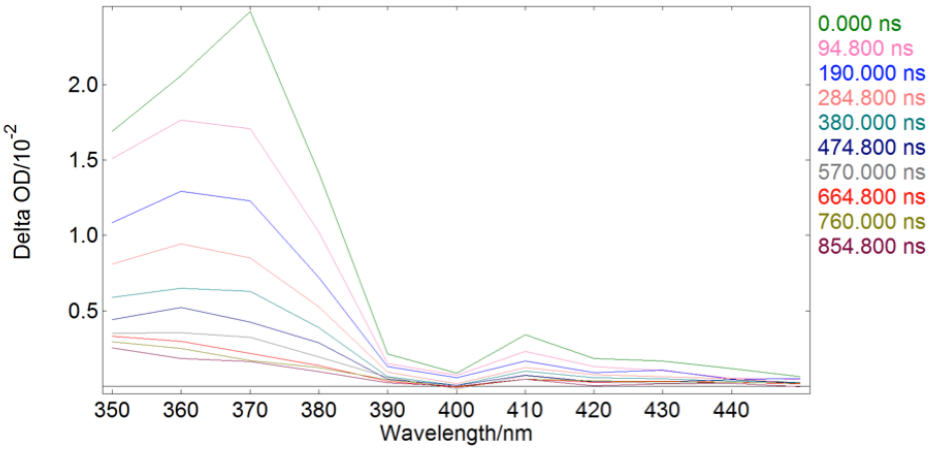

Figure 4.2.10. Time-dependent transient absorption spectrum for **4** at various time points in *n*-hexane solution collected between 0 and 900 ns.

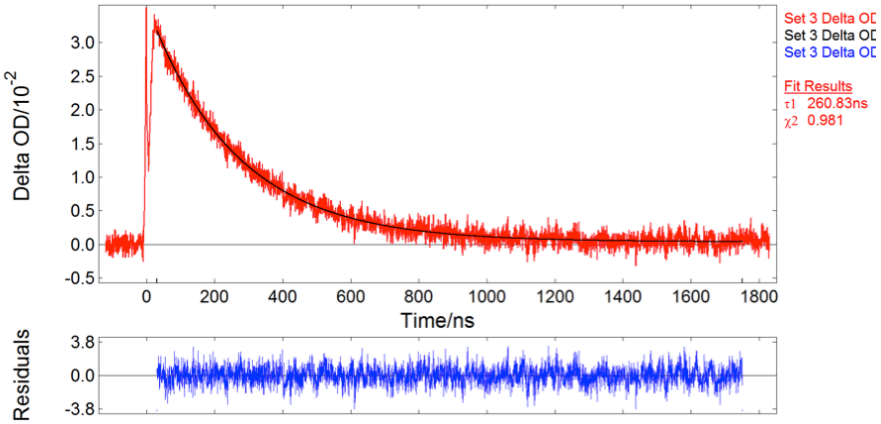

Figure 4.2.11. Transient decay at 370 nm for **4** measured in air-saturated *n*-hexane at 298 K. Fit line is shown in black.

In order to determine whether the transient we are observing at 370 nm is the same triplet 9-phenylfluorenyl species as that reported by Kirmse and coworkers, we performed a laser flash photolysis study on the cyclized product **4**. Our results showed a single transient species with a

λ_{max} = 370 nm, whose decay lifetime is affected by oxygen (Figures 4.2.10, 4.2.11, and 4.2.12), suggesting that this is indeed the same transient that we observed upon irradiation of **1**.

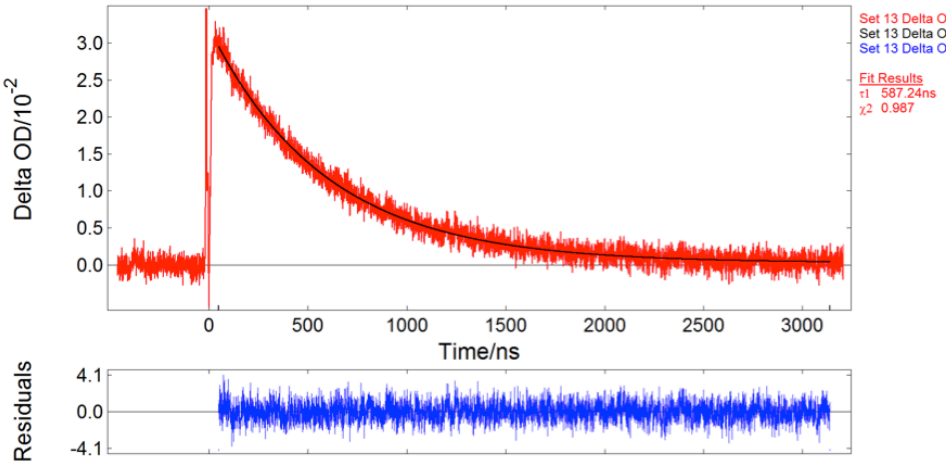

Figure 4.2.12. Transient decay at 370 nm for **4** measured in argon degassed *n*-hexane at 298 K. Fit line is shown in black.

With the results of our laser flash photolysis studies in solution now in hand, we can use this data to propose a photochemical mechanism for the photolysis of **1** to form **4**. Since it appears that the only transient we are able to observe is the triplet excited state of the 9-phenylfluorenyl product **4** (^{3}**4***), we will consider two possible mechanisms for how this transient might be generated, which are illustrated in Scheme 4.2.2. The first mechanism shown in part A follows the one proposed by Kirmse and coworkers in which the 9-phenylfluorenyl product is produced within the laser pulse where it can then be excited and subsequently detected.[12] Specifically, the mechanism begins with the excitation of the diphenyldiazomethane **1** to its first excited singlet state from which nitrogen gas (N_2) is lost to give the excited singlet carbene (^{1}**2***). Since it has been established that arylcarbenes have triplet ground states[5] the excited singlet carbene (^{1}**2***) can then undergo ISC to the lower energy ground state triplet carbene (^{3}**2**). Subsequent cyclization to form the triplet biradical (^{3}**BR**) is then followed by ISC to the ground state isofluorene (**3a**). **3a** then undergoes a [1,5]-H shift to give rise to the ground

state 9-phenylfluorenyl product (**4**). In order for this mechanism to hold true with our LFP results, the photochemical events from **1** → **4** just described must occur within the ca. 8 ns pulse width of our laser such that **4** can then be excited to its singlet excited state (^{1}**4***) and then intersystem cross to its excited triplet state (^{3}**4***). Finally, ^{3}**4*** would then relax back to the ground state (**4**) via ISC, and it is the decay of this triplet species (^{3}**4***) that we observe. The excitation of **4** and subsequent ISC to ^{3}**4*** can only occur if **4** has a reasonably high quantum yield of ISC (Φ_{ISC}). Since the Φ_{ISC} for fluorene is known to be 0.22,[40] and our UV-vis data (Figure 4.2.7) suggests that the main chromophore in **4** is the fluorene moiety, we can reasonably propose that **4** could have a similarly high Φ_{ISC} as fluorene, which supports the mechanism shown in Scheme 4.2.2.A.

Scheme 4.2.2

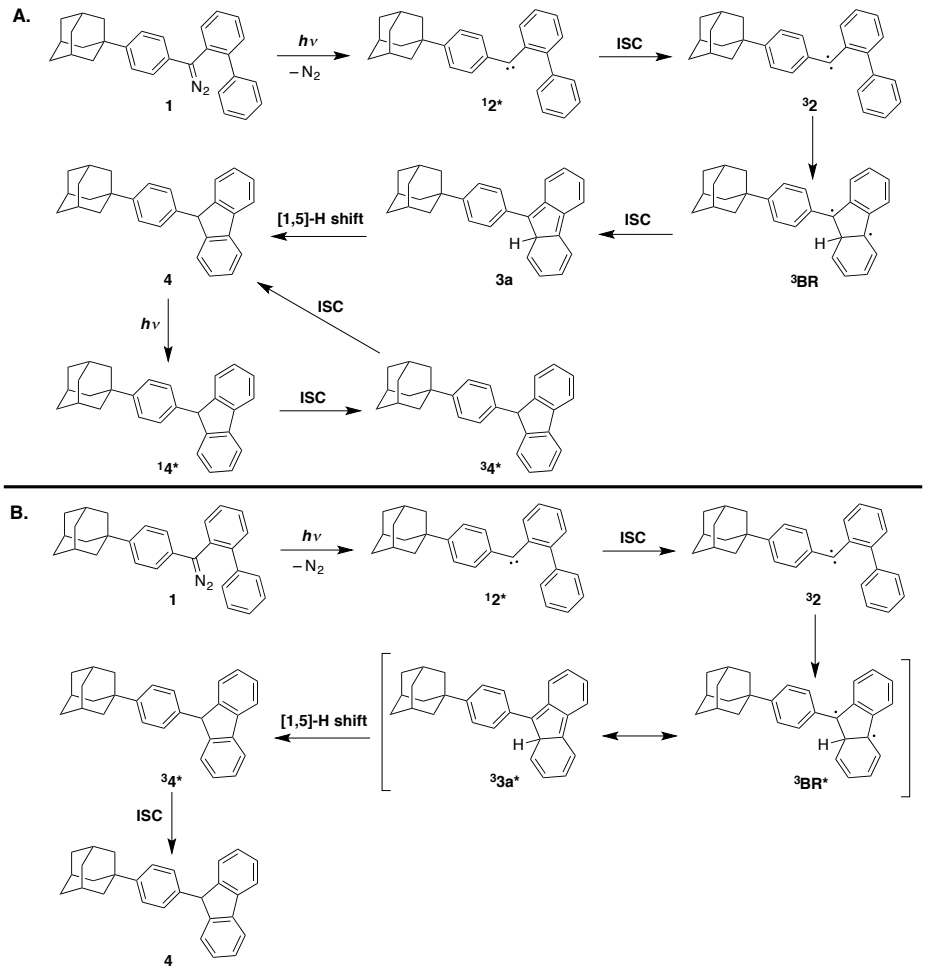

An alternative mechanism is shown in part B and differs from the one in part A in that the triplet 9-phenylfluorenyl species (^{3}**4***) is generated as a transient along the reaction pathway from **1** → **4** rather than being formed from a second excitation event. In this mechanism, the initial excitation of **1** proceeds to the excited singlet carbene (^{1}**2***) exactly the same way as was described for part A. However, this mechanism postulates that the reaction could continue on the excited state surface after ISC to the triplet carbene (^{3}**2**). Next, cyclization to the excited triplet biradical (^{3}**BR***), which may correspond to the excited triplet isofluorenyl species (^{3}**3a***), could occur followed by a [1,5]-H shift to give rise to the triplet excited state of the 9-phenylfluorenyl product (^{3}**4***). Subsequent ISC of ^{3}**4*** to the ground state product **4** is the transient decay that we are then able to measure. For this mechanism to hold true, the major assumption that has to be made is that the triplet excited state of the 9-phenylfluorene (^{3}**4***) must be energetically accessible from the triplet carbene (^{3}**2**).

In order to test the validity of the second photochemical mechanism (Scheme 4.2.2.B), we needed to determine the triplet energy of **4** and then correlate it to the triplet energy of the carbene (^{3}**2**) This was accomplished by acquiring an emission spectrum for **4** in a glass at 77 K (Figure 4.2.13, red line). The sharp spectral bands between 300–350 nm in the emission spectrum correlate to the excited singlet state energy or fluorescence of **4** (^{1}**4***), whereas the weaker and very broad spectral band between 420–500 nm corresponds to the excited triplet state energy or phosphorescence of **4** (^{3}**4***). Specifically, the onset of the phosphorescence spectrum is equal to the energy of the triplet state, which in this case occurs at 421 nm and thus gives a triplet energy of 67.9 kcal/mole for ^{3}**4***. This energy exactly matches the triplet energy for a pure sample of fluorene,[40] indicating that the fluorene moiety in **4** is the main chromophore in the molecule and thus is responsible for the emission spectrum we observe in Figure 4.2.13.

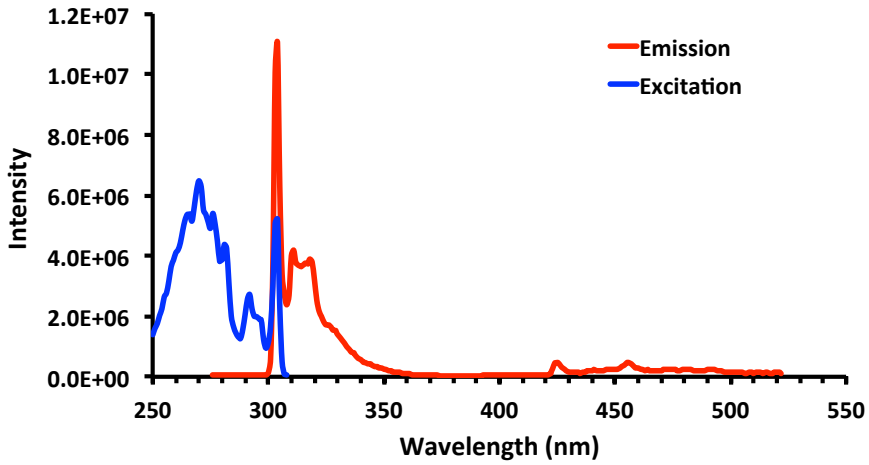

Figure 4.2.13. Excitation (blue line) and emission spectra (red line) for **4** in methylcyclohexane at 77 K. Excitation spectrum was collected using an emission wavelength of 318 nm, and emission spectrum using an excitation wavelength of 266 nm.

Since diarylcarbene **2** cannot be observed under our experimental conditions due to its extremely fast rate of cyclization, we decided to use diphenylcarbene as a model because it can be isolated and therefore has been extensively studied in a variety of solvents.[7–9,14,41–44] Using photoacoustic calorimetry, Simon and Peters were able to determine the enthalpy change for the reaction of diphenyldiazomethane to the triplet carbene to be 0 kcal/mol,[45,46] which strongly suggests that the energy difference between the triplet diphenylcarbene ^{3}**2** and the ground state 9-phenylfluorene product **4** is less than the energy difference between **4** and its triplet excited state (^{3}**4***) of 67.9 kcal/mol. This means that the adiabatic reaction mechanism proposed from **1** to ^{3}**4*** in part B of Scheme 4.2.2 would appear to be very unlikely to occur based on energetics. The possibility of an excited triplet carbene is not likely because the literature and the mechanism proposed in part B is that diarylcarbenes are known to undergo facile ISC from the singlet carbene to the more stable ground state triplet carbene,[4,5] Therefore, we exclude the mechanism in part B as a reasonable way to form ^{3}**4*** in favor of the mechanism proposed in part A.

However, although the proposed mechanism in part A appears to be more reasonable than the one in part B, we wanted to gather some more evidence to support its plausibility.

Scheme 4.2.3

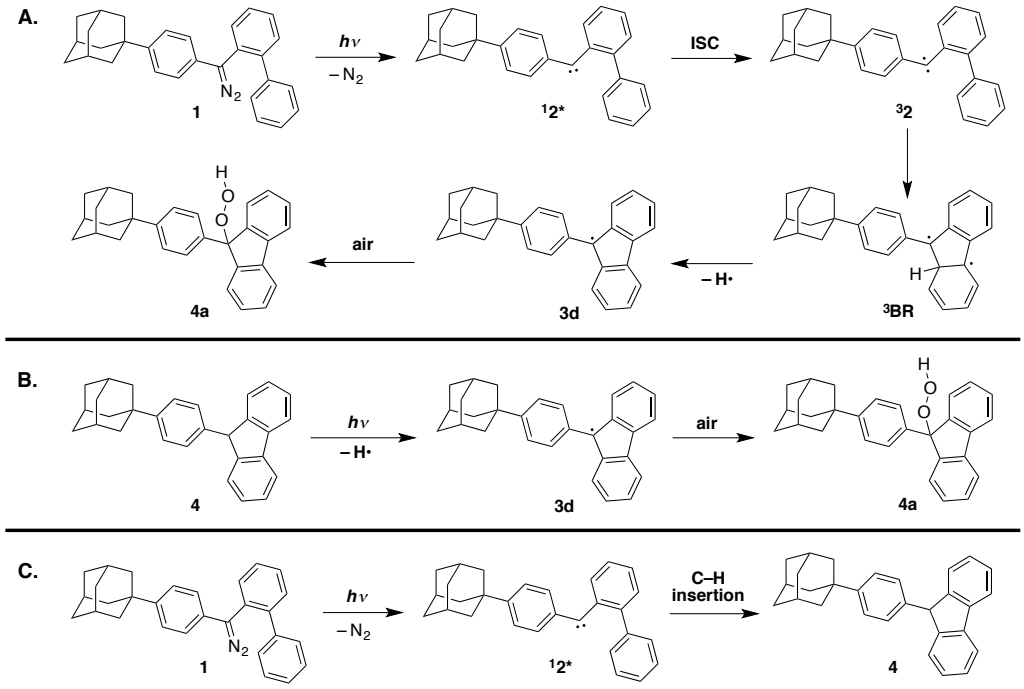

Since we know that the transient species we are able to detect upon the direct photolysis of either **1** or **4** can interact with oxygen, we postulated that instead of observing the triplet excited state of **4** (^{3}**4***), we could be detecting a radical species that then reacts with oxygen to form a peroxide derivative of **4** (**4a**) as illustrated in Scheme 4.2.3.A and B. To test this hypothesis, samples of **1** and **4** were purged with air and irradiated in a Hanovia photochemical reactor for 15 min. NMR and mass spectrometry analysis did not reveal the formation of **4a** or other similar peroxide species, suggesting that radical **3d** is not the transient species observed at 370 nm (see Appendix 4.5.3, Figures 4.5.3.1–4.5.3.3) and that the photochemical mechanism proposed in Scheme 4.2.2.A is more plausible than that of 4.2.2.B. One other possible mechanism to account for the formation of the 9-phenylfluorenyl product **4** after irradiation of the diaryldiazomethane **1** is the concerted singlet state C–H insertion reaction shown in Scheme

4.2.3.C. This mechanism assumes that direct C–H insertion of the excited singlet carbene (^{1}**2***) to form the final product (**4**) is faster than ISC to the ground state triplet carbene (^{3}**2**). However, a previous study found that the deuterium isotope effect for the formal C–H insertion of a carbene derived from the photolysis of 2-diazomethylbiphenyl in solution to produce fluorene was only 1.12 (k_H/k_D), which suggested that the rate-determining cyclization proceeds through a biradical or isofluorene intermediate with subsequent migration of the hydrogen via a [1,5]-H shift.[32] Thus, the direct C–H insertion of the singlet carbene ^{1}**2*** in Scheme 4.2.3.C to form **4** seems unlikely and suggests that ISC to the ground state triplet carbene (^{3}**2**) is incredibly fast, which lends more support to the photochemical mechanism proposed in Scheme 4.2.2.A.

With the investigation into the nanosecond transient kinetics of **1** and **4** in solution now complete, we turned our attention to studying the solid state kinetics of diaryldiazomethane **1**. Figure 4.2.14 shows the time-dependent transient absorption spectrum for **1** in NC suspension from 0–400 ns, which reveals a broad absorption between 340–500 nm with a λ_{max} = 370 nm that appears to decay very slightly over time. No further spectral changes in the transient absorption spectrum were observed from 400–4000 ns. Similar to our observations in solution, the solid state transient absorption spectrum also has a negative absorbance between 300–340 nm, which might correlate to the disappearance of the diaryldiazomethane starting compound **1** as it is converted to product. The UV-vis spectrum obtained prior to pulsed laser excitation seems to support this hypothesis as it shows that **1** has a significant absorption band between 270–360 nm with a λ_{max} ~ 300 nm (Figure 4.2.15, red line). A UV-vis spectrum was also collected after pulsed laser excitation of **1** in NC suspension, and just as was observed in solution it shows that the band at λ_{max} = 300 nm undergoes a blue shift to λ_{max} = 270 nm as well as decreases significantly in intensity (Figure 4.2.15, blue line). Interestingly, the post photolysis absorbance

spectrum in NC suspension also matches exactly with the spectrum for a pure sample of fluorene,[40] indicating that pulsed laser irradiation of **1** appears to produce 9-phenylfluorenyl **4** almost exclusively even in the solid state.

In order to reveal more about the nature of the transient that absorbs at 370 nm in NC suspensions, we measured the kinetics at 370 nm for a sample of **1**. Our results showed a very weak signal that could be fit using a single exponential decay function from which a lifetime of 47 μs was calculated (Figure 4.2.16). Although the UV-vis spectra in Figure 4.2.15 show very clearly the conversion of **1** to **4**, the kinetic data is difficult to interpret. Mechanistically, we speculate that the transient absorbing at 370 nm could be the same triplet species (^{3}**4***) that was observed in solution, suggesting that the solid state environment does not hinder the carbene from undergoing rapid intramolecular cyclization to the 9-phenylfluorenyl product (**4**) as illustrated in Scheme 4.2.2.A. Thus, within the laser pulse, excitation of **1** produces the 9-phenylfluorenyl product (**4**), which is also excited such that we can only observe the intersystem crossing of the triplet excited state of **4** (^{3}**4***) back to the ground state product (**4**).

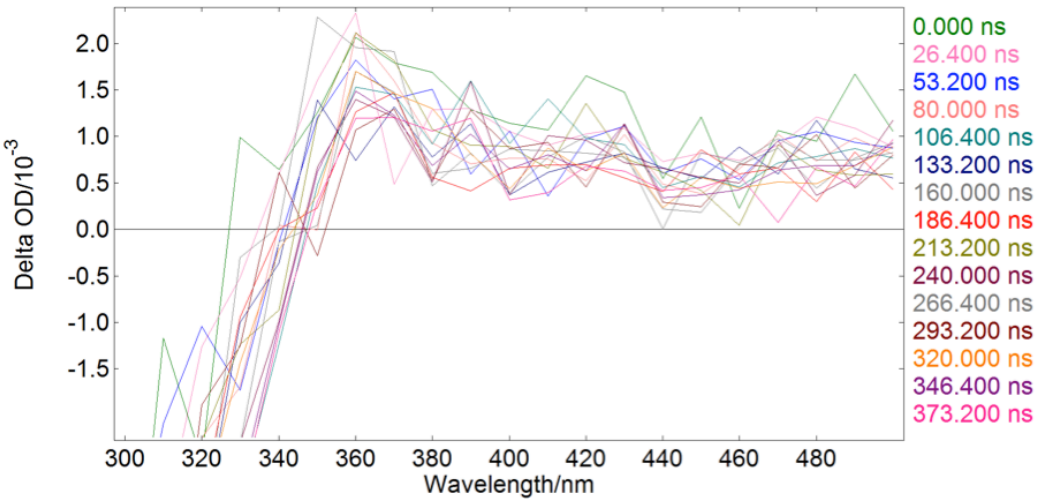

Figure 4.2.14. Time-dependent transient absorption spectrum for **1** at various time points in NC suspension collected between 0 and 400 ns.

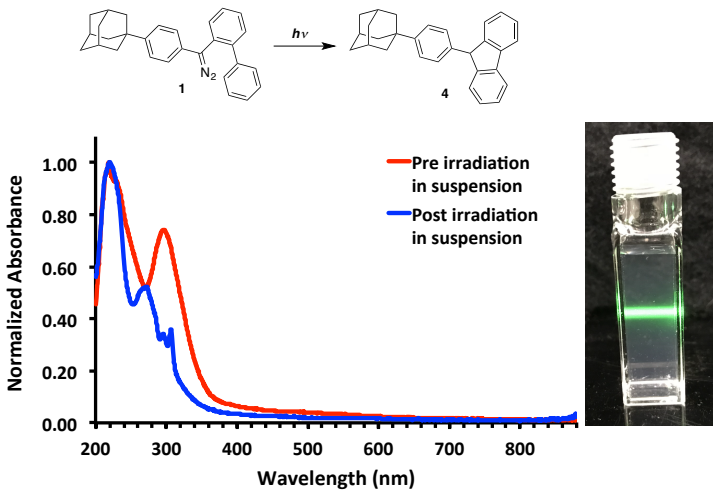

Figure 4.2.15. UV-vis spectra for **1** pre (red line) and post (blue line) pulsed laser irradiation in NC suspension. Picture: NC suspension of **1** with a green laser pointer shining through it to illustrate that suspended particles scatter light.

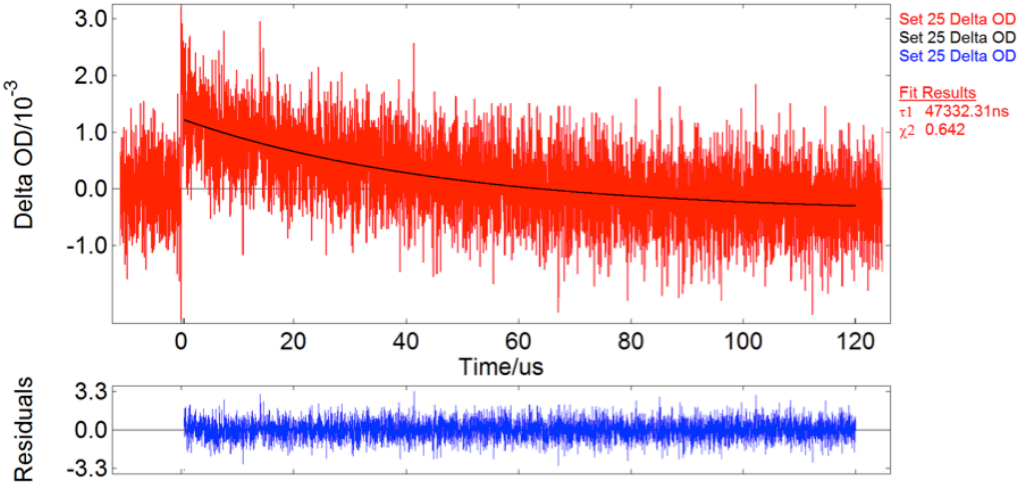

Figure 4.2.16. Transient decay at 370 nm for **1** in NC suspension at 298 K. Fit line is shown in black.

4.3 Conclusions

Using nanosecond transient absorption spectroscopy, we were able to measure the kinetics of the triplet excited state of a 9-phenylfluorenyl species (^{3}**4***) both in solution and in the

solid state and suggest a mechanism that involves the formation of the cyclized product **4** from initial excitation of the diaryldiazomethane **1** within the laser pulse such that **4** could then also be excited by the same pulse to generate the triplet excited state (^{3}**4***), which then relaxes back down to the ground state via ISC. NMR analysis of air-saturated solutions of both **1** and **4** did not reveal the formation of peroxide species such as **4a**, which ruled out the possibility that our observed transient is a radical species like **3d**. Subsequent studies in NC suspension revealed a relatively broad transient spectrum with a λ_{max} = 370 nm and a decay lifetime of 47 μs. UV-vis analysis of our NC suspensions pre and post irradiation strongly suggested the formation of **4**, just as we observed in solution, such that the solution and solid state photochemical mechanism could be the same with the only difference being the rate of ISC from ^{3}**4*** to **4**. Although we were not able to observe the triplet carbene (^{3}**2**) in the solid state spectroscopically, this report helps to demonstrate that NC suspensions are a simple and robust method for studying the solid state kinetics of photochemical reactions by reducing the challenges arising from optical effects and by reducing the probability of multiphotonic processes.

4.4 Experimental

4.4.1 General Information for Synthetic Procedures

All commercially obtained reagents/solvents were used as received without further purification. Unless stated otherwise, reactions were conducted in oven-dried glassware under argon atmosphere. ^{1}H and ^{13}C NMR spectra were acquired on a Bruker Avance spectrometer at 500 MHz (^{1}H) and 125 MHz (^{13}C). All chemical shifts are reported in ppm on the δ-scale relative to the residual solvent signal as reference ($CDCl_3$ δ 7.26 and δ 77.16 for proton and carbon, respectively). Coupling constants (*J*) are reported in hertz (Hz). Standard abbreviations

indicating multiplicity were used as follows: s (singlet), b (broad), d (doublet), t (triplet), q (quartet), m (multiplet), dd (doublet of doublets), dt (doublet of triplets), and td (triplet of doublets). High-resolution mass spectrum data was recorded on a DART spectrometer in positive (ESI+) ion mode. Melting point values were recorded on a Melt-Point II® apparatus. Infrared spectra were recorded on a PerkinElmer® Spectrum 100 spectrometer equipped with a universal ATR sampling accessory.

4.4.2 Synthetic Procedures

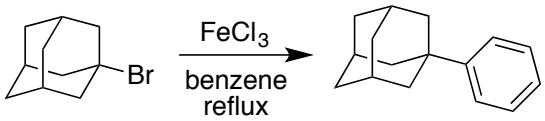

5 **6**

Synthesis of 1-Phenyladamantane (6): Activated 2.2920 g of $FeCl_3$ (5 wt. % on silica gel) by heating at 85–90 °C for 2 hours. Then added 1.0130 g (4.7085 mmol) of 1-bromoadamantane (**5**) along with 93 mL of dry benzene under argon and refluxed for 5.5 h. After cooling to room temperature, filtered the reaction through a fritted glass funnel using benzene and then concentrated the filtrate. Purified by flash chromatography on a short plug of silica with hexanes as eluent to obtain **6** (0.9960 g, 99% yield) as a white solid. m.p. 84.3–84.7 °C (lit. 84–85 °C).[47] IR (film): 3082, 3060. 3027, 2925, 2905, 2848, 1600, 1580, 1495, 1485, 1442, 1345, 1253, 1107, 1077, 1024, 974, 751, 694, 532 cm^{-1}. ^1H NMR ($CDCl_3$, 500 MHz): δ 7.38–7.36 (m, 2H), 7.34–7.30 (m, 2H), 7.20–7.16 (m, 1H), 2.09 (b, 3H), 1.92 (d, J = 2.63 Hz, 6H) 1.80–1.74 (m, 6H) ppm. ^{13}C NMR ($CDCl_3$, 125 MHz): δ 151.5, 128.2, 125.6, 125.0, 43.3, 37.0, 36.3, 29.1 ppm. HRMS (ESI-TOF) m/z: [M] calcd. for $C_{16}H_{20}$: 212.15650, found: 212.15751.

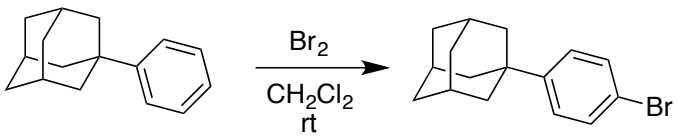

6 **7**

Synthesis of 1-(4-Bromophenyl)adamantane (7): Bromine (2 mL, 39.03 mmol) was added to a solution containing 1-phenyladamantane (**6**) (2 g, 9.42 mmol) in 40 mL of dry CH_2Cl_2 at room temperature under argon. After 19 h, the reaction was quenched by pouring into a flask containing crushed ice and then adding $NaHSO_3$ with the flask in an ice bath until both the organic and aqueous layers were colorless. Removed the organic layer and extracted the aqueous layer 3 times with DCM, washed the combined organic layers 1 time with DI H_2O, dried over $MgSO_4$, filtered and removed solvent under reduced pressure. The resulting solid was purified by flash chromatography on a short plug of silica with hexanes as eluent to obtain **7** (2.6933 g, 98% yield) as a white solid. m.p. 101.7–102.8 °C (lit. 101–102 °C).[47] IR (film): 3082, 3054, 3029, 2903, 2847, 1623, 1597, 1584, 1567, 1490, 1473, 1447, 1395, 1343, 1315, 1102, 1076, 1005, 831, 801, 715, 528 cm^{-1}. ^1H NMR ($CDCl_3$, 500 MHz): δ 7.44–7.41 (m, 2H), 7.25–7.22 (m, 2H), 2.09 (b, 3H), 1.88 (d, J = 2.66 Hz, 6H), 1.80–1.72 (m, 6H) ppm. ^{13}C NMR ($CDCl_3$, 125 MHz): δ 150.5, 131.2, 127.0, 119.4, 43.2, 36.8, 36.2, 29.0 ppm. HRMS (ESI-TOF) m/z: $[M]^{\bullet+}$ calcd. for $C_{16}H_{19}Br^{\bullet+}$: 290.06646, found: 290.06487.

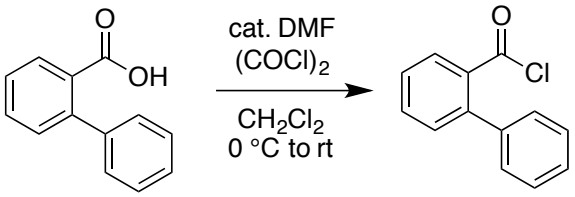

8 **9**

Synthesis of [1,1'-Biphenyl]-2-carbonyl chloride (9): [1,1'-Biphenyl]-2-carboxylic acid (**8**) (1.0001 g, 5.045 mmol) was dissolved in 30 mL of dry CH_2Cl_2 at 0 °C under argon. After 20 min, oxalyl chloride (1.30 mL, 15.36 mmol) was added dropwise along with 4 drops of DMF. Ice bath was removed after 1 h and the reaction was allowed to warm slowly to room temperature. After 3.5 h, the now light yellow reaction mixture was concentrated under reduced pressure. The resulting crude material was washed 3 x 6 mL of toluene with the solvent being removed under

reduced pressure between washes, which gave **9** as a white solid that was used without further purification in the next step.

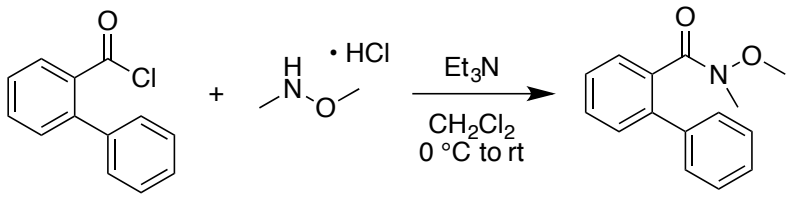

9 **10** **11**

Synthesis of *N*-methoxy-*N*-methyl-[1,1'-biphenyl]-2-carboxamide (11): *N,O*-dimethyldydroxylamine hydrochloride (**10**) (0.3691 g, 3.78 mmol) was dissolved in 40 mL of dry CH_2Cl_2 at 0 °C under argon. After 45 min, dry triethylamine (0.88 mL, 6.31 mmol) was added dropwise to the reaction. After another 1.5 h, added the acid chloride (0.5465 g, 2.52 mmol) from the previous in two portions using 2.5 mL of CH_2Cl_2 each time followed by the addition of 11 mL more of CH_2Cl_2. Let reaction warm slowly to room temperature over 14.5 h and then quenched with 7–8 mL of sat. $NaHCO_3$. After 10 min, separated the aqueous and organic layers and extracted the aqueous layer twice with CH_2Cl_2. Then washed the combined organic layers once with brine, dried over $MgSO_4$, and removed solvent under reduced pressure. The resulting yellow oil was purified by flash chromatography using 2:1 hexanes/ethyl acetate to give the Weinreb amide (**11**) (0.5453 g, 90% yield) as a colorless oil. IR (film): 3059, 3024, 2972, 2934, 2899, 2817, 1655, 1597, 1481, 1451, 1438, 1411, 1377, 1209, 1073, 990, 780, 746, 701 cm^{-1}. ^1H NMR ($CDCl_3$, 500 MHz): δ 7.47–7.35 (m, 9H), 3.50–2.67 (m, 6H) ppm. ^{13}C NMR ($CDCl_3$, 125 MHz): δ 172.1, 167.2, 140.7, 139.7, 139.3, 135.0, 134.4, 130.1, 129.7, 129.5, 128.8, 128.6, 128.4, 128.0, 127.9, 127.5, 127.01, 127.98, 61.2, 60.0, 35.9, 32.5 ppm. HRMS (ESI-TOF) m/z: $[M+H]^+$ calcd. for $C_{15}H_{16}NO_2^+$: 242.11756, found: 242.11791.

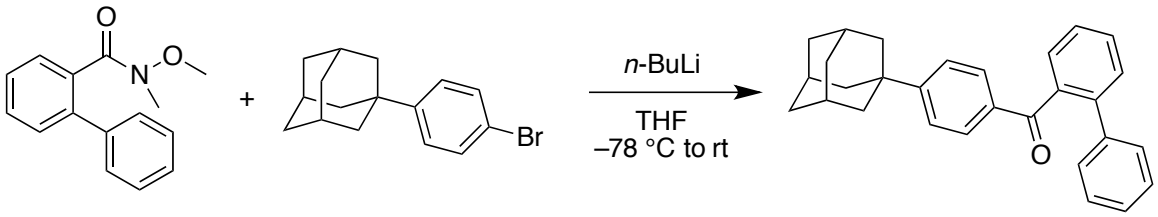

11 **7** **12**

Synthesis of [1,1'-biphenyl]-2-yl(4-(adamantan-1-yl)phenyl)methanone (12): 1-(4-Bromophenyl)adamantane (**7**) (0.6582 g, 2.26 mmol) was dissolved in 15 mL of dry THF and cooled to –78 °C under argon. After 30 min, *n*-BuLi (2 mL, 2.9 mmol) was added dropwise and the reaction was maintained at –78 °C for 1 hour upon which time the Weinreb amide (**11**) (0.5453 g, 2.26 mmol) in 3.6 mL of dry THF was then added over 30 min. The reaction was allowed to warm slowly to room temperature over 20 h before being quenched with 4 mL of a 10% HCl solution. Extracted the aqueous layer three times with ethyl acetate and then washed the combined organic layers once with brine, dried over $MgSO_4$, and removed solvent under reduced pressure to give a thick yellow oil. Purified by flash chromatography on silica using 2:1 CH_2Cl_2/hexanes as eluent to obtain **12** (0.4879 g, 55% yield) as a white solid. m.p. 131.7–133.6 °C. IR (film): 3058, 3029, 2902, 2848, 1665, 1603, 1565, 1475,1449, 1407, 1309, 1281, 1263, 1152, 1032, 930, 851, 776, 747, 697, 642 cm^{-1}. ^1H NMR ($CDCl_3$, 500 MHz): δ 7.64–7.62 (m, 1H), 7.55 (td, J = 7.45, 1.59 Hz, 1H), 7.49–7.41 (m, 3H), 7.29–7.26 (m, 4H), 7.22–7.14 (m, 3H), 2.08 (b, 3H), 1.85 (d, J = 2.66 Hz, 6H), 1.79–1.71 (m, 6H) ppm. ^{13}C NMR ($CDCl_3$, 125 MHz): δ 198.4, 156.8, 141.4, 140.4, 139.4, 135.0, 130.3, 130.24, 130.21, 129.1, 128.8, 128.4, 127.3, 127.0, 124.8, 42.9, 36.8, 28.9 ppm. HRMS (ESI-TOF) m/z: $[M+H]^+$ calcd. for $C_{29}H_{29}O^+$: 393.22129, found: 393.21470.

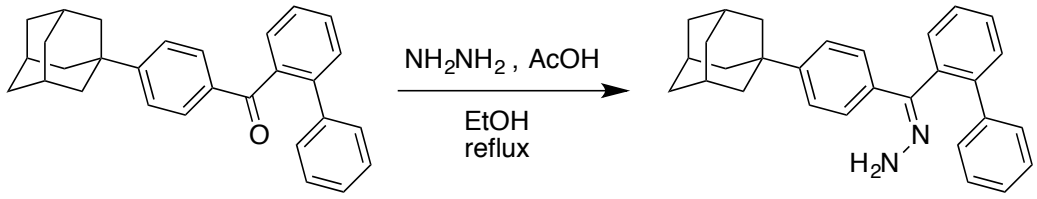

12 **13**

Synthesis of ([1,1'-biphenyl]-2-yl(4-(adamantan-1-yl)phenyl)methylene)hydrazine (13): Ketone **12** (0.0523 g, 0.133 mmol) was suspended in 1 mL of dry EtOH under argon and then heated to reflux to dissolve the ketone. Hydrazine (0.06 mL, 1.91 mmol) was then added along with 3 drops of acetic acid and the solution was allowed to continue to reflux. Two more portions of 0.06 mL of hydrazine were added at 1.5 h intervals. After 14 h, the reaction was cooled to room temperature and concentrated under reduced pressure to give a white solid. The solid was filtered and washed with cold EtOH to obtain **13** (0.0269 g, 50%) as a white solid, which was used without further purification in the next step.

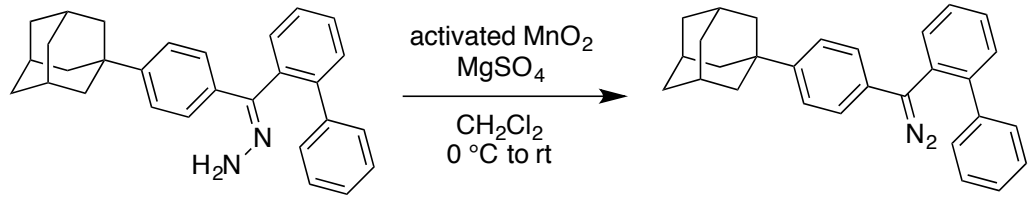

13 **1**

Synthesis of 1-(4-([1,1'-biphenyl]-2-yl(diazo)methyl)phenyl)adamantane (1): A solution of hydrazone **13** (0.014 g, 0.0344 mmol) in 1 mL of dry CH_2Cl_2 was added to $MgSO_4$ (0.0044 g, 0.0366 mmol) under argon and cooled to 0 °C. After 15 min, added in one portion activated MnO_2 (0.0124 g, 0.142 mmol), which was prepared as previously reported.[ref (JACS 1984, 106, 1043)] The reaction was allowed to warm slowly to room temperature over 14 h before being filtered and washed with CH_2Cl_2. The dark pink filtrate was dried using a stream of argon, which gave **1** (0.0091 g, 65% yield) as a dark pink/purple solid. m.p. at 137 °C the dark pink color started to fade and by 150 °C no color remained. The now white/pale yellow solid melted at 202.1–

204.0 °C. IR (film): 3054, 3027, 2901, 2846, 2036, 1601, 1513, 1476, 1451, 1313, 1101, 1008, 835, 806, 775, 756, 744, 702 cm^{-1}. ^1H NMR ($CDCl_3$, 500 MHz): δ 7.55–7.53 (m, 1H), 7.45–7.43 (m, 1H), 7.41–7.39 (m, 2H), 7.36–7.35 (m, 4H), 7.33–7.31 (m, 2H), 7.30–7.28 (m, 1H), 7.05–7.02 (m, 2H), 2.10 (b, 3H), 1.91 (d, J = 2.64 Hz, 6H), 1.81–1.74 (m, 6H) ppm. ^{13}C NMR ($CDCl_3$, 125 MHz): δ 147.8, 141.6, 140.5, 131.3, 130.7, 128.9, 128.5, 128.4, 128.1, 127.9, 127.2, 126.9, 125.7, 123.0, 61.9, 43.3, 36.9, 36.0, 29.1 ppm. HRMS (ESI-TOF) m/z: $[M+H]^+$ calcd. for $C_{29}H_{29}N_2^+$: 405.23253, found: 405.23253.

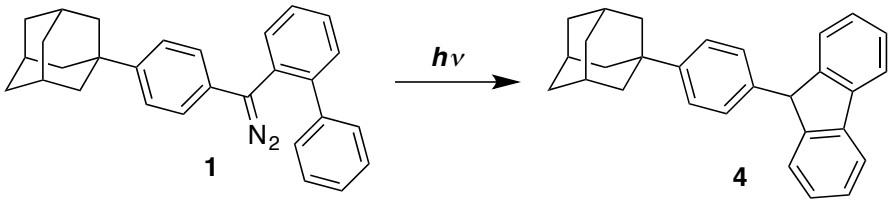

Synthesis of 1-(4-(9*H*-fluoren-9-yl)phenyl)adamantane (4): Dissolved 2 mg of **1** in 0.5 mL of benzene-d_6 and transferred to an NMR tube. Used a Pyrex beaker as a cutoff filter and irradiated in a Hanovia photochemical reactor (450 W, medium pressure Hg lamp). Took time points at 0 min, 2 min, 8 min, and 13 min and recorded the ^1H NMR spectrum to observe formation of **4**. After complete conversion to product was observed, removed the benzene-d_6 and then redissolved in $CDCl_3$ in order to fully characterize **4** via ^1H and ^{13}C NMR. m.p. 202.1–204.0 °C. IR (film): 3059, 3037, 3014, 2912, 2849, 1602, 1508, 1473, 1447, 1411, 1343, 1103, 1015, 798, 756, 740, 692 cm^{-1}. ^1H NMR ($CDCl_3$, 500 MHz): δ 7.79 (d, J = 7.61 Hz, 2H), 7.38 (t, J = 7.45 Hz, 2H), 7.35 (dd, J = 7.51, 0.76 Hz, 2H), 7.27–7.23 (m, 4H), 7.05–7.02 (m, 2H), 5.04 (s, 1H), 2.07 (b, 3H), 1.88 (d, J = 2.72 Hz, 6H), 1.79–1.71 (m, 6H) ppm. ^{13}C NMR ($CDCl_3$, 125 MHz): δ 149.9, 148.1, 141.1, 138.5, 128.0, 127.4, 127.3, 125.5, 125.3, 120.0, 54.1, 43.3, 36.9, 36.1, 29.1 ppm. HRMS (ESI-TOF) m/z: $[M]^{\bullet+}$ calcd. for $C_{29}H_{28}^{\bullet+}$: 376.21855, found: 376.21556.

4.4.2 Sample Preparation of Diaryldiazomethane 1 for Laser Flash Photolysis Experiments

Preparation of solutions for laser flash photolysis experiments

0.5964 mL of a stock solution (5 mM) in *n*-hexane was diluted to 100 mL to give a final sample concentration of ~3 x 10^{-5} M. Solutions had an optical density of ca. 0.3 at 266 nm.

Preparation of nanocrystalline suspensions for laser flash photolysis experiments

45 μL of a stock solution (6.76 mM) in THF was injected via a micropipette into a large culture tube containing 10 mL of vortexing Millipore water. Vortexing continued for 30 seconds after injection. The freshly made suspension was then used for LFP studies and new suspensions were made as needed. NC suspensions had an optical density of ca. 0.260 at 266 nm.

4.4.3 Laser Flash Photolysis of Diaryldiazomethane 1 in Solution (argon degassed and air-saturated)

Degassed *n*-hexane solutions of **1** were purged with argon for 3 hours prior to conducting laser flash photolysis experiments, and a continuous flow of argon was maintained in the reservoir flask for the duration of data collection. Air-saturated *n*-hexane solutions of **1** were allowed to equilibrate for several hours under normal atmospheric conditions prior to conducting laser flash photolysis experiments.

Time-resolved transient absorption maps were then recorded from 300–500 nm in 10 nm steps while continuously flowing the sample solutions through a quartz cell mounted on a home-built sample holder at a rate of 1.9 mL/min. One absorption band with a λ_{max} of 370 nm was observed, and the kinetics at 370 nm was then measured with a 1 nm bandwidth and 30 scans averaged together. The fluorescence background was also acquired and subtracted from the

transient absorption spectra. Flashlamp settings were set where the frequency was 10 Hz, width at 40 μs, and delay at 4000 μs. Q-switch settings were set where the frequency was at 1.0 Hz, width at 20 μs, and delay at 280 μs.

4.4.4 Laser Flash Photolysis of Diaryldiazomethane 1 in Nanocrystalline Suspensions

Suspensions were prepared immediately prior to performing kinetic measurements as described in section 4.5.3. Time-resolved transient absorption maps were then recorded from 300–500 nm in 10 nm steps while continuously flowing the sample through a quartz cell mounted on a home-built sample holder at a rate of at 1.9 mL/min. Kinetic measurements were made at 370 nm with a 1.75 nm bandwidth and 30 scans averaged together. The fluorescence background was also acquired and subtracted from the transient absorption spectra. Flashlamp settings were set where the frequency was 10 Hz, width at 40 μs, and delay at 4000 μs. Q-switch settings were set where the frequency was at 1.0 Hz, width at 20 μs, and delay at 220 μs.

4.4.5 Sample Preparation of 9-Phenylfluorenyl 4 for Laser Flash Photolysis and Emission Experiments

Preparation of solutions for laser flash photolysis experiments

0.60 mL of a stock solution (5 mM) in *n*-hexane was diluted to 100 mL to give a final sample concentration of ~3 x 10^{-5} M. Solutions had an optical density of ca. 0.32 at 266 nm.

Preparation of solutions for emission experiments

5 μL of a stock solution (5 mM) in methylcyclohexane was diluted to 4 mL to give a final sample concentration of ~6.2 x 10^{-6} M. Solution had an optical density of ca. 0.1 at 266 nm.

4.4.6 Laser Flash Photolysis of 9-Phenylfluorenyl 4 in Solution (argon degassed and air-saturated)

Experimental procedure and data collection parameters were the same as described in section 4.4.3.

4.4.7 Experimental Method of Emission Study of 9-Phenylfluorenyl 4 in a Frozen Glass Matrix at 77 K

0.5–1 mL of ~6.2 x 10^{-6} M solution of **4** in methylcyclohexane was transferred to a quartz EPR tube, which was placed in a quartz dewer and frozen into a glass using liquid nitrogen. The sample was maintained at 77 K for the duration of the experiment. Emission spectra were recorded with an excitation wavelength of 266 nm and scanning from 276–522 nm in 1 nm steps with a 0.2 second dwell time. Emission spectrum did not change when the dwell time was varied from 0.2–50 seconds. Excitation spectra were recorded with an emission wavelength of 318 nm and scanning from 250–308 nm in 1 nm steps with a 0.2 second dwell time. Identical excitation spectra were recorded using an emission wavelength of 304, 311, or 318 nm.

4.5 Appendix

Characterization and Supplemental Information for Chapter 4

4.5.1 General Information.....166

4.5.2 ^{1}H and ^{13}C NMR Spectra for Synthesized Compounds.....167

4.5.3 ^{1}H and ^{13}C NMR Spectra for Compounds **1** and **4** Post Photolysis in Air-Saturated Solutions.....179

4.5.4 UV-vis Spectra for Compounds **1** and **4**.....182

4.5.5 Dynamic Light Scattering Analysis for Compound **1**.....183

4.5.1 General Information

^{1}H and ^{13}C NMR spectra were acquired on a Bruker Avance spectrometer at 500 MHz (^{1}H) and 125 MHz (^{13}C). All chemical shifts are reported in ppm on the δ-scale relative to the residual solvent signal as reference ($CDCl_3$ δ 7.26 and δ 77.16 for proton and carbon, respectively, and C_6D_6 δ 7.16 and δ 128.06). UV-Vis absorption spectra were recorded on Ocean Optics spectrometer (DT-MINI-2-GS UV-VIS-NIR LightSource and USB2000+ using SpectraSuite software package). Dynamic Light Scattering (DLS) data were recorded using a Beckman-Coulter N4 Plus particle analyzer with a 10 mW helium-neon laser at 632.8 nm. The particle size was determined using the 62.6° detection angle and was calculated using the size distribution processor (SDP) analysis package provided by the manufacturer. Powder X-ray diffraction measurements were performed on a flat stage using a PANalytical Inc. X'Pert Pro Cu K-a = 1.5406 Å radiation at power settings of 45 kV and 40 mA and a slit width of 0.5°. Data were collected at room temperature in the range of 2θ = 4–45°. Nanosecond transient absorption experiments were performed using a laser flash photolysis (LFP) instrument from Edinburgh Instruments in conjunction with a Q-switched Nd:YAG laser (Brilliant b, Quantel®) with a 355 nm output wavelength, 5–8 ns pulse width, 1 Hz repetition rate, and 36–40 mJ pulse energy. The optical detection is based on a pulsed Xenon arc lamp (450 W), a monochromator (TMS300, Czerny-Turner), a photomultiplier detector (Hamamatsu R928), and a digital oscilloscope (TDS3012C, 100 MHz and 1.25 GS/s from Tektronix). Transient absorption data was processed using the L900 software package provided by Edinburgh Instruments. Laser flash photolysis experiments were performed with a 1 cm quartz flow cell mounted on a home-built sample holder that is placed at the cross-section of the laser incident beam and the probe flashlamp. Samples were flowed through a Masterflex L/S peristaltic pump at a rate of 1.9 mL/min for *n*-

hexane solutions and for nanocrystalline suspension samples. Emission spectra were acquired using an Edinburgh Instruments FLSP920 spectrometer equipped with a 450 W xenon arc lamp (Xe900) as the light source, a single photon counting PMT as the detector, and the F900 software program.

4.5.2 ^{1}H and ^{13}C NMR Spectra for Synthesized Compounds

^{1}H NMR of 1-Phenyladamantane (**6**) in $CDCl_3$ at 500 MHz

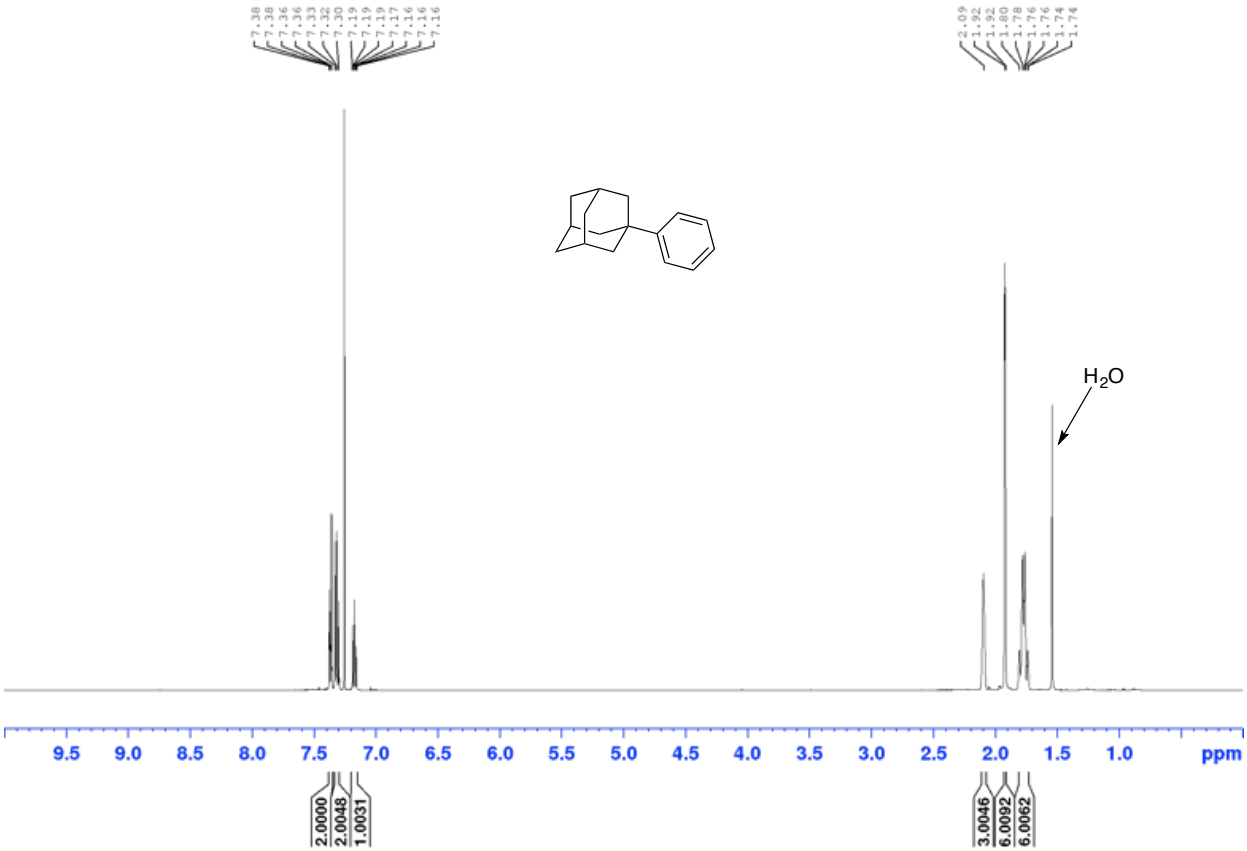

^{13}C NMR of 1-Phenyladamantane (**6**) in $CDCl_3$ at 125 MHz

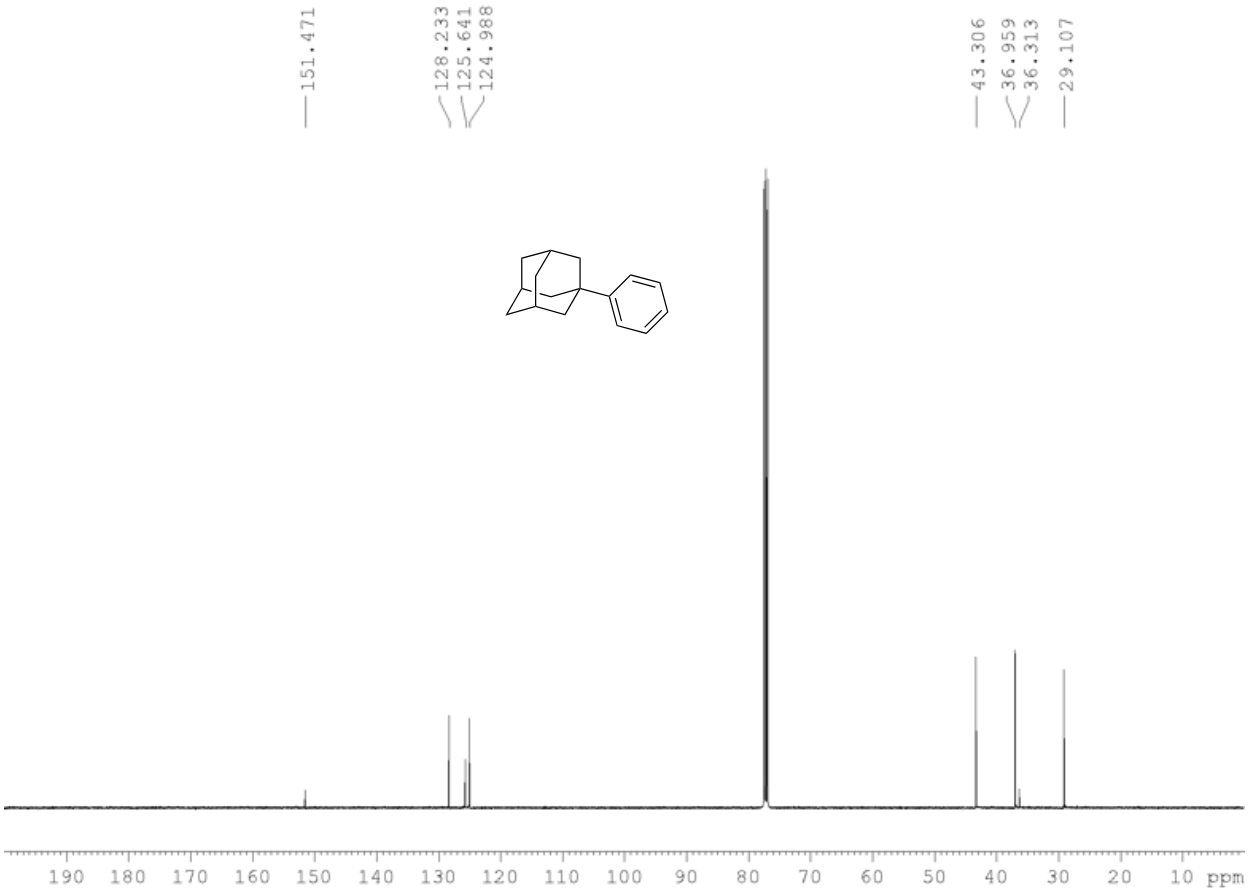

^{1}H NMR of 1-(4-Bromophenyl)adamantane (**7**) in $CDCl_3$ at 500 MHz

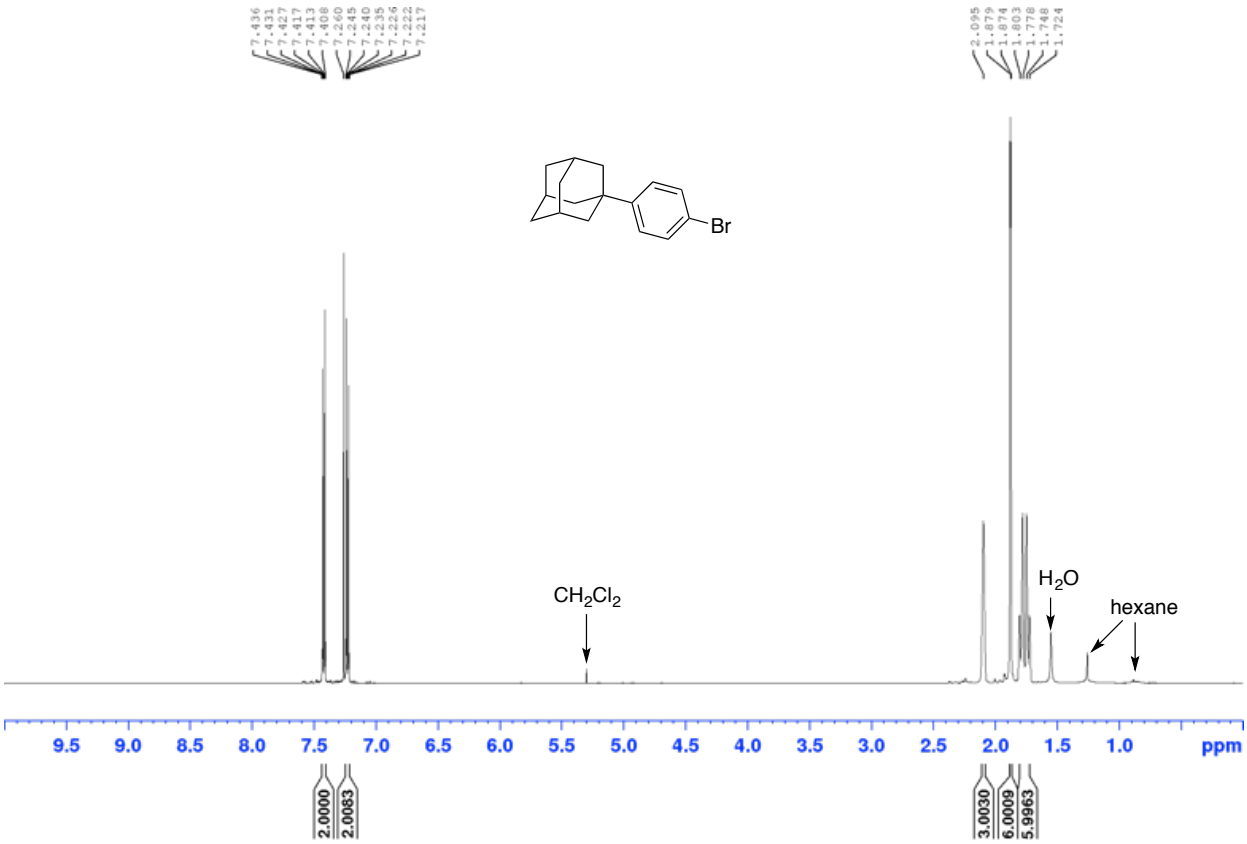

^{13}C NMR of 1-(4-Bromophenyl)adamantane (**7**) in $CDCl_3$ at 125 MHz

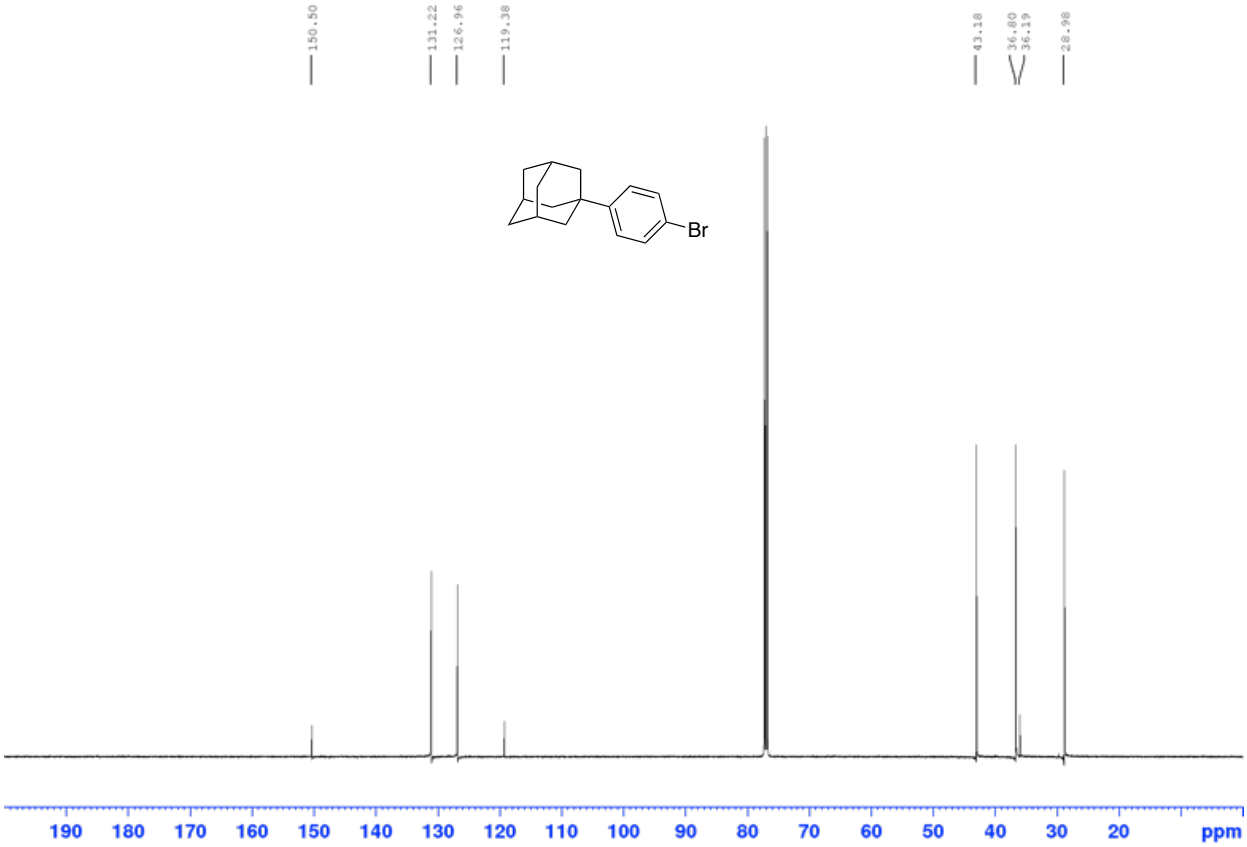

^{1}H NMR of *N*-methoxy-*N*-methyl-[1,1'-biphenyl]-2-carboxamide (**11**) rotamers at room temperature in $CDCl_3$ at 500 MHz

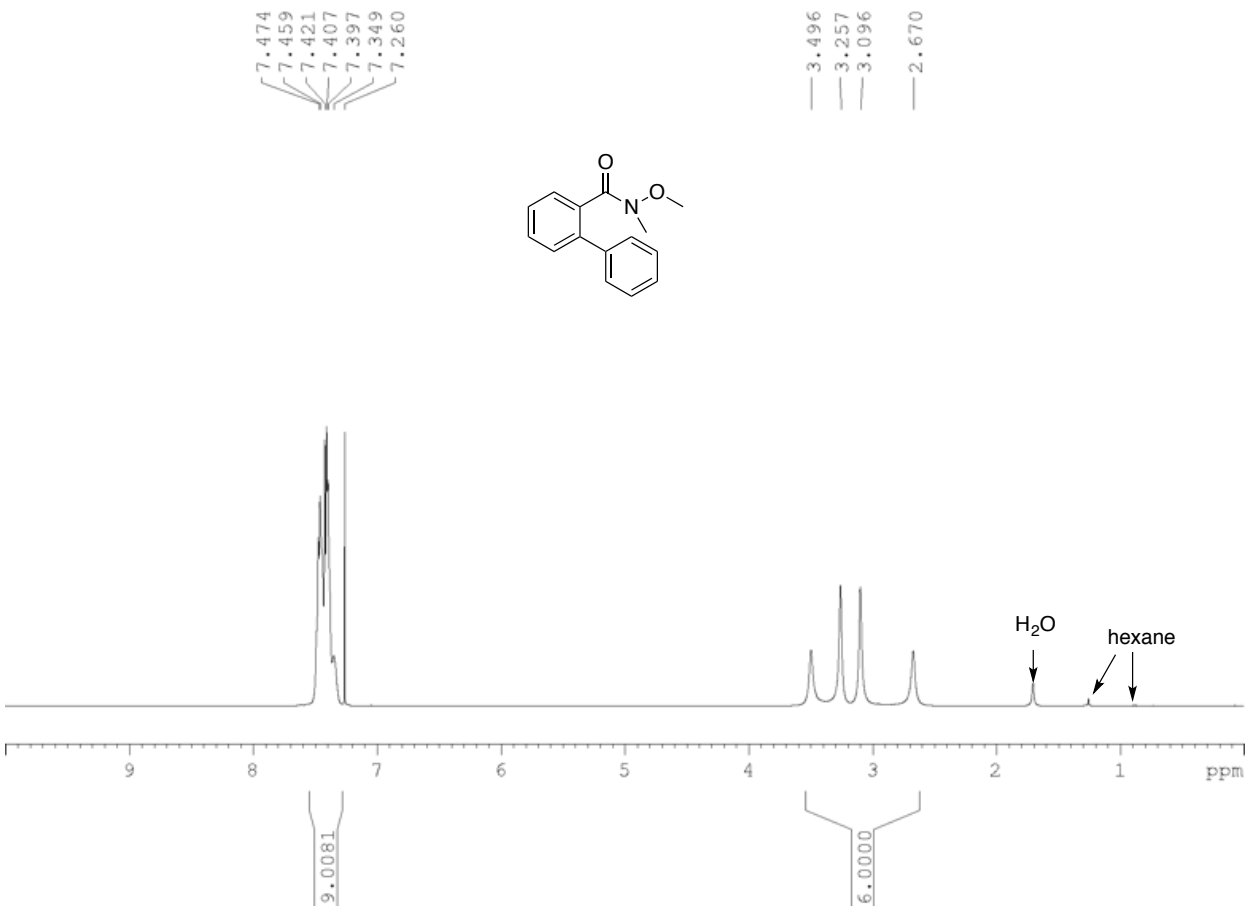

^{13}C NMR of *N*-methoxy-*N*-methyl-[1,1'-biphenyl]-2-carboxamide (**11**) rotamers at room temperature in $CDCl_3$ at 125 MHz

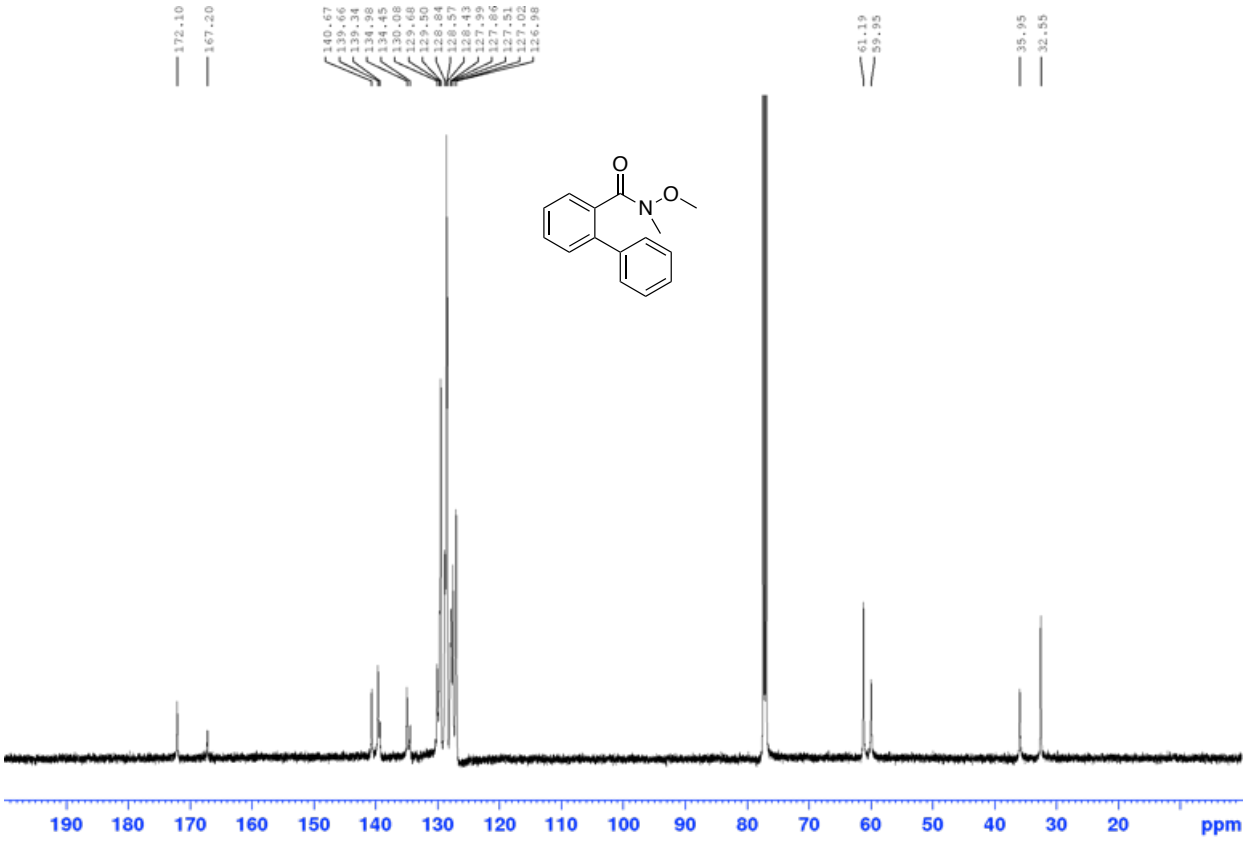

^{1}H NMR of [1,1'-biphenyl]-2-yl(4-(adamantan-1-yl)phenyl)methanone (**12**) in $CDCl_3$ at 500 MHz

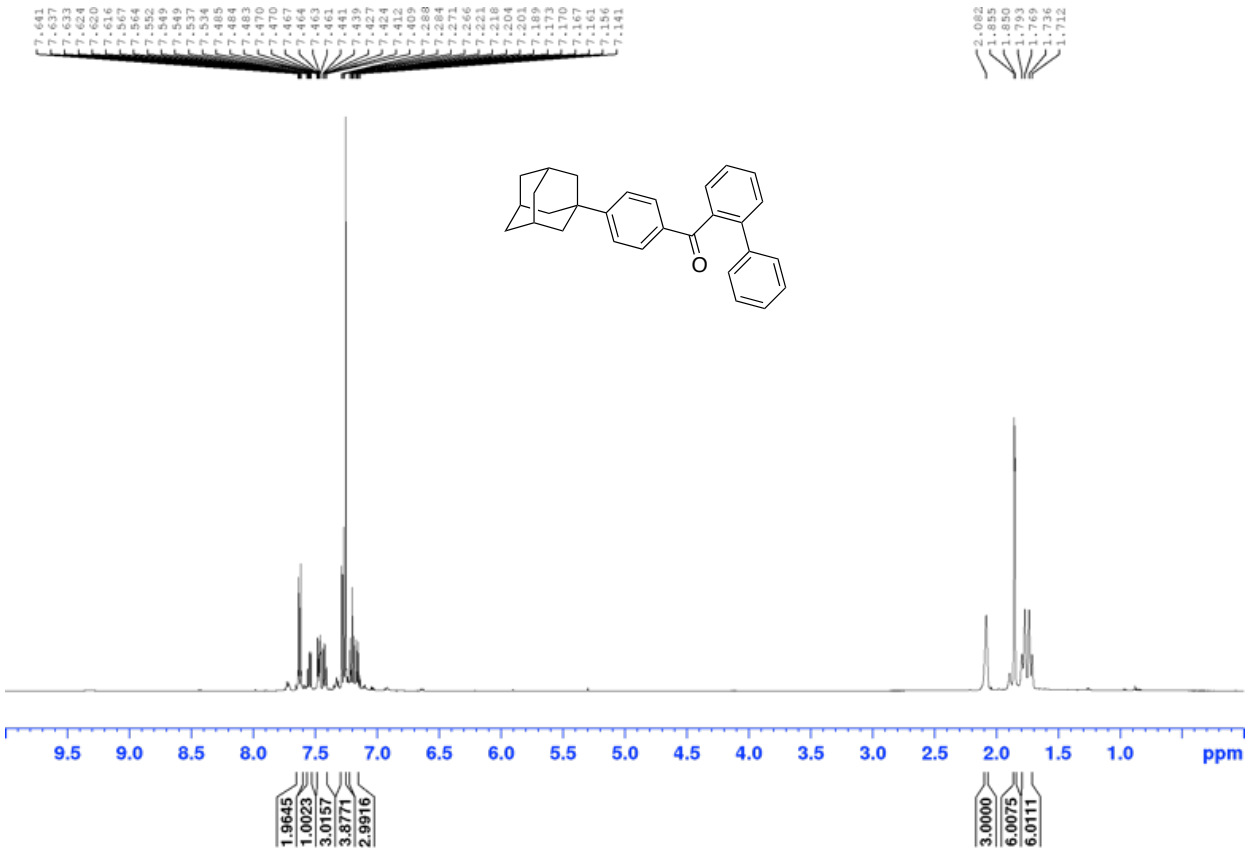

^{13}C NMR of [1,1'-biphenyl]-2-yl(4-(adamantan-1-yl)phenyl)methanone (**12**) in $CDCl_3$ at 125 MHz

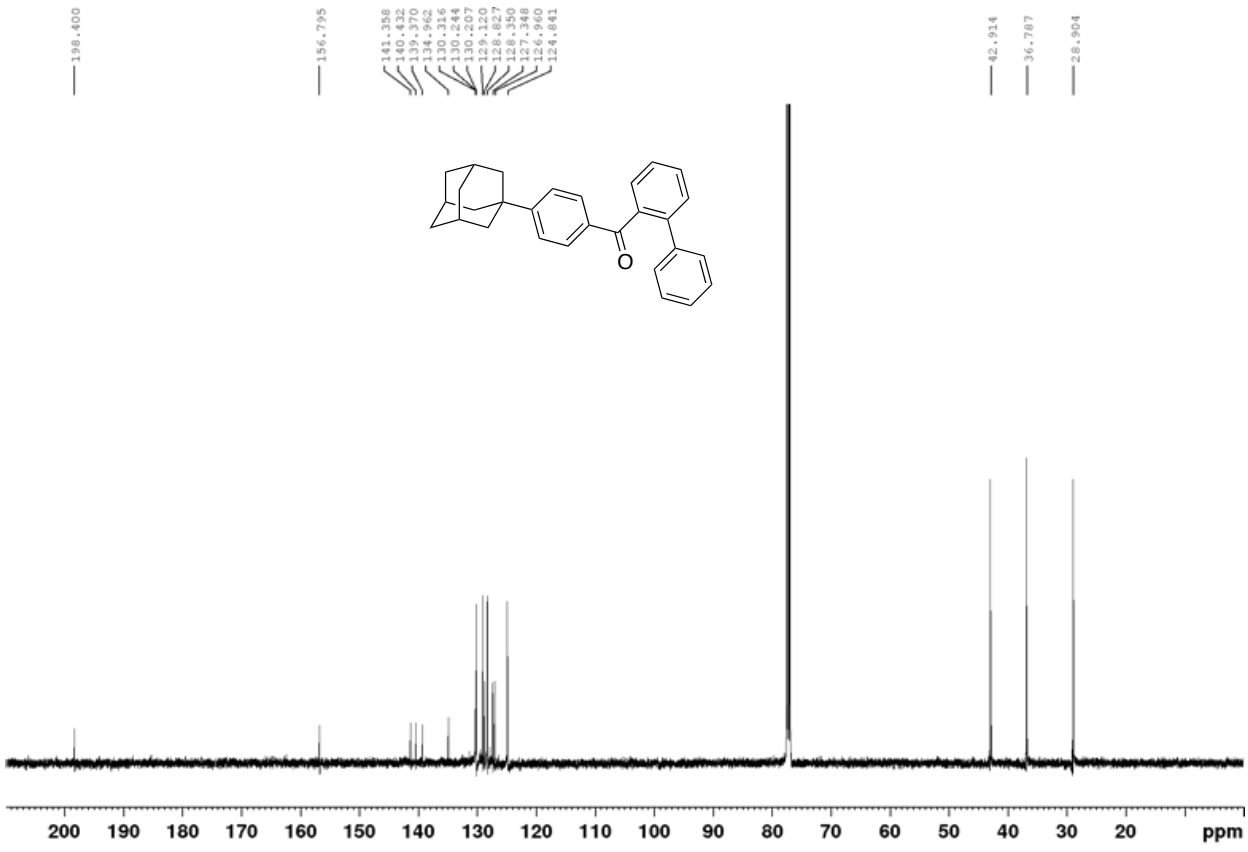

^{1}H NMR of 1-(4-([1,1'-biphenyl]-2-yl(diazo)methyl)phenyl)adamantane (**1**) in $CDCl_3$ at 500 MHz

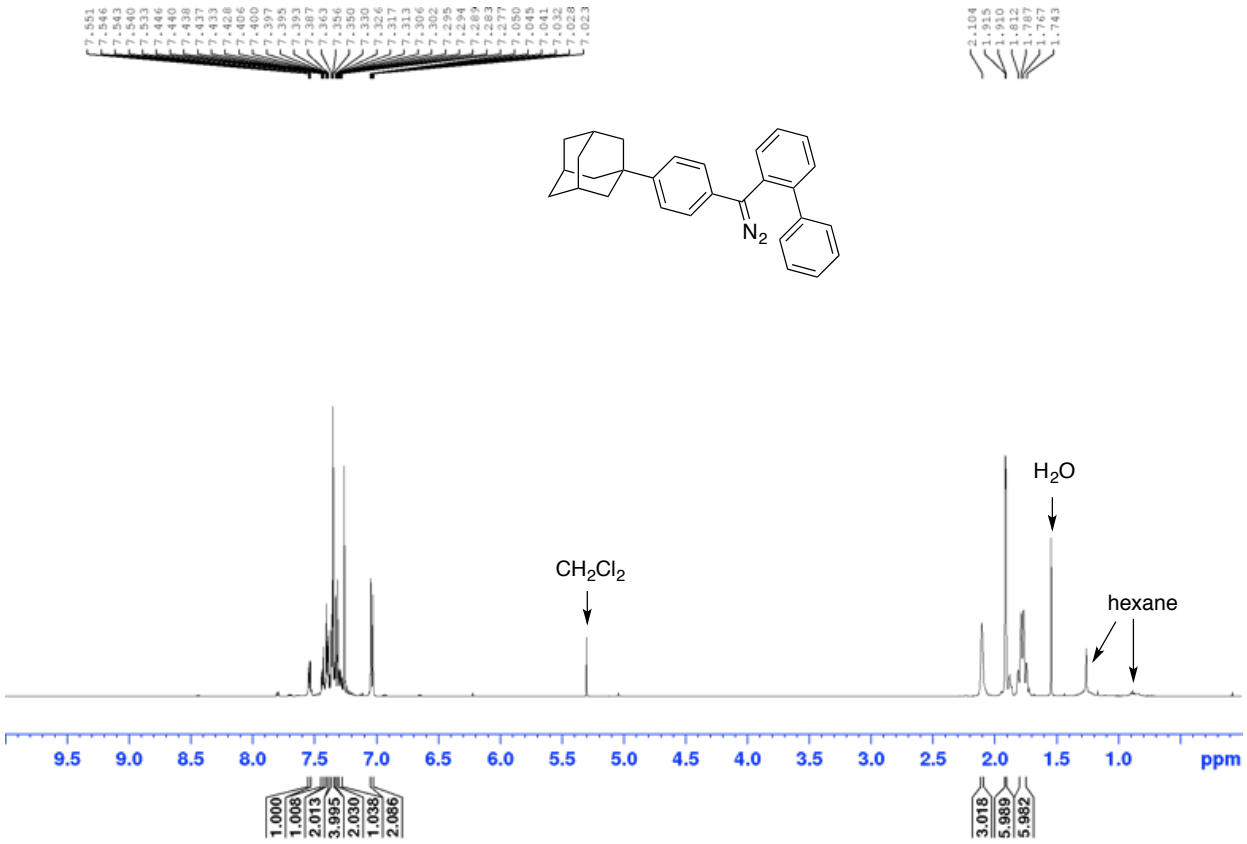

^{13}C NMR of 1-(4-([1,1'-biphenyl]-2-yl(diazo)methyl)phenyl)adamantane (**1**) in $CDCl_3$ at 125 MHz

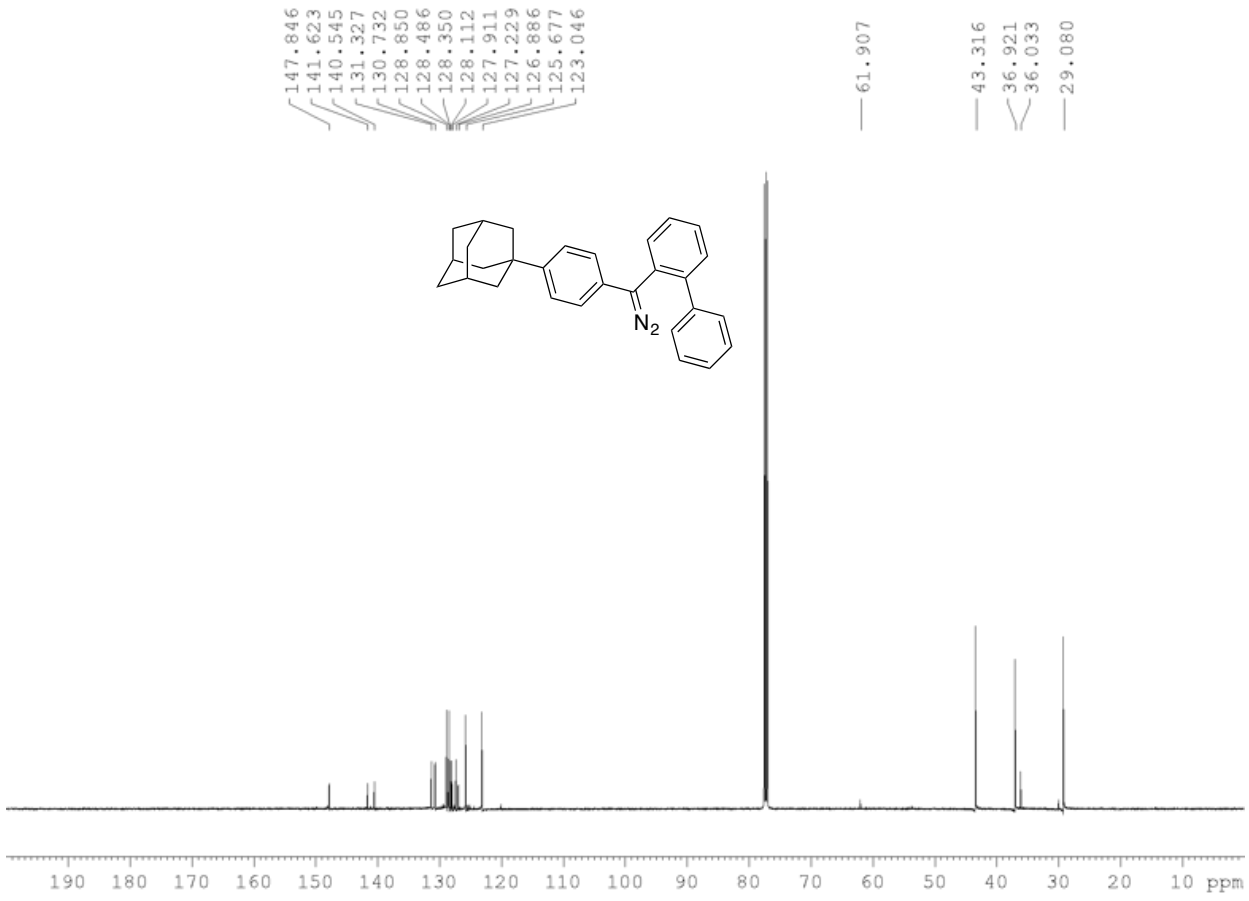

^{1}H NMR of 1-(4-(9*H*-fluoren-9-yl)phenyl)adamantane (**4**) in $CDCl_3$ at 500 MHz

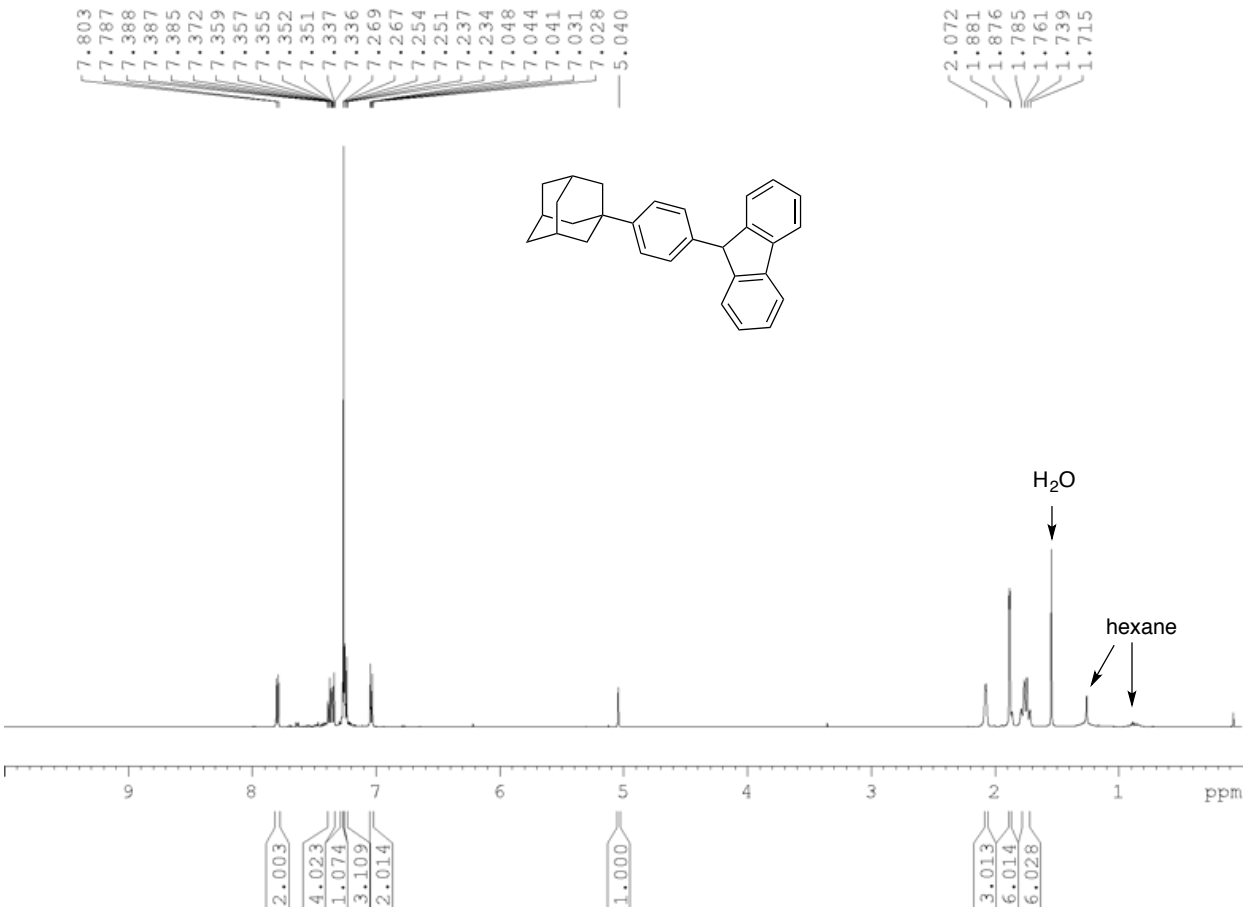

^{13}C NMR of 1-(4-(9*H*-fluoren-9-yl)phenyl)adamantane (**4**) in $CDCl_3$ at 125 MHz

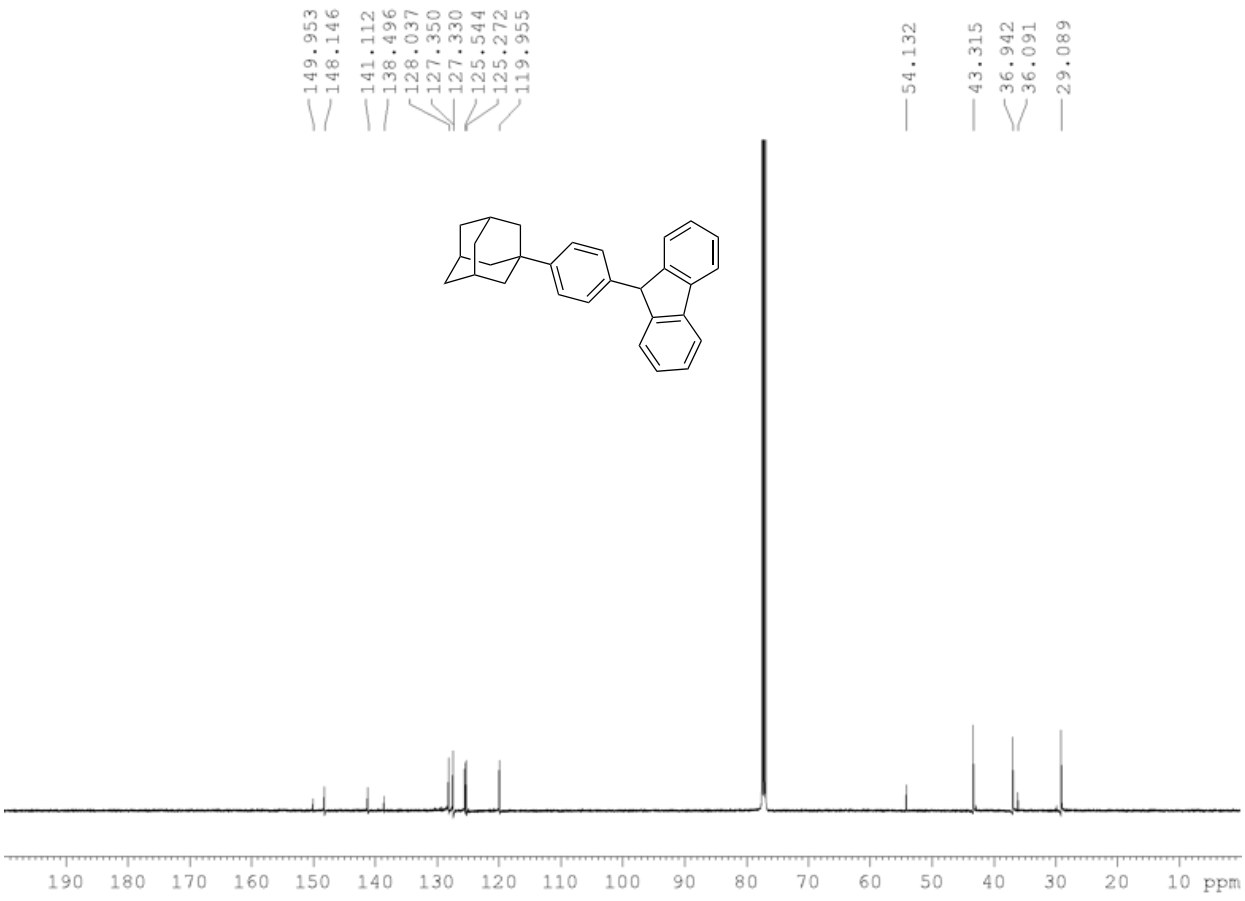

4.5.3 ^{1}H and ^{13}C NMR Spectra for Compounds 1 and 4 Post Photolysis in Air-Saturated Solutions

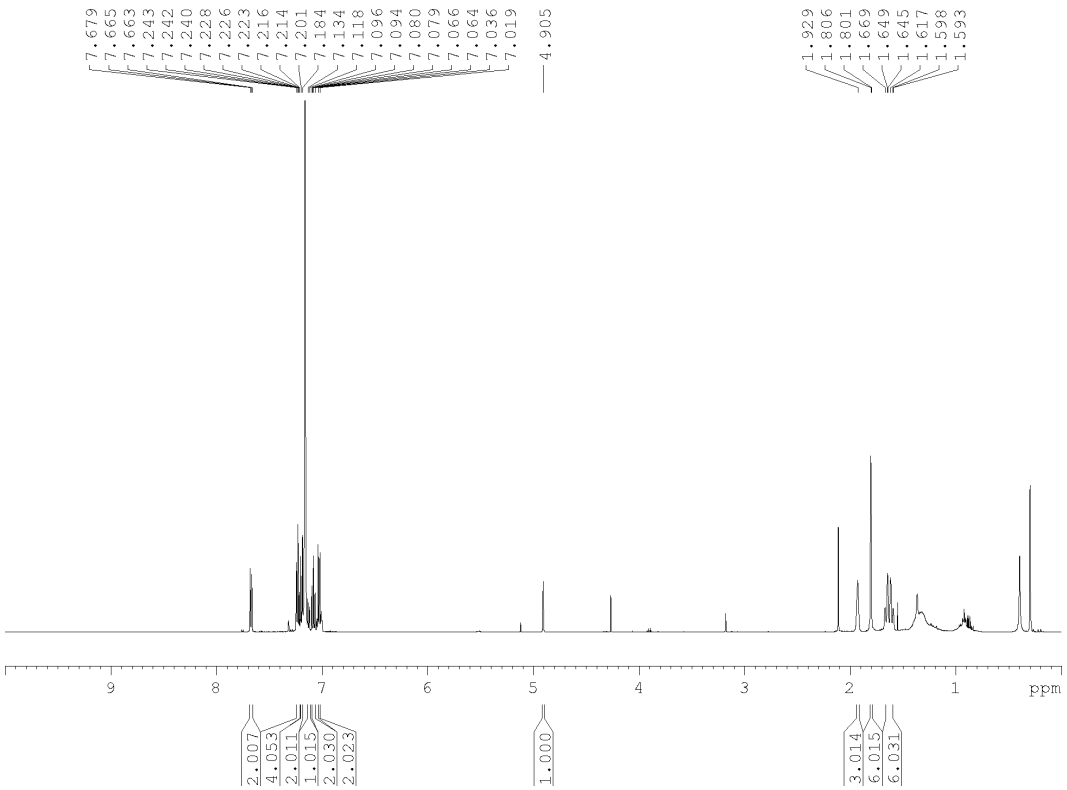

Figure 4.5.3.1. ^{1}H NMR of **4** post photolysis in air-saturated C_6D_6.

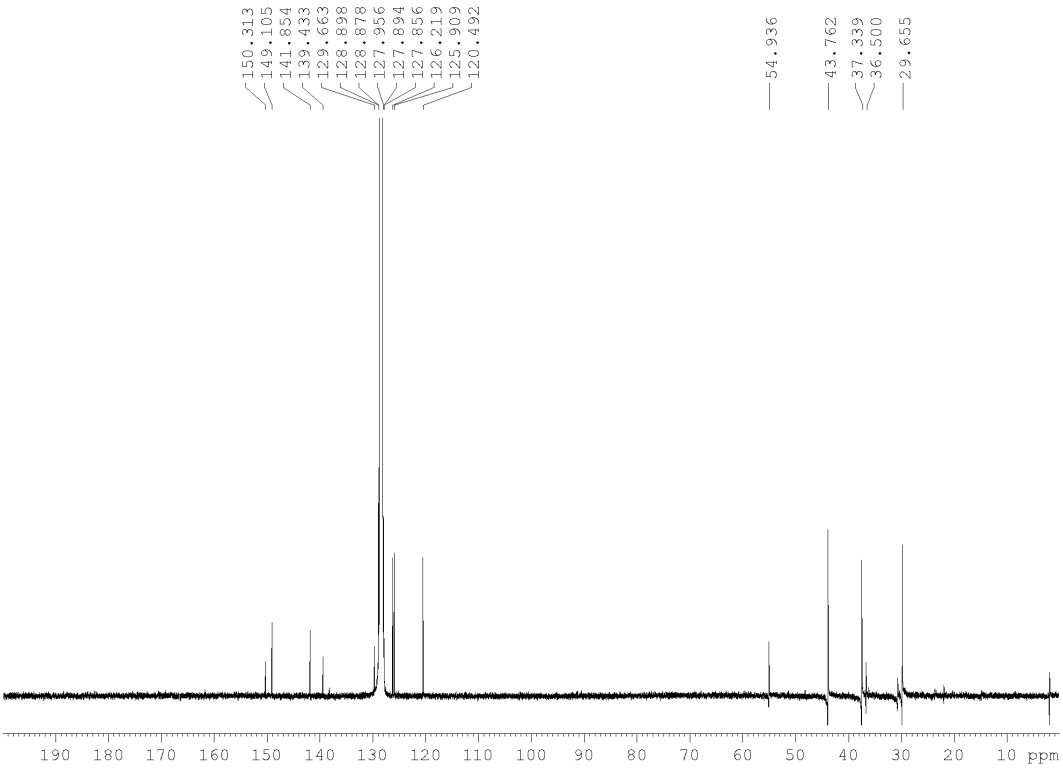

Figure 4.5.3.2. ^{13}C NMR of **4** post photolysis in air-saturated C_6D_6.

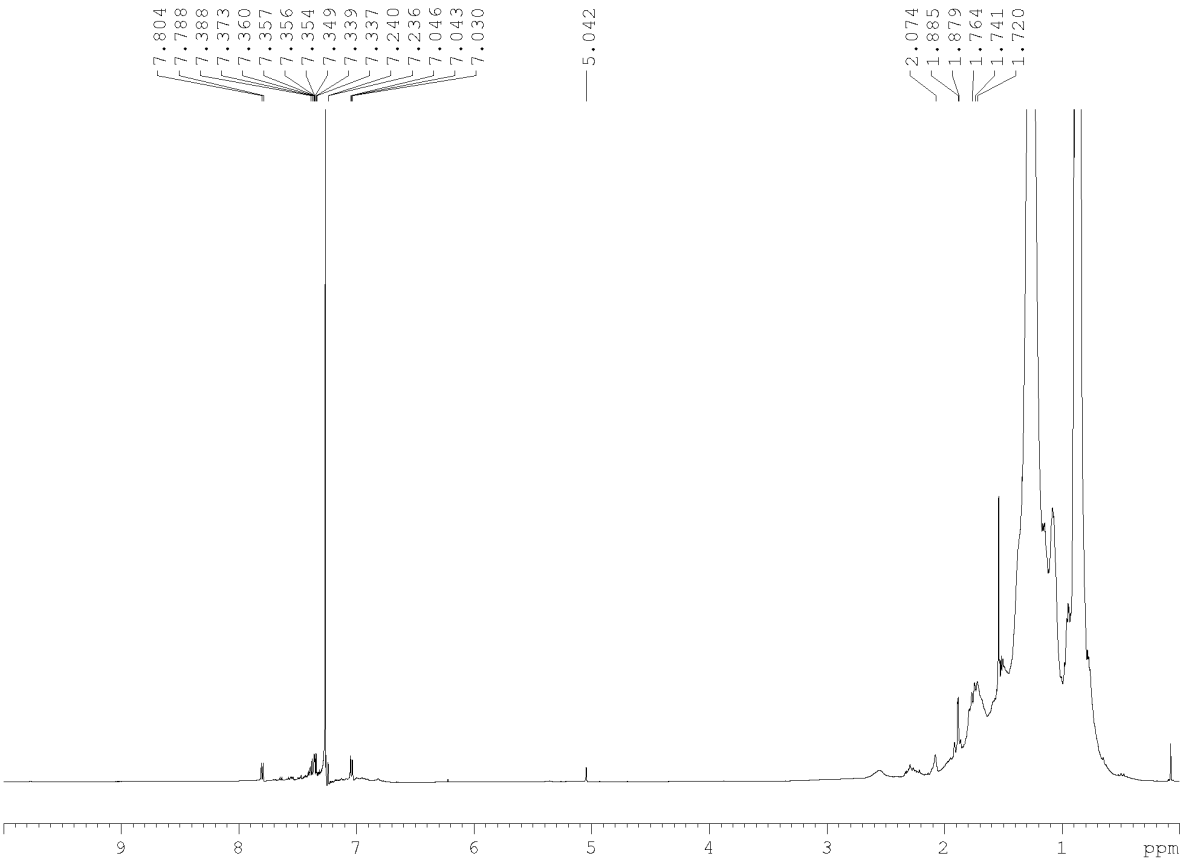

Figure 4.5.3.3. ^{1}H NMR of **1** post photolysis in air-saturated *n*-hexane. Spectrum acquired in $CDCl_3$.

4.5.4 UV-vis Spectra for Compounds 1 and 4 (Not Normalized)

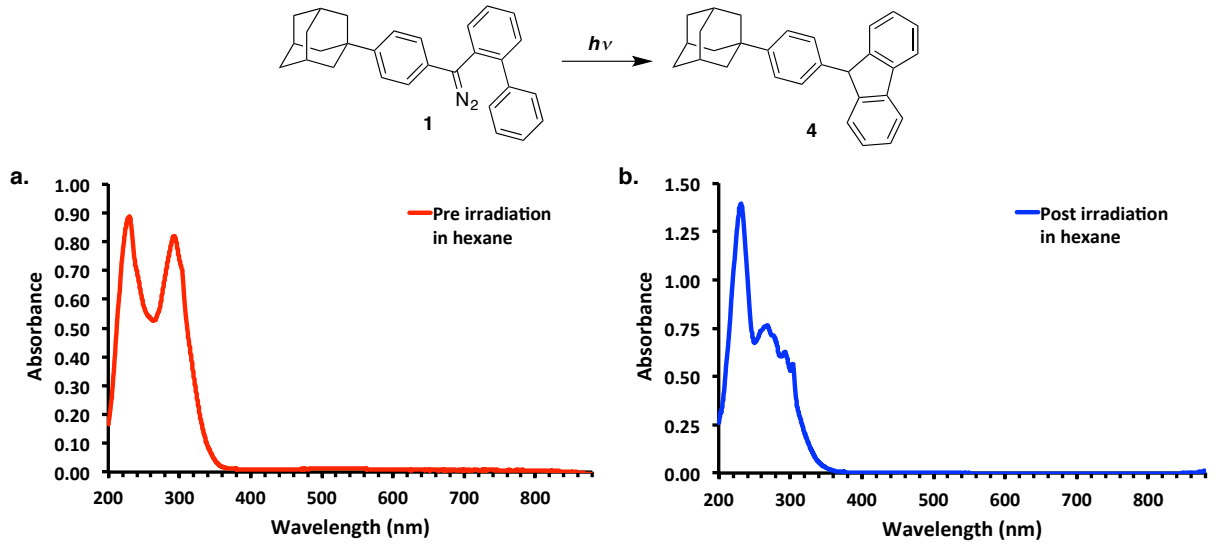

Figure 4.5.4.1. UV-vis spectra for diaryldiazomethane **1** in *n*-hexane solution (a) pre irradiation and (b) post irradiation via laser flash photolysis. The post irradiation spectrum (b) correlates to the 9-phenylfluorenyl product (**4**).

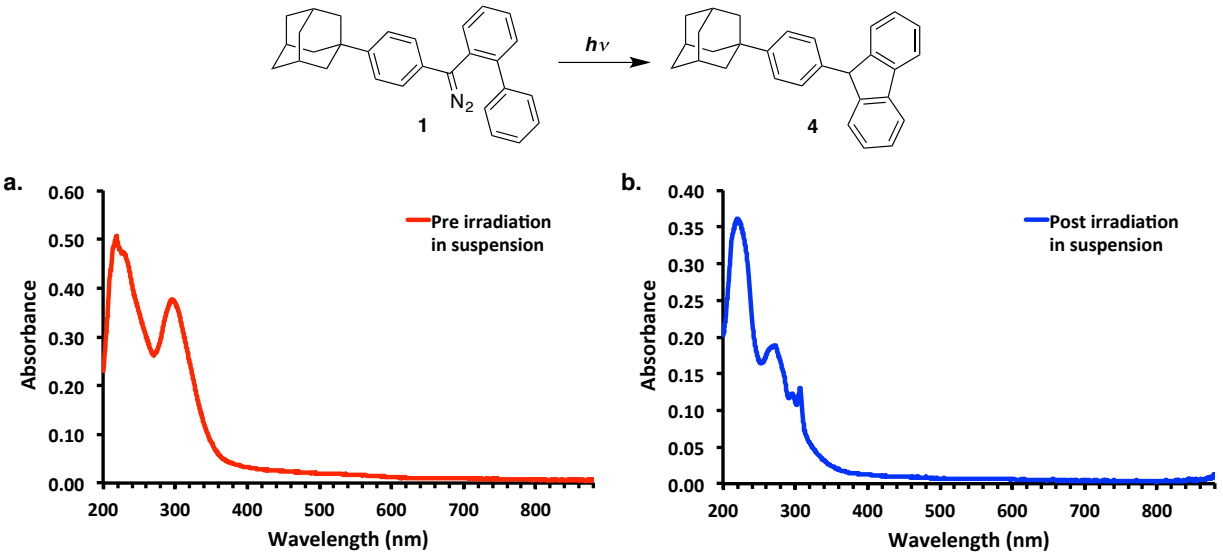

Figure 4.5.4.2. UV-vis spectra for diaryldiazomethane **1** in NC suspension (a) pre irradiation and (b) post irradiation via laser flash photolysis. The post irradiation spectrum (b) correlates to the 9-phenylfluorenyl product (**4**).

4.5.5 Dynamic Light Scattering Analysis for Compound 1

Unimodal Results Summary

Rept#.	Mean (nm)	Std.Dev (nm)	Baseline Error	P.I.	Counts/s	Diff.Coef (m^2/s)	Overflow
Rept.1	302.1	149.7	0.00%	6.610	7.72e+04	1.50e-12	1
Rept.2	134.0	66.6	0.00%	11.231	7.70e+04	3.38e-12	1
Rept.3	278.4	137.6	0.00%	5.343	7.68e+04	1.63e-12	0
Average	238.2	117.97		7.728			

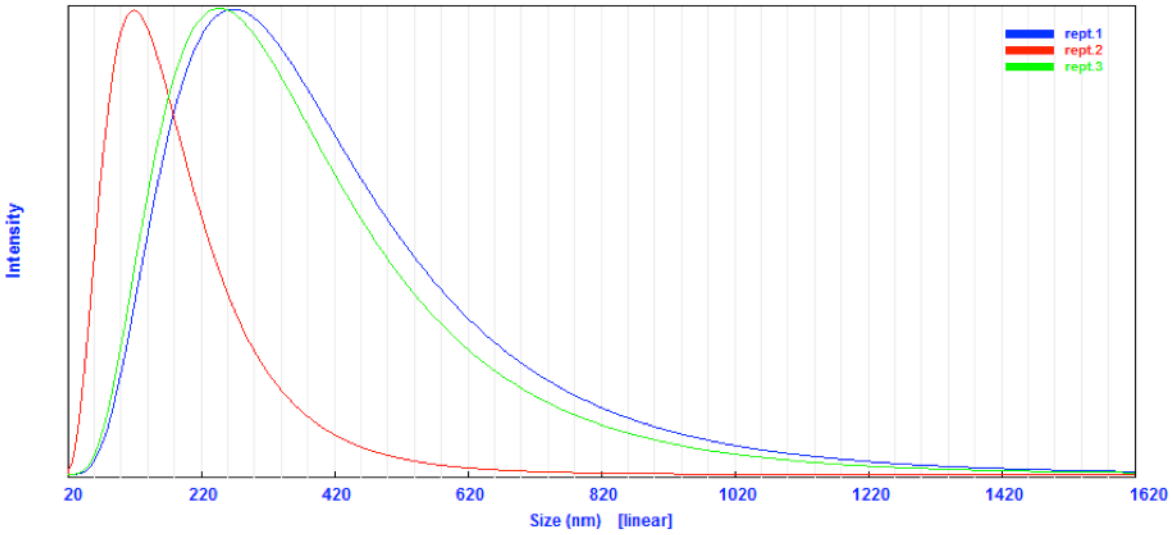

Figure 4.5.5.1. Dynamic light scattering (DLS) results for the nanocrystalline suspensions of diaryldiazomethane **1** showing the average particle size to be 238 nm.

4.6 References

1. Mulliken, R. *Phys. Rev.* **1932**, *41*, 751–758.

2. Chen, B.; Rogachev, A. Y.; Hrovat, D. A.; Hoffmann, R.; Borden, W. T. *J. Am. Chem. Soc.* **2013**, *135*, 13954–13964.

3. Schuster, G. B. *Adv. Phys. Org. Chem.* **1986**, *22*, 31–361.

4. Kirmse, W. *Carbene Chemistry*, Academic Press, New York, N. Y., 1971.

5. Wang, J.; Kubicki, J.; Peng, H.; Platz, M. S. *J. Am. Chem. Soc.* **2008**, *130*, 6604–6609.

6. Gilbert, B. C.; Griller, D.; Nazran, A. S. *J. Org. Chem.* **1985**, *50*, 4738–4742.

7. Bethell, D.; Stevens, G.; Tickle, P. *Chem. Commun.* **1970**, 792–794.

8. Griller, D.; Nazran, A. S.; Scaiano, J. C. *Acc. Chem. Res.* **1984**, *17*, 283–289.

9. Griller, D.; Nazran, A. S.; Scaiano, J. C. *J. Am. Chem. Soc.* **1984**, *106*, 198–202.

10. Kirmse, W.; Kund, K.; Ritzer, E.; Dorigo, A. E.; Houk, K. N. *J. Am. Chem. Soc.* **1986**, *108*, 6045–6046.

11. Woodworth, R. C.; Skell, P. S. *J. Am. Chem. Soc.* **1959**, *81*, 3383–3386.

12. Dorra, M.; Gomann, K.; Guth, M.; Kirmse, W. *J. Phys. Org. Chem.* **1996**, *9*, 598–610.

13. Langan, J. G.; Sitzmann, E. V.; Eisenthal, K. B. *Chem. Phys. Lett.* **1984**, *110*, 521–527.

14. Langan, J. G.; Sitzmann, E. V.; Eisenthal, K. B. *Chem. Phys. Lett.* **1986**, *124*, 59–62.

15. Sitzmann, E. V.; Langan, J. G.; Griller, D.; Eisenthal, K. B. *Chem. Phys. Lett.* **1989**, *161*, 353–360.

16. Sitzmann, E. V.; Langan, J.; Eisenthal, K. B. *J. Am. Chem. Soc.* **1984**, *106*, 1868–1869.

17. Jortner, J.; Rice, S. A.; Hochstrasser, R. M. *Adv. Photochem.* **1969**, *7*, 149–309.

18. Robinson, G. W.; Frosch, R. J. *J. Chem. Phys.* **1962**, *37*, 1962–1973.

19. Robinson, G. W.; Frosch, R. P. *J. Chem. Phys.* **1963**, *38*, 1187–1203.

20. Geise, C. M.; Wang. Y.; Mykhaylova, O.; Frink, B. T.; Toscano, J. P.; Hadad, C. M. *J. Org. Chem.* **2002**, *67*, 3079–3088.

21. Wang, Y.; Hadad, C. M.; Toscano, J. P. *J. Am. Chem. Soc.* **2002**, *124*, 1761–1767.

22. Wang, J.; Burdzinski, G.; Gustafson, T. L.; Platz, M. S. *J. Org. Chem.* **2006**, *71*, 6221–6228.

23. Wang, J.; Burdzinski, G.; Gustafson, T. L.; Platz, M. S. *J. Am. Chem. Soc.* **2007**, *129*, 2597–2606.

24. Wang, J.; Kubicki, J.; Hilinski, E. F.; Mecklenburg, S. L.; Gustafson, T. L.; Platz, M. S. *J. Am. Chem. Soc.* **2007**, *129*, 13683–13690.

25. Peon, J.; Polshakov, D.; Kohler, B. *J. Am. Chem. Soc.* **2002**, *124*, 6428–6438.

26. Wang, J.; Zhang, Y.; Kubicki, J.; Platz, M. S. *Photochem. Photobiol. Sci.* **2008**, *7*, 552–557.

27. Grasse, P. B.; Brauer, B. E.; Zupancic, J. J.; Kaufmann, K. J.; Schuster, G. B. *J. Am. Chem. Soc.* **1983**, *105*, 6833–6845.

28. Tomioka, H.; Hirai, K.; Fujii, C. *Acta Chem. Scand.* **1992**, *46*, 680–682.

29. Closs, G. L.; Rabinow, B. E. *J. Am. Chem. Soc.* **1976**, *98*, 8190–8198.

30. Hadel, L. M.; Platz, M. S.; Scaiano, J. C. *J. Am. Chem. Soc.* **1984**, *106*, 283–287.

31. Doss, S. H.; Abdel-Wahab, A. A.; Frühof, E. M.; Dürr, H. D.; Gould, I. R.; Turro, N. J. *J. Org. Chem.* **1987**, *52*, 434–438.

32. Denney, D. B.; Klemchuk, P. P. *J. Am. Chem. Soc.* **1958**, *80*, 3289–3290.

33. Palik, E. C.; Platz, M. S. *J. Org. Chem.* **1983**, *48*, 963–969.

34. Wood, E. A. Crystals and Light: An Introduction to Optical Crystallography, 2nd ed.; Dover Publications: New York, 1977.

35. Chin, K. K.; Natarajan, A.; Gard, M. N.; Campos, L. M.; Shepard, H.; Johansson, E.; Garcia-Garibay, M. A. *Chem. Commun.* **2007**, 4266–4268.

36. Kuzmanich, G.; Simoncelli, S.; Gard, M. N.; Spänig, F.; Henderson, B. L.; Guldi, D. M.; Garcia-Garibay, M. A. *J. Am. Chem. Soc.* **2011**, *133*, 17296–17306.

37. Simocelli, S.; Kuzmanich, G.; Gard, M. N.; Garcia-Garibay, M. A. *J. Phys. Org. Chem.,* 2010, **23**, 376–381.

38. Woo, J. C. S.; Fenster, E.; Dake, G. R. *J. Org. Chem.* **2004**, *69*, 8984–8986.

39. Kasai, H.; Nalwa, H. S.; Oikawa, H.; Okada, S.; Matsuda, H.; Minami, N.; Kakuta, A.; Ono, K.; Mukoh, A.; Nakanishi, H. *Jpn. J. Appl. Phys.* **1992**, *31*, L1132–L1134.

40. Murov, S. L.; Carmichael, I.; Hug, G. L. Handbook of Photochemistry, 2nd ed.; Marcel Dekker, Inc.: New York, 1993.

41. Trozzolo, A. M.; Wasserman, E. In *Carbenes*, Vol. 2; Moss, R. A., Jones, M., Jr., Eds.; Wiley: New York, 1975.

42. Dupuy, C.; Korenowski, G. M.; McAuliffe, M.; Hetherington, W. M., III: Eisenthal, K. B. *Chem. Phys. Lett.* **1981**, *77*, 272–274.

43. Wang, Y.; Sitzmann, E. V.; Novak, F.; Dupuy, C.; Eisenthal, K. B. *J. Am. Chem. Soc.* **1982**, *104*, 3238–3239.

44. Knorr, J.; Sokkar, P.; Schott, S.; Costa, P.; Thiel, W.; Sander, W.; Sanchez-Garcia, E.; Nuernberger, P. *Nat. Commun.* **2016**, *7*, 12968-1–8.

45. Simon, J. D.; Peters, K. S. *J. Am. Chem. Soc.* **1983**, *105*, 5156–5158.

46. Simon, J. D.; Peters, K. S. *J. Am. Chem. Soc.* **1988**, *110*, 3336–3336.

47. Kobayashi, S.; Matsuzawa, T.; Matsuoka, S.; Tajima, H.; Ishizone, T. *Macromolecules* **2006**, *39*, 5979–5986.